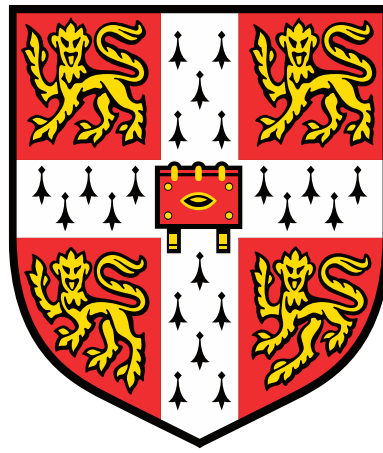
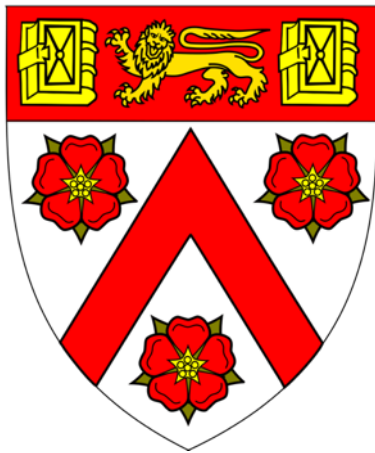


Novel pleiotropic regulators of flotation,
secondary metabolite production, and
virulence in *Serratia* sp. ATCC 39006



Amy Maria Hill
Trinity College
University of Cambridge

August 2021

This thesis is submitted for the degree of Doctor of Philosophy

Declaration

This thesis is the result of my own work and includes nothing which is the outcome of work done in collaboration except as declared in the Preface and specified in the text. It is not substantially the same as any that I have submitted, or, is being concurrently submitted for a degree or diploma or other qualification at the University of Cambridge or any other University or similar institution except as declared in the Preface and specified in the text. I further state that no substantial part of my thesis has already been submitted, or, is being concurrently submitted for any such degree, diploma or other qualification at the University of Cambridge or any other University or similar institution except as declared in the Preface and specified in the text. It does not exceed the prescribed word limit for the relevant Degree Committee.

Amy Maria Hill

August 2021

**Novel pleiotropic regulators of flotation, secondary metabolite production, and virulence
in *Serratia* sp. ATCC 39006**

Amy Maria Hill

Summary

Serratia sp. ATCC 39006 (S39006) is a Gram-negative, rod-shaped enterobacterium known for the production two antibiotics; the β -lactam, 1-carbapen-2-em-3-carboxylic acid (a carbapenem) and the red-pigmented tripyrrole, 2-methyl-3-pentyl-6-methoxyprodigiosin (prodigiosin; a prodiginine). It also produces plant cell wall degrading enzymes (PCWDEs) and is capable of flagellar-mediated swimming and swarming motility. S39006 is the only enterobacterium known to naturally produce gas vesicles (GVs). GV are proteinaceous, intracellular organelles that increase the buoyancy of a cell and enable flotation upwards through the water column and colonisation of air-liquid interfaces. The production and regulation of GV is a complex process with a range of regulatory inputs. GV are expressed from a cluster of 19 genes arranged in two contiguous operons, *gvpA1-gvpY* and *gvrA-gvrC*. Prior to this study, three regulators encoded within the GV cluster, which are essential for GV production, had been described: GvrA, GvrB, and GvrC. Other regulators that have been identified include the post-transcriptional regulator RsmA, the repressor of the ribose operon, RbsR, and the DeoR-family transcriptional regulator, FloR. This study employed random transposon mutagenesis, visual screening of mutant phenotypes, cloning and sequencing, and bioinformatic analysis to identify novel regulators of GV production. This included mutants with transposon insertions in genes encoding an O-antigen ligase (*walL*), the sigma factor σ^{54} (*rpoN*), and a transcription factor (*dksA*). The *walL* mutant exhibited increased transcription and expression of GV genes but was unable to float. Pleiotropic effects of the transposon insertion included an increase in carbapenem production and a decrease in motility and virulence in a *Caenorhabditis elegans* model. The *rpoN* mutant showed a reduction in GV and pectate lyase production, swimming and swarming motility, and an increase in carbapenem production. The *dksA* mutant showed a decrease in GV and antibiotic production, motility, and virulence in *C. elegans*. A quantitative proteomic analysis was undertaken comparing the *rpoN* and *dksA* mutants against wild type S39006 to understand their regulatory roles. Expression of proteins involved in GV biogenesis, antibiotic production and motility as well as previously identified transcriptional regulators were significantly altered in each mutant, compared to wild type.

Acknowledgements

This work would not have been possible without the help and support of many people. Firstly, I would like to thank my supervisor, Professor George Salmond, for his support and guidance over the course of my PhD. His helpful feedback and suggestions have greatly enriched my work and my time in his lab has allowed me to develop into an independent scientist. I would also like to extend my thanks to the postdocs in the lab, Dr. Rita Monson and Dr. Jessica Bergman. Your support, guidance, and friendship both within the lab and outside of it have been incredibly helpful. I would like to acknowledge my Postgraduate Thesis Panel and the help they gave me over the course of my degree; thank you Ross, Martin, and Dee for your support.

I am incredibly grateful to have been supported by the Woolf Fisher Trust and the Cambridge Trust over the past four years. I would not have been able to do this degree without their support. In particular, I would like to acknowledge the help that Nigel Evans, then secretary of the Woolf Fisher Trust, extended to all of the scholars at the start of the coronavirus pandemic, allowing many of us to return home to New Zealand when the university closed.

To all members of the Salmond lab, past and present, I say a massive thank you. To the lab members before me: Alex, Andy, Ray, Bihe, Chin Mei, Tracy, and Maxime, thank you for the advice and mentoring you provided. To all of the current lab members, and those that have recently finished: Kate, Carlo, Muriel, Anya, Isobel, Maria, Daniel, Tomás and Isabella, thank you for your friendship, advice, encouragement and help when I needed it most. I would also like to thank Josh and Diana for their expert technical help and all of the administration and support staff within the Biochemistry Department for their tireless work. I would like to thank the members of the Welch lab, past and present, for their help and advice during lab meetings and in the lab.

I would also like to thank the team at the Cambridge Advanced Imaging Centre for their help when taking TEM images. I thank Dr. Mike Deery, Renata Feret, and Yagnesh Umrana from the Cambridge Centre for Proteomics (CCP) for their collaboration on the proteomics

experiments and helpful advice on data analysis. The proteomics experiments were performed in conjunction with Carlo Sandoval, and I want to say an extra thank you to him for his patience, skill, and quiet resolve while we were performing these experiments.

To all of my friends both in Cambridge and outside of it, I want to say a huge thank you for keeping me sane during this endeavour, particularly over the last year. I want to thank the Woolf Fisher Scholars in Cambridge for their frequent catch ups for a meal or to watch the All Blacks play rugby, you were the little piece of home that made life so much easier. In particular, thank you to Liam, Steph, Tessa, Nick, Jono, and Abbey. To Bonnie and Sam, thank you for providing me with an escape and always being keen to see a concert or a stage show with me. To all my friends back in New Zealand, thank you and I can't wait to spend some more time with you now. Finally, I would like to thank my family for their unwavering support and belief in me. You have been there for me through all the ups and downs, both in person and over the phone and I have no words to say except thank you from the bottom of my heart.

Table of Contents

Declaration	ii
Summary	iii
Acknowledgements	iv
Table of Contents	vi
List of Figures	ix
List of Tables	xi
Abbreviations	xii
<i>Chapter 1. Introduction</i>	<i>1</i>
1.1 <i>Serratia</i> sp. ATCC 39006	1
1.2 Quorum Sensing	2
1.3 Secondary Metabolites	3
1.3.1 Prodigiosin	4
1.3.2 Carbapenem	7
1.4 Plant Cell Wall Degrading Enzymes	9
1.5 Flagellar Motility	10
1.6 Gas vesicles	12
1.6.1 Regulation of gas vesicles in S39006	17
1.7 Aims of this Study	20
<i>Chapter 2. Materials and Methods</i>	<i>21</i>
2.1 Media, Solutions, Antibiotics, and Supplements	21
2.2 Bacterial Strains, Bacteriophage, Plasmids, and Culture Conditions	21
2.3 Recombinant DNA Techniques	31
2.3.1 DNA separation, purification, digestion, and ligation	31
2.3.2 Polymerase chain reaction (PCR)	35
2.3.3 Random primed polymerase chain reaction (RP-PCR)	36
2.3.4 Plasmid construction	37
2.3.5 Allelic exchange	38
2.3.6 Bacterial transformation by heat shock	38
2.3.7 Transfer of plasmids via conjugation	39
2.3.8 DNA sequencing	39
2.4 Random Transposon Mutagenesis	40
2.4.1 Bypass mutagenesis screening	40
2.5 Bioinformatic Analysis	41
2.6 Generalised Transduction of S39006 using ΦOT8	41

2.6.1 Preparation of Φ OT8 lysate	41
2.6.2 Transduction of S39006 using Φ OT8	41
2.7 Phenotypic Assays	42
2.7.1 BHL detection assay	42
2.7.2 Carbapenem detection assay	42
2.7.3 Cellulase detection assay	42
2.7.4 Pectate lyase detection assay	43
2.7.5 Flotation assay	43
2.7.6 Colony morphology spot test	43
2.7.7 Swarming assay	44
2.7.8 Swimming assay	44
2.7.9 Quantification of carbapenem and BHL production	44
2.7.10 Quantification of prodigiosin production	45
2.8 <i>Caenorhabditis elegans</i> Virulence Assay	45
2.9 Analysis of Gene Expression by Measuring β-glucuronidase Activity	46
2.10 Microscopy Techniques	46
2.10.1 Phase contrast microscopy	46
2.10.2 Transmission electron microscopy	47
2.11 Protein Methods	47
2.11.1 Sodium dodecyl sulphate-polyacrylamide gel electrophoresis (SDS-PAGE)	47
2.11.2 Western blotting	47
2.11.3 Preparation of intracellular protein samples for proteomics	48
2.11.4 Tandem mass tag (TMT) labelling	48
2.11.5 High-pH first dimension reverse-phase fractionation	48
2.11.6 Liquid chromatography-mass spectrometry (LC-MS/MS) analyses	49
2.11.7 Database searching and analysis	50
2.12 Silver Stain for Lipopolysaccharides	51
2.13 Statistical Analysis	51
Chapter 3. A Random Transposon Mutagenesis Screen for <i>Serratia</i> sp. ATCC 39006 Gas Vesicle Mutants	52
3.1 Introduction	52
3.2 Results	52
3.2.1 Generation of a library of transposon insertion mutants	52
3.2.2 Determination of the transposon insertion location	55
3.2.3 Novel GV regulators show differences in flotation ability	58
3.2.4 IclR family transcriptional regulator, Orf6410	60
3.2.5 4' Phosphopantetheinyl transferase, Orf2785	65
3.2.6 RnfH family protein, RatB	69
3.2.7 RNA Chaperone, Hfq	74
3.3 Discussion	77
Chapter 4. The O-antigen ligase, <i>WaaL</i>, is essential for flotation of S39006	78
4.1 Introduction	78

4.2 Results	78
4.2.1 Sequence analysis and genomic context of <i>waaL</i>	78
4.2.2 The <i>waaL</i> mutant produces gas vesicles but is unable to float	81
4.2.3 Mutation of <i>waaL</i> causes diverse phenotypic impacts in S39006	85
4.2.4 Mutation in <i>waaL</i> can be complemented	89
4.2.5 A <i>waaL</i> knockout has the same effect as transposon insertion	91
4.2.6 LPS composition differs between the <i>waaL</i> mutant and wild type S39006	93
4.3 Discussion	94
Chapter 5. The alternative sigma factor RpoN (σ^{54}) controls gas vesicle production	98
5.1 Introduction	98
5.2 Results	98
5.2.1 Sequence analysis and genomic context of <i>rpoN</i>	98
5.2.2 The <i>rpoN</i> mutant shows reduced gas vesicle production	102
5.2.3 Transcription of <i>gvpA1-gvpY</i> is reduced in the <i>rpoN</i> mutant	103
5.2.4 Mutation in <i>rpoN</i> causes diverse phenotypic impacts in S39006	105
5.2.5 The transposon insertion in <i>rpoN</i> can be complemented	108
5.2.6 A <i>rpoN</i> knockout has the same effect as the transposon insertion	111
5.2.7 Intracellular protein extraction and quantification in S39006 and the <i>rpoN</i> mutant	113
5.2.8 Proteins showing differential abundance between S39006 and the <i>rpoN</i> mutant	118
5.2.9 Prediction of RpoN binding sites in S39006	130
5.3 Discussion	132
Chapter 6. The transcription factor DksA regulates production of gas vesicles and secondary metabolites in <i>Serratia sp. ATCC 39006</i>.	139
6.1 Introduction	139
6.2 Results	140
6.2.1 Sequence analysis and genomic context of <i>dksA</i>	140
6.2.2 The <i>dksA</i> mutant shows reduced GV production and flotation ability	142
6.2.3 Transcription of the <i>gvpA1</i> and <i>gvrA</i> operons is reduced in the <i>dksA</i> mutant	144
6.2.4 Mutation in <i>dksA</i> causes diverse phenotypic impacts in S39006	145
6.2.5 Transposon insertion in <i>dksA</i> can be complemented	149
6.2.6 A <i>dksA</i> knockout has the same effect as transposon insertion	151
6.2.7 The mutation of <i>dksA</i> can be partially bypassed by the disruption of <i>guaBA</i>	151
6.2.8 Intracellular protein extraction and quantification in S39006 and the <i>dksA</i> mutant	154
6.2.9 Proteins showed differential abundance between S39006 and the <i>dksA</i> mutant	159
6.3 Discussion	170
Chapter 7. Final Discussion	178
References	184

List of Figures

Figure 1.1 – The <i>smalR</i> regulatory system in S39006.	3
Figure 1.2 – S39006 produces the red pigmented antibiotic prodigiosin.	4
Figure 1.3 – A hierarchical model of the regulatory network controlling prodigiosin and carbapenem production in S39006.	7
Figure 1.4 – S39006 produces the β -lactam antibiotic carbapenem.	8
Figure 1.5 – Swimming and swarming motility in S39006.	11
Figure 1.6 – S39006 makes gas vesicles for flotation.	13
Figure 1.7 – The GV gene clusters of S39006 and related strains.	15
Figure 3.1 – Random transposon mutagenesis of NWA19 using plasmid pKRCPN1.	54
Figure 3.2 – Examples of different gas vesicle phenotypes observed following random transposon mutagenesis of NWA19.	55
Figure 3.3 – Determination of the transposon insertion location using random primed PCR.	56
Figure 3.4 – Flotation and spot test assays for novel GV regulators with accompanying PCM images.	59
Figure 3.5 – Organisation of genes surrounding the AMH101, AMH133, and AMH137 transposon insertion sites.	61
Figure 3.6 – The transposon insertion in <i>orf6410</i> is pleiotropic.	64
Figure 3.7 – Organisation of genes surrounding the AMH105 transposon insertion site.	66
Figure 3.8 – The transposon insertion in <i>orf2785</i> is pleiotropic.	68
Figure 3.9 – Transposon insertion in <i>orf2785</i> significantly increases prodigiosin production.	69
Figure 3.10 – Organisation of genes surrounding the AMH129 transposon insertion site.	70
Figure 3.11 – The transposon insertion in <i>ratB</i> is pleiotropic.	72
Figure 3.12 – Transposon insertion in <i>ratB</i> significantly increases carbapenem production.	73
Figure 3.13 – Organisation of genes surrounding the AMH105 transposon insertion site.	74
Figure 3.14 – The transposon insertion in <i>hfq</i> is pleiotropic.	76
Figure 4.1 – Organisation of genes surrounding the AMH113 and AMH157 transposon insertion sites.	80
Figure 4.2 – Transposon insertion in <i>waal</i> abolishes flotation and disrupts colony morphology.	82
Figure 4.3 – <i>gvpA1</i> and <i>gvrA</i> expression in wild type and the <i>waal</i> mutant under aerobic and microaerophilic conditions.	84
Figure 4.4 – The transposon insertion in <i>waal</i> is pleiotropic.	86
Figure 4.5 – Transposon insertion in <i>waal</i> increases carbapenem but not prodigiosin production.	87
Figure 4.6 – Transposon insertion in <i>waal</i> attenuates virulence in a <i>C. elegans</i> model.	88
Figure 4.7 – Transposon insertion in <i>waal</i> can be complemented.	90
Figure 4.8 – The <i>waal</i> knockout strain AMH37 displays the same phenotypes as the <i>waal</i> transposon mutant AMH157.	92
Figure 4.9 – The <i>waal</i> mutants show different LPS banding patterns to wild type S39006.	94
Figure 5.1 – Organisation of genes surrounding the AMH109 transposon insertion site.	100
Figure 5.2 – Transposon insertion in <i>rpoN</i> reduces flotation and gas vesicle production.	102
Figure 5.3 – <i>gvpA1</i> and <i>gvrA</i> expression in wild type and the <i>rpoN</i> mutant under aerobic and microaerophilic conditions.	104
Figure 5.4 – The transposon insertion in <i>rpoN</i> is pleiotropic.	106

Figure 5.5 – Transposon insertion in <i>rpoN</i> increases carbapenem but not prodigiosin production.	107
Figure 5.6 – Transposon insertion in <i>rpoN</i> attenuates virulence in a <i>C. elegans</i> model.	107
Figure 5.7 – Transposon insertion in <i>rpoN</i> can be complemented.	109
Figure 5.8 – Transcription of the <i>gvpA1</i> can be restored by expression of <i>rpoN</i> <i>in trans</i> .	110
Figure 5.9 – The <i>rpoN</i> knockout strain AMH31 displays the same phenotypes as the <i>rpoN</i> transposon mutant AMH109.	112
Figure 5.10 – Western blot for GvpC in wild type, AMH109, and GPA1 after 12, 14, and 16 hours growth.	113
Figure 5.11 – Intracellular protein samples extracted from S39006 and AMH109.	114
Figure 5.12 – Pearson correlation coefficients between replicates of S39006 and AMH109.	116
Figure 5.13 – Boxplot of protein abundances in S39006 and AMH109.	116
Figure 5.14 – The PCA of the protein quantification in S39006 and AMH109.	117
Figure 5.15 – p-value distribution of proteome quantitation in AMH109.	117
Figure 5.16 – Volcano plot of differential protein abundances in AMH109.	118
Figure 5.17 – RpoN modulates proteins of the <i>gvpA1</i> and <i>gvrA</i> operons.	123
Figure 5.18 – RpoN modulates the expression of the prodigiosin and carbapenem operons.	124
Figure 5.19 – Genomic organisation and changes in protein abundance of Orf24450 to Orf22425.	127
Figure 5.20 – Genomic organisation and changes in protein abundance of Orf16280 to Orf16160.	128
Figure 5.21 – Predicted binding site of RpoN in S39006 generated by MEME.	130
Figure 5.22 – Schematic diagram of the proposed method of σ^{54} regulation of GV production.	134
Figure 6.1 – Organisation of genes surrounding the AMH141 transposon insertion site.	140
Figure 6.2 – Transposon insertion in <i>dksA</i> abolishes flotation and gas vesicle production.	143
Figure 6.3 – <i>gvpA1</i> and <i>gvrA</i> expression in wild type and the <i>dksA</i> mutant under aerobic and microaerophilic conditions.	145
Figure 6.4 – The transposon insertion in <i>dksA</i> is pleiotropic.	147
Figure 6.5 – Transposon insertion in <i>dksA</i> decreases carbapenem and prodigiosin production.	148
Figure 6.6 – Transposon insertion in <i>dksA</i> attenuates virulence in a <i>C. elegans</i> model.	148
Figure 6.7 – Transposon insertion in <i>dksA</i> can be complemented.	150
Figure 6.8 – The <i>dksA</i> knockout strain AMH32 displays the same phenotypes as the <i>dksA</i> transposon mutant AMH141.	152
Figure 6.9 – A second transposon insertion in <i>guaB</i> can bypass the <i>dksA</i> gas vesicle phenotype.	153
Figure 6.10 – Western blot for GvpC in wild type, AMH141 and GPA1 after 12, 14, and 16 hours growth.	154
Figure 6.11 – Intracellular protein samples extracted from S39006 and AMH141.	155
Figure 6.12 – Pearson correlation coefficients between replicates of S39006 and AMH141.	157
Figure 6.13 – Boxplot of protein abundances in S39006 and AMH141.	157
Figure 6.14 – The PCA of the protein quantification in S39006 and AMH141.	158
Figure 6.15 – p-value distribution of proteome quantitation in AMH141.	158
Figure 6.16 – Volcano plot of differential protein abundances in AMH141.	159
Figure 6.17 – DksA modulates proteins of the <i>gvpA1</i> and <i>gvrA</i> operons.	165
Figure 6.18 – DksA modulates the expression of the prodigiosin and carbapenem operons.	166
Figure 7.1 – Model of the regulatory network in S39006 for GV production, motility, and secondary metabolite production in S39006.	182

List of Tables

Table 2.1 – Media and solutions used in this study.	22
Table 2.2 – Antibiotics and supplements used in this study.	26
Table 2.3 – Bacterial strains and bacteriophage used in this study.	27
Table 2.4 – Plasmids used in this study.	30
Table 2.5 – Restriction enzyme digestion.	32
Table 2.6 – Ligation reaction.	32
Table 2.7 – Sequence of the oligonucleotides used in this study.	32
Table 2.8 – PCR reaction mixture used in this study.	35
Table 2.9 – PCR amplification conditions.	35
Table 2.10 – RP-PCR reaction mixture used in this study.	36
Table 2.11 – RP-PCR amplification conditions.	37
Table 3.1 – Transposon insertion sites in <i>S39006 ΔpigC</i> gas vesicle mutants.	57
Table 3.2 – Amino acid sequence similarity search of Orf6410 using BLASTP.	62
Table 3.3 – Predicted function of genes surrounding <i>orf6410</i> .	62
Table 3.4 – Amino acid sequence similarity search of Orf2785 using BLASTP.	66
Table 3.5 – Predicted function of genes surrounding <i>orf2785</i> .	66
Table 3.6 – Amino acid sequence similarity search of RatB using BLASTP.	70
Table 3.7 – Predicted function of genes surrounding <i>ratB</i> .	70
Table 3.8 – Amino acid sequence similarity search of Hfq using BLASTP.	75
Table 3.9 – Predicted function of genes surrounding <i>hfq</i> .	75
Table 4.1 – Predicted functions of genes surrounding <i>waalL</i> .	80
Table 4.2 – Amino acid sequence similarity search of WaaL using BLASTP.	81
Table 5.1 – Amino acid sequence similarity search of RpoN using BLASTP.	100
Table 5.2 – Predicted function of genes surrounding <i>rpoN</i> .	101
Table 5.3 – The top thirty most upregulated proteins quantified AMH109.	120
Table 5.4 – The top thirty most downregulated proteins quantified AMH109.	122
Table 5.5 – The fold change of proteins involved in flagellar biosynthesis and chemotaxis in AMH109.	125
Table 5.6 – Predicted functions of proteins encoded by <i>orf22450</i> to <i>orf22425</i> .	127
Table 5.7 – Predicted functions of proteins encoded by <i>orf16280</i> to <i>orf16160</i> .	128
Table 5.8 – Fold change in abundance of known regulators in the <i>rpoN</i> mutant.	129
Table 5.9 – The location of predicted RpoN binding sites in <i>S39006</i> .	131
Table 6.1 – Amino acid sequence similarity search of DksA using BLASTP.	141
Table 6.2 – Predicted function of genes surrounding <i>dksA</i> .	141
Table 6.3 – The top thirty most upregulated proteins quantified AMH141.	162
Table 6.4 – The top thirty most downregulated proteins quantified AMH141.	164
Table 6.5 – The fold change of proteins involved in flagellar biosynthesis and chemotaxis in AMH141.	168
Table 6.6 – Fold change in abundance of known regulators in the <i>dksA</i> mutant.	169

Abbreviations

AHL	<i>N</i> -acyl homoserine lactone
Ap	ampicillin
APS	ammonium persulfate
ATCC	American Type Culture Collection
ATP	adenosine triphosphate
bEBP	bacterial enhancer binding protein
BHL	<i>N</i> -butanoyl-L-homoserine lactone
BLAST	Basic Local Search Alignment Tool
BLASTP	protein-protein BLAST
bp	base pair
car	carbapenem
carbapenem	1-carbapen-2-em-carboxylic acid
CCP	Cambridge Centre for Proteomics
Cm	chloramphenicol
CMC	carboxymethyl cellulose
cRAP	common repository of adventitious proteins
DAPA	diaminopimelic acid
DEA	differential expression analysis
dH ₂ O	distilled water
DMSO	dimethyl sulfoxide
DNA	deoxyribonucleic acid
DNTP	deoxyribonucleoside triphosphate
DTT	dithiothreitol
EDTA	ethylenediaminetetraacetic acid disodium salt
Em	erythromycin
EMSA	electrophoretic mobility shift assay
ESS	<i>Escherichia coli</i> super sensitive
g	gram
GDP	guanosine 5'-diphosphate
GMP	guanosine 5'-monophosphate
GTP	guanosine 5'-triphosphate
GV	gas vesicle
HHL	<i>N</i> -hexanoyl-L-homoserine lactone
IMP	inosine 5'-monophosphate
IPTG	isopropyl- β -D-1-thiogalactopyranoside
kb	kilobase pairs
kDa	kilodalton
Km	kanamycin
L	litre

LB	Lysogeny broth
LBA	Lysogeny broth agar
LC-MS/MS	liquid chromatography-tandem mass spectrometry
LPS	lipopolysaccharide
m	milli (10^{-3})
M	molar (mol/L)
MAP	2-methyl-3-amylypyrrole
MBC	4-methoxy-2,2'-bipyrrrole-5-carboxyaldehyde
MES	2-(<i>N</i> -Morpholino)ethanesulfonic acid monohydrate
MRI	magnetic resonance imaging
mRNA	messenger RNA
MUG	4'-methylumbelliferyl- β -D-glucuronide
MW	molecular weight
NCE	normalised collision energy
nm	nanometre
OD	optical density
OHHL	<i>N</i> -(3-oxohexanoyl)-homoserine lactone
ORF	open reading frame
PBS	phosphate buffered saline
PCA	principal component analysis
PCM	phase contrast microscopy
PCR	polymerase chain reaction
PCWDE	plant cell wall degrading enzyme
P _i	inorganic phosphate
ppGpp	guanosine tetraphosphate
pppGpp	guanosine pentaphosphate
PPTase	phosphopantetheinyl transferase
pQE	pQE80- <i>oriT</i>
Prodigiosin	2-methyl-3-pentyl-6-methoxyprodigiosin
QS	quorum sensing
RNA	ribonucleic acid
RNAP	RNA polymerase
RP-PCR	random primed polymerase chain reaction
rpm	revolutions per minute
RTM	random transposon mutagenesis
s	seconds
S39006	<i>Serratia</i> sp. ATCC 39006
SDS-PAGE	sodium dodecyl sulphate-polyacrylamide gel electrophoresis
Sm	streptomycin
TA	toxin-antitoxin
Tc	tetracycline

TEM	transmission electron microscopy
TEMED	<i>N,N,N',N'</i> -tetramethylethylenediamine
TMT	tandem mass tag
v/v	volume by volume
wild type	<i>Serratia</i> sp. ATCC 39006 LacA
w/v	weight by volume
X-gal	5-bromo-4-chloro-3-indoyl- β -D-galactopyranoside
μ	micro (10^{-6})
μ L	microlitres
$^{\circ}$ C	degrees Celsius

Chapter 1. Introduction

1.1 *Serratia* sp. ATCC 39006

Serratia species are Gram-negative, motile, rod shaped facultative anaerobes that belong to the Enterobacteriaceae family (Grimont & Grimont, 2006). Members of the *Serratia* genus are closely related to plant pathogens such as *Dickeya* spp. and *Pectobacterium* spp. (Retchless & Lawrence, 2010; Sproer et al., 1999). A key characteristic of some *Serratia* species is the production of a red pigment known as prodigiosin (Williamson et al., 2006). *Serratia* species are commonly found in both soil and aquatic environments and have also been isolated from insects, plants, and vertebrates (Grimont & Grimont, 2006; Yu, 1979). Some *Serratia marcescens* species are opportunistic human pathogens, capable of causing nosocomial infections through colonisation of catheters or wounds (Maltezou et al., 2012).

Serratia sp. ATCC 39006 (S39006) was originally isolated from channel water and the roots of *Salicornia alterniflora* in a salt marsh in Cheesequake, New Jersey during a screen for producers of novel antibiotics (Parker et al., 1982). Phenotypic characterisation led to S39006 originally being designated as a strain of *Serratia marcescens* however more recent analysis has shown it to be taxonomically ill-defined, atypical strain of *Serratia* (Fineran et al., 2013; Parker et al., 1982; Slater et al., 2003). Genome sequencing and bioinformatic analysis has found that S39006 has greater similarity with some *Dickeya* and *Pectobacterium* species than many *Serratia* species (Fineran et al., 2013). Recent analysis has even suggested that S39006 represents a sister lineage of *Dickeya* and should be reclassified into a new genus, *Prodigiosinella* with proposed species name for S39006 of *Prodigiosinella confusarubida* (Duprey et al., 2019). For the purposes of this dissertation the strain will continue to be referred to as *Serratia* sp. ATCC 39006 or S39006.

S39006 produces two key secondary metabolites: the tripyrrole red-pigment 2-methyl-3-pentyl-6-methoxyprodigiosin (prodigiosin), and the β -lactam antibiotic 1-carbapen-2-em-3-carboxylic acid (carbapenem) (Parker et al., 1982; Thomson et al., 1997; Williamson et al., 2006). S39006 is also capable of infecting and rotting plants through the secretion of two

plant cell wall degrading enzymes (PCWDEs), pectate lyase and cellulase, that act as virulence factors (Fineran et al., 2007). This bacterium can also infect and kill the nematode worm *Caenorhabditis elegans* (Coulthurst et al., 2004). S39006 is flagellated and capable of both swimming and swarming motility (Williamson et al., 2008). As a third means of movement, S39006 can produce gas vesicles (GVs) enabling flotation (Ramsay et al., 2011). Many of these phenotypes are under quorum sensing (QS) control through the production of *N*-acyl homoserine lactones (Thomson et al., 2000).

1.2 Quorum Sensing

Quorum sensing is a cell-to-cell communication system utilised by bacteria to detect the density of the bacterial population within the immediate environment (Waters & Bassler, 2005). These systems function through the detection of diffusible signalling molecules, called autoinducers, which then results in the synchronisation of gene expression and coordination of behaviours (Waters & Bassler, 2005). A key class of autoinducer molecules used by Gram-negative proteobacteria are *N*-acyl homoserine lactones (AHLs). QS was first described in the bioluminescent marine bacterium *Vibrio fischeri* where it is encoded by the LuxI/LuxR regulatory system (Nealson & Hastings, 1979). LuxI is QS autoinducer synthase, producing *N*-(3-oxohexanoyl)-homoserine lactone (OHHL) which is freely diffusible across the cell membrane (Engebrecht et al., 1983). As cell density increases, so too does the OHHL concentration until, at a certain threshold, OHHL binds to LuxR, a DNA binding transcriptional activator (Engebrecht et al., 1983). The LuxR-OHHL complex then activates transcription of the *lux* operon, which is responsible for bioluminescence (Engebrecht et al., 1983; Waters & Bassler, 2005).

In S39006 secondary metabolite production, exoenzyme production, and flotation are all under quorum sensing control (Ramsay et al., 2011; Thomson et al., 2000). The QS system in S39006 is homologous to the LuxIR system and is encoded by the convergently transcribed *smalR* locus (ssecondary metabolite activator) (Thomson et al., 2000). Smal synthesises two signalling molecules, the major product *N*-butanoyl-L-homoserine lactone (BHL) and the minor product *N*-hexanoyl-L-homoserine lactone (HHL) (Thomson et al., 2000). Smar is an atypical LuxR-type regulator that is active only in the absence of AHLs

when it acts to inhibit transcription of target genes (Figure 1.1A). This inhibition is lifted when BHL/HHL binds to SmaR once the AHL concentration reaches a sufficient threshold (Figure 1.1B) (Tsai & Winans, 2010). Bioassays to detect the production of BHL and HHL in S39006 have been developed with BHL found to be the most common QS molecule used in this strain (Poulter et al., 2010; Thomson et al., 2000).

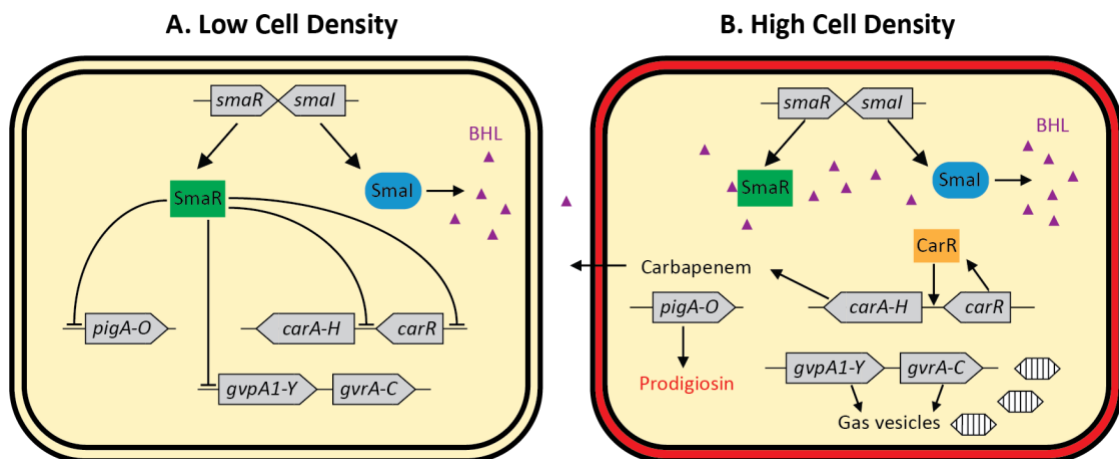


Figure 1.1 – The *smaIR* regulatory system in S39006.

The S39006 QS system is encoded by the *smaIR* operon. *SmaI* synthesises the QS signalling molecules (predominantly BHL). At low cell densities *SmaR* represses expression of prodigiosin (*pig*), carbapenem (*car*) and gas vesicle (*gvp/gvr*) operons. At high cell densities the concentration of BHL is increased causing de-repression of *SmaR* regulated genes, allowing the production of prodigiosin, carbapenem and gas vesicles to occur. Activation is shown by pointed arrowheads and repression by flat arrowheads. This figure is adapted from Slater et al. (2003).

1.3 Secondary Metabolites

S39006 produces two key secondary metabolites that exhibit antimicrobial activity. The first, 2-methyl-3-pentyl-6-methoxyprodigiosin (prodigiosin) belongs to the prodiginine family, members of which have antibacterial, antiprotozoal, antimalarial, antifungal, and antiproliferative properties (Williamson et al., 2007, 2006; Yenkejeh et al., 2017). A simple carbapenem antibiotic, 1-carbapen-2-em-3-carboxylic acid, is also produced by S39006 (Parker et al., 1982). Carbapenem antibiotics are active against a range of Gram-positive and Gram-negative bacteria and the increasing resistance to them is posing a serious public health threat (Bradley et al., 1999; Elshamy & Aboshanab, 2020). The production of both of these secondary metabolites is under quorum sensing control as well as an overlapping series of other regulators (Thomson et al., 2000).

1.3.1 Prodigiosin

The red colony appearance characteristic of some *Serratia* strains, including S39006, is caused by prodigiosin, a linear tripyrrole belonging to the prodiginine family (Figure 1.2A & B) (Williamson et al., 2006). A typical secondary metabolite, prodigiosin production only occurs during the late stages of growth (Williams et al., 1971). The exact physiological role prodigiosin plays in S39006 remains unknown however it has been suggested that the biosynthesis of prodigiosins could act to store light energy, in anion exchange, to protect from UV, or as a 'metabolic sink' to consume excess proline or NAD(P)H from primary metabolism (Borić et al., 2011; Hood et al., 1992; Ryazantseva et al., 1995; Seganish & Davis, 2005). Prodiginines have proven antimicrobial activity against a range of Gram-negative and Gram-positive bacteria including *Salmonella enterica* serovar Typhimurium, *Escherichia coli*, *Enterococcus faecalis*, *Staphylococcus aureus* and *Streptococcus pyogenes* (Lapenda et al., 2014; Lee et al., 2011). The method of action of prodigiosin is not well understood but recent studies have shown it can induce autolysins in *Bacillus subtilis* and can cause damage to the plasma membrane and subsequent leakage of intracellular components in *E. coli* (Danevčič et al., 2016a, 2016b; Suryawanshi et al., 2016).

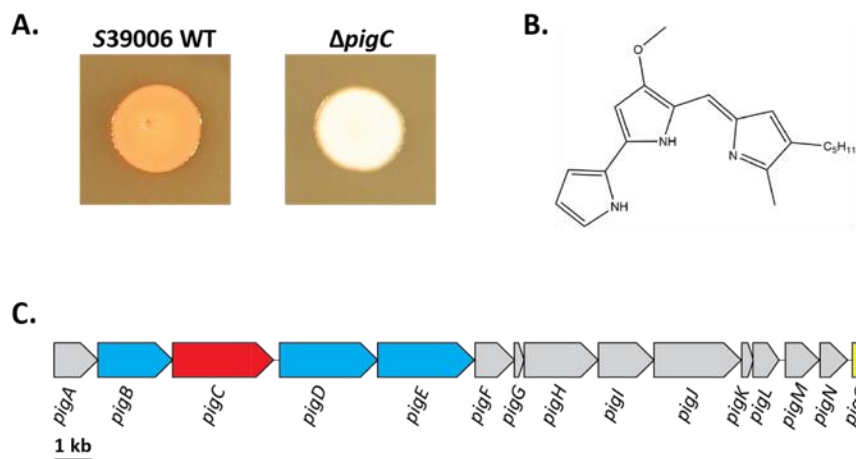


Figure 1.2 – S39006 produces the red pigmented antibiotic prodigiosin.

(A) S39006 (left) produces the red pigment prodigiosin while a $\Delta pigC$ mutant (NWA19, right) does not. (B) The chemical structure of prodigiosin. (C) The genetic cluster responsible for the biosynthesis of prodigiosin. Open reading frames (ORFs) in blue encode proteins for 2-methyl-3-n-amylyl-pyrrole (MAP) synthesis, grey ORFs encode proteins responsible for 4-methoxy-2,2'-bipyrrrole-5-carbaldehyde (MBC) synthesis. The red ORF, *pigC*, encodes the condensing enzyme and the function of *pigO* (yellow) is unknown. This figure is adapted from Williamson et al. (2006).

In S39006 prodigiosin is synthesised through the condensation of the final products of two separate pathways, 2-methyl-3-n-amylopyrrole (MAP) and 4-methoxy-2,2'-bipyrrrole-5-carbaldehyde (MBC) (Williamson et al., 2005). The prodigiosin cluster is made up of 15 genes, *pigA-O*, transcribed as a polycistronic mRNA with the promoter located upstream of *pigA*. There are additional regulatory proteins and external factors such as media composition, temperature and phosphate availability that control the production of prodigiosin (Slater et al., 2003; Williams et al., 1971; Williamson et al., 2006). The *pigB*, *pigD*, and *pigE* genes encode enzymes responsible for the production of MAP, while *pigC* encodes the condensing enzyme necessary for making prodigiosin from MAP and MBC. The other genes of the cluster, with the exception of *pigO*, encode proteins required for the production of MBC (Williamson et al., 2005).

The regulatory network governing the production of prodigiosin in S39006 is complex and overlapping with novel regulators still being discovered. Many of the regulators that control prodigiosin production also control the production of the β -lactam antibiotic, carbapenem (Figure 1.3). As previously described, QS is a key regulator of secondary metabolite production with SmaR acting to repress transcription of the prodigiosin and carbapenem clusters until a sufficient population density and BHL concentration has been reached (Fineran et al., 2005b; Thomson et al., 2000). This system controls transcription of three regulators, *pigQ*, *pigR*, and *rap*, with PigQ and Rap subsequently regulating transcription of the *pigA-O* operon to affect prodigiosin production (Figure 1.3) (Fineran et al., 2005a). Rap (regulator of antibiotic and pigment), a SlyA homologue, is a DNA binding protein containing a helix-turn-helix motif (Thomson et al., 1997). Rap induces transcription of the prodigiosin biosynthetic cluster, the carbapenem regulator CarR, and reduces swarming motility (Fineran et al., 2005b; Slater et al., 2003). PigQ is a response regulator that together with the sensor histidine kinase PigW forms the PigQW two component system (Fineran et al., 2005a). The S39006 PigQW system is a homologue of GacAS which has been shown to control the production of secondary metabolites and extracellular enzyme production in *Pseudomonas* spp. (Heeb & Haas, 2001). *pigR* is predicted to encode a class IV adenylate cyclase; the mechanism through which PigR affects prodigiosin production remains unknown.

Another key regulator of prodigiosin production is the master regulator PigP, which regulates transcription of six prodigiosin regulators (Fineran et al., 2005b). Mutation of *pigP* caused decreased transcription of *pigQ*, *pigS*, and *rap* while also causing increased transcription of *pigR*, *pigV*, and *pigX* (Fineran et al., 2005b). PigS is homologous to DNA binding proteins of the ArsR/SmtB family which coordinate bacterial resistance to heavy metals (Busenlehner et al., 2003; Fineran et al., 2005a). PigV, also known as YgfX, has been shown to form a complex with SdhE (McNeil et al., 2012). SdhE is essential for the flavinylation and activation of SdhA, a subunit of succinate dehydrogenase and part of the tricarboxylic acid cycle and electron transport chain (McNeil et al., 2012, 2013). PigX is a pleiotropic regulator that, in addition to repressing transcription of *pigA-O*, also represses exoenzyme production and *in planta* virulence (Fineran et al., 2007). PigX is predicted to be anchored in the inner membrane and contains GGDEF and EAL domains that modulate c-di-GMP levels (Fineran et al., 2007).

Environmental inputs such as phosphate availability have also been shown to regulate antibiotic production in S39006 (Slater et al., 2003). The Pst transport system is a key route for the uptake of inorganic phosphate (P_i) under P_i-limiting conditions in many bacteria (Gardner & McCleary, 2019). In *E. coli*, the *pstSCAB-phoU* operon encodes the ABC transporter PstSCAB and the chaperone PhoU which, at high P_i concentrations, inhibits the activation of PhoR, a sensory histidine kinase (Gardner & McCleary, 2019). PhoR phosphorylates the response regulator and transcription factor PhoB which then alters gene expression. The *pstSCAB-phoU* operon functions in the same manner in S39006 where PhoBR controls the production of carbapenem and prodigiosin as well as flagellar motility (Gristwood et al., 2009; Slater et al., 2003). At low phosphate concentrations, PhoBR controls the expression of *smal*, *rap*, and *pigA-O*, representing both a direct and indirect mechanism of controlling prodigiosin production and indirect control of carbapenem production via increased QS molecule production (Gristwood et al., 2009; Slater et al., 2003). Another physiological cue that controls the production of prodigiosin is the presence of gluconate which decreases prodigiosin production even in complex media (Fineran et al., 2005a). This reduction was hypothesised to be the result of deactivation of the GntR family transcriptional regulator PigT, which has a predicted binding site upstream of *pigA* (Fineran et al., 2005a).

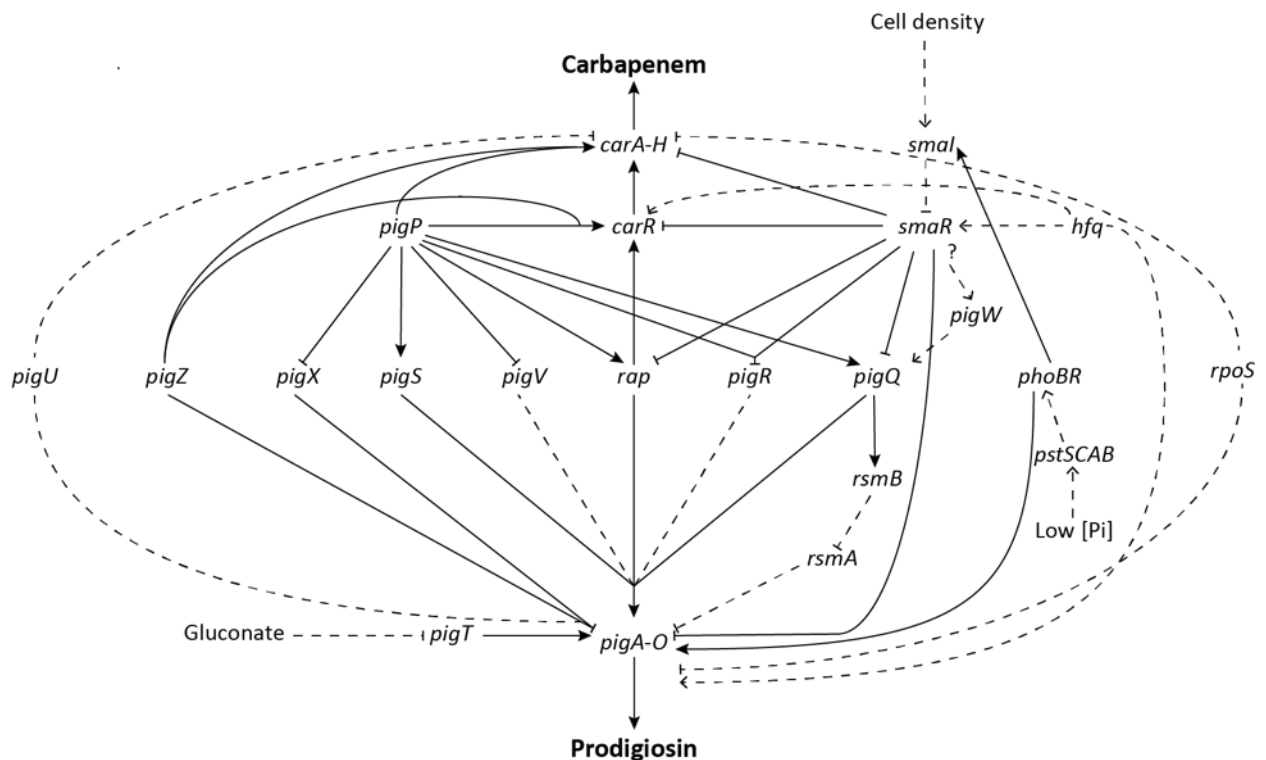


Figure 1.3 – A hierarchical model of the regulatory network controlling prodigiosin and carbapenem production in S39006.

The known environmental inputs into the regulatory network include cell density, gluconate, and phosphate. *pigP* is a master regulator that controls seven other regulators (*pigX*, *pigS*, *rap*, *pigR*, *pigQ*, and *carR*) and controls transcription of the *carA-H*, and *pigA-O* directly or indirectly. *SmaR* represses transcription of *carR*, *pigQ*, *pigR*, *rap*, *carA-H*, and *pigA-O*. Solid lines and arrowheads represent activation while flat arrowheads represent repression. Dashed lines indicate non-transcriptional regulation including environmental factors and post transcriptional effects (*rsmAB* and *hfq* regulation), or that the mode of regulation is unknown (*pigU*, *pigV*, *pigR*, and *rpoS*). This figure is adapted from Fineran et al. (2005b).

1.3.2 Carbapenem

The other key secondary metabolite produced by S39006 is the β -lactam antibiotic carbapenem (Figure 1.4A). Antibiotics of the carbapenem class are important clinically due to their effectiveness against a wide range of bacteria (El-Gamal et al., 2017). The structure of carbapenems is similar to penicillins with an unsaturated five-membered ring fused with a β -lactam ring (Figure 1.4B) (El-Gamal et al., 2017). Carbapenems also have a C2-C3 double bond and a carbon at C1 (instead of a sulphur as in penicillins) (El-Gamal et al., 2017). There are several clinically available carbapenems with varying side chains including imipenem and meropenem. The carbapenem antibiotic produced by S39006, 1-carbapen-2-em-3-carboxylic acid, has a much simpler structure than clinical carbapenems (Figure 1.4B). Carbapenem antibiotics prevent bacterial growth by inhibiting the synthesis of the key cell

wall component, peptidoglycan (Codjoe & Donkor, 2017). The antibiotics bind penicillin binding proteins inhibiting transpeptidase activity and preventing the formation of cross-links that strengthen the cell wall (Codjoe & Donkor, 2017).

The genes required for S39006 to produce the carbapenem antibiotic are located in the *car* cluster (Figure 1.4C) (Thomson et al., 2000). The genes *carA-E* encode biosynthetic enzymes, *carF* and *carG* encode components involved in the intrinsic resistance mechanism, and *carH* encodes a protein of unknown function, the mutation of which does not alter carbapenem synthesis (Thomson et al., 2000). The intrinsic resistance mechanism of CarF and CarG is unknown however the proteins are predicted to be located in the periplasm and both are required for resistance (McGowan et al., 1996; Tichy et al., 2017, 2014). The carbapenem cluster is under the control of two LuxR-family transcriptional regulators. CarR binds to the *carA* promoter in an AHL-independent manner to activate transcription (Poulter et al., 2011). SmaR binds to the promoters of *carR* and *carA*, repressing transcription until the cell density reaches a level where the concentration of AHLs (produced by SmaI) is sufficient to relieve the repression of SmaR, enabling transcription of CarR and subsequent production of the carbapenem antibiotic (Fineran et al., 2005b; Slater et al., 2003; Thomson et al., 2000).

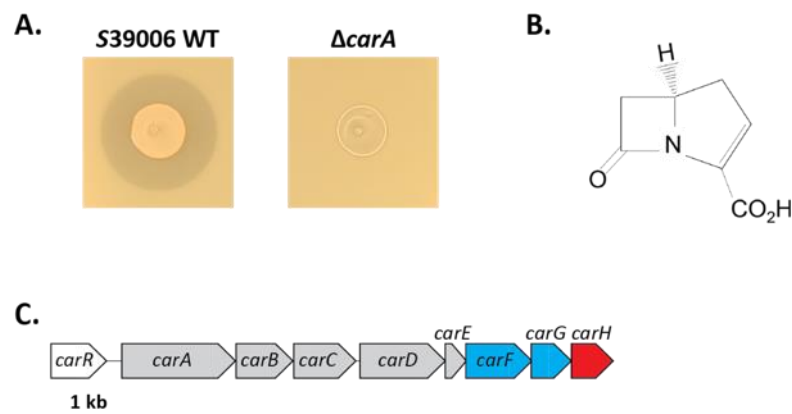


Figure 1.4 – S39006 produces the β -lactam antibiotic carbapenem.

(A) A halo of inhibition surrounding S39006 wild type (left) on a lawn of *E. coli* ESS (a β -lactam supersensitive mutant) caused by the carbapenem antibiotic, no zone of clearance was observed around a *carA* mutant that did not produce carbapenem. (B) The chemical structure of the carbapenem antibiotic produced by S39006. (C) The genetic cluster responsible for the biosynthesis of carbapenem. Biosynthetic enzymes are encoded by *carA-E*, shown in grey. *carF-G* (blue) encode proteins involved in the intrinsic β -lactam resistance mechanism. The function of the *carH* (red) gene product is unknown. The carbapenem operon is controlled by CarR (white) in the absence of QS signalling molecules. This diagram is adapted from Coulthurst et al. (2005).

Many regulators are involved in the production of carbapenem in *S39006* and there is often overlap with regulators that control prodigiosin production (Figure 1.3). Previously described regulators of prodigiosin production that also control carbapenem production include Rap, PigP, and the SmaR system. The highly pleiotropic RNA binding protein Hfq positively controls the production of both prodigiosin and carbapenem through regulation of CarR and SmaR (Wilf et al., 2011). This regulation is thought to occur via Hfq-dependent small RNAs (sRNA) that activate translation of *smaR* and *carR* mRNA and protect these transcripts from degradation (Wilf et al., 2011). Another post-transcriptional method of regulation utilised by *S39006* is the Rsm (regulator of secondary metabolism) system, which is homologous to the Csr (carbon storage regulator) system characterised in *E. coli* (Williamson et al., 2008). RsmA acts as a negative regulator of antibiotic production with prodigiosin and carbapenem production increased in an *rsmA* mutant (Wilf et al., 2013; Williamson et al., 2008). RsmA is a RNA binding protein that itself is regulated by the sRNA RsmB which can sequester multiple copies of RsmA (Babitzke & Romeo, 2007; Williamson et al., 2008). Another negative regulator of prodigiosin and carbapenem production is the stationary phase sigma factor RpoS, the deletion of which causes increased antibiotic production in *S39006* (Wilf & Salmond, 2012).

1.4 Plant Cell Wall Degrading Enzymes

PCWDEs are a virulence factor utilised by plant pathogens to facilitate the entry and colonisation of plant hosts (Walton, 1994). *S39006* secretes two key PCWDEs, pectate lyase and cellulase, which cause tissue maceration in potato tubers (Fineran et al., 2007). Pectins are a key component of plant cell walls and are often found in the intercellular layer between the primary cell wall of adjoining cells (Thakur et al., 1997). Pectins are predominantly a polymer of D-galacturonic acid and rhamnogalacturonan but other sugars such as arabinose, galactose, and xylose can be found in the side chains (Thakur et al., 1997). Pectinases are a group of enzymes that degrade pectin through a variety of reactions with pectate lyases catalysing the cleavage of de-esterified pectin (Marin-Rodriguez et al., 2002). Cellulose is the main component of the plant cell wall and is comprised of polymers of glucose connected by β -1, 4-glycosidic bonds (Sadhu & Maiti, 2013). Cellulases are

enzymes that break down cellulose by hydrolysing these β -1, 4-glycosidic bonds (Tomme et al., 1995).

The production of PCWDEs in *S39006* is modulated by QS in an AHL dependent manner (Slater et al., 2003). The previously described regulators PigP, PigQ, and PigW have also been shown to positively regulate exoenzyme production (Fineran et al., 2005b). PigX was found to negatively regulate pectate lyase production, further highlighting the pleiotropic role of many regulators in *S39006* (Fineran et al., 2007). Higher cellulase and pectate lyase activity was observed in an *rsmA* mutant indicating that RsmA usually plays a role in repressing the production of these enzymes while an *hfq* mutant showed attenuated virulence in potato rotting assays (Wilf et al., 2013, 2011).

1.5 Flagellar Motility

Bacteria exist in varied and swiftly changing environments and as such employ many methods (including swimming, swarming, twitching, floating, and gliding) to move towards more favourable conditions (Jarrell & McBride, 2008). The range of environmental signals sensed by bacteria include oxygen levels, pH, osmolarity, light intensity, and the concentrations of nutrients and toxins (Wadhams & Armitage, 2004). *S39006* is capable of movement via swimming, swarming, and floating (Figure 1.5). Swimming and swarming are two methods of active motility requiring flagella (Jarrell & McBride, 2008; Kearns, 2010). Bacteria swim by rotating their flagella allowing for movement of individual cells through liquid or low percentage agar in the laboratory (Berg & Anderson, 1973). Swarming is the collective movement of a group of bacteria across a semi-solid surface (Eberl et al., 1999; Fraser & Hughes, 1999). As with swimming motility, swarming requires flagella however it also requires the secretion of a surfactant to reduce surface tension (Lindum et al., 1998). The collective movement is caused by a group of hyper flagellated, elongated bacteria which suppress cell division (Alberti & Harshey, 1990; Hoeniger, 1965). Both swimming and swarming motility have been associated with increased virulence, enabling bacterial cells to reach their host and facilitating colonisation of surfaces before biofilm formation (Fraser & Hughes, 1999; Guttenplan & Kearns, 2013).

The mechanism of regulation of swimming motility, swarming motility, and surfactant production in S39006 has been the subject of some study. The SmaIR quorum sensing system is a key regulator with SmaR repressing surfactant production and swarming motility, which is then de-repressed in at high AHL concentrations (Williamson et al., 2008). The previously described regulators RpoS, RsmA, and PigX are negative regulators of swarming and swimming motility, in addition to regulating the production of antibiotics and PCWDEs (Fineran et al., 2007; Wilf & Salmond, 2012; Williamson et al., 2008). Expression of *rhIA* and *flhC* was increased in *pigX* and *rsmA* mutants compared to wild type S39006 but not altered in *rap* mutants, which also showed a hyper motile phenotype (Williamson et al., 2008). The *rhIA* gene is required for surfactant production in S39006 and encodes a protein homologous to RhIA from *Pseudomonas aeruginosa* PAO1 (Williamson et al., 2008). RhIA is required for the synthesis of rhamnolipid precursors in PAO1 and a similar role has been presumed in S39006 (Williamson et al., 2008). Hfq is a positive regulator of swimming and swarming motility, with an *hfq* mutant showing a reduction in swimming motility and an inability to swarm (Wilf et al., 2011). The pleiotropic regulator YgfX also controls flagellar motility and is repressed by RsmA inhibition of the flagellar master regulator FlhDC (Hampton et al., 2016).

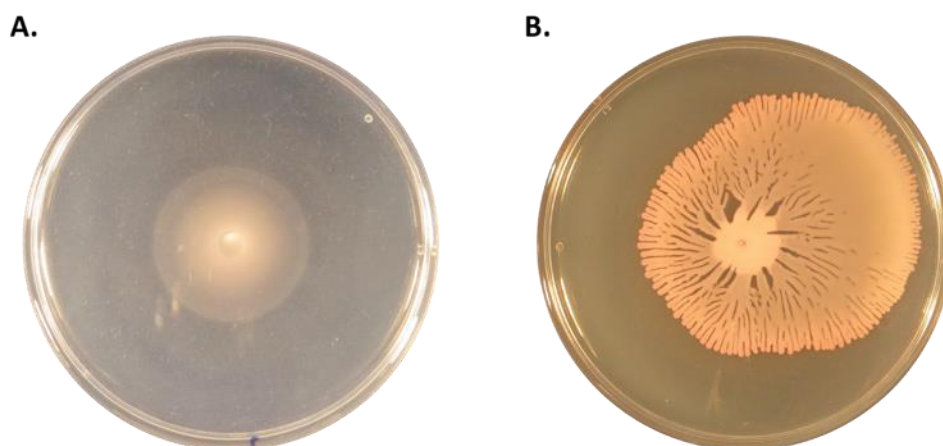


Figure 1.5 – Swimming and swarming motility in S39006.

(A) Swimming motility shown by S39006 moving through semi-solid agar. (B) Swarming motility shown by S39006 moving across the surface of an Eiken agar plate.

1.6 Gas vesicles

Some bacteria and archaea are capable of producing gas vesicles (GVs) to increase cell buoyancy and facilitate movement through the water column (Figure 1.6) (Jarrell & McBride, 2008). *S39006* utilises this method and thus far is the only member of the Enterobacteriaceae family shown to naturally produce GV's (Ramsay et al., 2011). Gas vesicles are intracellular proteinaceous organelles that are permeable to surrounding gases but impervious to water (Walsby, 1969). GV's enable flotation by reducing the overall cell density and have been used by bacteria to move to more oxygen-rich environments (Walsby, 1972, 1994). Some cyanobacteria use gas vesicles to move upwards in the water column in response to a reduction in light intensity allowing for the capture of more sunlight for photosynthesis (Pfeifer, 2012; Walsby, 1994). Gas vesicles are found in a range of organisms including the haloarchaeon *Halobacterium salinarum*, cyanobacteria such as *Microcystis aeruginosa*, and heterotrophic bacteria including *Psychromonas ingrahamii*, among others (Pfeifer, 2012).

Gas vesicles are formed when gas vesicle proteins initially aggregate into a small bicone which then expands into a spindle or cylindrical shaped hollow structure that allows gases such as oxygen, methane, nitrogen and carbon dioxide to diffuse in from the cytoplasm (Figure 1.6A) (Pfeifer, 2012; Walsby, 1972). The gas vesicles are at equilibrium with gases in the cytoplasm and will irreversibly collapse under increased pressure (Walsby & Bleything, 1988). The critical collapse pressure of GV's can be measured using pressure nephelometry and varies depending on the organism producing the GV's, the shape of the GV's, and the GV protein components (Tashiro et al., 2016; Walsby, 1994). GV size and shape is species dependent however mature gas vesicles tend to be 0.045 – 0.2 μm wide and 0.1 – 2 μm long (Pfeifer, 2012). GV's refract light making colonies that produce them appear opaque (Figure 1.6C). This feature can be utilised to help visualise GV's as they cluster together to form a gas 'vacuole', which appears as a phase bright structure when cells are viewed using phase contrast microscopy (PCM, Figure 1.6C) (Oren, 2013; Walsby, 1994). Individual GV's can also be visualised inside cells using transmission electron microscopy (TEM, Figure 1.6B)

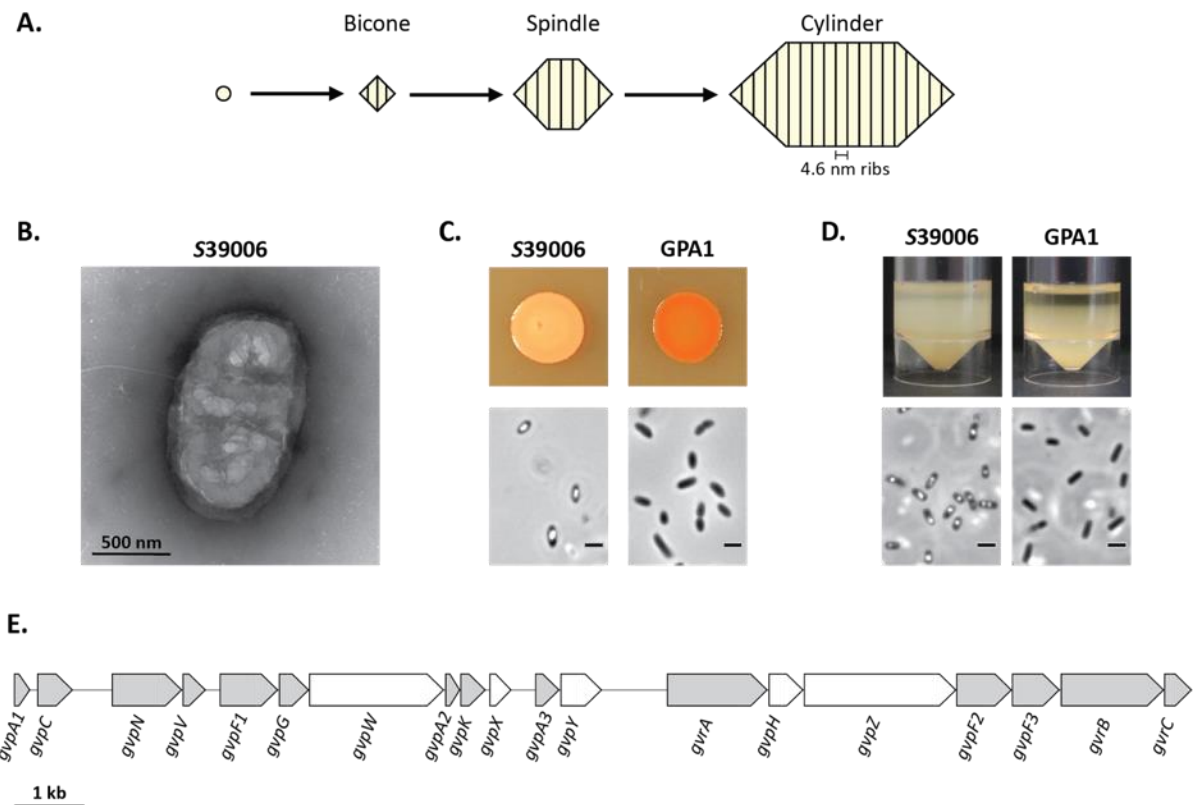


Figure 1.6 – S39006 makes gas vesicles for flotation.

(A) Morphogenesis of gas vesicles, starting from aggregated proteins that form a bicone then a spindle/cylinder-shaped gas vesicle. This figure is adapted from Pfeifer (2012). (B) GVs of S39006 can be observed under TEM, the scale bar represents 500 nm. (C) Patch morphology and PCM images of S39006 and GV deficient mutant GPA1, the scale bar on the PCM image represents 1 µm. (D) Flotation assays for wild type S39006 and GPA1 with accompanying PCM images below, the scale bar represents 1 µm. (E) The S39006 GV gene cluster is comprised of 19 genes in two operons. Genes essential for GV production are shown in grey, genes that are not essential are shown in white.

The genes required for the formation of gas vesicles varies widely across species, however at least one homologue of *gvpA* is necessary for GV formation (Figure 1.7). *gvpA* encodes the primary gas vesicle structural protein, GvpA, a small, hydrophobic protein that forms a single layer gas vesicle wall with a thickness of 2 nm (Walsby, 1994). GvpA is arranged in a tandem repeat to form 4.6 nm ‘ribs’ that run perpendicular to the long axis of the vesicle (Walsby, 1994; Walsby & Hayes, 1989). A secondary gas vesicle structural protein, GvpC, is commonly found and attaches to the exterior surface of the gas vesicle acting to strengthen and stabilize the structure (Englert & Pfeifer, 1993; Hayes et al., 1992). It remains unclear exactly which other proteins encoded by GV clusters are found in mature GVs however there is evidence to suggest that GvpF is found in GVs of *Microcystis aeruginosa* and *Halobacterium salinarum* NRC-1 (Shukla & DasSarma, 2004; Xu et al., 2014). GvpB has also been detected in GVs of *H. salinarum* NRC-1 using western blotting (DasSarma & Arora,

1997). A mass spectrometry study of *H. salinarum* NRC-1 was able to detect GV proteins found in low abundance and suggested that GvpJ, GvpI, GvpN, GvpO and GvpH may also be minor GV structural proteins although their exact function remains unknown (Chu et al., 2011). Determining the exact protein composition of GVs is problematic due to technical challenges isolating the GVs, their resistance to protease digestion, and their hydrophobic nature making it difficult to solubilise the vesicle membrane (Belenky et al., 2004; Chu et al., 2011; Krantz & Ballou, 1973).

GV gene clusters are conserved across haloarchaea but vary more between bacteria (Pfeifer, 2012). Generally, 8 – 14 genes are necessary to produce GVs in different microorganisms, some GV clusters such as those from *H. salinarum*, have been extensively studied (DasSarma et al., 1994; Jones et al., 1991). *H. salinarum* strains PHH1 and NRC-1 both contain two distinct gas vesicle gene clusters each containing 14 genes, expression of each cluster is dependent on the growth phase and salinity and can alter the GV shape (Englert et al., 1992; Ng et al., 2000; Pfeifer, 2012). The GV clusters of bacteria are comprised of homologues of archaeal GV genes with additional genes of unknown function (Figure 1.7) (Pfeifer, 2012). GV-producing cyanobacteria often contain multiple copies of *gvpA*, for instance *Microcystis aeruginosa* contains three copies and *Planktothrix rubescens* contains up to seven copies of *gvpA* (Beard et al., 2000, 2002; Hayes & Powell, 1995). Recently GVs were reported in *Streptomyces* sp. CB03234-S, the first example of functional expression of a GV gene cluster in streptomycetes, which had previously only been shown to carry a GV gene cluster (Bentley et al., 2002; Huang et al., 2019).

GVs have long been proposed as a biotechnological tool. Understanding the regulation and morphogenesis of GVs will help this work and may provide a mechanism to control toxic cyanobacterial blooms in the environment (Paerl & Huisman, 2008). GvpC from *H. salinarum* NRC-1 has been engineered to display antigens from *Chlamydia trachomatis*, *Salmonella enterica*, *Plasmodium falciparum*, and simian immunodeficiency virus to create gas vesicle based vaccine nanoparticles that can elicit an immune response (Childs & Webley, 2012; DasSarma et al., 2015; Dutta et al., 2015; Stuart et al., 2004). GVs from *H. salinarum* and *Anabaena flos-aquae* are currently being investigated for use in magnetic resonance imaging (MRI) (Bourdeau et al., 2018; Farhadi et al., 2019; Shapiro et al., 2014).

γ -Proteobacteria

Serratia sp.
ATCC39006



Psychromonas
ingrahamii 37



Legionella
drancourtii LLAP12



δ -Proteobacteria

Desulfomonile tiedjei
DCB-1



β -Proteobacteria

Burkholderia
thailandensis MSMB43



α -Proteobacteria

Bradyrhizobium
oligotrophicum S58



Rhodobacter
capsulatus SB1003



Cyanobacteria

Anabaena flos-aquae
CCAP 1403/13F



1 kb

Firmicutes

Bacillus megaterium
DSM319



Actinobacteria

Rhodococcus
jostii RHA1



Streptomyces
coelicolor A3(2)



Archaea

Halobacterium
salinarum PHH1



Figure 1.7 – The GV gene clusters of S39006 and related strains.

Each ORF is represented by an arrow block, blocks of the same colour indicate ORFs with similar predicted functions. The scale bar represents 1 kb. This figure is taken from Tashiro et al. (2016).

The gas vesicle cluster of S39006 is 16.6 kb long and comprised of 19 open reading frames in two contiguous operons (Figure 1.6E) (Ramsay et al., 2011). The gene products from 13 out of 19 genes in the GV locus were most similar to proteins encoded by the psychrophilic Alaskan sea-ice isolate *Psychromonas ingrahamii* (Ramsay et al., 2011). There are three genes encoding homologues of GvpA (*gvpA1*, *gvpA2* and, *gvpA3*) and a homologue of GvpC (*gvpC*) present in this cluster (Ramsay et al., 2011). The GV gene cluster also encodes homologues of known GV proteins GvpF/L, GvpG, GvpH, GvpK, and GvpN and five putative GV genes of unknown function (GvpV, GvpW, GvpX, GvpY, and GvpZ) (Ramsay et al., 2011; Tashiro et al., 2016). Three GV regulatory proteins are encoded within the cluster: *gvrA*, *gvrB*, and *gvrC*; these genes are required for expression of GVs (Ramsay et al., 2011; Tashiro et al., 2016). Gene deletion studies in S39006 demonstrated that 11 out of the 19 genes in the GV cluster were essential for GV formation (Tashiro et al., 2016). Individual gene knockouts of *gvpA1*, *gvpF1*, *gvpG*, *gvpA2*, *gvpK*, *gvpA3*, *gvpF2*, *gvpF3*, *gvrA*, and *gvrB* showed that no GVs could be observed by PCM or TEM. When *gvrC* was disrupted no GVs were detected in planktonic cells but a small number could be observed in cells grown on an agar plate (Tashiro et al., 2016). Additionally, *gvpN* and *gvpV* mutants could not produce mature GVs and lost the ability to float (Tashiro et al., 2016).

The GVs of a *gvpC* mutant were analysed and found to have the same size and shape but a much lower critical collapse pressure than wild type GVs indicating that GvpC plays a strengthening role in S39006 GVs as it does in other systems (Hayes et al., 1992; Tashiro et al., 2016; Walsby & Hayes, 1988). GV production in S39006 was further analysed by overexpressing each gene *in trans* on a plasmid. Overexpression of *gvpA3*, *gvpF1*, *gvpF2*, *gvrA*, *gvrB*, and *gvrC* significantly reduced the amount of GVs produced (Monson et al., 2016). Cells that were overexpressing GvpG were slow growing but did contain GVs while cells that were overproducing GvpV contained small bicone vesicles (Monson et al., 2016). Additionally, overproduction of GvpC did not have any effect on GV production and did not increase the strength of the GVs in a collapse pressure assay (Monson et al., 2016). The S39006 GV cluster has also been expressed in a heterologous host with *E. coli* W3110 able to produce GVs that were indistinguishable from wild type S39006 GVs when expressing genes from the cosmid pGAS (Ramsay et al., 2011; Tashiro et al., 2016).

1.6.1 Regulation of gas vesicles in S39006

Since the GV cluster of S39006 was first described 10 years ago a significant amount of study has been performed to determine the regulatory elements that control GV production in this strain. The three regulatory genes of the GV cluster (*gvrA*, *gvrB*, and *gvrC*) are essential for GV formation but overexpression of these regulators causes reduced transcription of *gvpA1* and reduced GV synthesis (Monson et al., 2016; Tashiro et al., 2016). Other factors have been linked to GV regulation and buoyancy in S39006 including quorum sensing, the Rsm system, oxygen availability, and other pleiotropic regulators (Lee et al., 2017; Quintero-Yanes et al., 2020; Ramsay et al., 2011; Tashiro et al., 2016). GvrA belongs to the NtrC family of σ^{54} -dependent transcriptional regulators (Ramsay et al., 2011). There is a predicted σ^{54} binding site located upstream of *gvpA1*, consistent with previous reports that GvrA controls transcription of *gvpA1* (Ramsay et al., 2011; Tashiro et al., 2016). GvrB is a NtrB family protein that is predicted to be located in the cytoplasm and contains a PAS sensor domain and a histidine kinase domain (Monson et al., 2016; Ramsay et al., 2011). GvrC is a CheY-like response regulator protein (Ramsay et al., 2011). Using transcriptional fusions, it has been shown that GvrA, GvrB, and GvrC are all required independently for full expression of the *gvpA1* operon and GV production in S39006 (Tashiro et al., 2016). These cognate GV regulators also show some evidence of pleiotropy with prodigiosin production increased when GvrA and GvrB were overproduced in S39006 (Monson et al., 2016).

As with the production of antibiotics and PCWDEs, GV production is under quorum sensing control in S39006. A *smal* mutant of S39006, which cannot make the QS signalling molecule BHL, was unable to synthesise GVs but could produce them if BHL was supplied exogenously (Ramsay et al., 2011). To test the effect of SmAR on transcription of the two operons of the GV cluster, the promoters upstream of *gvpA1* and *gvrA* were cloned upstream of a β -galactosidase reporter fusion. The expression of the two promoters was then determined in *E. coli* carrying either the *gvpA1* or *gvrA* promoter in the presence of a plasmid expressing SmAR or an empty vector control (Tashiro et al., 2016). SmAR reduced expression from the *gvpA1* promoter by 75 %; this repression could be relieved by the addition of BHL (Tashiro et al., 2016). There was no change in *gvrA* expression when SmAR was present indicating that QS-dependent regulation of flotation in S39006 occurs through direct transcriptional repression of *gvpA1* not *gvrA* (Tashiro et al., 2016). In a *smal/smaR* double mutant that

cannot make or respond to BHL, there was no difference in GV production compared to wild type S39006. There was no precocious or increased production of GVs in a *smaR* mutant indicating that other regulatory factors must be required for GV production (Ramsay et al., 2011). Having GV production under QS control may act to increase the fitness of S39006 by providing an early warning system for oxygen and nutrient deprivation as well as allowing a population with higher cell density to achieve a high floating velocity according to Stoke's law (Ramsay et al., 2011; Walsby, 1994)

RsmA, a CsrA homologue, has also been reported to regulate GV production with expression of *gvpA1* and *gvrA* reduced in a *rsmA* mutant, indicating RsmA is a positive regulator of GV production (Ramsay et al., 2011). RsmA negatively regulates flagella-based motility and surfactant production through repression of *rhIA* and *flhC* respectively, indicating that flotation and flagellar motility are oppositely regulated (Ramsay et al., 2011; Williamson et al., 2008). RsmB, an RsmA antagonist and CsrB homologue, is a negative regulator of GVs with *gvpA1* and *gvrA* genes more highly expressed in a *rsmB* mutant (Ramsay et al., 2011). Mutation of another RsmA antagonist, *pigQ*, also increased transcription of *gvpA1* and *gvrA*. Disruption of *pigX*, which encodes a CsrD homologue, moderately reduced expression of both *gvpA1* and *gvrA* (Ramsay et al., 2011). In *E. coli* CsrD is responsible for the RNase-E mediated decay of CsrB, increasing the amount of CsrA available (Suzuki et al., 2006).

A recently discovered gene involved in the regulation of gas vesicle production in S39006 is *rbsR*, which encodes a LacI family transcriptional regulator of the putative ribose operon (Lee et al., 2017). An *rbsR* mutant was identified following a random transposon mutagenesis screen searching for gas vesicle negative mutants (Lee et al., 2017). In addition to gas vesicles, RbsR also regulates the production of carbapenem, prodigiosin, and PCWDEs with all of these reduced in an *rbsR* mutant compared to wild type, while swimming and swarming motility was increased (Lee et al., 2017). Mutants defective in *rbsR* were highly pleiotropic and it was suspected that other, as yet unknown, regulators of gas vesicle production would be similarly pleiotropic.

Another screen for gas vesicle mutants identified a new global regulator in S39006, FloR, a DeoR family transcription factor (Quintero-Yanes et al., 2020). Compared to wild type, a

floR mutant had diminished transcription of the *gvpA1* and *gvrA* operons leading to a reduction in GV production and buoyancy (Quintero-Yanes et al., 2020). This mutant also had increased flagellar motility compared to wild type, consistent with previous observations that flotation and flagellar motility are oppositely regulated. FloR is also a regulator of antibiotic production and virulence in a *C. elegans* model. Proteomic analysis determined that FloR regulates PigU and RpoS to control gas vesicle production (Quintero-Yanes et al., 2020). Increased levels of RsmA were also observed in the *floR* mutant indicating that FloR may control cell buoyancy via RsmA-GvrABC and motility via RsmA-FlhDC (Quintero-Yanes et al., 2020).

Expression of the *gvpA1* operon was upregulated in flask-grown cultures entering stationary phase or when mineral oil was overlaid on top of cultures to create microaerophilic conditions (Ramsay et al., 2011). Even higher expression of the *gvpA1* operon was observed in cultures grown in smaller sealed tubes and static cultures indicating that gas vesicle synthesis was stimulated by reduced oxygen concentrations (Ramsay et al., 2011). Changes in oxygen concentration had no effect on *gvrA* expression and the oxygen-dependent increase in *gvpA1* expression was abolished if the *gvrA* operon was disrupted. This indicates that the proteins encoded by the *gvrA* operon transduced the *gvpA1* expression response to reduced aeration (Ramsay et al., 2011). It has been suggested that S39006 makes GVs to facilitate colonisation of the air-liquid interface and may be used to decrease fitness of competing aerobes that cannot rise through the water column through competitive oxygen consumption (Ramsay et al., 2011).

Another physiological input that affects the production of GVs in S39006 is the environmental potassium concentration (Quintero-Yanes et al., 2019). A GV hyper-producing mutant was identified with a transposon insertion in *trkH*, a gene encoding a low-affinity potassium transporter. This mutation was pleiotropic with cells showing reduced flagellar motility and higher prodigiosin production (Quintero-Yanes et al., 2019). Further studies found that transcription of the *gvpA1* operon was increased at low potassium concentrations and flotation was reduced at high potassium concentrations in wild type S39006 (Quintero-Yanes et al., 2019). S39006 utilises gas vesicles to respond not

just to oxygen concentration but other nutritional cues and this suggests that there may be more environmental inputs into GV regulation that are yet to be determined.

1.7 Aims of this Study

The coordinated regulation of GV and secondary metabolite production in *S39006* has been a subject of a great deal of scrutiny with novel regulators being identified and characterised that are highly pleiotropic in nature (Lee et al., 2017; Quintero-Yanes et al., 2020, 2019). However, due to the complexity of the regulatory network of *S39006*, it is likely that novel regulatory inputs remain undiscovered. *S39006* is a very genetically tractable organism with many well-described methods existing to identify novel regulatory elements. *S39006* (and recombinant *E. coli* strains expressing GVs) may have future biotechnological utility especially as the potential use of GVs as antigen display systems and MRI contrast agents are being investigated in greater detail. This study aims to (i) identify novel regulators of GV and secondary metabolite production in *S39006*, (ii) determine the pleiotropic nature of these novel regulators, and (iii) investigate the mechanism through which these regulators alter the production of GVs and secondary metabolites.

This study describes the use of a random transposon mutagenesis screen to identify eight genes not previously linked to the production of GVs, and the effect of transposon insertions in these genes on different phenotypes (Chapter 3). Three genes were chosen for more detailed study, described in Chapters 4 – 6. Two mutants were then subjected to a comprehensive proteomic analysis that revealed the true extent of the pleiotropic impacts of disruption of the two genes of interest (Chapter 5 & 6).

Chapter 2. Materials and Methods

2.1 Media, Solutions, Antibiotics, and Supplements

All media and solutions used in this study are described in Table 2.1. Antibiotics and supplements used are shown in Table 2.2. Media and solutions were sterilized by autoclaving at 121 °C for 15 minutes, components that required autoclaving separately before addition are indicated in Table 2.1. Antibiotics and supplements were filter sterilized with a 0.2 µm syringe filter before use.

2.2 Bacterial Strains, Bacteriophage, Plasmids, and Culture Conditions

Bacterial strains, bacteriophage, and plasmids used in this study are described in Table 2.3 and Table 2.4. *Serratia*, *Pectobacterium*, and *Pseudomonas* strains were grown at 30 °C and *E. coli* strains were grown at 37 °C in Lysogeny Broth (LB) unless otherwise indicated. Liquid cultures, also called overnight cultures, were grown in 5 mL of LB inoculated with a single bacterial colony in a 30 mL plastic universal tube and aerated on a rotary wheel overnight (14 – 16 hours). Bacterial strains were maintained by mixing 1 mL of liquid culture with 500 µL 50% glycerol and then stored at -80 °C. Strains were streaked out to single colonies on LB agar supplemented with the relevant antibiotics from freezer stocks before use. Bacterial growth was determined by measuring optical density (OD₆₀₀) using a Unicam Heλios spectrophotometer at 600 nm wavelength.

Data for growth curves were produced from cultures in 250 mL flasks containing 25 mL LB inoculated with the indicated strain to an initial OD₆₀₀ of 0.05. Flasks were incubated at 30 °C in a water bath with shaking at 215 rpm. For growth curves in microaerophilic conditions, 25 mL of mineral oil was overlaid on top of 25 mL LB and the shaking was reduced to 80 rpm. For each strain, three independent replicates were performed. Samples were taken every 2 hours throughout the growth curve to check OD₆₀₀ until strains reached stationary phase. Additional samples were also taken at the same time for use in β-glucuronidase assays, and to quantify prodigiosin, carbapenem and BHL production where necessary.

Table 2.1 – Media and solutions used in this study.

Solution	Components (per L)¹
Media	
Lysogeny Broth (LB)	10 g Bacto Tryptone 5 g Bacto Yeast Extract 5 g NaCl
Lysogeny Broth Agar (LBA)	20 g LB 15 g Bacto Agar
CMC-Sucrose Agar	0.5 g MgSO ₄ .7H ₂ O 0.5 g KH ₂ PO ₄ 2 g K ₂ HPO ₄ 2.5 g L-asparagine 10 g Sucrose 16 g Bacto Agar (500 mL 1 % (w/v) carboxymethyl cellulose (CMC))
Pel Agar	16 g Bacto Agar (5 mL 20 % (w/v) Bacto Yeast Extract) (10 mL 10 % (w/v) (NH ₄) ₂ SO ₄) (1 mL 1 M MgSO ₄) (10 mL 50 % (w/v) glycerol) (250 mL 2 % (w/v) polygalacturonic acid) (200 mL Pel phosphate buffer)
Pel Phosphate Buffer	15 g Na ₂ HPO ₄ 0.7 g NaH ₂ PO ₄ .H ₂ O [pH 8.0]
Tryptone Swarm Agar (Swimming Agar)	10 g Bacto Tryptone 5 g NaCl 3 g Bacto Agar
Eiken Agar (Swarming Agar)	10 g Bacto Tryptone 5 g NaCl 5 g Bacto Yeast Extract 7.5 g Eiken Agar
0.7 % Top Agar	20 g LB 7 g Bacto Agar
0.35% Top Agar	20 g LB 3.5 g Bacto Agar

Solution	Components (per L)¹
Minimal Medium	(20 mL 50 X Phosphate) (10 mL 10 % (w/v) (NH ₄) ₂ SO ₄) (0.41 mL 1 M MgSO ₄) (10 mL 20 % carbon source)
Minimal Agar	1 L Minimal Medium 15 g Bacto Agar
50 X Phosphate	350 g K ₂ HPO ₄ 100 g KH ₂ PO ₄ [pH 6.9 – 7.1]
NGM Agar	3 g NaCl 2.5 g Peptone 20 g Agar (1 mL 1 M MgSO ₄) (25 mL 1 M Phosphate Buffer [pH 6.0]) (1 mL 1 M CaCl ₂) (1 mL 5 mg/mL Cholesterol (in ethanol))
1 M Phosphate Buffer	54.1 g KH ₂ PO ₄ 17.8 g K ₂ HPO ₄ [pH 6.0]
M9 Media	3 g KH ₂ PO ₄ 6 g Na ₂ HPO ₄ 5 g NaCl (1 mL 1 M MgSO ₄)
Phosphate Buffered Saline (PBS)	1 PBS tablet dissolved in 100 mL dH ₂ O to provide: 8 g/L NaCl 0.2 g/L KCl 1.15 g/L Na ₂ HPO ₄ 0.2 g/L KH ₂ PO ₄ [pH 7.3]
<u>Solutions</u>	
<u>Agarose gel electrophoresis</u>	
Agarose gel	1 % Agarose in 1 X TAE buffer 500 ng/mL Ethidium Bromide
50 X TAE Buffer	242.2 g Tris base 57.1 mL Glacial acetic acid 18.612 g Ethylenediaminetetraacetic acid disodium salt (EDTA)

Solution	Components (per L)¹
<u><i>C. elegans</i> virulence assay</u>	
40% Bleaching Solution (for 10 mL)	2.5 mL 4 M NaOH 3.5 mL H ₂ O 4 mL thin bleach (5 % sodium hypochlorite)
<u>Transformation</u>	
Solution A	9.9 mL 1 M MnCl ₂ 49.5 mL 1 M CaCl ₂ 198 mL 50 mM MES
Solution A + glycerol	Solution A 15 % Glycerol
<u>SDS-PAGE</u>	
Resolving gel (15%) (per 10 mL)	5 ml 30% Acrylamide 5 ml 0.75 M Tris-HCl [pH 8.3] 50 µl 20% Sodium dodecyl sulphate (SDS) 100 µl 8% Ammonium persulfate (APS) 5 µl <i>N,N,N',N'</i> -tetramethylethylenediamine (TEMED)
Resolving gel (18%) (per 10 mL)	6 ml 30% Acrylamide 2.5 ml 1.5 M Tris-HCl [pH 8.3] 1.5 ml H ₂ O 50 µl 20% SDS 100 µl 8% APS 5 µl TEMED
Stacking gel (6%) (per 10 mL)	2 ml 30% Acrylamide 1 ml 1.25 M Tris-HCl [pH 6.8] 7 mL H ₂ O 50 µl 20% SDS 100 µl 8% APS 5 µl TEMED
10 X Electrode buffer	150 g Glycine 30 g Tris-HCl [pH 8.3]
Running Buffer	100 mL Electrode buffer 5 mL 20% SDS
<u>Western blotting</u>	
Western transfer buffer	14.4 g Glycine 3.03 g Tris base 150 mL Methanol

Solution	Components (per L)¹
Wash buffer	1.09 g Na ₂ HPO ₄ 0.32 g NaH ₂ PO ₄ 9 g NaCl 1 mL Tween 20 [pH 7.2]
Blocking solution	5 % (w/v) skim milk powder in wash buffer
<u>Protein extraction</u>	
Lysis buffer	100 mM Tris-HCl 50 mM NaCl 10 % (v/v) glycerol 1 mM Tris(2- carboxyethyl)phosphine) [pH 7.5] cComplete Mini protease inhibitor cocktail (Roche)
<u>Lipopolysaccharide (LPS) staining</u>	
LPS buffer I	187.5 mM Tris-HCl [pH 6.8], 6% (w/v) SDS 30% (w/v) glycerol
LPS buffer II	62.5 mM Tris-HCl [pH 6.8] 0.1% SDS 10 % (w/v) glycerol 0.1% (w/v) bromophenol blue
Fixing solution	40 % Ethanol 5 % Glacial acetic acid
Periodic acid solution	40 % Ethanol 5 % Glacial acetic acid 0.7 % Periodic acid
Staining reagent	18.67 mM NaOH 0.39 % Ammonium hydroxide 0.67 % Silver nitrate
Developing solution	0.24 mM Citric acid 0.0185 % Formaldehyde
Stop solution	5 % Glacial acetic acid

¹Items in brackets are sterilised separately and added after autoclaving.

Table 2.2 – Antibiotics and supplements used in this study.

Chemical	Abbreviation	Stock Concentration (mg/mL)¹	Final Concentration (µg/mL)
Ampicillin	Ap	100 in H ₂ O	100
Chloramphenicol	Cm	50 in EtOH	25
Erythromycin	Em	200 in EtOH	200
Kanamycin	Km	50 in H ₂ O	50
Spectinomycin	Sp	50 in H ₂ O	50
Streptomycin	Sm	100 in H ₂ O	100
Tetracycline	Tc	5 in EtOH	15
Diaminopimelic acid	DAPA	30 mM = 5.7 mg/mL in H ₂ O	300 µM
Isopropyl-β-D-1- thiogalactopyranoside	IPTG	100 mM = 24 mg/mL in H ₂ O	0.1 mM
5-bromo-4-chloro-3-indolyl- β-D-galactopyranoside	X-gal	20 in dimethyl sulfoxide (DMSO)	20

¹All stock solutions stored at -20 °C except for DAPA which was stored at 4 °C.

Table 2.3 – Bacterial strains and bacteriophage used in this study.

Strain/phage	Genotype/phenotype	Reference
<i>Escherichia coli</i>		
β2163	(F ⁻) RP4-2-Tc::Mu <i>dapA</i> ::(<i>erm-pir</i>), Km ^R Em ^R	(Demarre et al., 2005)
CC118λ <i>pir</i>	<i>araD</i> , Δ(<i>ara</i> , <i>leu</i>), Δ <i>lacZ74</i> , <i>phoA20</i> , <i>galk</i> , <i>thi-1</i> , <i>rspE</i> , <i>rpoB</i> , <i>argE</i> , <i>recA1</i> , λ <i>pir</i>	(Herrero et al., 1990)
DH5α	(F ⁻), Φ80Δ <i>lacZM15</i> , Δ(<i>lacZYA-argF</i>)U169, <i>endA1</i> , <i>recA1</i> , <i>hsdR17</i> (<i>rκ⁻ mκ⁺</i>), <i>deoR</i> , <i>thi-1</i> , <i>supE44</i> , λ ⁻ , <i>gyrA96</i> , <i>relA1</i>	Laboratory stock
ESS	β-lactam super sensitive indicator strain	(Bainton et al., 1992)
OP50	Uracil auxotroph	(Brenner, 1974)
<i>Serratia sp.</i>		
S39006	<i>Serratia sp.</i> ATCC 39006, Parental strain	(Parker et al., 1982)
S39006 LacA	<i>lacZ</i> derivative of S39006. Referred to as wild type in this study.	(Thomson et al., 2000)
Strains derived from S39006 LacA:		
NWA19	Δ <i>pigC</i>	(Ramsay et al., 2011)
GPA1	<i>gvpA1</i> ::Tn-DS1028- <i>uidA</i> , Cm ^R	(Ramsay et al., 2011)
GRA	<i>gvrA</i> ::Tn-DS1028- <i>uidA</i> , Cm ^R	(Ramsay et al., 2011)
LIS	<i>smal</i> ::mini-Tn5Sm/Sp, Sp ^R	(Thomson et al., 2000)
SP19	<i>smal</i> ::mini-Tn5Sm/Sp, <i>pigX</i> ::Tn-DS1028, <i>pigZ</i> ::miniTn5 <i>lacZ1</i> , Sp ^R , Cm ^R , Km ^R	(Poulter et al., 2010)
MCA54	<i>carA</i> ::mini-Tn5 <i>lacZ1</i> , Km ^R	(Thomson et al., 2000)
AMH1	Δ <i>pigC orf6410</i> ::TnKRCPN1, Km ^R (untransduced)	This study
AMH2	Δ <i>pigC orf2785</i> ::TnKRCPN1, Km ^R (untransduced)	This study
AMH3	Δ <i>pigC rpoN</i> ::TnKRCPN1, Km ^R (untransduced)	This study
AMH4	Δ <i>pigC waaL</i> ::TnKRCPN1, Km ^R (untransduced)	This study
AMH5	Δ <i>pigC pigP</i> ::TnKRCPN1, Km ^R (untransduced)	This study
AMH6	Δ <i>pigC cyoA</i> ::TnKRCPN1, Km ^R (untransduced)	This study
AMH7	Δ <i>pigC orf2785</i> ::TnKRCPN1, Km ^R (untransduced)	This study
AMH8	Δ <i>pigC hfq</i> ::TnKRCPN1, Km ^R (untransduced)	This study
AMH9	Δ <i>pigC ratB</i> ::TnKRCPN1, Km ^R (untransduced)	This study
AMH10	Δ <i>pigC orf6410</i> ::TnKRCPN1, Km ^R (untransduced)	This study
AMH11	Δ <i>pigC orf6410</i> ::TnKRCPN1, Km ^R (untransduced)	This study

Strain/phage	Genotype/phenotype	Reference
AMH12	<i>ΔpigC dksA::TnKRCPN1</i> , Km ^R (untransduced)	This study
AMH13	<i>ΔpigC gvpN::TnKRCPN1</i> , Km ^R (untransduced)	This study
AMH14	<i>ΔpigC gvpC::TnKRCPN1</i> , Km ^R (untransduced)	This study
AMH15	<i>ΔpigC gvrA::TnKRCPN1</i> , Km ^R (untransduced)	This study
AMH16	<i>ΔpigC waaL::TnKRCPN1</i> , Km ^R (untransduced)	This study
AMH17	<i>ΔpigC proQ::TnKRCPN1</i> , Km ^R (untransduced)	This study
AMH18	<i>ΔpigC gvrB::TnKRCPN1</i> , Km ^R (untransduced)	This study
AMH19	<i>ΔpigC orf17860::TnKRCPN1</i> , Km ^R (untransduced)	This study
AMH31	<i>ΔrpoN</i>	This study
AMH32	<i>ΔdksA</i>	This study
AMH37	<i>ΔwaaL</i>	This study
AMH101	<i>orf6410::TnKRCPN1</i> , Km ^R	This study
AMH102	<i>ΔpigC orf6410::TnKRCPN1</i> , Km ^R	This study
AMH105	<i>orf2785::TnKRCPN1</i> , Km ^R	This study
AMH106	<i>ΔpigC orf2785::TnKRCPN1</i> , Km ^R	This study
AMH109	<i>rpoN::TnKRCPN1</i> , Km ^R	This study
AMH110	<i>ΔpigC rpoN::TnKRCPN1</i> , Km ^R	This study
AMH111	<i>gvpA1::Tn-DS1028-uidA</i> , <i>rpoN::TnKRCPN1</i> , Cm ^R , Km ^R	This study
AMH112	<i>gvrA::Tn-DS1028-uidA</i> , <i>rpoN::TnKRCPN1</i> , Cm ^R , Km ^R	This study
AMH113	<i>waaL::TnKRCPN1</i> , Km ^R	This study
AMH114	<i>ΔpigC waaL::TnKRCPN1</i> , Km ^R	This study
AMH117	<i>pigP::TnKRCPN1</i> , Km ^R	This study
AMH118	<i>ΔpigC pigP::TnKRCPN1</i> , Km ^R	This study
AMH121	<i>orf2785::TnKRCPN1</i> , Km ^R	This study
AMH122	<i>ΔpigC orf2785::TnKRCPN1</i> , Km ^R	This study
AMH125	<i>hfq::TnKRCPN1</i> , Km ^R	This study
AMH126	<i>ΔpigC hfq::TnKRCPN1</i> , Km ^R	This study
AMH129	<i>ratB::TnKRCPN1</i> , Km ^R	This study
AMH130	<i>ΔpigC ratB::TnKRCPN1</i> , Km ^R	This study
AMH133	<i>orf6410::TnKRCPN1</i> , Km ^R	This study
AMH134	<i>ΔpigC orf6410::TnKRCPN1</i> , Km ^R	This study
AMH137	<i>orf6410::TnKRCPN1</i> , Km ^R	This study
AMH138	<i>ΔpigC orf6410::TnKRCPN1</i> , Km ^R	This study
AMH141	<i>dksA::TnKRCPN1</i> , Km ^R	This study
AMH142	<i>ΔpigC dksA::TnKRCPN1</i> Km ^R	This study
AMH143	<i>gvpA1::Tn-DS1028-uidA</i> , <i>dksA::TnKRCPN1</i> , Cm ^R , Km ^R	This study

Strain/phage	Genotype/phenotype	Reference
AMH144	<i>gvrA::Tn-DS1028-uidA, dksA::TnKRCPN1, Cm^R, Km^R</i>	This study
AMH145	<i>gvpN::TnKRCPN1, Km^R</i>	This study
AMH146	<i>ΔpigC gvpN::TnKRCPN1, Km^R</i>	This study
AMH149	<i>gvpC::TnKRCPN1, Km^R</i>	This study
AMH150	<i>ΔpigC gvpC::TnKRCPN1, Km^R</i>	This study
AMH153	<i>gvrA::TnKRCPN1, Km^R</i>	This study
AMH154	<i>ΔpigC gvrA::TnKRCPN1, Km^R</i>	This study
AMH157	<i>waaL::TnKRCPN1, Km^R</i>	This study
AMH158	<i>ΔpigC waaL::TnKRCPN1, Km^R</i>	This study
AMH159	<i>gvpA1::Tn-DS1028-uidA, waaL::TnKRCPN1, Cm^R, Km^R</i>	This study
AMH160	<i>gvrA::Tn-DS1028-uidA, waaL::TnKRCPN1, Cm^R, Km^R</i>	This study
AMH161	<i>proQ::TnKRCPN1, Km^R</i>	This study
AMH162	<i>ΔpigC proQ::TnKRCPN1, Km^R</i>	This study
AMH165	<i>gvrB::TnKRCPN1cZ1, Km^R</i>	This study
AMH166	<i>ΔpigC gvrB::TnKRCPN1cZ1, Km^R</i>	This study
AMH169	<i>orf17860::TnKRCPN1, Km^R</i>	This study
AMH170	<i>ΔpigC orf17860::TnKRCPN1, Km^R</i>	This study
<u>Other species</u>		
	<i>Pectobacterium atrosepticum</i> SCRI1043	(Hinton et al., 1989)
	<i>Pseudomonas tolaasii</i> NCPPB 2192	Lab collection
<u>Bacteriophage</u>		
ΦOT8	<i>Serratia</i> generalised transducing phage	(Evans et al., 2010)

Table 2.4 – Plasmids used in this study.

Plasmid	Genotype/phenotype	Reference
pKRCPN1	<i>tetA, tnp, 'lacZ, oriR6K, aph, Km^R</i>	(Monson et al., 2015)
pDS1028	<i>tetA, tnp, oriR6K, cat, Cm^R</i>	(Monson et al., 2015)
pQE80-oriT	pQE80L carrying the RK2 origin of transfer cloned as an <i>NdeI</i> fragment, Ap ^R	(Ramsay et al., 2011)
pBlueScript II KS+	Cloning vector, ColE1 replicon, Ap ^R	(Alting-Mees & Short, 1989)
pKNG101	Marker exchange suicide vector, <i>sacBR</i> , <i>mobRK2, oriR6K, Sm^R</i>	(Kaniga et al., 1991)
pAH1	pQE80-oriT with <i>rpoN</i> inserted between the <i>BamHI</i> and <i>SacI</i> restriction sites, Ap ^R	This study
pAH4	pQE80-oriT with <i>dkxA</i> inserted between the <i>BamHI</i> and <i>SacI</i> restriction sites, Ap ^R	This study
pAH5	pQE80-oriT with <i>waaL</i> inserted between the <i>BamHI</i> and <i>SacI</i> restriction sites, Ap ^R	This study
pAH6	pBlueScript containing <i>rpoN</i> deletion construct cloned into the <i>BamHI</i> and <i>Apal</i> restriction sites, Ap ^R	This study
pAH7	pKNG101 with <i>rpoN</i> deletion construct from pAH6 subcloned into the <i>BamHI</i> and <i>Apal</i> restriction sites, Sm ^R	This study
pAH8	pBlueScript containing <i>dkxA</i> deletion construct cloned into the <i>XbaI</i> and <i>Apal</i> restriction sites, Ap ^R	This study
pAH10	pKNG101 with <i>dkxA</i> deletion construct from pAH8 subcloned into the <i>XbaI</i> and <i>Apal</i> restriction sites, Sm ^R	This study
pAH11	pBlueScript containing <i>waaL</i> deletion construct cloned into the <i>XbaI</i> and <i>Apal</i> restriction sites, Ap ^R	This study
pAH12	pKNG101 with <i>waaL</i> deletion construct from pAH11 subcloned into the <i>XbaI</i> and <i>Apal</i> restriction sites, Sm ^R	This study

2.3 Recombinant DNA Techniques

2.3.1 DNA separation, purification, digestion, and ligation

All molecular biological techniques were performed using standard methods (Sambrook & Green, 2012) unless otherwise stated. Genomic and plasmid DNA was extracted using a Thermo Scientific GeneJET Genomic DNA Purification Kit and a Thermo Scientific GeneJET Plasmid Miniprep Kit respectively, both according to the manufacturer's instructions. The resulting DNA concentration was determined using a NanoDrop 1000 spectrophotometer (Thermo Scientific). DNA was eluted in H₂O and stored at -20 °C.

DNA molecules were separated by gel electrophoresis using 1 % agarose gel in 1X TAE running buffer. DNA was stained with 500 ng/mL ethidium bromide and visualized using a Gene Genius Bio-Imaging System. Samples were mixed with 6X loading buffer before being loaded into the gel and a linear DNA ladder (Henrici et al., 2017) was included in every gel. Where necessary, bands of the appropriate size were excised from the agarose gel and the DNA extracted using a Thermo Scientific GeneJET Gel Extraction Kit following the manufacturer's instructions.

DNA was digested using restriction endonuclease enzymes according to the instructions supplied with each enzyme. A general digestion mixture is shown in Table 2.5, restriction digests were incubated at 37 °C for 1 hour before samples were separated using 1 % gel electrophoresis and the DNA extracted from the gel as above. If two enzymes were used that were incompatible, two single digests were performed successively. Alkaline phosphatase was added to restriction digestions of plasmid vectors to prevent re-ligation.

Ligation reactions were performed using T4 DNA Ligase (Thermo Scientific), vector and insert DNA were mixed in 1:1 and 5:1 (v/v) ratios. An additional no insert control was also performed to ensure that the vector digestion was successful with no re-ligation or incomplete digestion. The ligation mixtures are shown in Table 2.6. Ligation reactions were incubated at 22 °C for at least 1 hour before being used to transform competent *E. coli*.

Table 2.5 – Restriction enzyme digestion.

Reagents	Volume (μL)
10X Buffer	2
Restriction Enzyme 1	1
Restriction Enzyme 2	1
DNA (~1 μg of plasmid)	x ¹
H ₂ O	x ¹
Total	20

¹Volume was adjustable depending on the concentration of the input DNA

Table 2.6 – Ligation reaction.

Reagents	Reaction 1 (μL)	Reaction 2 (μL)	Reaction 3 (μL)
10X Buffer	2	2	2
T4 DNA Ligase	1	1	1
Vector	5	5	5
Insert	5	1	0
H ₂ O	7	11	12
Total	20	20	20

Table 2.7 – Sequence of the oligonucleotides used in this study.

Name	Oligonucleotide Sequence (5'-3') and description ¹	Reference
oPF106	GACCACACGTCGACTAGTGCNNNNNNNNNAGAG Random primed PCR primer 1	(Fineran et al., 2005a)
oPF107	GACCACACGTCGACTAGTGCNNNNNNNNNACGCC Random primed PCR primer 2	(Fineran et al., 2005a)
oPF108	GACCACACGTCGACTAGTGCNNNNNNNNNGATAC Random primed PCR primer 3	(Fineran et al., 2005a)
oPF109	GACCACACGTCGACTAGTGC Random primed PCR adapter primer	(Fineran et al., 2005a)
oMAMV1- KRCPN1	GGAATTGATCCGGTGGATG Sequencing primer for pKRCPN1 transposon	(Matilla et al., 2012)
oMAMV2- KRCPN1	GCATAAAGCTTGCTCAATCAATCAC Sequencing primer for pKRCPN1 transposon	(Matilla et al., 2012)
oREM7	CTAGAGTCGACCTGCAGGC Sequencing primer for pDS1028 transposon	(Monson et al., 2015)
oREM8	CACAGGAACACTTAACGGC Sequencing primer for pDS1028 transposon	(Monson et al., 2015)
oAMH5	CGCGGGATCCATGAAGCAAGTTTGCAACTCA Forward primer for cloning <i>rpoN</i> into pQE80-oriT, restriction site <i>Bam</i> HI	This study

Name	Oligonucleotide Sequence (5'-3') and description¹	Reference
oAMH6	CGCG GAGCTC TCAGACCAGCTGCTTACGC Reverse primer for cloning <i>rpoN</i> into pQE80- <i>oriT</i> , restriction site <i>SacI</i>	This study
oAMH7	GTGAGCGGATAACAATTTCA Sequencing primer for pQE80- <i>oriT</i>	This study
oAMH9	TAGGTACATTGAGCAACTGACT Sequencing primer for pQE80- <i>oriT</i>	This study
oAMH10	CGCG GGATCC ATGGCCTGTCATTTTCGTACG Forward primer for cloning <i>orf2785</i> into pQE80- <i>oriT</i> , restriction site <i>BamHI</i>	This study
oAMH11	CGCG GAGCTC CTACAATGCAAATAGGGAAGT Reverse primer for cloning <i>orf2785</i> into pQE80- <i>oriT</i> , restriction site <i>SacI</i>	This study
oAMH13	CGCG GGATCC GTGCCTGAACTTCACGTGG Forward primer for cloning <i>ratB</i> into pQE80- <i>oriT</i> , restriction site <i>BamHI</i>	This study
oAMH14	CGCG GAGCTC TTATTTTTTTGCGCGTTCTGCA Reverse primer for cloning <i>ratB</i> into pQE80- <i>oriT</i> , restriction site <i>SacI</i>	This study
oAMH15	CGCG GGATCC ATGCAAGAAGGGCAAACCG Forward primer for cloning <i>dkxA</i> into pQE80- <i>oriT</i> , restriction site <i>BamHI</i>	This study
oAMH16	CGCG GAGCTC TTACCCTGCCATCTGTTTTTCG Reverse primer for cloning <i>dkxA</i> into pQE80- <i>oriT</i> , restriction site <i>SacI</i>	This study
oAMH17	CGCG GGATCC ATGTCCCAGTTATCCTTTCACC Forward primer for cloning <i>waaL</i> into pQE80- <i>oriT</i> , restriction site <i>BamHI</i>	This study
oAMH18	CGCG GAGCTC TTAAATAAATCGTTGCTTATCCT Reverse primer for cloning <i>waaL</i> into pQE80- <i>oriT</i> , restriction site <i>SacI</i>	This study
oAMH19	CGCG GGATCC ACCTGCCTCAGGAAGCATCC Forward primer to amplify the region upstream of <i>rpoN</i> for allelic exchange, restriction site <i>BamHI</i>	This study
oAMH20	TCAGACCAGTTGCTTCATAAATAGCGC Reverse primer to amplify the region upstream of <i>rpoN</i> for allelic exchange	This study
oAMH21	ATGAAGCAACTGGTCTGACCCTAATTG Forward primer to amplify the region downstream of <i>rpoN</i> for allelic exchange	This study

Name	Oligonucleotide Sequence (5'-3') and description ¹	Reference
oAMH22	CGCG GGGCC CACTGATGATTTCCAGGGCACG Reverse primer to amplify the region downstream of <i>rpoN</i> for allelic exchange, restriction site <i>Apal</i>	This study
oAMH23	CGACGTTTTATATGGTGGTAGG Forward primer to confirm by PCR the allelic exchange to make <i>rpoN</i> mutant	This study
oAMH24	CCAAGTGCACCCAGTGTA Reverse primer to confirm by PCR the allelic exchange to make <i>rpoN</i> mutant	This study
oAMH26	CGCG GGGCC CTGTTATTAAGCACCCGCA Forward primer to amplify the region upstream of <i>dksA</i> for allelic exchange, restriction site <i>Apal</i>	This study
oAMH27	TTACCCTGCTTCTTGCATGTTGCTTCT Reverse primer to amplify the region upstream of <i>dksA</i> for allelic exchange	This study
oAMH28	ATGCAAGAAGCAGGGTAATTCGCCAA Forward primer to amplify the region downstream of <i>dksA</i> for allelic exchange	This study
oAMH29	GCT CTAG ATGGATTTACCGCGCAAC Reverse primer to amplify the region downstream of <i>dksA</i> for allelic exchange, restriction site <i>XbaI</i>	This study
oAMH30	CGCTAGTACATGAAGCGTTA Forward primer to confirm by PCR the allelic exchange to make <i>dksA</i> mutant	This study
oAMH31	ACAATCTCGGTGATACCC Reverse primer to confirm by PCR the allelic exchange to make <i>dksA</i> mutant	This study
oAMH32	CGCG GGGCC CAATCCCTTATGTGGTTTTGC Forward primer to amplify the region upstream of <i>waaL</i> for allelic exchange, restriction site <i>Apal</i>	This study
oAMH33	TTAAATAAACTGGGACATTAGTTTTTT Reverse primer to amplify the region upstream of <i>waaL</i> for allelic exchange	This study
oAMH34	ATGTCCAGTTTATTTAATAAGCATAA Forward primer to amplify the region downstream of <i>waaL</i> for allelic exchange	This study
oAMH35	GCG CTAG AACTATCAGAAGCTTGCCAG Reverse primer to amplify the region downstream of <i>waaL</i> for allelic exchange, restriction site <i>XbaI</i>	This study

Name	Oligonucleotide Sequence (5'-3') and description ¹	Reference
oAMH36	CCGATGGCATGGAGTGATG Forward primer to confirm by PCR the allelic exchange to make <i>waal</i> mutant	This study
oAMH37	GAGCGTAAAGGATTGGCTGG Reverse primer to confirm by PCR the allelic exchange to make <i>waal</i> mutant	This study

¹Sequences in bold show the restriction sites indicated in the description

2.3.2 Polymerase chain reaction (PCR)

Purified genomic DNA was used as a template for PCR amplification, with the exception of random primed PCR (RP-PCR), when a colony PCR was performed. Oligonucleotide primers were purchased from Sigma-Aldrich and are detailed in Table 2.7 above. Annealing and extension temperatures and times were adjusted to suit the individual PCR reaction. Phusion polymerase was used for all PCRs, following the enzyme instructions. General PCR reactions and amplification conditions are shown in Table 2.8 and Table 2.9. All PCR reactions were performed in a Veriti Thermo Cycler (Applied Biosystems).

Table 2.8 – PCR reaction mixture used in this study.

Reagents	Volume (µL)
5X Phusion HF Buffer	5
10 mM dNTPs	0.5
10 µM Forward Primer	1.25
10 µM Reverse Primer	1.25
DMSO	0.75
Phusion DNA Polymerase	0.25
Template DNA	1
H ₂ O	15
Total	25

Table 2.9 – PCR amplification conditions.

Stage	Temperature (°C)	Time	Cycles
1. Initial denaturation	95	1 min	1
2a. Denaturation	95	15 s	
b. Annealing	5 °C below primer melting temperature	30 s	30
c. Extension	72	15 s/kb	
3. Final Extension	72	7 mins	1
4. End	12	Indefinitely	1

2.3.3 Random primed polymerase chain reaction (RP-PCR)

Random primed PCR was carried out as per Jacobs et al. (2003) to identify the transposon location following random transposon mutagenesis screens. Briefly, two PCRs were performed, reaction 1 used random primers paired with a transposon-specific primer. The second reaction used the product of reaction 1 as the template DNA and an adapter primer and second transposon-specific primer to only amplify areas that contain the transposon and a small section of the surrounding DNA. The PCR reagents and conditions used are listed in Tables 2.10 and 2.11 below. Template DNA for reaction 1 was produced by boiling cells in H₂O five minutes at 99 °C. All reactions were performed in a Veriti Thermo Cycler (Applied Biosystems). The PCR products of reaction 2 were separated on a 1 % agarose gel and bands of interest were excised, the DNA purified from them, and sent for sequencing using primer oMAMV2-KRCPN1.

Table 2.10 – RP-PCR reaction mixture used in this study.

Reagents	Reaction 1 (µL)	Reaction 2 (µL)
5X Phusion HF Buffer	5	5
10 mM dNTPs	0.5	0.5
10 µM Forward Primer		
oMAMV1-KRCPN1	1.25	
oMAMV2-KRCPN1		1.25
10 µM Reverse Primer		
oPF106	0.42	
oPF107	0.42	
oPF108	0.42	
oPF109		1.25
DMSO	0.75	0.75
Phusion DNA Polymerase	0.25	0.25
Template DNA	2	1
H ₂ O	14	15
Total	25	25

Table 2.11 – RP-PCR amplification conditions.

Stage	Temperature (°C)	Time	Cycles
Reaction 1:			
1. Initial denaturation	94	3 mins	1
2a. Denaturation	94	15 s	
b. Annealing	42	30 s	6
c. Extension	72	3 mins	
3a. Denaturation	94	15 s	
b. Annealing	55	30 s	15
c. Extension	72	3 mins	
4. Final Extension	72	7 mins	1
5. End	12	Indefinitely	1
Reaction 2:			
1. Initial denaturation	94	1 min	1
2a. Denaturation	94	15 s	
b. Annealing	55	30 s	35
c. Extension	72	30 s	
3. Final Extension	72	7 mins	1
4. End	12	Indefinitely	1

2.3.4 Plasmid construction

Plasmids used in this study are listed in Table 2.4. To construct plasmids for complementation assays, the gene of interest was amplified using PCR with purified S39006 wild type genomic DNA used as the starting DNA template. Oligonucleotides used to amplify each gene are listed in Table 2.7. The PCR product and relevant vector were then digested separately using the restriction enzymes indicated. The digested insert was ligated into the compatibly digested, alkaline phosphatase-treated vector. Restriction digest and ligation reactions are detailed in Tables 2.5 and 2.6 respectively. The ligation mixtures were then used to transform chemically competent *E. coli* β 2163 cells. Putative transformants were streaked out to single colonies twice on selective agar before plasmids were extracted and the presence of the insert confirmed via PCR and DNA sequencing. The confirmed plasmids were then transferred to S39006 strains by conjugation.

Plasmids used for allelic exchange were made in the same manner as above with blue-white selection also used to screen for successful insertion of the mutator fragment into pBlueScript.

2.3.5 Allelic exchange

Allelic exchange was carried out using the previously published methodology (Kaniga et al., 1991; Muhl & Filloux, 2014). Briefly, a mutator fragment was created by amplifying regions 500 bp upstream and downstream of the gene of interest. These fragments were amplified using oligonucleotides that contained an 18 bp overlap region (the first 9 bp and last 9 bp of the gene of interest). This overlap region allowed the upstream and downstream fragments to be joined together via PCR. The product of this reaction was then run on a 1 % agarose gel and the 1000 bp band purified for digestion and ligation into pBlueScript. The ligation mixture was used to transform *E. coli* DH5 α . LBA supplemented with X-gal and IPTG were used to screen for successful transformants using blue-white selection. Putative successful transformants were streaked out twice to single colonies and confirmed by PCR and DNA sequencing of the plasmid. This plasmid was then digested to provide a greater quantity of mutator fragment that was then sub-cloned into the suicide vector, pKNG101. This vector contains the *Bacillus subtilis sacB* gene, the product of which is lethal to Gram-negative bacteria in the presence of sucrose (Kaniga et al., 1991). This second plasmid was then transferred into chemically competent *E. coli* β 2163 by heat shock transformation. The suicide vector containing the mutator fragment was then introduced into S39006 wild type by conjugation and allowed to integrate into the chromosome by homologous recombination across the cloned fragment. Derivatives in which the plasmid had then excised spontaneously from the genome and been lost from the bacteria were selected by growing the strain on 5 % sucrose, either reverting to wild type or removing the gene of interest by recombination. Putative knockouts were then subjected to PCR to amplify the area of interest and then sequenced to confirm the absence of the gene of interest.

2.3.6 Bacterial transformation by heat shock

Competent *E. coli* cells were made using standard methods (Sambrook & Green, 2012). Briefly, 25 mL of the relevant *E. coli* strain was grown to an OD₆₀₀ of 0.6 – 0.8 in LB supplemented with 375 μ L 1M MgCl₂ and DAPA if necessary in a 250 mL conical flask, with shaking at 215 rpm in a 37 °C water bath. The culture was then chilled on ice for 1 hour before being centrifuged at 2219 g for 10 minutes at 4 °C. The pellet was then resuspended in 10 mL solution A and incubated at 4 °C for 20 minutes. Cells were pelleted by centrifugation as previously stated, resuspended in 10 mL solution A, and centrifuged again

before a final resuspension in 1.25 mL of solution A + glycerol and then frozen at -80 °C or used immediately.

To transform competent cells, 75 µL of competent cells were mixed with 10 µL of ligation reaction or 2 µL of plasmid DNA and incubated on ice for 1 hour. The mixtures were then incubated at 42 °C for 90 seconds before 1 mL of LB (+ DAPA if necessary) was added and cells were allowed to recover for 1 hour at 37 °C. After cells had recovered, they were spread on LB agar supplemented with the relevant antibiotics and DAPA if necessary.

2.3.7 Transfer of plasmids via conjugation

Donor and recipient strains were grown overnight in 5 mL LB. Cultures were then normalised to an OD₆₀₀ of 1 and mixed together in a 1:3 donor to recipient ratio. 30 µL of this mixture was then spotted onto LBA (supplemented with DAPA if the donor strain was *E. coli* β2163) and incubated at 30 °C for 16 hours. Mating patches were then scraped off each plate and resuspended in 1 mL LB. Cells were then pelleted by centrifugation and resuspended in 1 mL fresh LB twice. The cell mixture was diluted and plated on the relevant selective agar. Plates were incubated at 30 °C for 48 hours before putative transconjugants were streaked out to single colonies twice on selective agar, to confirm resistance phenotypes.

2.3.8 DNA sequencing

DNA products to be sequenced were extracted from 1 % agarose gels using Thermo Scientific GeneJET Gel Extraction Kits, following the manufacturer's instructions. Plasmids to be sequenced were extracted from liquid cultures using Thermo Scientific GeneJET Plasmid Miniprep Kit as per the manufacturer's instructions. DNA was eluted in H₂O and the concentration checked using a NanoDrop 1000 spectrophotometer. DNA sequencing was carried out by Eurofins Genomics with 7.5 µL of DNA and 2.5 µL of 10 µM forward or reverse oligonucleotide sent for each reaction. Sequencing was carried out using an Applied Biosystems 3730XL DNA Analyser.

2.4 Random Transposon Mutagenesis

The random transposon mutagenesis was performed using a plasmid-transposon (plasposon) hybrid system, pKRCPN1 (Monson et al., 2015). The pKRCPN1 plasposon contains a R6K DNA replication origin (*oriR6K*) that requires the *pir*-encoded π protein to replicate, which is present only in the donor strain. The transposon is derived from Tn5 and the transposase gene (*tnp*) is located outside of the transposon so that after transposition the *tnp* gene is lost, resulting in stable insertions. Liquid cultures of *E. coli* β 2163 carrying plasmid pKRCPN1 (donor) and NWA19 (*S39006* Δ *pigC*) (recipient) were grown in 5 mL LB and normalised to an OD₆₀₀ of 1. Donor and recipient cultures were mixed at either a 1:2 or 1:3 ratio and 30 μ L spots placed onto LBA + DAPA plates and allowed to dry. Conjugation patches were then incubated at 30 °C for 8 or 16 hours before being scraped off, resuspended in LB, and plated onto selective agar (LB + Km) as described in section 2.3.7. The absence of DAPA in selective plates prevented any donor from growing while the kanamycin ensured only successful NWA19 transconjugants could grow. Donor- and recipient-only spots were also plated out onto selective agar as controls.

After the mating patches were diluted and plated onto selective agar, colonies were visually screened for any likely difference in gas vesicle production compared to NWA19. Colonies that appeared noticeably more translucent, slightly less opaque (intermediate), hyper opaque or that had an unusual colony morphology (bull's eye), were streaked out twice onto selective agar as putative gas vesicle mutants. These putative mutants were then subjected to RP-PCR (see section 2.3.3) to determine the transposon insertion site with the most interesting mutants selected for further study. To confirm the change in gas vesicle phenotype was the result of the transposon insertion and not another mutation, the transposon insertion was transduced into a clean background (*S39006* wild type and NWA19) and these transduced strains were used for subsequent analysis.

2.4.1 Bypass mutagenesis screening

Bypass mutagenesis screens were performed on strains AMH110 and AMH142 to determine if a secondary transposon insertion could restore the ability to produce gas vesicles. The transposon was delivered into cells as described in section 2.4, the only difference being the plasmid used was pDS1028 and transconjugants were selected on LBA + Km + Cm. Colonies were screened visually for any change in opacity, indicative of GV production. The transposon insertion site was determined for putative GV bypass mutants using the procedure described in section 2.3.3.

2.5 Bioinformatic Analysis

Sequence similarity values were determined by comparison to sequences available in GenBank (Benson et al., 2005) using the Basic Local Alignment Search Tool (BLAST) (Altschul et al., 1990). The predicted amino acid sequence encoded by each gene of interest was analysed for any conserved domains using Pfam (El-Gebali et al., 2019) and protein-protein BLAST (BLASTP) (Boratyn et al., 2012). Genomes were visualised using Artemis version 16.0 (Carver et al., 2012). Binding motifs were predicted using the FIMO program in the MEME Suite (Bailey et al., 2015; Grant et al., 2011).

2.6 Generalised Transduction of *S39006* using Φ OT8

2.6.1 Preparation of Φ OT8 lysate

Lysates of Φ OT8 were prepared by mixing 10 μ L of phage or phage dilution with 200 μ L of *S39006* wild type liquid culture and 4 mL of molten 0.35 % top agar. This mixture was then poured onto LBA and left to set before being incubated at 30 °C for 16 hours. 10-fold dilutions of phage from 10^{-1} to 10^{-5} were used in order to identify the dilution that resulted in semi-confluent lysis. The top agar was then harvested from this plate using a glass spreader and transferred into a 30 mL glass universal tube. The plate was then rinsed with 3 mL LB and this was also transferred to the same universal. Next, 500 μ L of NaHCO₃-saturated chloroform was added to the universal and the mixture was vortexed for two minutes to break up the agar. The mixture was then centrifuged at 2219 g for 20 minutes at 4 °C. The supernatant was then transferred to a sterile glass bijou and 100 μ L of NaHCO₃-saturated chloroform was added. This lysate was then stored at 4 °C over chloroform until required for transduction assays.

2.6.2 Transduction of *S39006* using Φ OT8

The use of Φ OT8 to transduce *S39006* and derivative strains has already been well established (Evans et al., 2010). Briefly, Φ OT8 was grown on the appropriate donor strain (with the transposon/genetic marker to be transduced) and a lysate was made as per section 2.6.1 above. After lysates were made, 25 μ L of lysate was mixed with 1 mL of an overnight culture of the recipient strain and the mixture was incubated at 30 °C for 1 hour. After incubation, cells were pelleted by centrifugation and resuspended in fresh LB twice to

remove any excess phage. The mixture was then diluted and spread onto LBA plates supplemented with the appropriate antibiotics to select for successful transductants. A 100 μ L aliquot of the lysate was spread onto an LBA plate and 100 μ L of the recipient strain was spread onto the selective agar plates as controls for phage lysate sterility and spontaneous drug resistance, respectively. Putative transductants were then streaked out to single colonies twice to reduce the risk of any Φ OT8 carryover, before being frozen.

2.7 Phenotypic Assays

2.7.1 BHL detection assay

BHL detection assays were carried out as previously described (Poulter et al., 2010). Indicator plates were made by mixing 100 μ L of *Serratia* biosensor strain SP19 with 4 mL of molten 0.7 % top agar and poured over an LBA plate. Top lawns were allowed to set and dry for at least 30 minutes. Liquid cultures of the strains to be tested were grown and normalized to an OD₆₀₀ of 1 to ensure similar starting cell numbers. 10 μ L of the strain to be tested, wild type S39006 and the negative control strain LIS (a *smal* mutant) were spotted onto the SP19 top lawn at evenly spaced intervals. The spots were allowed to dry before plates were incubated at 30 °C for 48 hours. The production of BHL was indicated by the presence of a red halo around a spot.

2.7.2 Carbapenem detection assay

Carbapenem detection assays were performed as previously described (Slater et al., 2003). Carbapenem detection plates were made by mixing 100 μ L of *E. coli* super sensitive strain (ESS) with 4 mL of molten 0.7 % top agar which was then poured over an LBA plate. After allowing the top lawn to set and dry, 10 μ L of a liquid culture of each strain to be tested was spotted onto each plate and allowed to dry. The OD₆₀₀ of each culture was normalized to 1. Plates were then incubated at 30 °C for 48 hours. Carbapenem production was indicated by a zone of clearance on the top lawn around the test spot where the ESS was unable to grow.

2.7.3 Cellulase detection assay

The cellulase detection assay was performed as described by Andro et al. (1984). CMC-sucrose agar plates were made according to the recipe in Table. 2.1, the agar was measured

so each plate contained exactly 25 mL of agar, plates were allowed to set and dry before use in the assay. Overnight cultures of the test strain and S39006 wild type were grown and normalized to an OD₆₀₀ of 1 before 10 µL of each strain was spotted onto the plate and allowed to dry. Plates were then incubated at 30 °C for 48 hours before they were developed. To develop the plates, they were first flooded with 0.2 % (w/v) congo red for 20 minutes before being rinsed twice with 1 M NaCl then covered once more with 1 M NaCl and left for five minutes to bleach the plates. The NaCl was then discarded, and plates were stained with 1 M HCl for 5 minutes. Cellulase activity was indicated by a bleached yellow halo surrounding the bacterial spot.

2.7.4 Pectate lyase detection assay

The pectate lyase detection assay was performed as previously described (Andro et al., 1984). Briefly, overnight cultures of test strains were normalized to an OD₆₀₀ of 1 before 10 µL of each strain was spotted onto Pel agar plates. Spots were left to dry then plates were incubated at 30 °C for 48 hours. To assess enzyme activity, plates were flooded with 7.5 % (w/v) copper acetate for 1 – 2 hours. Pectate lyase activity was indicated by the presence of two cream halos formed around a bacterial spot.

2.7.5 Flotation assay

Flotation assays were performed as described by Tashiro et al. (2016). Overnight cultures of each test strain were used to start a second 5 mL culture with a starting OD₆₀₀ of 0.05 in a 30 mL clear plastic universal tube. These cultures were then grown at 30 °C on a rotary wheel for 24 hours. After growth, tubes were left standing as static cultures at room temperature for at least 48 hours before imaging and sampling for phase contrast microscopy (PCM).

2.7.6 Colony morphology spot test

To assess colony morphology, overnight cultures of test strains were grown and normalized to an OD₆₀₀ of 1. 10 µL of each strain was spotted onto LBA, left to dry and then incubated at 30 °C for 48 hours. After incubation, spots were imaged and compared to wild type

S39006 for any differences in opacity or spot morphology. Samples were also taken from each spot and assessed using PCM.

2.7.7 Swarming assay

To assess the swarming ability of each strain, overnight cultures were normalized to an OD₆₀₀ of 0.2 and 5 µL was spotted onto an Eiken agar plate. Each plate contained a spot of the test strain and S39006 wild type to account for any plate to plate variation. Eiken agar was measured when pouring to ensure each plate contained exactly 25 mL. Plates were also allowed to set on a level surface to ensure the agar was the same thickness across the plate. Spots were allowed to dry for 10 minutes before plates were incubated at 30 °C for 48 hours.

2.7.8 Swimming assay

Swimming motility was assessed using tryptone swarm agar plates, as described previously (Williamson et al., 2008). Liquid cultures of each test strain were normalized to an OD₆₀₀ of 0.2 and 5 µL of each strain spotted onto swimming plates. Agar was measured when each plate was poured to ensure every plate contained 25 mL. Plates were also allowed to set on a level surface to ensure the agar was the same thickness across on the plate. Spots were allowed to dry for 10 minutes then incubated at 30 °C for 16 hours. The diameter of the swimming halo was then compared between wild type and test strains.

2.7.9 Quantification of carbapenem and BHL production

Samples of 1 mL were taken every two hours throughout growth curve assays and centrifuged to pellet cells. The supernatant was filter sterilized using a 0.22 µm syringe filter and incubated on ice until they could be assessed at the end of the growth curve. To prepare the quantification plates, 400 mL of LBA was poured into a 245 x 245 x 25 bioassay dish and allowed to set. A top lawn of ESS (to measure carbapenem production) or SP19 (to measure BHL production) was then poured over each plate by mixing 1 mL of the relevant strain with 100 mL of 0.75 % top agar. Once the top agar was set, wells were cut into the agar using a sterile 0.5 cm cork borer. 200 µL of supernatant from each strain at each time point was used to fill the wells. Plates were then incubated at 30 °C for 48 hours before the

halo size was measured. Halo sizes were then normalized to the OD₆₀₀ of each culture at each time point to measure the difference in production of carbapenem or BHL over time.

2.7.10 Quantification of prodigiosin production

Samples of 1 mL were taken every two hours throughout growth curve assays and centrifuged at 13,000 rpm for 5 minutes to pellet the cells. The supernatant was filter sterilized for other analysis (see section 2.7.9) and the pellet used to quantify prodigiosin production. Cell pellets were resuspended in 1 mL of acidified ethanol to extract prodigiosin. The cells were then pelleted by centrifugation at 13,000 rpm for 5 minutes. The supernatant was transferred to a plastic cuvette to measure the absorbance at 534 nm (A₅₃₄) in a Unicam Helios spectrophotometer. 1 mL of acidified ethanol was used as a blank. This measurement was then normalized to the OD₆₀₀ of the culture at that specific time point to give prodigiosin concentration as A₅₃₄ mL⁻¹ OD₆₀₀⁻¹.

2.8 *Caenorhabditis elegans* Virulence Assay

Assays of S39006 killing of *C. elegans* are based on those used by Kurz et al. (2003). *C. elegans* strain DH26 was used for these assays. Worms were maintained on NGM agar covered with an *E. coli* OP50 lawn. Worms were synchronized prior to each virulence assay to ensure all worms used were at the same stage. To synchronize, all worms and eggs were washed off a maintenance plate with 5 mL of M9 medium and all worms were killed using a 40% bleach solution (see Table 2.1). To stop bleaching, 14 mL of M9 medium was added and dead worms and eggs were pelleted by centrifugation at 4,000 rpm for 2 minutes. The supernatant was then removed and another 14 mL M9 medium added to resuspend the pellet and wash the worm eggs. This mixture was then centrifuged under the same conditions and washed as above. This washing was repeated a further three times to ensure there was no bleach carried over. The washed solution was incubated at 25 °C for 16 hours to allow the eggs to hatch. The worms were pelleted, resuspended in 100 µL M9 medium and transferred to an NGM agar plate with an OP50 lawn. These worms were left for 26-36 hours before L4 stage worms were picked for the virulence assay. For each strain tested, 50 L4 stage worms were used. Ten worms per plate were placed onto NGM agar plates containing a 50 µL spot of the test strain (grown at 30 °C for 24 hours prior to the

worm addition). Plates were then incubated at 25 °C and scored for live worms every 24 hours. Worms were considered dead when they no longer responded to touch and live worms were transferred onto new plates each day.

2.9 Analysis of Gene Expression by Measuring β -glucuronidase Activity

β -glucuronidase activity was measured as described by Ramsay et al. (2011). A 100 μ L sample of each culture was taken at each time point over the course of a growth curve and frozen at -80 °C in a 96-well plate. Samples were then defrosted at 37 °C and 10 μ L aliquots made of each sample into a new 96-well plate which was then frozen at -80 °C. The aliquots were then defrosted at room temperature before 100 μ L of reaction mixture was added immediately prior to the samples being read. The reaction mixture was made of phosphate-buffered saline (PBS) with 20 mg mL⁻¹ lysozyme and 250 μ g mL⁻¹ 4'-methylumbelliferyl- β -D-glucuronide (MUG) added. Samples were read using a Gemini XPS plate reader using the following parameters: excitation: 360 nm, emission: 450 nm, cut-off: 435 nm, 8 reads per well, measured every 30 seconds for 30 minutes. RFUs produced per minute were calculated from a period of linear increase in fluorescence and normalised to the OD₆₀₀ of each sample to give a measurement of RFU min⁻¹ OD₆₀₀⁻¹.

2.10 Microscopy Techniques

2.10.1 Phase contrast microscopy

PCM images were obtained either from liquid cultures or cells grown on LBA plates. For liquid cultures, a 1 μ L sample was taken from the flotation assay cultures after 48 hours of standing incubation and loaded onto a glass microscope slide. The cultures were mixed before sampling to ensure an accurate representation of the whole culture. Samples were also taken from the colony morphology spot tests, which were mixed with 50 μ L LB before 1 μ L was taken to be loaded onto the microscope slide. Slides were then immediately covered with a glass coverslip and analyzed under oil immersion using an Olympus BX-51 microscope with the 100 X lens. Images were taken with a QICAM monochrome camera using QCapture Pro-6 software. Image J was then used to crop images to a consistent size and add the scale bar.

2.10.2 Transmission electron microscopy

Cells for TEM analysis were obtained from flotation assay cultures after standing for 48 hours at room temperature. Sample preparations were performed as described by Ramsay et al. (2011). Briefly, cells were attached to a carbon-coated glow-discharged grid for 5 – 10 minutes before grids were washed twice with H₂O to remove excess cells. Fixed cells were stained with 2 % phosphotungstic acid (pH 7.0) for 1 minute. Grids were viewed using a FEI Tecnai G2 TEM at the Cambridge Advanced Imaging Centre, University of Cambridge.

2.11 Protein Methods

2.11.1 Sodium dodecyl sulphate-polyacrylamide gel electrophoresis (SDS-PAGE)

SDS-PAGE was used to analyse samples prior to proteomic analysis and to determine the amount of GvpC produced at various points of the growth curve. Samples for proteomic analysis were loaded following protein extraction, growth curves samples were boiled for 10 minutes before 3 X SDS Blue Loading Buffer (NEB) and 1 mM dithiothreitol (DTT) was added. Samples were boiled for a further 10 minutes prior to loading, with 10 µL of each sample loaded. Thermo Scientific PageRuler Plus Prestained Protein Ladder was used as a reference. SDS-PAGE gels were prepared according to standard protocols (Sambrook & Green, 2012) and the gel electrophoresis was performed using a Bio-Rad Mini-PROTEAN Tetra Cell system. The solutions used for SDS-PAGE are described in Table 2.1.

2.11.2 Western blotting

After samples were separated by electrophoresis, protein bands were transferred from the gel to an Immobilon PVDF membrane using a Bio-Rad Mini Trans-Blot Cell system. Transfers were carried out for 16 h at 100 mA at 4 °C in western transfer buffer. After the transfer, the membrane was washed three times in wash buffer, for 5 minutes per wash. The membrane was then blocked for 1 hour in blocking solution before the primary antibody, a rabbit anti-GvpC, was added (1:10,000 dilution) for another hour. The membrane was washed another 4 times in wash buffer for 5 minutes per wash. The secondary antibody (horseradish peroxidase-conjugated goat anti-rabbit IgG) was added to 30 mL blocking solution (1:10,000 dilution) and incubated for 40 minutes. The membrane was washed

another three times in wash buffer before it was developed with a chemiluminescent substrate (Millipore). Finally, the membrane was exposed to X-ray film for signal detection.

2.11.3 Preparation of intracellular protein samples for proteomics

The protocol followed to extract proteins for proteomic analysis was performed largely as described by Dolan et al. (2020). Briefly, 25 mL of LB was inoculated with S39006, the *rpoN* mutant (AMH109) or the *dksA* mutant (AMH157) at a starting OD₆₀₀ of 0.05. Cells were grown for 14 hours in 250 mL flasks at 30 °C and 215 rpm. These cultures were then normalised to an OD₆₀₀ of 2 and 25 mL of cells was harvested by centrifugation (2739 g, 10 min, 4 °C). Pellets were resuspended in 500 µL lysis buffer, followed by three rounds of sonication (3 x 10 s) on ice. Samples were then centrifuged again (21,130 g, 15 min, 4 °C) to remove cell debris. Protein concentrations were determined using a Bradford assay (Bio-Rad) and normalised to 2 mg/mL. At this stage samples were separated by SDS-PAGE and stained with Coomassie and a western blot for GvpC was performed as quality controls. Protein samples of 100 µg were then sent to the Cambridge Centre for Proteomics (CCP) for quantitative proteomic analysis. Three independent replicates were performed for each strain analysed. The preparation of protein samples was performed in conjunction with Carlo Sandoval, who was analysing two other mutants of S39006 and as such the wild type control samples were shared. The protocol below in sections 2.11.4 – 2.11.7 was kindly provided by Dr. Mike Deery from the Cambridge Centre for Proteomics.

2.11.4 Tandem mass tag (TMT) labelling

TMT-16plex labelling was performed following the manufacturer's instructions (Thermo Fisher Scientific). Each strain was labelled with the following TMT tags, S39006 wild type: 126, 127N, 127C; AMH109: 128N, 128C, 129N; and AMH157: 129C, 130N, 130C. All protein samples were combined and cleaned using a Sep-Pak C18 cartridge.

2.11.5 High-pH first dimension reverse-phase fractionation

Desalted peptides were resuspended in 0.1 ml 20 mM ammonium formate (pH 10.0) and 4 % (v/v) acetonitrile. Peptides were subjected to a 60 min linear gradient of 5 – 60 % acetonitrile and 20 mM ammonium formate (pH 10.0) at a flow rate of 0.25 mL min⁻¹ over

an Acquity bridged ethyl hybrid C18 UPLC column (Waters; 2.1 mm i.d. x 150 mm, 1.7 μ m particle size). Chromatographic performance was monitored by sampling eluate with a diode array detector (Acquity UPLC, Waters), scanning between wavelengths of 200 and 400 nm. To reduce dryness by vacuum centrifugation, samples were collected in 1 min increments.

2.11.6 Liquid chromatography-mass spectrometry (LC-MS/MS) analyses

Samples from the high pH reverse-phase separations were resuspended in 30 μ L of 0.1 % formic acid and placed into a glass vial. 1 μ L of each fraction was injected by the HPLC autosampler and separated by the LC method detailed below. A total of 17 combined fractions were analysed by LC-MS/MS.

LC-MS/MS experiments were performed using a Dionex Ultimate 3000 RSLC nanoUPLC system (Thermo Fisher Scientific) and a Lumos Orbitrap mass spectrometer (Thermo Fisher Scientific). The peptides were loaded onto a pre-column (Thermo Fisher Scientific PepMap 100 C18, 5 mm particle size, 100 Å pore size, 300 mm i.d. x 5 mm length) from the Ultimate 3000 auto-sampler with 0.1 % formic acid for 3 min at a flow rate of 10 μ L min⁻¹. The column valve was then switched to allow elution of peptides from the pre-column onto the analytical column. The peptides were separated by C18 reverse-phase chromatography at a flow rate of 300 nl min⁻¹ using a Thermo Scientific reverse-phase nano Easy-spray column (Thermo Fisher Scientific PepMap C18, 2 mm particle size, 100 Å pore size, 75 mm i.d. x 50 cm length). Solvent A was 0.1 % formic acid and solvent B was 80 % acetonitrile and 0.1 % formic acid. Elution was performed using a linear gradient of 2 – 40 % solution B over 93 minutes.

The eluted peptides were sprayed into the mass spectrometer by an Easy-Spray Source (Thermo Fisher Scientific). All m/z values of eluted peptide ions were measured in an Orbitrap mass analyser, with a resolution of 120,000 and were scanned between m/z of 380 – 1500 Da. Data dependent MS/MS scans (top speed) were used to automatically isolate and fragment precursor ions by collision-induced dissociation with normalised collision energy (NCE) of 35 %, which were analysed in the linear ion trap. Singly charged ions and ions with unassigned charge states were excluded for MS/MS and a dynamic exclusion

window of 70 seconds was used. Synchronous Precursor Selection MS3 was used to select the top 10 most abundant fragment ions from each MS/MS event using High energy Collisional Dissociation, with NCE set at 55 % (McAlister et al., 2014). MS/MS data were collected with mass range from 100 – 500 Da with a resolution of 60,000. This was performed in cycles of 10 MS3 events before the Lumos instrument reverted to scanning the m/z ratios of the intact peptide ions and the cycle continued.

2.11.7 Database searching and analysis

Analysis of the MS raw data was performed using Proteome Discoverer version 2.1 (Thermo Fisher Scientific) and Mascot version 2.6 (Matrix Science). Data were aligned against the UniProt *Serratia* sp. ATCC 39006 database and the common repository of adventitious proteins (cRAP) version 1.0 with trypsin set as the enzyme specificity. Protein identification allowed an MS tolerance of ± 10 ppm and an MS/MS tolerance of ± 0.8 Da along with permission of up to 2 missed tryptic cleavages. The minimum peptide length was set at six amino acids. Protein with at least one peptide was set as the acceptable score thresholds for protein identification. Quantification was performed by calculating the sum of centroided reporter ions with a ± 2 millimass unit window around the expected m/z for each of the four TMT reporter ions.

All comparative analyses were performed using R (R Core Team, 2020) and RStudio (RStudio Team, 2021). The MSnbase package (Gatto et al., 2021; Gatto & Lilley, 2012) was used to process the proteomics data. This entailed the removal of missing values (instances where a protein was identified but not quantified in all channels and was rejected from further analysis), \log_2 -transformation of the raw data, and sample normalisation using the 'diff.median' method. The differential abundance of each protein was evaluated using the Limma package (Ritchie et al., 2015). The significance of differences in protein abundance was determined using the Student's t-test with variances moderated by Limma's empirical Bayes method. P-values were adjusted for multiple testing by the Benjamini Hochberg method (Benjamini & Hochberg, 1995). Volcano plots were created using OmicsVolcano (Kuznetsova et al., 2021).

2.12 Silver Stain for Lipopolysaccharides

Lipopolysaccharide (LPS) preparations were performed as described by Preston et al. (1996). Briefly, overnight cultures of each strain were normalised to an OD₆₀₀ of 1, 3 mL of each culture was centrifuged to pellet cells, washed once in 1 mL PBS then resuspended in 500 µL PBS. 250 µL LPS buffer I was added, and cells were lysed by boiling for 5 minutes. 10 µL of cell lysate was added to 35 µL LPS buffer II and 10 µL Proteinase K (25 mg/mL). Samples were then incubated for 12 – 16 h at 55 °C. LPS samples were separated by SDS-PAGE, with 15 µL of each sample was loaded onto the gel (18 % resolving gel, 6 % stacking gel). The LPS was stained as previously described by Tsai & Frasch (1982) and Fomsgaard et al. (1990). Briefly, LPS was fixed for 2 h in fixing solution before being exposed to the periodic acid solution for 5 minutes to oxidise the LPS. The gel was then washed three times in H₂O before being placed in the staining reagent for 20 minutes. Following a further three washes, the gel was developed for 2 – 5 minutes in developer solution until LPS turned dark brown. At this point the developing process was stopped by replacing the developing solution with stop solution. All incubations and washes were carried out on a rotary platform at room temperature with 25 mL of the relevant solution.

2.13 Statistical Analysis

The statistical significance of any differences seen in RFU or antibiotic production over the course of a growth curve was determined using a repeated measures ANOVA, p-values of less than 0.05 were considered significant. Differences in the virulence of *C. elegans* was assessed using a Mantel-Cox log-rank test. Asterisks in figure legends indicate p-values: *, p < 0.05; **, p < 0.01; ***, p < 0.001; NS, not significant. Statistical analysis was carried out using R (R Core Team, 2020), RStudio (RStudio Team, 2021), and GraphPad Prism version 9.1.0 for Mac.

Chapter 3. A Random Transposon Mutagenesis Screen for *Serratia* sp. ATCC 39006 Gas Vesicle Mutants

3.1 Introduction

Serratia sp. ATCC 39006 (S39006) produces gas vesicles that enable it to float and colonize air-liquid interfaces in a more energy efficient way than flagellar-mediated migration (Monson et al., 2016; Ramsay et al., 2011; Tashiro et al., 2016). The gas vesicle cluster of S39006 is composed of 19 genes in two contiguous operons (Ramsay et al., 2011). Previous work in this laboratory established that 11 of these genes are essential for the production of gas vesicles (*gvpA1*, *gvpF1*, *gvpG*, *gvpA2*, *gvpK*, *gvpA3*, *gvpF2*, *gvpF3*, *gvrA*, *gvrB*, and *gvrC*) and that overexpression of some genes within the cluster resulted in either a reduction (*gvpF1*, *gvpF2*, *gvrA*, *gvrB*, and *gvrC*) or complete loss of gas vesicles (*gvpV* and *gvpA3*) (Monson et al., 2016; Tashiro et al., 2016). Random transposon mutagenesis (RTM) screens have been utilized to identify novel regulators of gas vesicle production in S39006 including RbsR, FloR and TrkH (Lee et al., 2017; Quintero-Yanes et al., 2020, 2019). These results show that the regulatory network of S39006 is complex and although we have some understanding of how regulation of various phenotypes overlap, there is still much to be understood. This chapter details the creation of a bank of transposon mutants that were then screened for differences in gas vesicle production. The locations of the transposon insertions were identified for promising mutants and further analysis of any pleiotropy was carried out. This screen provided a number of interesting potential regulatory genes to investigate, three of which are investigated in greater detail in chapters 4-6.

3.2 Results

3.2.1 Generation of a library of transposon insertion mutants

Gas vesicles are found in the cytoplasm and refract light. They appear as bright spots (“gas vacuoles”) under phase contrast microscopy (PCM) and bacterial colonies producing gas vesicles appear opaque. Therefore, by performing a random transposon mutagenesis and screening for colonies with differences in opacity, novel regulators of gas vesicles can be identified. Wild type S39006 produces the red pigmented antibiotic, prodigiosin, the

production of which is also altered in certain mutants. To overcome the potentially confounding effects of changes in pigment production, the random transposon mutagenesis was carried out in the strain NWA19, which does not produce prodigiosin. NWA19 contains an in-frame deletion of the *pigC* gene which is essential for the production of prodigiosin; colonies of this strain appear white on agar plates (due to the presence of gas vesicles and absence of prodigiosin).

The transposon was delivered to cells via conjugation of the plasmid pKRCPN1 (Monson et al., 2015) which can replicate only in the donor strain *E. coli* β 2163 due to the presence of the *pir*-encoded π protein. The plasmid contained tetracycline and kanamycin resistance genes, with only the kanamycin resistance gene located on the transposon. Therefore, by screening for kanamycin resistance and tetracycline sensitivity, it can be easily confirmed that only the transposon has integrated into the recipient cell and not the entire plasmid. The donor strain, *E. coli* β 2163 is an auxotroph that cannot grow in the absence of DAPA, and this trait was exploited to select against the *E. coli* donor while positively selecting for kanamycin resistant S39006 transconjugants (Figure 3.1).

In total, 86,892 transposon insertion mutants were screened from 24 independent conjugation patches. From this library of mutants, 534 were identified as showing a difference in opacity or colony morphology, when compared to the wild type strain. After streaking the putative gas vesicle mutants to single colonies multiple times, 77 failed to show any visible, reproducible difference in opacity when compared to the original recipient strain NWA19 and so were not pursued further. The remaining 457 putative gas vesicle mutants fell into four distinct categories: translucent, intermediate, hyper opaque, and bull's eye. An example of the appearance of each type of mutant is shown in Figure 3.2 along with the number identified for each class. Mutants were classified on a visual basis with translucent mutants appearing not to make any gas vesicles and intermediate mutants appearing opaque but to a lesser degree than NWA19. Hyper opaque mutants were defined as looking more opaque than NWA19, or they appeared opaque at an earlier stage of colony growth than NWA19. Bull's-eye mutants were first described as such due to their distinctive colony shape and opacity (Quintero-Yanes, 2019).

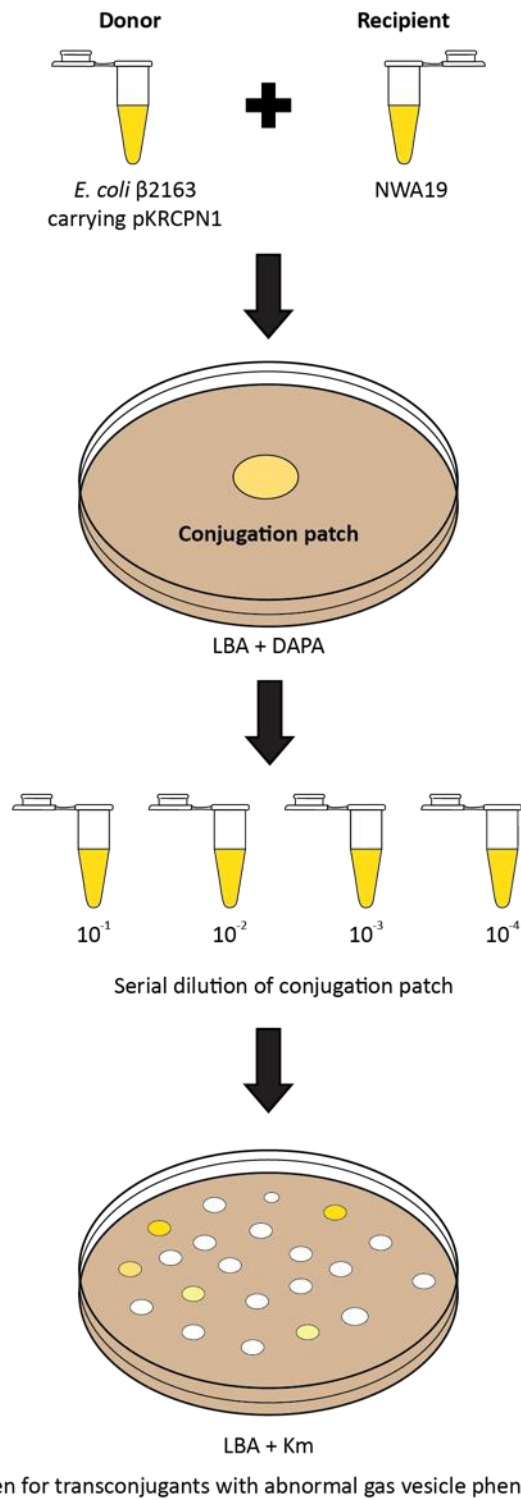


Figure 3.1 – Random transposon mutagenesis of NWA19 using plasmid pKRCPN1.

The donor strain *E. coli* β2163 was mixed with the recipient NWA19 and grown on LBA supplemented with DAPA at 30 °C for 8 or 16 hours. The conjugation patch was then scraped off the plate and serially diluted before being plated on LBA supplemented with kanamycin to select for putative transconjugants.

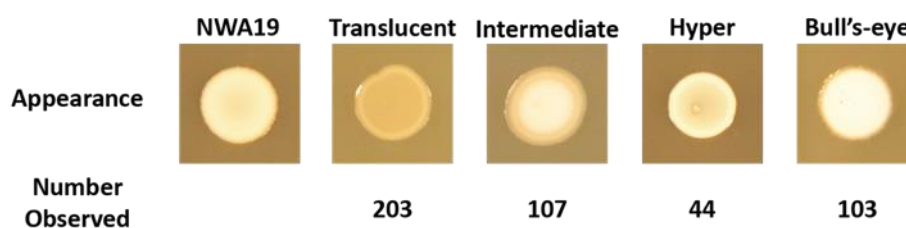


Figure 3.2 – Examples of different gas vesicle phenotypes observed following random transposon mutagenesis of NWA19.

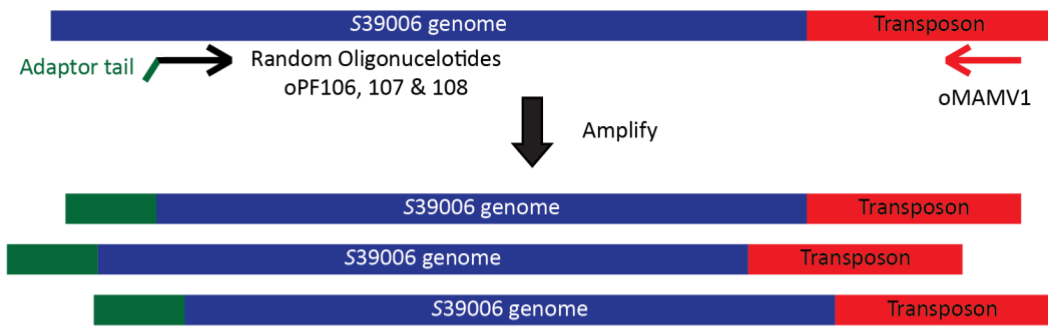
Bacteria were grown in liquid culture; cell numbers were normalised to an OD₆₀₀ of 1 and spotted onto LBA then incubated at 30 °C for 48 hours.

3.2.2 Determination of the transposon insertion location

Random primed PCR (RP-PCR) was used to determine the transposon insertion location in the gas vesicle mutants (Figure 3.3). The region bordering the transposon was amplified using a transposon-specific oligonucleotide and a random oligonucleotide with a known adaptor sequence. The desired PCR product was then further amplified using a second transposon-specific oligonucleotide and an adaptor oligonucleotide complementary to the known sequence of the random oligonucleotides used in the first PCR. This product was then sequenced and used to determine the precise location where the transposon had inserted in any given mutant.

The location of the transposon insertion was determined for 19 gas vesicle mutants with varying GV phenotypes (Table 3.1). Of these 19 mutants, the transposon insertions were found in 15 different genes, some of which had been linked previously to GV production in S39006. After the transposon insertion location had been determined, the transposon was transduced from the original mutant back into S39006 wild type using the generalized transducing phage Φ OT8 (Evans et al., 2010). This simple transduction step was an important control to confirm that the difference in opacity observed in each mutant was caused by the transposon insertion rather than by any unknown, random mutation. The transposon was also transduced back into strain NWA19 to confirm the GV phenotype was as expected, and into GPA1 and GRA transcriptional fusion strains for use in assays of the impacts of the transposon insertions on regulation of either of the two GV operons. The names given to each mutant before and after transduction are given in Table 3.1, from this point on, all work was performed using strains that had the transposon transduced into the “clean” wild type background so any effect on prodigiosin production could be observed.

First PCR:



Second PCR:

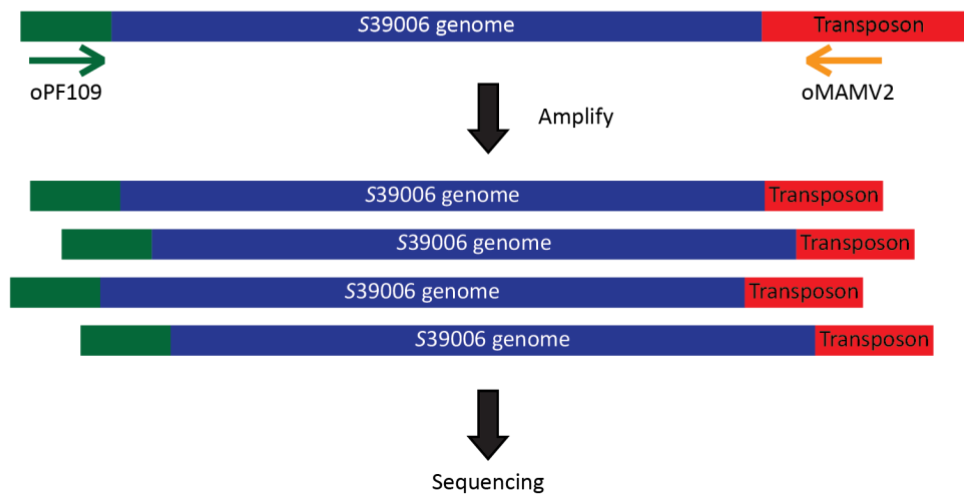


Figure 3.3 – Determination of the transposon insertion location using random primed PCR. In the first PCR oligonucleotide primers oPF106, 107 and 108 anneal randomly throughout the S39006 genome. This, in combination with the transposon-specific oligonucleotide oMAMV1, allowed for amplification of a region bordering the transposon insertion. The resulting DNA was then used as a template for a second PCR using the adaptor oligonucleotide oPF109 and a second transposon-specific oligonucleotide oMAMV2.

Table 3.1 – Transposon insertion sites in S39006 $\Delta pigC$ gas vesicle mutants.

Mutant	GV Phenotype	Insertion Site	Predicted Function	Transduced Name
AMH1	Intermediate	<i>orf6410</i>	IcIR family transcriptional regulator	AMH101
AMH2 [†]	Intermediate	<i>orf2785</i>	4' phosphopantetheinyl transferase	AMH105
AMH3	Translucent	<i>rpoN</i>	RNA polymerase sigma factor, σ^{54}	AMH109
AMH4	Bull's-eye	<i>waal</i>	O-antigen ligase family protein	AMH113
AMH5	Translucent	<i>pigP</i>	Global regulator of prodigiosin and carbapenem production	AMH117
AMH6	Hyper	<i>cyaA</i>	Class I adenylate cyclase	*
AMH7 [†]	Intermediate	<i>orf2785</i>	4' phosphopantetheinyl transferase	AMH121
AMH8	Translucent	<i>hfq</i>	RNA chaperone, Hfq	AMH125
AMH9	Hyper	<i>ratB</i>	RnfH family protein	AMH129
AMH10	Intermediate	<i>orf6410</i>	IcIR family transcriptional regulator	AMH133
AMH11	Intermediate	<i>orf6410</i>	IcIR family transcriptional regulator	AMH137
AMH12	Translucent	<i>dksA</i>	RNA polymerase-binding transcription factor, DksA	AMH141
AMH13 ^{**}	Translucent	<i>gvpN</i>	Gas vesicle protein GvpN	AMH145
AMH14 ^{**}	Translucent	<i>gvpC</i>	Gas vesicle structural protein GvpC	AMH149
AMH15	Translucent	<i>gvrA</i>	Gas vesicle regulatory protein GvrA	AMH153
AMH16	Bull's-eye	<i>waal</i>	O-antigen ligase family protein	AMH157
AMH17	Intermediate	<i>proQ</i>	RNA chaperone, ProQ	AMH161
AMH18	Translucent	<i>gvrB</i>	Gas vesicle regulatory protein GvrB	AMH165
AMH19	Hyper	<i>orf17860</i>	NAD-dependent epimerase	AMH169

[†]AMH2 and AMH7 were from the same conjugation, the transposon insertion locations are identical.

*Attempts to transduce the transposon in AMH6 were unsuccessful.

**Indicates transposon insertion was located upstream of the open reading frame.

Transposon insertions were found in four genes in the gas vesicle cluster: *gvpC*, *gvpN*, *gvrA*, and *gvrB*. Mutants with transposon insertions in each of these genes had a translucent colony phenotype. This was expected given that the transposon contains a transcriptional terminator, preventing transcription of the rest of the relevant gas vesicle operon, both of which contain genes essential for gas vesicle production (Tashiro et al., 2016). Other previously identified regulatory genes included *pigP* and *cyaA* (Lee, 2019; Quintero-Yanes, 2019). The RNA chaperone Hfq has also been studied in S39006 but has not previously been identified in a transposon mutagenesis of this strain and has not been linked to gas vesicle production (Wilf et al., 2013, 2011). The *waal* gene encoding an O-antigen ligase family protein was identified by a previous lab member and partially characterized, however, many unanswered questions remained (Quintero-Yanes, 2019). This mutant is further investigated in Chapter 4 due to the unusual phenotype as a strain that makes gas vesicles but is unable to float. The identification of a mixture of known regulators, gas vesicle structural genes, and “novel” genes confirmed that the screen was functioning correctly and that the new results were valid.

Of the 19 mutants where the transposon location was identified, 11 had the transposon inserted into a gene not previously linked to gas vesicle production in S39006. A few mutants were found with the transposon inserted into the same gene, therefore eight genes in total not previously linked to gas vesicle production were identified. In addition to the aforementioned *hfq*, novel genes included *orf6410*, *orf2785*, *rpoN*, *ratB*, *dksA*, *proQ*, and *orf17860*. After identifying the transposon insertion locations and transducing the transposons into a clean genetic background a representative of each of these genes was assayed to determine how disruption of these genes affected flotation and GV production. Two mutants in particular, AMH109 and AMH141 with transposon insertions in *rpoN* and *dksA* respectively are investigated in greater detail in Chapters 5 and 6.

3.2.3 Novel GV regulators show differences in flotation ability

The initial screen for regulators of gas vesicle production was carried out in the prodigiosin deficient strain, NWA19. The transposon insertions in these putative regulatory mutants were then transduced back into wild type S39006 to determine if there was any difference in prodigiosin production in addition to gas vesicle production. Flotation assays, spot tests

and PCM were performed for each of the novel gas vesicle mutants identified in the screen to visualise changes in GV production (Figure 3.4).

These mutants were initially classed as either translucent, intermediate, or hyper producers of gas vesicles. The *hfq* mutant, AMH125, was classified as translucent based on colony appearance. Consistent with this classification, it did not float to the same degree as wild type and there are no bright spots in PCM images of the cells. The flotation ability of this strain was closer to that of the negative control GPA1 than wild S39006. In section 3.2.7 this mutant is further investigated to determine if the pleiotropic effects seen in a S39006 *hfq* knockout mutant are consistent with those seen in this transposon insertion mutant.

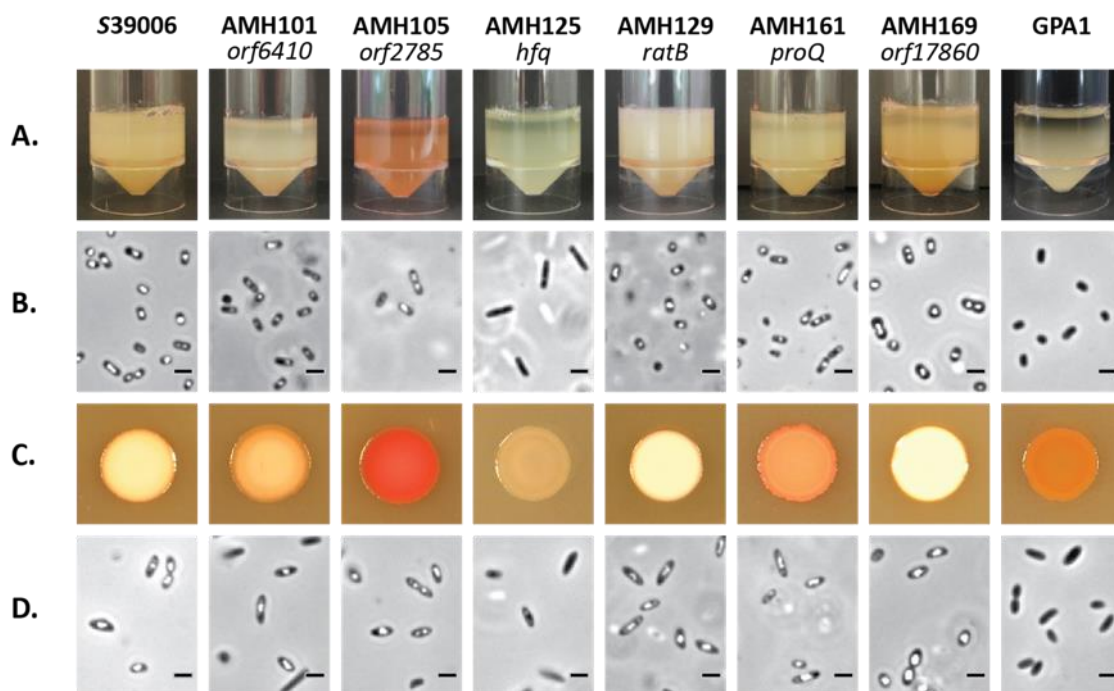


Figure 3.4 – Flotation and spot test assays for novel GV regulators with accompanying PCM images.

Novel GV regulators identified in a RTM screen were transduced into the wild type S39006 background to give the strains shown above. The gene in which the transposon inserted was indicated in italics below each strain name with S39006 and GPA1 shown in the first and last columns as positive and negative controls respectively. Flotation assays were imaged after 48 hours static culture at room temperature and are shown in row A. Row B shows PCM image of cells from the flotation assay above. Spot tests are of normalised OD₆₀₀, grown for 48 h at 30 °C and shown in row C. Row D shows PCM images of cells from the spot test immediately above.

Three of the mutants of interest were initially classified as intermediate producers of gas vesicles, meaning that as colonies on agar plates they appeared less opaque than wild type but not fully translucent. AMH101, AMH105, and AMH161 were shown to have transposon insertions in the genes *orf6410*, *orf2785*, and *proQ* respectively. The flotation assays for these strains showed a slight decrease in flotation, as seen by a layer of culture more thinly populated by the bacteria towards the air-liquid interface, when compared to wild type. However, this effect is much less pronounced than AMH125 or the negative control GPA1. In addition to this, there were early indications of pleiotropy in AMH101 and AMH105 which are explored in greater detail in sections 3.2.4 and 3.2.5, the most obvious of which is the overproduction of prodigiosin in AMH105, an unexpected observation given it was originally identified in a prodigiosin deficient strain.

Two mutants were initially classified as hyper producers of gas vesicles, AMH129 and AMH169. It is difficult to quantify the amount of gas vesicles produced in any given strain based solely on PCM images, however in a flotation assay AMH129 in particular appeared to float at least as well, if not better than wild type S39006. In contrast, AMH169, although initially identified as a hyper producer did not exhibit the same level of flotation ability as wild type or AMH129. Although some of the differences in flotation were clear across the gas vesicle mutants, others were much more subtle. Therefore, other techniques were used, outlined further in chapters 4-6, to study in much greater detail the gas vesicle production of the three key mutants of interest investigated in this study. In addition to this, four mutants of interest were briefly interrogated to determine if there were any pleiotropic effects of the relevant transposon insertion. These mutants, with transposon insertions in *orf6410*, *orf2785*, *ratB*, and *hfq* are detailed in subsequent sections with information about their genomic context and effects on antibiotic production, motility and plant cell wall degrading enzyme production also presented.

3.2.4 IclR family transcriptional regulator, Orf6410

Transposon insertions in the gene *orf6410* were identified in three mutants, AMH101, AMH133, and AMH137, all from independent conjugations. These mutants were identified as intermediate producers of gas vesicles and had diminished flotation ability compared to wild type (Figure 3.4). Further investigation of the genomic context and the gene itself

revealed that *orf6410* is predicted to encode a 255 amino acid IclR family transcriptional regulator that contains a helix-turn-helix domain and an effector binding domain (Figure 3.5). These domains are consistent with the classification as an IclR family transcriptional regulator (Molina-Henares et al., 2006). Of the three transposon insertions, two were located within the helix-turn helix domain (AMH101 and AMH133) and one within the effector binding domain (AMH137). Based on the similarity of this region to that of other organisms, *orf6410* is predicted to be at the end of a five-gene operon and may play a role in the regulation of the three gene operon immediately downstream (*orf6395-orf6405*) (Shimada et al., 2017). As *orf6410* does not have any genes immediately downstream of it that could be co-transcribed, the transposon insertion would not have any polar effects.

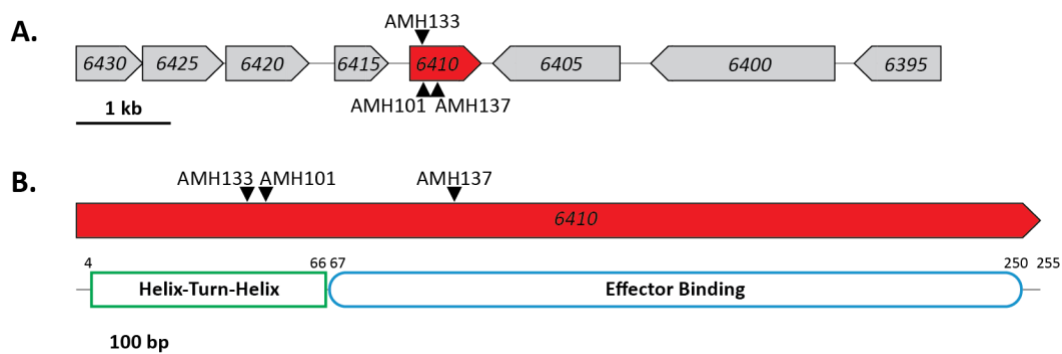


Figure 3.5 – Organisation of genes surrounding the AMH101, AMH133, and AMH137 transposon insertion sites.

(A) The transposons were inserted in *orf6410*, highlighted in red, the location of each insertion is shown by a black triangle. (B) The predicted protein domains of Orf6410, the numbers above indicate the amino acid position of the start and end of each domain.

A BLASTP search found that strains with the highest degree of amino acid sequence similarity and identity belonged to other IclR family transcriptional regulators from *Brenneria* and *Pectobacterium* species (Tables 3.2 and 3.3). A broader search found that the predicted protein had a shared identity of 66% (87% similarity) with the XynR protein from *E. coli* K12 and 38% identity (75% similarity) with the KdgR protein from *Dickeya chrysanthemi*. The XynR protein has been characterized as a regulator of the xylonate catabolism enzymes YagE and YagF, encoding xylonate dehydratase and 2-keto-3-deoxygluconate aldolase respectively (Shimada et al., 2017). The genomic organisation of this region in S39006 is comparable to that of *E. coli* with the proteins predicted to be encoded by *orf6395* sharing 62% identity with YagE and *orf6400* sharing 77% identity to

YagF. In *Dickeya chrysanthemi* (formerly *Erwinia chrysanthemi*), KdgR is responsible for the repression of genes involved in the degradation of pectin (Nasser et al., 1992; Reverchon et al., 1991). As S39006 is a known to make pectate lyase and cellulase and is capable of causing rot in potatoes (Slater et al., 2003), it is possible that *orf6410* may be partly responsible for the regulation of these plant cell wall degrading enzymes, due to its similarity to KdgR in other plant pathogens.

Table 3.2 – Amino acid sequence similarity search of Orf6410 using BLASTP.

Species	Identity (%)	Similarity (%)	Accession Number
<i>Brenneria alni</i>	86	94	WP_121572665.1
<i>Brenneria sp. hezel4-2-4</i>	85	94	WP_172291118.1
<i>Brenneria sp. L3-3C-1</i>	85	94	WP_199378489.1
<i>Brenneria sp. CFCC 11842</i>	84	94	WP_136166158.1
<i>Pectobacterium wasabiae</i>	84	94	WP_005975072.1
<i>Pectobacterium parmentieri</i>	83	94	WP_103807983.1

Table 3.3 – Predicted function of genes surrounding *orf6410*.

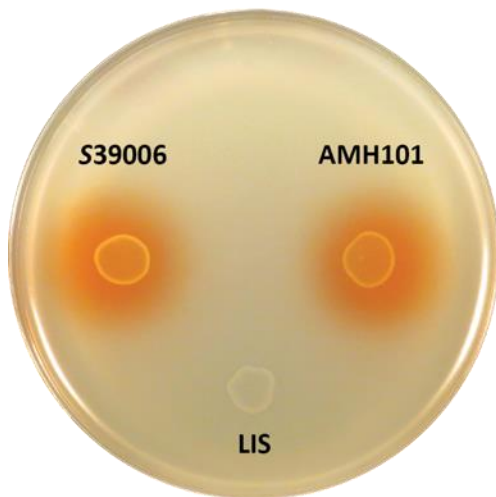
ORF	Size (bp)	Predicted Function	Species/Strain	Identity (%)	Similarity (%)
<i>orf6430</i>	705	ABC Transporter ATP-binding protein	<i>Dickeya zeae</i>	74	85
<i>orf6425</i>	855	Metal ABC Transporter permease	<i>Lonsdalea britannica</i>	87	92
<i>orf6420</i>	879	Metal ABC Transporter substrate-binding protein	<i>Pectobacterium aquaticum</i>	82	90
<i>orf6415</i>	567	TIGR00730 family Rossmann fold protein	<i>Dickeya sp. NCPPB 3274</i>	70	87
<i>orf6410</i>	768	IcIR family transcriptional regulator	<i>Brenneria alni</i>	86	94
<i>orf6405</i>	1347	Gluconate permease	<i>Brenneria alni</i>	87	93
<i>orf6400</i>	1968	YjhG/YagF family D-xylonate dehydratase	<i>Brenneria sp. CFCC 11842</i>	88	94
<i>orf6395</i>	918	Dihydrodipicolinate synthase family protein	<i>Brenneria alni</i>	83	91

As homologues of *orf6410* have been linked to the regulation of pathways distinct from gas vesicle production, any pleiotropic effects of the transposon insertion were investigated by first performing a series of plate assays shown in Figure 3.6. These assays utilise different agars or top lawns to determine the production of the quorum sensing signalling molecule BHL, the carbapenem antibiotic, pectate lyase, and cellulase as well as swarming and swimming motility. AMH101 showed no change in production of the quorum sensing signalling molecule BHL but had markedly reduced production of the β -lactam antibiotic carbapenem (Figure 3.6A & B), both of these assays also show a negative control strain. This indicates that *orf6410* positively regulates the production of the carbapenem antibiotic.

There appears to be no difference in pectate lyase production in AMH101 compared to wild type and only very slight differences in cellulase production based on the spot test assays of Figure 3.6 C & D. Quantitative spectrophotometric assays to determine pectate lyase and cellulase production might show a greater difference in PCWDEs in this strain, or it might be that the plate conditions are not appropriate for the expression of *orf6410*. Future experiments in a potato model would be interesting to determine if there is any difference in the virulence of this strain compared to wild type. However, AMH101 was hyper-motile compared to wild type S39006. This was seen most obviously in the swarming assay although an increase in swimming motility was also observed (Figure 3.6 E & F).

Due to time constraints, no further experiments were performed on the *orf6410* mutants however there is definite scope for further investigation into the mechanism through which this gene is able to repress gas vesicles and flagellar motility while also activating production of the carbapenem antibiotic. Any changes in virulence in plant and animal models would also be of interest based on the known effects of similar mutations on virulence in other bacteria.

A. BHL



B. Carbapenem



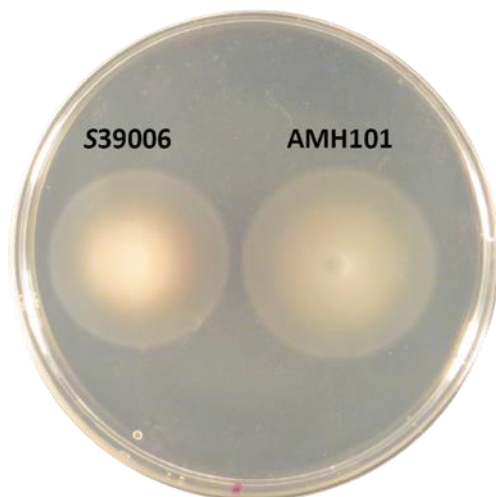
C. Pectate Lyase



D. Cellulase



E. Swimming



F. Swarming



Figure 3.6 – The transposon insertion in *orf6410* is pleiotropic.

Overnight cultures of the indicated strains were adjusted to an OD_{600} of 1 (A – D) or 0.2 (E & F) and spotted onto different agar plates to assay the production of BHL (A), carbapenem (B), pectate lyase (C) and cellulase (D). Swimming (E) and swarming (F) motility were also assayed. LIS and MCA54 act as negative controls for the production of BHL and carbapenem respectively.

3.2.5 4' Phosphopantetheinyl transferase, Orf2785

Another mutant of interest identified in the initial screen for gas vesicle mutants was AMH105. This strain contained a transposon insertion in *orf2785* which is predicted to encode a 4' phosphopantetheinyl transferase (4' PPTase). PPTases form part of non-ribosomal peptide synthetases, fatty acid synthases, and polyketide synthases and carry out post-translational modifications of acyl carrier protein domains, activating them (Lambalot et al., 1996). Specifically, 4' PPTases are responsible for the transfer of the 4'-phosphopantetheinyl moiety of coenzyme A to a conserved serine residue in the acyl carrier protein domain (Lambalot et al., 1996). The transposon was found 18 bp into the 726 bp gene, just before the start of the 4' PPTase domain (Figure 3.7). A transmembrane helix is predicted from amino acids 44 – 63 of Orf2785, with the region preceding the helix annotated as a cytoplasmic domain and the C-terminal predicted to be a non-cytoplasmic domain.

The *orf2785* gene does not appear to be part of an operon, and as such there are no polar effects expected from the transposon insertion. This gene shares a high degree of similarity and identity to other predicted 4' PPTases from various *Dickeya* species (Table 3.4). Surrounding genes also share a high degree of similarity to genes from closely related species including *Brenneria*, *Dickeya*, and *Pectobacterium* species (Table 3.5). The 4' PPTase encoded by *orf2785* shares 35.5 % identity with the uncharacterised YieE protein from *E. coli* K12. A search of the analogous region in *E. coli* shows some similarities with the presence of *adeP* (encoding a NCS2 permease) and *yieH* in the same location and orientation of *orf2780* and *yieH* in S39006.

This mutant was originally identified as an intermediate producer of gas vesicles but upon transduction of the transposon insertion from the original $\Delta pigC$ background to the wild type background it became clear that this mutant was a hyper producer of prodigiosin. This prompted a further investigation any pleiotropic impacts of the transposon insertion in *orf2785* (Figure 3.8) and quantification of the extent of the prodigiosin hyper-production (Figure 3.9).

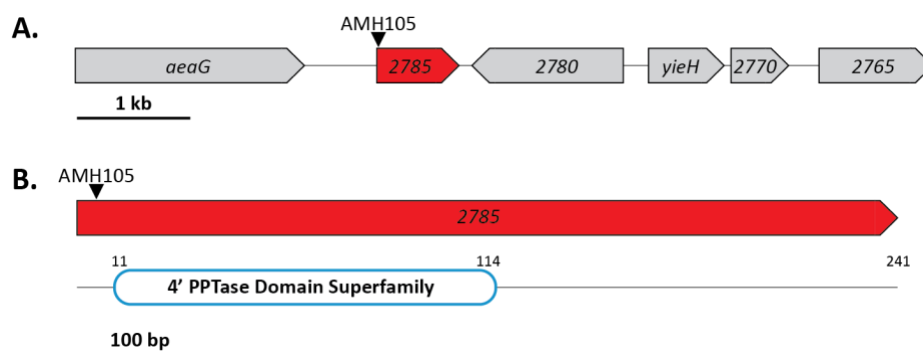


Figure 3.7 – Organisation of genes surrounding the AMH105 transposon insertion site.

(A) The transposon was inserted in *orf2785*, highlighted in red, the exact location of the transposon is indicated by a black triangle. (B) The predicted protein domains of Orf2785, the numbers above indicate the amino acid position of the start and end of each domain.

Table 3.4 – Amino acid sequence similarity search of Orf2785 using BLASTP.

Species	Identity (%)	Similarity (%)	Accession Number
<i>Dickeya dianthicola</i>	83	91	WP_024107899.1
<i>Dickeya zeae</i>	83	91	WP_019844262.1
<i>Dickeya dadantii</i>	83	91	WP_038924402.1
<i>Dickeya undicola</i>	83	90	WP_033568178.1
<i>Dickeya chrysanthemi</i>	83	90	WP_040003222.1
<i>Dickeya aquatica</i>	81	90	SLM65207.1

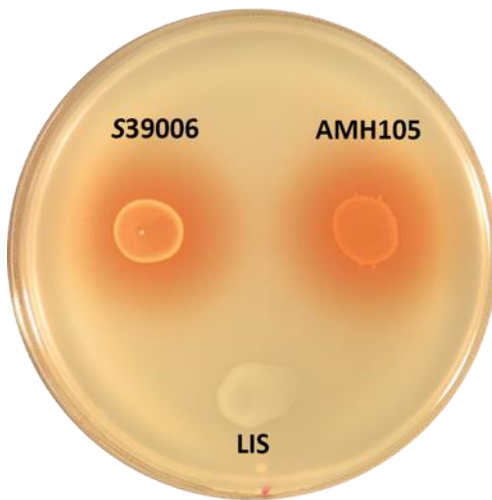
Table 3.5 – Predicted function of genes surrounding *orf2785*.

ORF	Size (bp)	Predicted Function	Species/Strain	Identity (%)	Similarity (%)
<i>aegA</i>	2025	Formate-dependent uric acid utilisation protein	<i>Brenneria roseae</i>	81	89
<i>orf2785</i>	726	4'-phosphopantetheinyl transferase	<i>Dickeya dianthicola</i>	83	91
<i>orf2780</i>	1338	NCS2 family permease	<i>Dickeya dianthicola</i>	90	95
<i>yieH</i>	669	6-phosphogluconate phosphatase	<i>Pectobacterium brasiliense</i>	75	85
<i>orf2770</i>	510	Lrp/AsnC ligand binding domain-containing protein	<i>Brenneria alni</i>	92	97
<i>orf2765</i>	1017	1-aminocyclopropane-1-carboxylate deaminase	<i>Brenneria alni</i>	97	98

To determine if there were any further pleiotropic effects of the transposon insertion in *orf2785* plate assays were carried out, similar to those performed for AMH101. Spot tests comparing the production of BHL and carbapenem showed no obvious differences between wild type S39006 and the *orf2785* transposon insertion mutant AMH105 (Figure 3.8 A & B). Similarly, pectate lyase and cellulase production halos showed only minor differences that were partly the result of spots of AMH105 culture spreading more than wild type spots (Figure 3.8 C & D). The most obvious differences, other than the prodigiosin phenotype already mentioned, were in the motility assays. Both swimming and swarming motility was increased in AMH105 compared to wild type, and this is likely due, at least in part, to the overproduction of surfactant. A clear halo of surfactant could be observed circling both wild type and AMH105 colonies on swimming agar plates when viewed under the correct light conditions. Although difficult to see by photography the amount of surfactant produced by AMH105 far exceeded that made by wild type.

The amount of prodigiosin produced by AMH105 was quantified over the course of a growth curve and shown compared to wild type in Figure 3.9. Prodigiosin production was increased in this mutant from the start and reached a final level that was 7.8 times higher than the wild type. As this gene is predicted to encode a 4' PPTase, it is not expected that regulation of these phenotypes would occur at a transcriptional level and the exact mechanism is still unclear. However, it appears that the disruption of this gene allows for the more efficient production of prodigiosin and surfactant, perhaps by freeing up precursor molecules or shifting activity to a more efficient enzyme. In a transposon mutagenesis of *Serratia marcescens* 274 a transposon insertion in *pswP*, predicted to encode a PPTase, was responsible for the failure of prodigiosin and surfactant production, the opposite of what was observed here (Sunaga et al., 2004). Further investigation of this gene is required, including perhaps an assay of transcription of the prodigiosin gene cluster, through an mRNA assay or use of a *lacZ* fusion to determine whether or not these changes are occurring at a transcriptional or translational level.

A. BHL



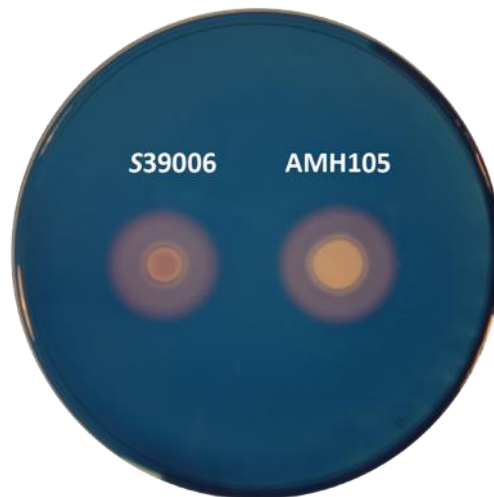
B. Carbapenem



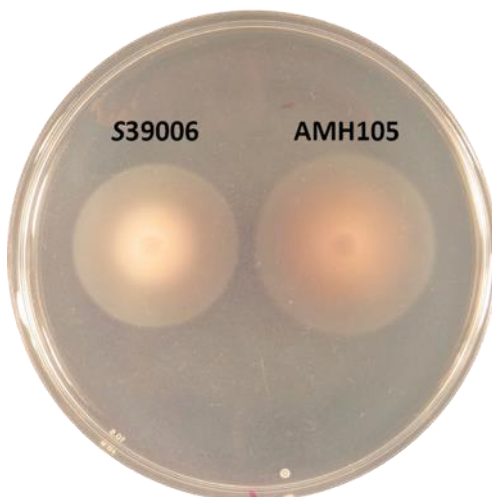
C. Pectate Lyase



D. Cellulase



E. Swimming



F. Swarming

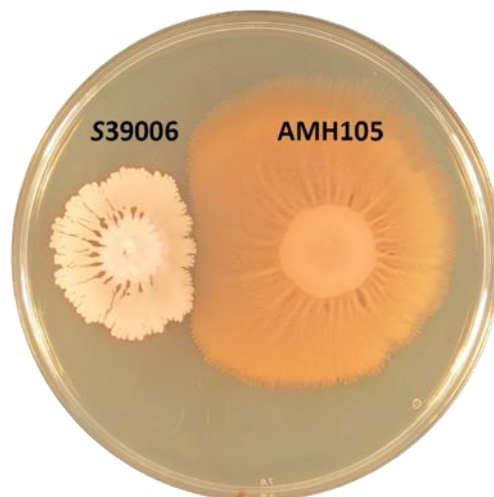


Figure 3.8 – The transposon insertion in *orf2785* is pleiotropic.

Overnight cultures of the indicated strains were adjusted to an OD_{600} of 1 (A – D) or 0.2 (E & F) and spotted onto different agar plates to assay the production of BHL (A), carbapenem (B), pectate lyase (C) and cellulase (D). Swimming (E) and swarming (F) motility were also assayed. LIS and MCA54 act as negative controls for the production of BHL and carbapenem respectively.

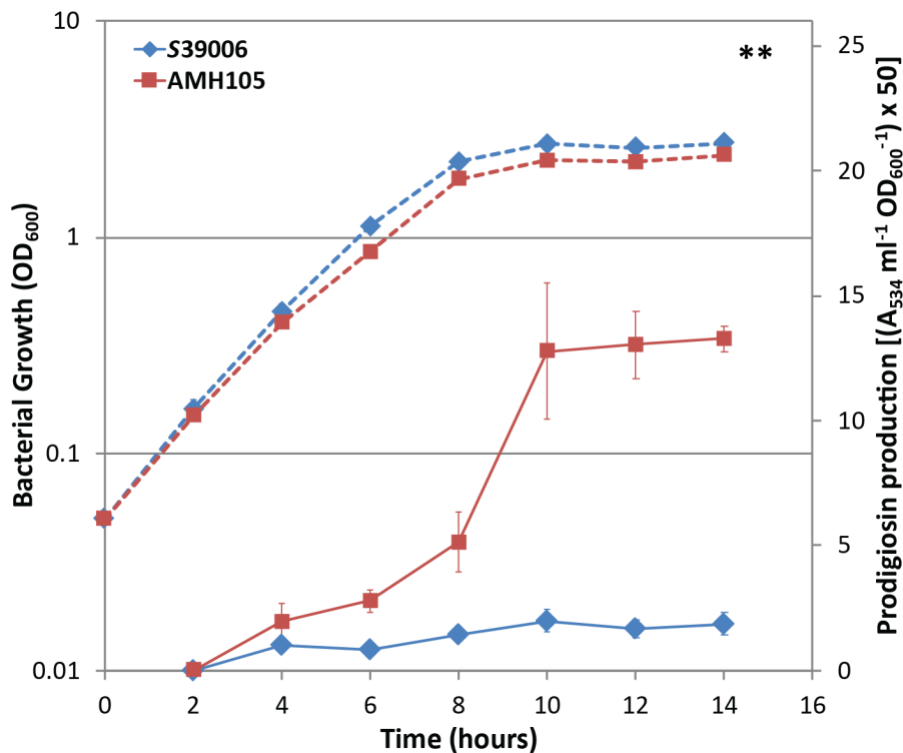


Figure 3.9 – Transposon insertion in *orf2785* significantly increases prodigiosin production. Prodigiosin production was measured over the course of a growth curve for S39006 (blue) and *orf2785* transposon mutant AMH105 (red). Solid lines indicate prodigiosin production while dashed lines show OD₆₀₀ measurements. Data shown are the mean values \pm SD (n = 3), asterisks indicate p-values comparing prodigiosin production between strains: *, p < 0.05; **, p < 0.01; ***, p < 0.001; NS, not significant.

3.2.6 RnfH family protein, RatB

In addition to the identification of various intermediate gas vesicle producers outlined in sections 3.2.4 and 3.2.5, a hyper opaque mutant was found and investigated in greater detail. AMH129 was shown to have a transposon insertion in the uncharacterized gene *orf21060*, predicted to encode an RnfH family protein. The RnfH family is part of the ubiquitin superfamily, genes encoding these proteins tend to be found near *smfB* or are part of a membrane associated complex transporting electrons for reactions including nitrogen fixation (Iyer et al., 2006). Based on the similarity of this region and the predicted protein products, this gene was renamed *ratB*, as it is positioned directly downstream of a homologue of the gene encoding a ribosome associated toxin, RatA, in *E. coli*. *ratB* is predicted to be the second gene of a two gene operon with *ratA* and as such no polar effects of the transposon insertion were expected. The transposon was inserted 122 bp into the 285 bp gene. Figure 3.10 shows the genomic context surrounding the operon, with the protein domains of RatA and RatB also shown.

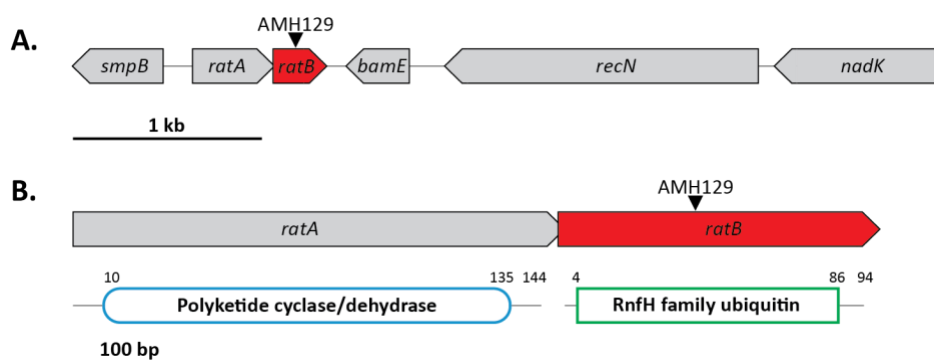


Figure 3.10 – Organisation of genes surrounding the AMH129 transposon insertion site.

(A) The transposon was inserted in *ratB*, highlighted in red, the exact location of the transposon is indicated by a black triangle. (B) The predicted protein domains of RatB, the numbers above indicate the amino acid position of the start and end of each domain.

Table 3.6 – Amino acid sequence similarity search of RatB using BLASTP.

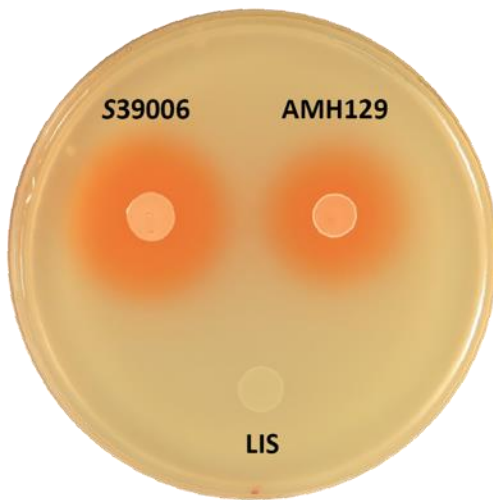
Species	Identity (%)	Similarity (%)	Accession Number
<i>Pectobacterium brasiliense</i>	81	92	WP_180791218.1
<i>Dickeya dadantii</i>	81	92	WP_013316583.1
<i>Chimaeribacter coloradensis</i>	81	94	WP_101824540.1
<i>Serratia rubidaea</i>	81	90	WP_126531634.1
<i>Pectobacterium parmentieri</i>	80	91	WP_012822682.1
<i>Samsonia erythrinae</i>	80	93	WP_132454406.1

Table 3.7 – Predicted function of genes surrounding *ratB*.

ORF	Size (bp)	Predicted Function	Species/Strain	Identity (%)	Similarity (%)
<i>smpB</i>	483	SsrA-binding protein SmpB	<i>Brenneria</i> sp. CFCC 11842	97	100
<i>ratA</i>	435	Type II toxin-antitoxin system RatA family toxin	<i>Pectobacterium</i> <i>fontis</i>	91	92
<i>ratB</i>	285	RnfH family protein	<i>Dickeya dadantii</i>	81	92
<i>bamE</i>	336	Outer membrane protein assembly factor BamE	<i>Lonsdalea britannica</i>	85	91
<i>recN</i>	1662	DNA repair protein RecN	<i>Brenneria roseae</i>	88	92
<i>nadK</i>	879	NAD(+) kinase	<i>Brenneria roseae</i>	88	94

The region surrounding *ratAB* is well conserved across enterobacteria, this can be seen in the high levels of identity and similarity in Tables 3.6 and 3.7. The order and orientation of these genes is conserved in *E. coli*, where the toxin RatA was first described. It is unclear whether RatAB is a functional toxin-antitoxin (TA) system in S39006. The induction of RatA in *E. coli* led to the inhibition of protein synthesis and purified RatA was shown to inhibit the formation of ribosomes in the presence of Mg^{2+} (Zhang & Inouye, 2011). However, there was no proof that any complex was formed between RatA and RatB, despite the prediction that the two encoded a type II TA system (Zhang & Inouye, 2011). Also, a *ratB* deletion strain has been isolated in the Keio collection, which suggests this gene is not essential, or at least not under normal laboratory conditions (Baba et al., 2006). A similar observation was made in S39006 where the putative antitoxin was disrupted by the transposon, but the putative toxin was left intact. There was a slight growth defect in this strain and the colonies on agar plates appeared smaller than wild type (Figure 3.12). The *ratAB* locus was studied in uropathogenic *E. coli* (where it was renamed *pasTI*) and was found to be critical for survival within the kidneys and enhanced persister cell formation (Norton & Mulvey, 2012). The authors also found that overexpression of the toxin was toxic, inducing bacterial stasis, but this could be rescued by over-expression of the antitoxin (Norton & Mulvey, 2012). This suggests that the RatAB could be a functional TA system, but it may only be functional under certain physiological conditions. However, a recent functional genomics screen of the S39006 TA systems did not identify the *ratAB* locus as a TA system (Hampton et al., 2020).

A. BHL



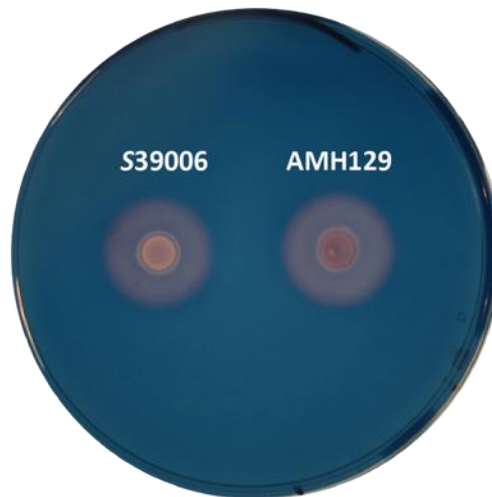
B. Carbapenem



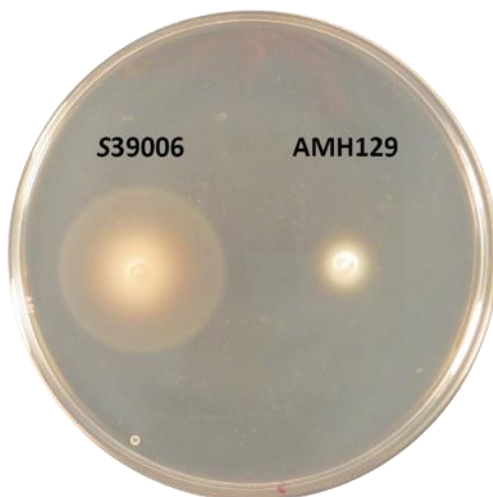
C. Pectate Lyase



D. Cellulase



E. Swimming



F. Swarming

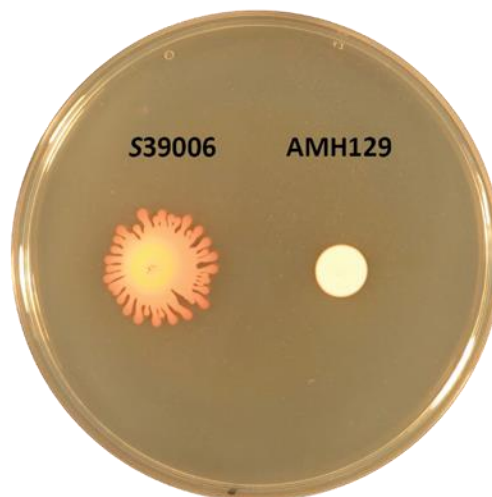


Figure 3.11 – The transposon insertion in *ratB* is pleiotropic.

Overnight cultures of the indicated strains were adjusted to an OD_{600} of 1 (A – D) or 0.2 (E & F) and spotted onto different agar plates to assay the production of BHL (A), carbapenem (B), pectate lyase (C) and cellulase (D). Swimming (E) and swarming (F) motility were also assayed. LIS and MCA54 act as negative controls for the production of BHL and carbapenem respectively.

AMH129, the *ratB* transposon insertion mutant, was screened to determine if there were any pleiotropic impacts of the disruption of this gene (Figure 3.11). There appeared to be a slight decrease in the amount of quorum sensing signalling molecule BHL produced, but an increase in carbapenem production (Figure 3.11 A & B). These assays can be confounded by differences in growth rates, and when these assays were performed over the course of a growth curve, there was no statistically significant difference in BHL production once corrected for OD₆₀₀ (Figure 3.12A). Over the course of a growth curve, carbapenem production was significantly increased in AMH129 compared to wild type (Figure 3.12B). There was a slight decrease in pectate lyase production however the most striking differences were in swimming and swarming motility (Figure 3.11 C – F). AMH129 showed nearly abolished swimming and no swarming ability, indicating that this gene, regardless of whether it is part of a functional TA system or not, has significant impacts on the physiology of S39006.

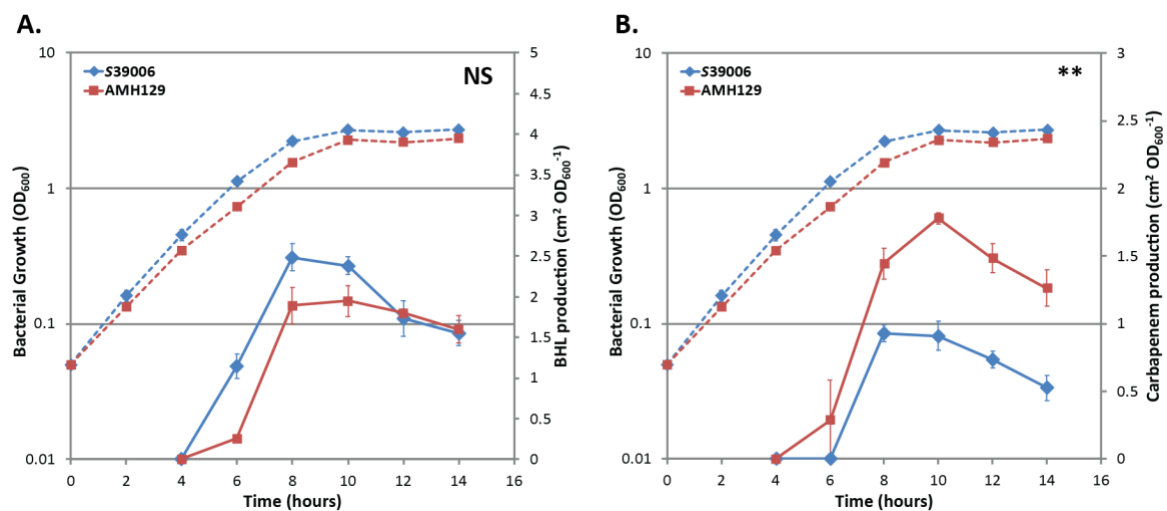


Figure 3.12 – Transposon insertion in *ratB* significantly increases carbapenem production. BHL (A) and carbapenem (B) production was measured over the course of a growth curve for S39006 (blue) and *ratB* transposon mutant AMH129 (red). Solid lines indicate BHL/carbapenem production while dashed lines show OD₆₀₀ measurements. Data shown are the mean values ± SD (n = 3), asterisks indicate p-values comparing BHL/carbapenem production between strains: *, p < 0.05; **, p < 0.01; ***, p < 0.001; NS, not significant.

3.2.7 RNA Chaperone, Hfq

The regulatory network of Hfq has been well characterised in many bacteria, including work in S39006 (Wilf et al., 2013, 2011). Hfq is an RNA chaperone involved in post-transcriptional regulation of various stress response and virulence pathways (Chao & Vogel, 2010). The genomic organisation of the *hfq* locus in S39006 is orthologous to that of *E. coli* (Figure 3.13, Tables 3.8 & 3.9). In *E. coli* transcription of *hfq* occurs from multiple promoter regions and *hfq* is co-transcribed with *hflX* immediately downstream (Tsui et al., 1996, 1994). This work represents the first time an *hfq* transposon insertion mutant was found in S39006, previous work characterised the effect of an engineered *hfq* knockout (Wilf et al., 2013, 2011). To determine if there were any polar effects of this transposon insertion (which contains a transcriptional terminator), a number of plate assays were carried out. Consistent with previously reported results, disruption of *hfq* saw no changes in BHL production but carbapenem and cellulase production was abolished completely, while pectate lyase production was greatly reduced (Figure 3.13 A – D). Similarly, swarming motility was abolished, and swimming motility was greatly reduced (Figure 3.13 E & F). The consistency of these results compared to those previously reported in an *hfq* deletion strain indicate that there are no polar effects of the transposon insertion on the phenotypes measured.

There was also no link made between disruption of *hfq* and changes in the flotation of S39006. As outlined earlier in this chapter, the transposon insertion caused *hfq* mutant strain AMH125 to appear translucent – as no gas vesicles were produced less light was refracted. There were no bright spots (“gas vacuoles”) observed when cells were viewed under PCM and in a static culture the cells sank compared to wild type (Figure 3.4).

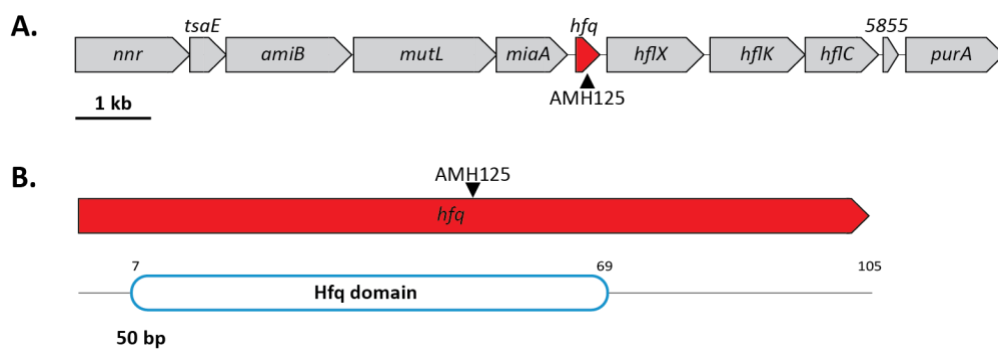


Figure 3.13 – Organisation of genes surrounding the AMH105 transposon insertion site.

(A) The transposon was inserted in *hfq*, highlighted in red, the exact location of the transposon is indicated by a black triangle. (B) The predicted protein domains of Hfq, the numbers above indicate the amino acid position of the start and end of each domain.

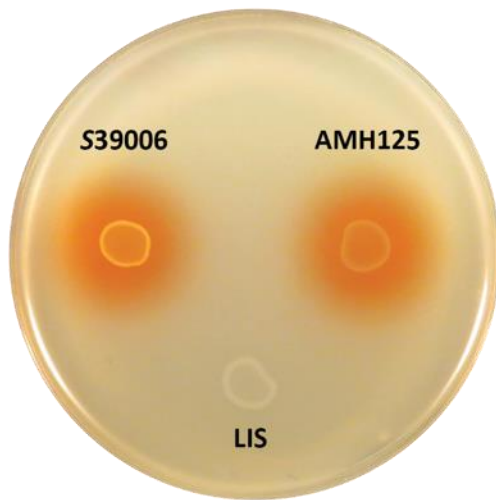
Table 3.8 – Amino acid sequence similarity search of Hfq using BLASTP.

Species	Identity (%)	Similarity (%)	Accession Number
<i>Yersinia pestis</i>	90	92	WP_016678432.1
<i>Brenneria salicis</i>	90	92	WP_113868200.1
<i>Yersinia ruckeri</i>	90	91	WP_038241862.1
<i>Yersinia pseudotuberculosis</i>	90	91	WP_129192835.1
<i>Serratia liquefaciens</i>	89	92	WP_048762802.1
<i>Yersinia enterocolitica</i>	89	90	WP_019080716.1

Table 3.9 – Predicted function of genes surrounding *hfq*.

ORF	Size (bp)	Predicted Function	Species/ Strain	Identity (%)	Similarity (%)
<i>nnr</i>	1530	Bifunctional ADP-dependent NAD(P)H-hydrate dehydratase/ NAD(P)H-hydrate epimerase	<i>Lonsdalea iberica</i>	78	85
<i>tsaE</i>	483	tRNA (adenosine(37)-N6)-threonylcarbamoyltransferase complex ATPase subunit type I TsaE	<i>Dickeya poaceiphila</i>	83	88
<i>amiB</i>	1665	N-acetylmuramoyl-L-alanine amidase AmiB	<i>Brenneria roseae</i>	71	79
<i>mutL</i>	1896	DNA mismatch repair endonuclease MutL	<i>Brenneria goodwinii</i>	76	83
<i>miaA</i>	942	tRNA (adenosine(37)-N6)-dimethylallyltransferase MiaA	<i>Brenneria sp. L3-3C-1</i>	87	93
<i>hfq</i>	318	RNA chaperone Hfq	<i>Yersinia pestis</i>	90	92
<i>hflX</i>	1281	GTPase HflX	<i>Brenneria sp. CFCC 1182</i>	91	95
<i>hflK</i>	1260	FtsH protease activity modulator HflK	<i>Dickeya chrysanthemi</i>	81	89
<i>hflC</i>	993	protease modulator HflC	<i>Lonsdalea iberica</i>	87	95
<i>orf5585</i>	201	DUF2065 domain-containing protein	<i>Brenneria goodwinii</i>	86	93
<i>purA</i>	1299	Adenylosuccinate synthase	<i>Brenneria roseae</i>	94	96

A. BHL



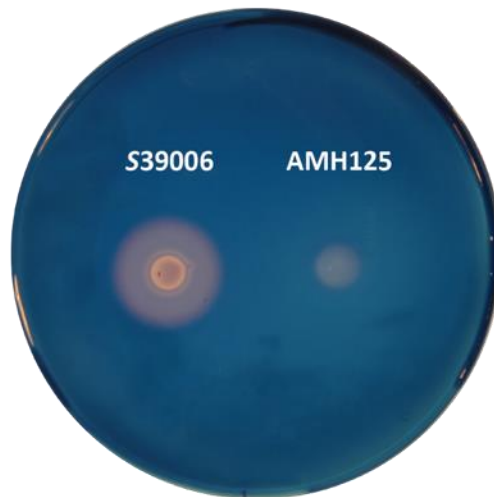
B. Carbapenem



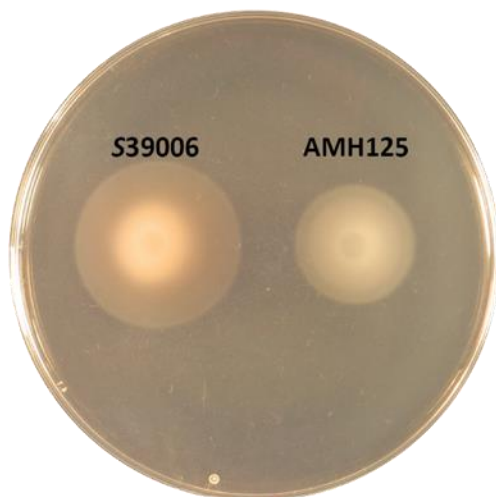
C. Pectate Lyase



D. Cellulase



E. Swimming



F. Swarming



Figure 3.14 – The transposon insertion in *hfq* is pleiotropic.

Overnight cultures of the indicated strains were adjusted to an OD_{600} of 1 (A – D) or 0.2 (E & F) and spotted onto different agar plates to assay the production of BHL (A), carbapenem (B), pectate lyase (C) and cellulase (D). Swimming (E) and swarming (F) motility were also assayed. LIS and MCA54 act as negative controls for the production of BHL and carbapenem respectively.

3.3 Discussion

This chapter has outlined the use of a random transposon mutagenesis screen to identify a panel of putative gas vesicle mutants in *S39006*. As previous screens had focused only on translucent mutants, this screen investigated mutants of varying colony appearances. Four interesting mutants were discussed in this chapter, with three key mutants discussed in chapters 4-6. The wide range of mutants that have been identified by the screen and the open avenues of investigation that could be pursued further are testimony to the relative paucity of information about the regulation of flotation and other key phenotypes in *S39006*. It also strongly implies that this screen has not been saturated and further, as yet unidentified, regulators of gas vesicle and secondary metabolite production remain undiscovered.

The regulatory network of *S39006* is clearly complex and our understanding of it is constantly expanding. Preliminary results from this chapter found that a protein homologous to repressors of xylonate and pectin degradation is involved in activating gas vesicle and carbapenem production while repressing flagellar motility. Further work to determine the impacts of xylonate on GV and secondary metabolite production would be interesting, particularly as other sugars have already been implicated in the gas vesicle regulatory network with the repressor of the ribose operon, RbsR, shown to activate gas vesicle production (Lee et al., 2017). Further work is also needed to understand how the disruption of a 4' PPTase and an RnfH family protein that may act as part of a toxin-antitoxin system are able to increase the production of prodigiosin and carbapenem respectively. Transcriptional fusions in the *pigA* and *carA* genes could be used to determine if these changes are taking place at a transcriptional level or post-transcriptionally. Although there is no evidence of a DNA binding function for these proteins they may act through one of a wide range of regulators that have already been characterised in *S39006*. Other key regulatory mutants are discussed in chapters 5 and 6 in much greater depth, with a comparative proteomic analysis carried out for the *rpoN* and *dksA* transposon mutants. Chapter 4 investigates the mechanism through which the 'bull's-eye' mutants are unable to float but can still produce gas vesicles.

Chapter 4. The O-antigen ligase, *WaaL*, is essential for flotation of S39006

4.1 Introduction

Chapter 3 described a random transposon mutagenesis screen for gas vesicle mutants in S39006. After screening over 80,000 mutants and performing random-primed PCR, the transposon insertion location was determined for 19 mutants. These mutants included previously identified regulators of gas vesicle production, genes in the gas vesicle cluster, and novel regulators that were assayed to determine if there were any pleiotropic effects of the transposon insertion. Several of these regulators were described in Chapter 3 and three genes of particular interest have been investigated in much greater detail. The first of these genes, *waaL*, is described in this chapter. The transposon insertion in *waaL* was identified twice in this screen, in two mutants isolated from independent conjugations, both of which had the distinctive ‘bull’s-eye’ appearance. This gene was identified as having importance in the regulation of flotation in S39006 by a previous lab member, however it was not characterized in any depth (Quintero-Yanes, 2019).

This chapter aims to understand how this gene is involved in flotation of S39006, what pleiotropic effects are caused by disruption of this gene, and how the O-antigen ligase impacts on the flotation process.

4.2 Results

4.2.1 Sequence analysis and genomic context of *waaL*

As previously mentioned, a transposon insertion was identified in the gene *waaL*, and caused the mutant to have an abnormal colony phenotype. This type of mutant, previously referred to as a ‘bull’s-eye’ mutant has been seen in previous screens, but was not thoroughly interrogated (Quintero-Yanes, 2019). The gene was originally referred to as *S39006_0591*, however, based on the amino acid sequence similarity of the predicted product to other O-antigen ligase proteins, the gene will be referred to as *waaL* in this work. The genomic context of this gene is shown in Figure 4.1A; *waaL* is the final gene of a three

gene operon. The upstream genes are predicted to encode two glycosyltransferase family proteins (a family 4 and a family 9 glycosyltransferase). Directly downstream of *waaL* is another divergently transcribed five gene operon, that is predicted to encode glycosyltransferases and heptosyltransferases. Both of these operons are predicted to be involved in the synthesis of lipopolysaccharide (LPS) in S39006.

The predicted function of each gene and the organisms sharing the highest amino acid sequence identity and similarity with each is detailed in Table 4.1. As is common with this strain, the sequences are most similar to various *Dickeya* species and share an identity level of 70-80%. Interestingly, the *waaD* gene, at the start of the second operon, shares a very high level of identity with *Serratia marcescens* (94%). S39006 was originally classified as a strain of *Serratia* (Parker et al., 1982) when deposited in the ATCC and later viewed as a *Serratia marcescens* strain, in part due to production of prodigiosin (Cox et al., 1998; Thomson et al., 1997). However, subsequent analysis considered S39006 to be an atypical *Serratia* (Harris et al., 2004) and more recent genome sequencing has suggested that S39006 is more closely related to *Dickeya* sp. than it is to other *Serratia* or *Pectobacterium* strains (Duprey et al., 2019; Fineran et al., 2013). Table 4.2 shows the other organisms that carry genes encoding proteins with high levels of identity and similarity to the amino acid sequence of WaaL. These are all various *Dickeya* species and, with ~68% identity, the sequence is reasonably well conserved between the species. This protein is predicted to include a Wzy_C domain, which is conserved amongst O-antigen ligases. As is indicated by the name, O-antigen ligases are integral to the synthesis of the O-antigen, the outermost component of LPS. Specifically, the O-antigen ligase catalyses the addition of polysaccharides to the lipid A core (Whitfield et al., 1997). The WaaL protein is also predicted to include 11 transmembrane helices, as shown in Figure 4.1B.

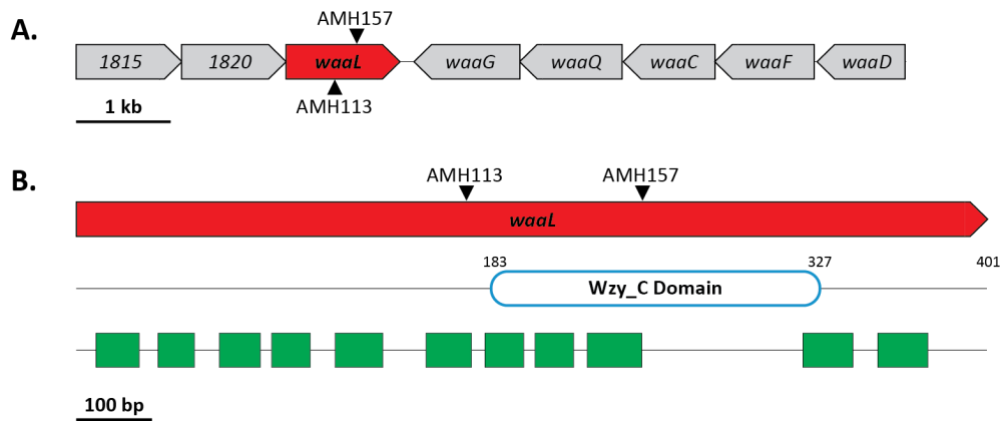


Figure 4.1 – Organisation of genes surrounding the AMH113 and AMH157 transposon insertion sites.

(A) The transposons were inserted in *waaL*, highlighted in red, the location of each insertion is shown by a black triangle. (B) The predicted protein domains of WaaL, the numbers above indicate the length of the protein in amino acids and the start and end of each domain. Transmembrane helices are represented by green boxes.

Table 4.1 – Predicted functions of genes surrounding *waaL*.

ORF	Size (bp)	Predicted Function	Species/Strain	Identity (%)	Similarity (%)
<i>orf1815</i>	1131	Glycosyltransferase family 4 protein	<i>Dickeya paradisiaca</i>	79	87
<i>orf1820</i>	1107	Glycosyltransferase family 9 protein	<i>Dickeya dadantii</i>	73	81
<i>waaL</i>	1206	O-antigen ligase family protein	<i>Dickeya chrysanthemi</i>	68	81
<i>waaG</i>	1121	Glycosyltransferase family 4 protein	<i>Dickeya chrysanthemi</i>	83	90
<i>waaQ</i>	1086	Lipopolysaccharide heptosyltransferase III	<i>Dickeya chrysanthemi</i>	88	94
<i>waaC</i>	972	Lipopolysaccharide heptosyltransferase WaaC	<i>Dickeya dadantii</i>	86	91
<i>waaF</i>	1053	ADP-heptose—LPS heptosyltransferase WaaF	<i>Dickeya dadantii</i>	85	91
<i>waaD</i>	933	ADP-glyceromanno-heptose 6-epimerase	<i>Serratia marcescens</i>	94	97

Table 4.2 – Amino acid sequence similarity search of WaaL using BLASTP.

Species	Identity (%)	Similarity (%)	Accession Number
<i>Dickeya chrysanthemi</i>	68	81	WP_027713466.1
<i>Dickeya fangzhongdai</i>	68	81	WP_038663487.1
<i>Dickeya sp. NCPPB 3724</i>	68	80	WP_042861533.1
<i>Dickeya dadantii</i>	67	80	WP_038912220.1
<i>Dickeya solani</i>	67	80	WP_022631695.1
<i>Dickeya paradisiaca</i>	66	82	WP_192456405.1

4.2.2 The *waaL* mutant produces gas vesicles but is unable to float

The transposon insertion in *waaL* was transduced from the screening strain NWA19 (a prodigiosin-deficient S39006 strain) into the wild type S39006 to confirm that the altered GV phenotype was the result of the transposon insertion. This enabled any possible impact of the transposon insertion on prodigiosin production to be determined. In a flotation assay AMH157 sank rapidly and completely, forming an aggregate at the bottom of the tube (Figure 4.2A). This lack of flotation was especially pronounced when compared to the gas vesicle negative strain GPA1 which has a transposon insertion in the first gene of the first GV operon, *gvpA1*. In PCM images taken of cells from this flotation assay, there was clear evidence that the cells still made GVs (Figure 4.2B). Phase bright structures (“gas vacuoles”) were clearly visible in all AMH157 and wild type cells, whereas the GPA1 negative control showed no bright spots. This unusual phenotype indicated that gas vesicles are necessary, but not sufficient, for flotation and so this mutant was investigated in greater detail. When viewed by microscopy AMH157 cells were found in clumps more often than seen in the wild type, something that was also noted by a previous lab member (Quintero-Yanes, 2019).

In a spot test using cells of normalised OD₆₀₀, the opacity of the *waaL* mutant strain AMH157 culture spot did not appear significantly different from the wild type S39006, and cells viewed by PCM showed the bright spots indicative of GVs (Figure 4.2C & D). However, during the initial mutagenesis screen, these mutants were chosen due to an unusual colony morphology that was characterised as a “bull’s-eye” morphology, where cells at the outer edge of the colony appeared less opaque than those in the middle. These cells also had an unusually fragile colony phenotype that characteristically would break apart rather than

smear when streaked out. For this reason, within the lab, they were referred to colloquially as “crunchy” mutants.

In addition to appearing as bright spots under PCM, individual GVs can also be visualised by TEM. AMH157 had gas vesicles clearly visible under TEM, further confirming what was observed under PCM (Figure 4.2E). To quantify this observation, a western blot using an antibody raised against GvpC (MW 18 kDa) was performed to determine whether there was more gas vesicle structural protein present in AMH157 compared to wild type (Figure 4.2F). There was a clear increase in the amount of GvpC detected in this assay in the *waaL* mutant compared to wild type, with nothing detected for the GPA1 negative control.

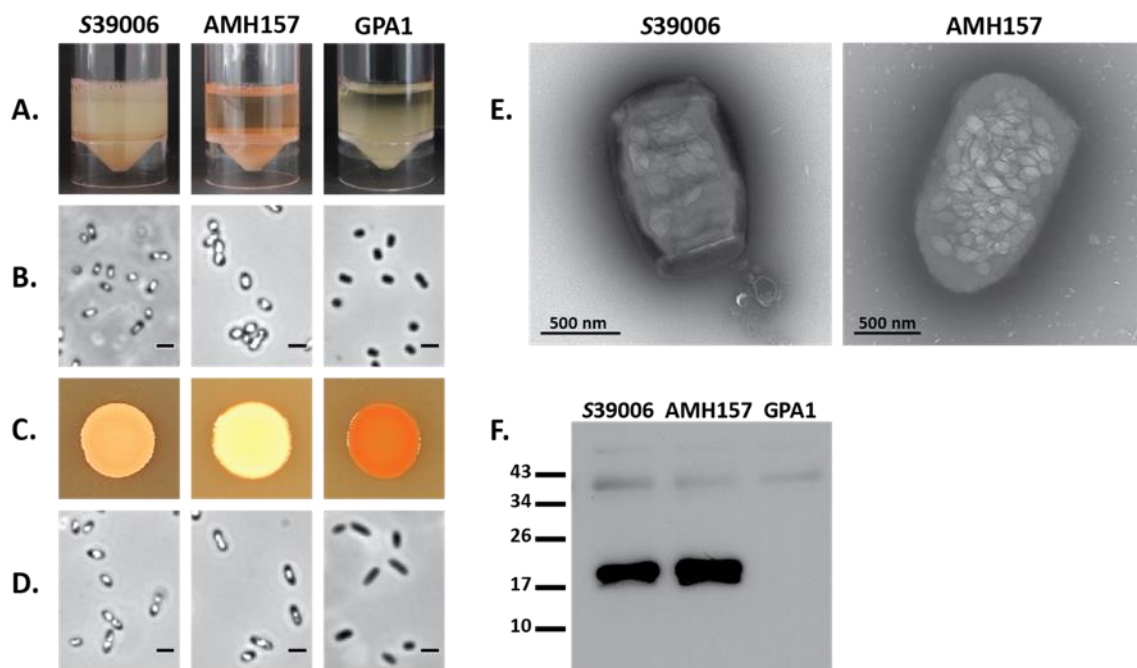


Figure 4.2 – Transposon insertion in *waaL* abolishes flotation and disrupts colony morphology. (A) Flotation assays for S39006, *waaL* transposon mutant AMH157, and gas vesicle negative control strain GPA1 after 48 h standing at room temperature. (B) PCM images from the flotation assay shown directly above, the scale bar indicates 1 μ m. (C) Spot tests of each strain with normalised cell number, grown for 48 h at 30 $^{\circ}$ C and associated PCM images directly below (D). (E) Representative TEM images showing AMH157 still made GVs. The S39006 image is also shown in Figure 5.2 and Figure 6.2. (F) Western blot using an antibody against GvpC, which has a molecular weight of 18 kDa.

The impact of the transposon insertion on transcription of the two operons of the GV cluster was assessed using *uidA* gene fusions in the initial gene of each operon, *gvpA1* and *gvrA*. The activity of β -glucuronidase (the product of the *uidA* gene) was used as a proxy for transcription of each operon over the course of a growth curve. These experiments were performed under aerobic and microaerophilic conditions, with a significant increase in transcription of *gvpA1* seen in both conditions (Figure 4.3A & C). This was consistent with the western blot shown above and the number of GVs seen in cells viewed under TEM. However, a loading control would be required to confirm any increase in protein production seen in the western blot. In contrast, when *gvrA* transcription was assessed there was a significant increase under aerobic conditions but no change in transcription under microaerophilic conditions (Figure 4.3B & D). There was no growth defect observed in the *waal* mutant, and all values were normalised to OD₆₀₀. GvrA is a known activator of transcription of the *gvpA1* operon (Ramsay et al., 2011). However, when any of *gvrA*, *gvrB*, or *gvrC* were overexpressed, as individual genes, this caused a decrease in transcription of *gvpA1* (Monson et al., 2016). It is therefore counter to our previous results to see an increase in both *gvrA* and *gvpA1* transcription at the same time. It is possible that the increase in expression of *gvrA* seen here is less than that caused by IPTG induction in the previous study, and as a result *gvrA* still had a positive impact on *gvpA1* expression. It remains unknown at what threshold *gvrA* might switch from an activator role and starts to repress *gvpA1* expression. An alternative explanation is that there is some unknown mechanism that is increasing transcription of the *gvpA1* operon independent of *gvrA* expression.

Previous work has shown that transcription of *gvpA1* was increased under microaerophilic conditions while no change in *gvrA* transcription was observed, leading to the hypothesis that the proteins encoded by the *gvrA* operon transduced the response to aeration (Ramsay et al., 2011). The level of *gvpA1* transcription observed in the late-exponential and stationary phases was approximately doubled in microaerophilic conditions compared to aerobic conditions for both wild type and AMH157 (Figure 4.3 A & C). The expression of *gvpA1* in microaerophilic conditions in the *waal* mutant is consistent with the wild type response to diminished oxygen, but simply at a higher level. However, this is inconsistent with the earlier hypothesis that an increase in *gvrA* expression was responsible for the

increased *gvpA1* expression seen in aerobic conditions. This suggests that the disruption of *waal* causes an increase in *gvpA1* expression in a *gvrA* and oxygen independent manner, while causing an oxygen-dependent increase in *gvrA* transcription.

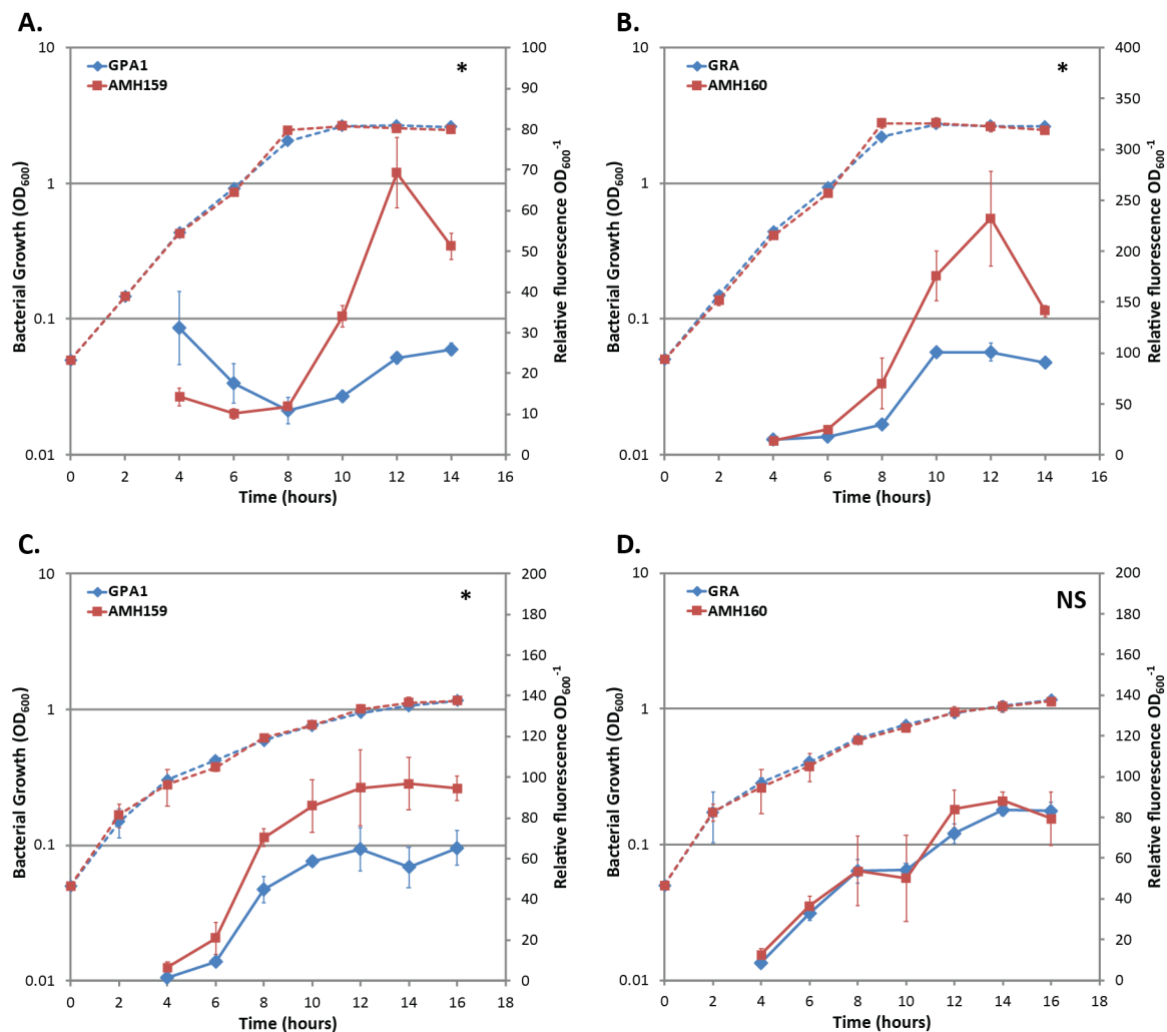


Figure 4.3 – *gvpA1* and *gvrA* expression in wild type and the *waal* mutant under aerobic and microaerophilic conditions.

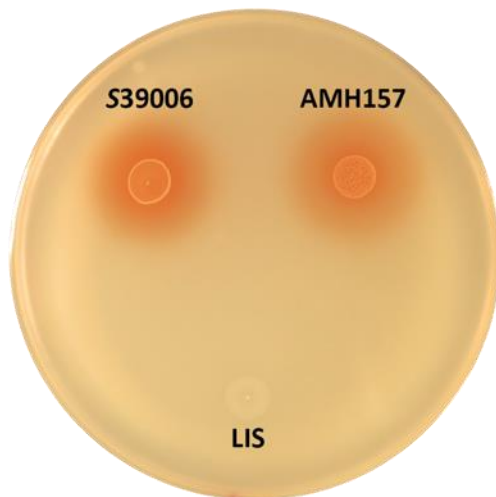
β -glucuronidase activity from a chromosomal *gvpA1::uidA* fusion was assayed in wild type (GPA1, blue) and *waal* transposon mutant backgrounds (AMH159, red) under aerobic (A) and microaerophilic (C) conditions. β -glucuronidase activity from a chromosomal *gvrA::uidA* fusion was assayed in wild type (GRA, blue) and *waal* transposon mutant backgrounds (AMH160, red) under aerobic (B) and microaerophilic (D) conditions. Solid lines indicate β -glu activity while dashed lines show OD₆₀₀ measurements. Data shown are the mean values \pm SD (n = 3), asterisks indicate p-values comparing β -glu activity: *, p < 0.05; **, p < 0.01; ***, p < 0.001; NS, not significant.

4.2.3 Mutation of *waal* causes diverse phenotypic impacts in S39006

S39006 produces two antibiotics (a carbapenem and a prodigiosin), along with pectate lyase and cellulase that degrade plant cell walls (Coulthurst et al., 2005; Fineran et al., 2007; Williamson et al., 2006). It is also motile via both swimming and swarming (Williamson et al., 2008). Most of these phenotypes are under quorum sensing control, via the signalling molecule, BHL (Thomson et al., 2000; Williamson et al., 2008). Previous work has shown that GV production is also under quorum sensing control, and that other regulators of GVs often have pleiotropic impacts on the phenotypes outlined above (Lee et al., 2017; Quintero-Yanes et al., 2020, 2019; Ramsay et al., 2011). The amount of QS signalling molecule produced by a strain can be quantified using the BHL detector strain SP19, which is unable to produce BHL itself but turns red in the presence of the molecule. The halo sizes shown in Figure 4.4A suggest that there was no detectable difference in BHL production and so this is unlikely to be the reason for the pleiotropic impacts of the transposon insertion observed. A similar assay was used to check for any difference in carbapenem production using the carbapenem sensitive strain ESS which is killed in the presence of the antibiotic. The relative amount of carbapenem produced can therefore be determined by the size of the halo of inhibition around the test strain. There appeared to be a difference in carbapenem production with a larger halo seen around AMH157 compared to wild type (Figure 4.4B).

In plate assays to determine the amount of PCWDEs produced no difference was observed in pectate lyase production, however cellulase detection plates showed increased production in AMH157 compared to wild type (Figure 4.4C & D). The transposon insertion in *waal* caused severe impacts on swarming and swimming motility with the strain unable to move across the surface of the swarming agar or through the swimming agar (Figure 4.4E & F). This strain could still be infected by the flagellum-dependent Φ OT8, therefore it is likely that AMH157 still makes flagella, but it is still unable to swim or swarm.

A. BHL



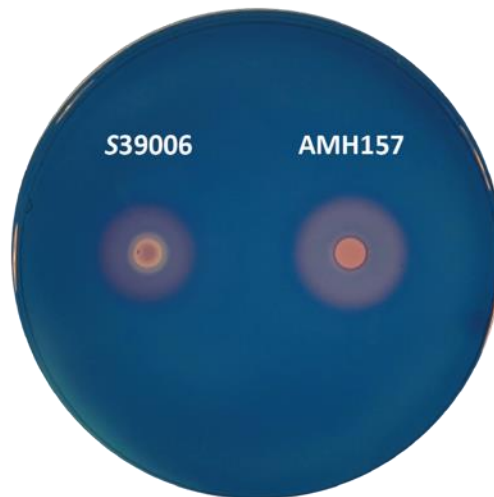
B. Carbapenem



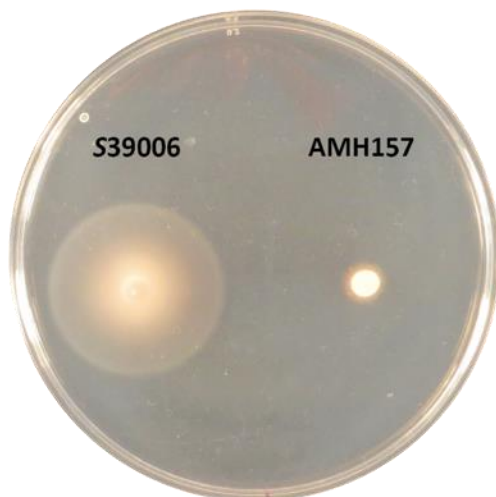
C. Pectate Lyase



D. Cellulase



E. Swimming



F. Swarming

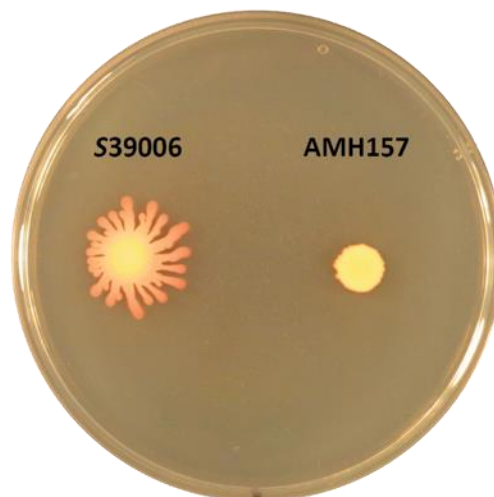


Figure 4.4 – The transposon insertion in *waal* is pleiotropic.

Overnight cultures of the indicated strains were adjusted to an OD_{600} of 1 (A – D) or 0.2 (E and F) and spotted onto different agar plates to assay the production of BHL (A), carbapenem (B), pectate lyase (C) and cellulase (D). Swimming (E) and swarming (F) motility were also assayed.

Based on the results of the carbapenem plate assay (Figure 4.4B) and previous observations that the *waaL* mutant cultures appeared more red than wild type cultures (Figure 4.2A), antibiotic production in AMH157 was quantified. The production of both antibiotics was measured throughout growth to determine if there was any significant difference in the amount of carbapenem or prodigiosin made in the *waaL* transposon insertion mutant. There was a significant increase in carbapenem production, possibly reflecting precocious induction compared to wild type (Figure 4.5A). Despite appearing more red in liquid cultures, there was no statistically significant difference in prodigiosin production between the two strains over the course of a 14 hour growth curve (Figure 4.5B).

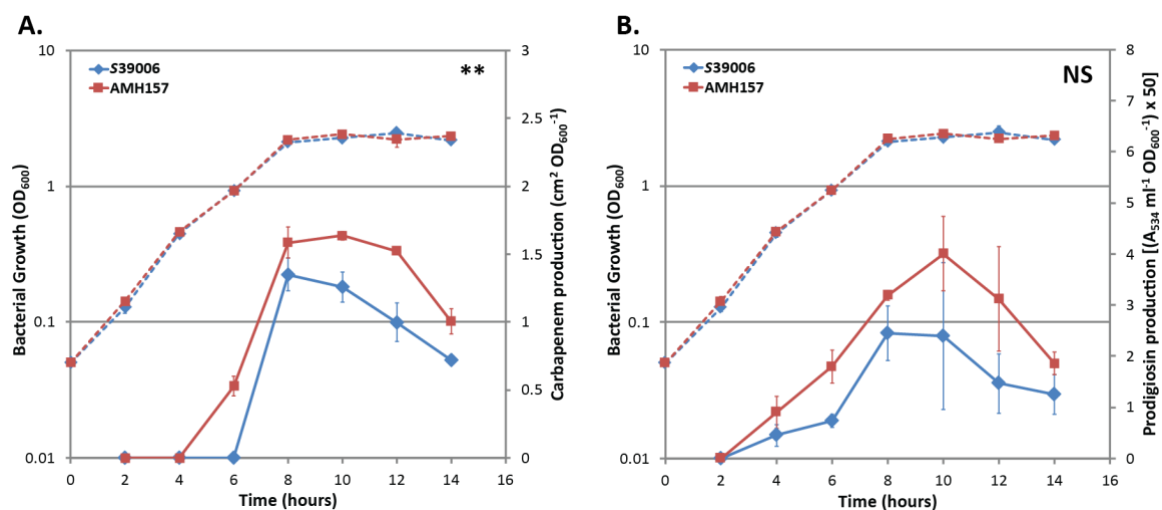


Figure 4.5 – Transposon insertion in *waaL* increases carbapenem but not prodigiosin production. Carbapenem (A) and prodigiosin (B) production was measured over the course of a growth curve for S39006 (blue) and *waaL* transposon insertion mutant AMH157 (red). Solid lines indicate carbapenem/prodigiosin production while dashed lines show OD₆₀₀ measurements. Data shown are the mean values ± SD (n = 3), asterisks indicate p-values comparing carbapenem/prodigiosin production between strains: *, p < 0.05; **, p < 0.01; ***, p < 0.001; NS, not significant

As there were many pleiotropic impacts of the transposon insertion in *waaL*, virulence in a *C. elegans* model was also assessed. Previous studies showed that mutants with pleiotropic impacts, particularly with decreased swimming and swarming motility (e.g. as in a *hfq* mutant) also show reduced virulence in *C. elegans* (Wilf et al., 2011). Figure 4.6 shows a survival curve comparing the percentage of worms surviving over time when fed the indicated strain. Wild type S39006 kills *C. elegans* far quicker than the maintenance strain *E. coli* OP50. Although AMH157 still kills the worms faster than OP50, it is also significantly slower than wild type S39006, with worms surviving two days longer on average. Other identified regulators of S39006 virulence in *C. elegans* include *rpoS* and *hfq* (Wilf et al., 2013, 2011).

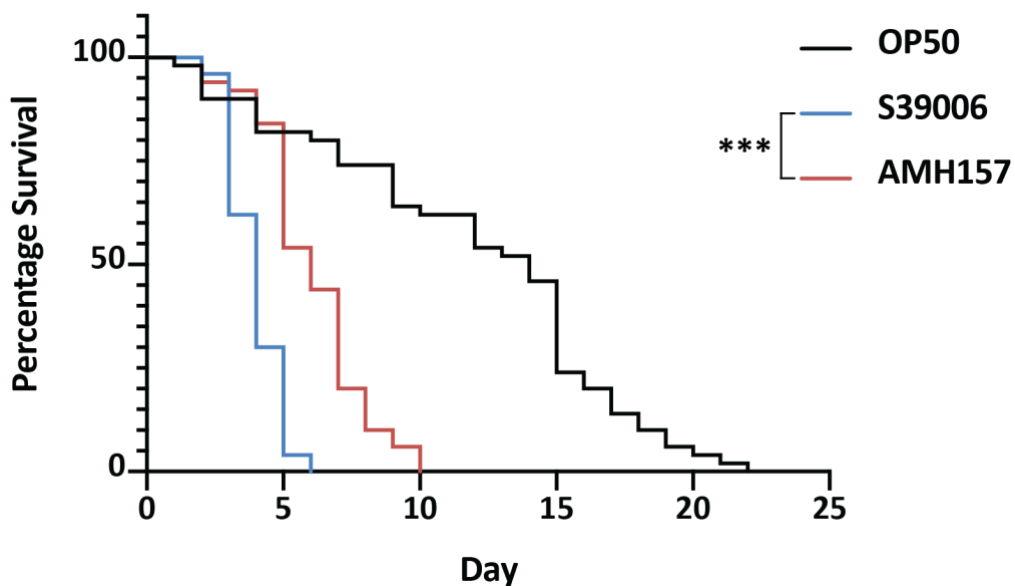


Figure 4.6 – Transposon insertion in *waaL* attenuates virulence in a *C. elegans* model.

Survival curves are shown for *C. elegans* fed S39006 (blue), AMH157 (red) and the control feeder strain *E. coli* OP50 (black). Fifty L4 stage worms were used for each bacterial strain, a log-rank test was used to determine if there was a significant difference in survival between S39006 and AMH157: *, $p < 0.05$; **, $p < 0.01$; ***, $p < 0.001$; NS, not significant. This experiment was also performed with AMH141 (shown in Figure 6.6), S39006 and OP50 controls are shared across the two figures.

4.2.4 Mutation in *waal* can be complemented

To determine whether the transposon insertion in *waal* could be complemented, the native gene was cloned into the pQE80-*oriT* (pQE) vector (Ramsay et al., 2011). To ensure that any burden of carrying the plasmid was accounted for, all comparisons were between wild type S39006 carrying the empty vector, AMH157 carrying the empty vector, and AMH157 with the complementation vector, pAH5. Both the wild type strain and AMH157 carrying the empty vector behaved as expected from assays of the non-plasmid carrying strains.

Expression of *waal* from the vector pAH5 restored the wild type flotation phenotype in AMH157 (Figure 4.7A). These assays were performed without induction with IPTG, but simply using “leaky” expression from the plasmid. As expected from the flotation assays, PCM images and spot tests of the complemented strain also appeared more similar to wild type than AMH157 carrying the empty vector (Figure 4.7B – D). In a western blot using an antibody against GvpC, AMH157 + pAH5 had a clear reduction in protein abundance compared to AMH157 + pQE (Figure 4.7E). Similarly swimming and swarming motility could be restored in AMH157 by *waal* expression, and PCWDE production returned to wild type levels (Figure 4.7 F – I).

As *waal* is the final gene of an operon, there are no expected polar effects and the phenotypes described were attributed solely to disruption of *waal*. The complementation assays performed tested a wide range of phenotypes, all of which could be restored to wild type levels through expression of *waal in trans* without induction by IPTG. This confirmed that the pleiotropic effects seen in AMH157 were the result of disruption to *waal*.

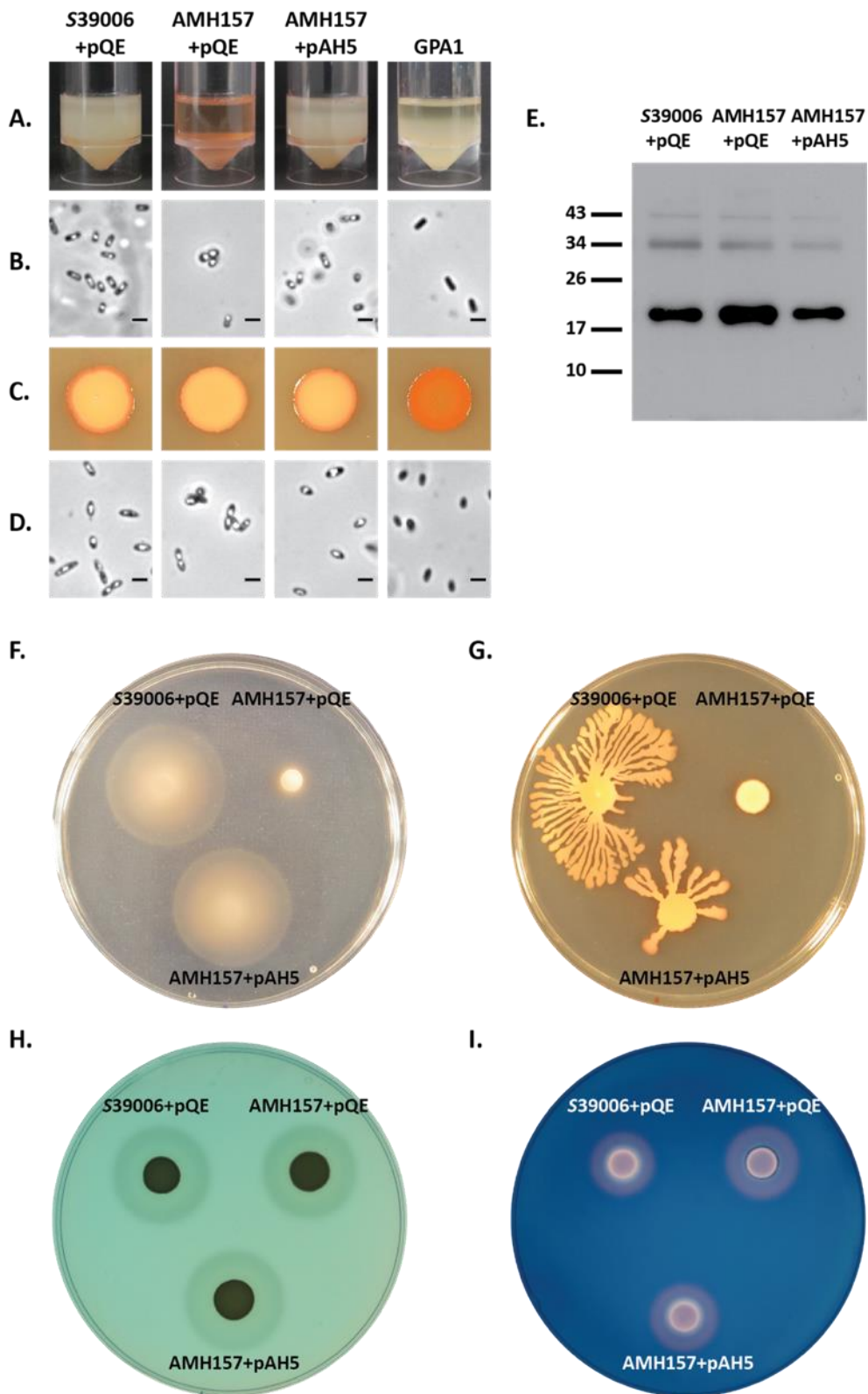


Figure 4.7 – Transposon insertion in *waaL* can be complemented.

(A) Flotation assays and (C) Spot tests with associated PCM images shown directly below in (B) and (D) for wild type S39006 carrying empty vector (pQE), AMH157 (*waaL* transposon mutant) carrying empty vector, and AMH157 with *waaL* expressed *in trans* (pAH5). (E) A western blot against using an antibody raised against GvpC for the same strains. Assays to determine if expression of *waaL* can complement swimming (F), swarming (G), pectate lyase (H) and cellulase (I) phenotypes previously observed in AMH157.

4.2.5 A *waaL* knockout has the same effect as transposon insertion

The various phenotype and complementation assays shown above confirm the pleiotropic impacts of a transposon insertion in *waaL*. As part of the initial random transposon mutagenesis screen, two mutants with transposon insertions in *waaL* were identified, AMH113 and AMH157. In initial testing, no differences were observed in the phenotypes of these two mutants and as such only AMH157 data has been presented here. However, when a previous lab member identified two *waaL* transposon insertion mutants, they found these mutants had decreased carbapenem antibiotic activity compared to wild type (Quintero-Yanes, 2019). These insertions were located 400-600 bp upstream of those described in this chapter; however, it does suggest that the specific location of the transposon insertion may change the phenotypes observed. To test whether these effects were the result of a partially active protein made in some transposon insertion strains, a *waaL* knockout mutant, AMH37, was created by allelic exchange. The effect of this deletion was very similar to the effect of the transposon insertion previously described in section 4.2.3. AMH37 cells were completely unable to float and formed an aggregate at the bottom of the flotation assay tube, produced more carbapenem antibiotic, were unable to swim or swarm and had increased amounts of GvpC present in a western blot (Figure 4.8).

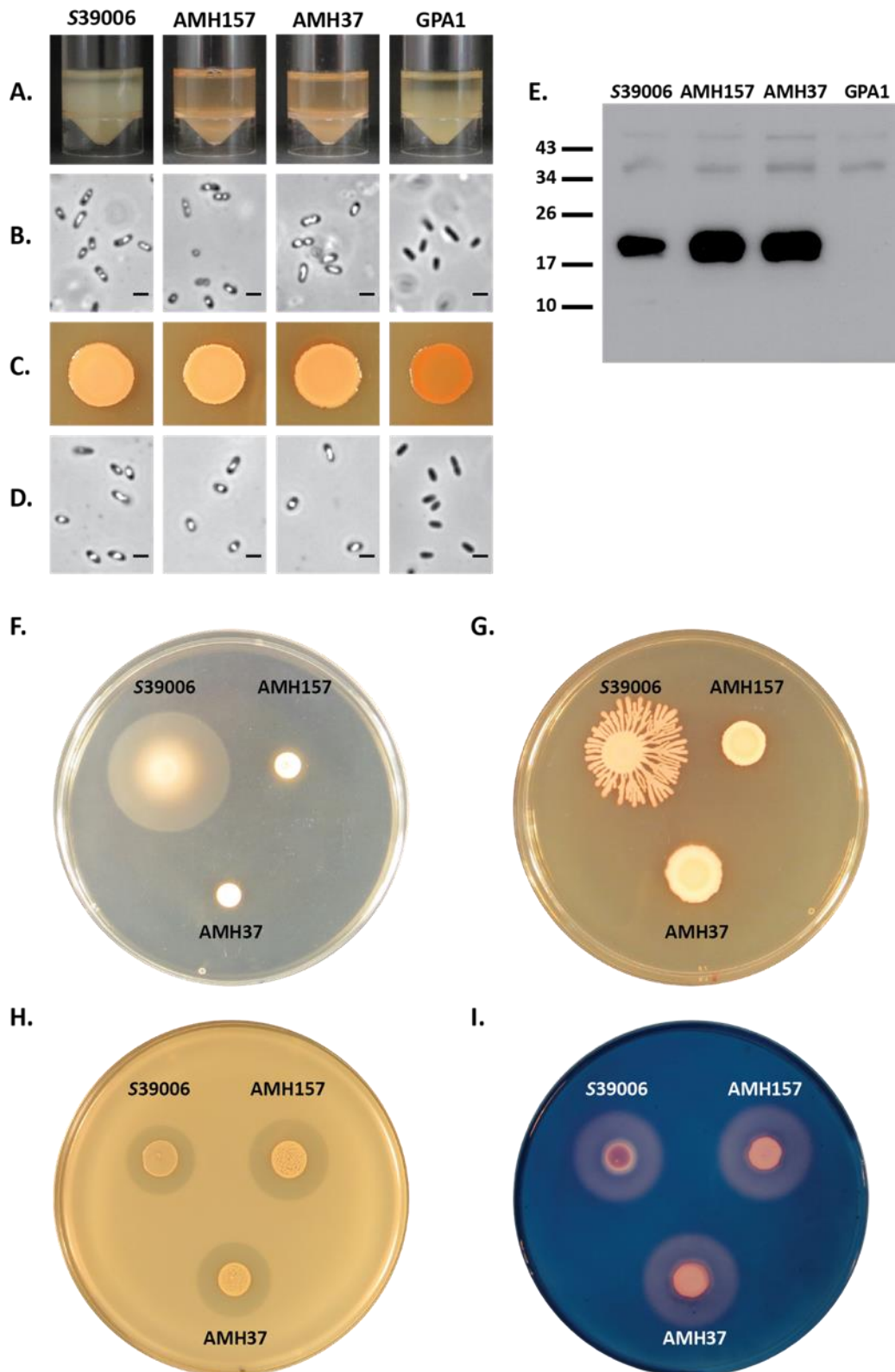


Figure 4.8 – The *waal* knockout strain AMH37 displays the same phenotypes as the *waal* transposon mutant AMH157.

(A) Flotation assays and (C) Spot tests with associated PCM images shown directly below in (B) and (D) for wild type S39006, AMH157 (*waal* transposon mutant), and AMH37 (*waal* knockout mutant). (E) A western blot against using an antibody raised against GvpC for the same strains. The effect of *waal* knockout on swimming (F) and swarming motility (G), and carbapenem (H) and cellulase (I) production.

4.2.6 LPS composition differs between the *waaL* mutant and wild type S39006

The gene *waaL* is predicted to encode an O-antigen ligase, a key enzyme for LPS synthesis. To determine if disruption in this gene caused any changes to the LPS structure of S39006, the LPS was extracted, separated by SDS-PAGE, and stained to identify any differences between AMH157 and the wild type. Wild type S39006 showed an unusual LPS structure without the laddering that is often seen, representing the different sizes of the O-antigen, depending on the number of oligosaccharide monomers present (Figure 4.9A). The LPS extraction was performed on two other strains available in the lab from other projects, *Pectobacterium atrosepticum* and *Pseudomonas tolaasii*, both of these strains showed a more typical laddering pattern with multiple bands visible (Figure 4.9C). However, even with the simple LPS structure seen in the wild type S39006, there is a clear difference in AMH157 with only one band seen (Figure 4.9A), representing the core oligosaccharide. The *waaL* knockout strain AMH37 showed the same LPS structure as the transposon insertion mutant AMH157.

This change in LPS structure could be complemented by the expression of *waaL* from the plasmid pAH5, which is in line with the restoration of the other phenotypes tested (Figure 4.9B). This assay also showed that overexpression of *waaL* in wild type S39006 had no discernible effect on the LPS structure (Figure 4.9B). These LPS stains provide strong evidence that changes in the cell surface are responsible for some, if not all, of the pleiotropic phenotypes observed in this strain.

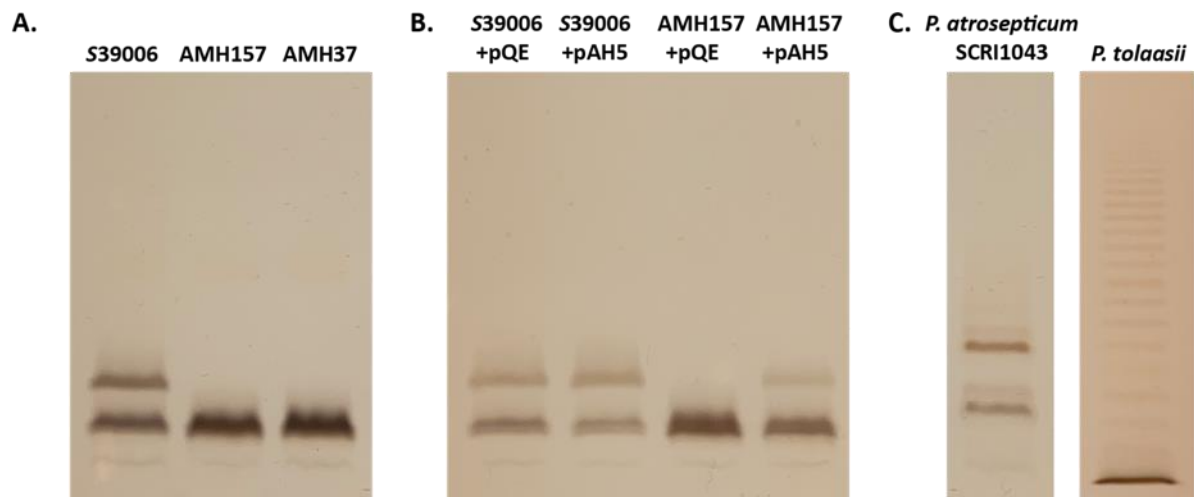


Figure 4.9 – The *waaL* mutants show different LPS banding patterns to wild type S39006. (A) LPS stain for wild type S39006, *waaL* transposon insertion mutant AMH157 and *waaL* gene knockout AMH37. (B) LPS stain of AMH157 with complementation vector pAH5 shows that the wild type LPS banding pattern can be restored by expression of *waaL* in trans. (C) Examples of LPS banding in *Pectobacterium atrosepticum* SCRI1043 and *Pseudomonas tolaasii*.

4.3 Discussion

The inputs affecting the production of GVs in S39006 have been studied for the past decade. Previous work has identified the 19 genes of the gas vesicle cluster and 11 of those genes that are essential for GV production (Ramsay et al., 2011; Tashiro et al., 2016). It has also been shown that gene products must be maintained at the correct stoichiometry to enable GV production (Monson et al., 2016). Previous screens for regulators of GV production have focused on genes that cause a translucent colony phenotype when disrupted and make no gas vesicles. These regulators often co-regulate other phenotypes of interest including antibiotic and PCWDE production. Two of the previously described regulators are predicted DNA-binding proteins: the ribose operon repressor, RbsR, and a DeoR family transcription factor, FloR. This provides a clear link establishing the mechanism through which these regulators affect GV synthesis, either by affecting transcription of the cluster itself like RbsR (which has a predicted binding site just upstream of *gvrA* (Lee et al., 2017)), or by acting through other known regulators such as FloR (which is predicted to act via RsmA and FlhDC to change GV and prodigiosin production as well as motility (Quintero-Yanes et al., 2020)). Quorum sensing is another key regulator of GV production; a *smal* mutant that cannot produce the BHL signalling molecule is unable to produce GVs or float (Ramsay et al., 2011). Environmental factors such as oxygen and potassium availability are also known to affect GV production, with oxygen limitation leading to increased transcription of the *gvpA1* operon

(Ramsay et al., 2011). Mutation in the potassium transporter TrkH resulted in a hyper opaque GV phenotype, and potassium-rich environments had a negative impact on GV production in wild type S39006 (Quintero-Yanes et al., 2019).

In this chapter a novel class of GV mutant has been discussed; one which makes GVs but is unable to float – proving that GVs are necessary but not sufficient for flotation. These mutants were identified following a random transposon mutagenesis screen that identified a transposon insertion in *waaL*, which encodes an O-antigen ligase. The production of GVs was upregulated in this mutant, suggesting the presence of a feedback mechanism transducing a signal from the cell surface possibly monitoring surface integrity. This upregulation potentially acts in a *gvrA* dependent manner under aerobic conditions but is independent of *gvrA* in microaerophilic conditions. In addition to changes in GV production the *waaL* mutant also demonstrated increased carbapenem and cellulase activity. It is not known whether the increased activity is the result of increased production or changes in cell permeability that leads to increased release and detection of the compounds.

AMH157 also demonstrated severe reductions in swimming and swarming motility. This is consistent with previous observations that GV production and flagellar motility are inversely regulated (Lee et al., 2017; Quintero-Yanes et al., 2020; Ramsay et al., 2011). However, the inability of the *waaL* mutant to float, swim, or swarm is unusual in our investigations into motility in S39006. Previously reported mutants that are unable to float such as *rbsR*, *floR*, and *rsmA* mutants all showed a hyper-motile phenotype (Lee et al., 2017; Quintero-Yanes et al., 2020; Williamson et al., 2008). There are known links between LPS and motility in other bacteria, for instance in *Myxococcus xanthus* where LPS mutants are defective in social motility, which is mediated by type IV pili (Bowden & Kaplan, 1998). Similarly, *waaL* mutants in *Pseudomonas aeruginosa* had drastically reduced swimming and twitching motility (Abeyrathne et al., 2005) and in *Proteus mirabilis* a transposon insertion in *waaL* prevented swarming motility but not swimming motility (Morgenstein et al., 2010). *Salmonella enterica* subsp. Typhimurium also requires LPS for swimming motility (Bogomolnaya et al., 2014). It has been suggested that LPS acts as a surfactant to aid swarming and swimming motility as *S. Typhimurium* strains defective in LPS production were unable to swarm on normal agar but could swarm on the more wettable Eiken agar

(Toguchi et al., 2000). Similarly *E. coli* K-12, which does not have an O-antigen layer, can only swarm on Eiken agar while other *E. coli* strains with an intact O-antigen can swarm on Bacto agar (Harshey & Matsuyama, 1994). In this study no swarming was observed in the S39006 *waaL* mutant even when Eiken agar was used, although it is possible that lower agar concentrations could lead to a restoration of this phenotype.

The *waaL* mutant also showed a significant decrease in virulence in a nematode worm model indicating that LPS may be a key factor in S39006 killing of *C. elegans*. Other regulators of S39006 virulence in *C. elegans* have been identified but the exact mechanisms of toxicity remain unknown (Wilf et al., 2013, 2011). However, LPS has been implicated as a key factor in determining the virulence of various bacteria towards *C. elegans*. LPS isolates from *Pseudomonas aeruginosa* and *Cronobacter sakazakii* were sufficient to cause lethality in *C. elegans* at concentrations of 2 µg/mL and 3.75 µg/mL respectively (Sivamaruthi et al., 2015; Vigneshkumar et al., 2012). Similar experiments in *Klebsiella pneumoniae* showed LPS dose-dependent mortality in *C. elegans* with concentrations as low as 0.1 µg/mL sufficient to kill all worms after 210 hours (Kamaladevi & Balamurugan, 2016). The p38 MAPK pathway was shown to play a major role in the host immune response to challenges from the LPS of *Salmonella enterica*, *Klebsiella pneumoniae*, and *Cronobacter sakazakii* (Aballay et al., 2003; Kamaladevi & Balamurugan, 2016; Sivamaruthi et al., 2015). Experiments in enterohemorrhagic *E. coli* O157:H7 showed that O-antigen side chains were required for virulence in *C. elegans* (Youn et al., 2013). A *perA* mutant strain that had no O-antigen side chains visible on an LPS stain was severely attenuated for virulence in *C. elegans*, with a TD₅₀ that was 60 hours longer than wild type O157:H7 (Youn et al., 2013). These data support the hypothesis that LPS, in particular the O-antigen side chain, is a key virulence factor allowing S39006 killing of *C. elegans*. It is possible that the LPS activates the host immune response via the p38 MAPK pathway as for other bacteria, however further experiments would be required to confirm this.

LPS is also a key factor in the innate resistance Gram-negative bacteria have to many antimicrobials (Bertani & Ruiz, 2018; Rosenfeld & Shai, 2006). Studies performed on an O-antigen ligase mutant of *Edwardsiella tarda*, a fish pathogen, showed the absence of any O-antigen side chains increased sensitivity to hydrogen peroxide, polymyxin B, and reduced

virulence *in vivo* (Xu et al., 2010). It would be interesting to determine if there was any similar increased sensitivity to antimicrobials seen in the *waal* mutant of S39006.

It was hypothesised that there was a feedback mechanism from the cell surface that changed transcription of the GV operons of S39006. One previously suggested mechanism is that inhibition of regular LPS synthesis could result in an accumulation of misfolded or mistargeted outer membrane proteins that are detected by the sensor protein DegS, eventually resulting in activation of the σ^E -dependent envelope stress response system (Alba & Gross, 2004; Walsh et al., 2003; G. Zhang et al., 2013). It was also shown that *waal* mutants of *Proteus mirabilis* failed to activate the *flhDC* operon during growth on agar (Morgenstein et al., 2010). Expression of the *flhDC* operon is required for high-level flagellin expression that is necessary for swarming cells. Overexpression of *flhDC* or a loss of function mutation in the response regulator *rcsB* restored swarming motility in the O-antigen ligase *P. mirabilis* mutant (Morgenstein et al., 2010). This led to the hypothesis that the O-antigen is a key part of a surface signalling pathway that increases expression of the master regulator *flhDC*. It is possible that a similar response pathway may operate in S39006, which would explain the lack of swimming and swarming motility in the *waal* mutant. In S39006 *flhC* is negatively regulated by RsmA, which also positively regulates GV production (Ramsay et al., 2011; Williamson et al., 2008). Any potential differences in *rsmA* and *flhDC* expression should be investigated in S39006 to determine if the changes in motility of the *waal* mutant is caused by disruption of these pathways.

Chapter 5. The alternative sigma factor RpoN (σ^{54}) controls gas vesicle production

5.1 Introduction

Chapter 3 described the use of a random transposon mutagenesis screen to identify novel regulators of gas vesicle production in S39006. This screen found eight genes that had not previously been linked to the production of GVs in S39006. The pleiotropic impacts of transposon insertions in four of these genes were determined and included altered antibiotic production, PCWDE production, swimming motility, and swarming motility. Chapter 4 described in greater detail the effect of a transposon insertion in the gene *waaL* which was predicted to encode an O-antigen ligase. This transposon insertion reduced motility and virulence in a *C. elegans* model and changed the external cell structure with LPS synthesis truncated. The *waaL* mutant was unable to float but still produced gas vesicles and therefore proved that gas vesicles were necessary but not sufficient for flotation.

This chapter describes another mutant of interest, AMH109, which has a transposon insertion in *rpoN*, a gene that encodes the alternative sigma factor σ^{54} . In addition to utilizing previously described methods to determine changes in GV gene transcription, antibiotic production, motility and virulence, a quantitative proteomic analysis was performed comparing the *rpoN* transposon mutant and wild type. The proteomic analysis and a bioinformatic screen for putative *rpoN* binding sites within the S39006 genome has provided insight into the σ^{54} regulon in S39006.

5.2 Results

5.2.1 Sequence analysis and genomic context of *rpoN*

The *rpoN* gene encodes the alternative sigma factor σ^{54} (also known as RpoN or σ^N), which was originally identified as the sigma factor required for the transcription of nitrogen-regulated genes in *E. coli* (Hunt & Magasanik, 1985). σ^{54} has since been identified and characterized in a range of species including *Legionella pneumophila* (Jacobi et al., 2004), *Campylobacter jejuni* (Jagannathan et al., 2001), *Pseudomonas spp.* (Hendrickson et al.,

2000; Ishimoto & Lory, 1989; Köhler et al., 1989), *Listeria monocytogenes* (Robichon et al., 1997), and *Bacillus subtilis* (Débarbouillé et al., 1991). σ^{54} has been linked to the expression of genes encoding a range of virulence determinants including flagella (Dasgupta et al., 2003), pili (Totten et al., 1990), Type III secretion (Chatterjee et al., 2002; Hutcheson et al., 2001), and the production of alginate (Boucher et al., 2000; Zielinski et al., 1992). Bacterial sigma factors fall into two families, the σ^{70} family and the σ^{54} family. σ^{54} proteins are different from σ^{70} proteins in sequence and domain structure, have promoter elements found at -12 and -24 from the transcriptional start site (instead of -10 and -35 for σ^{70} proteins), and require activator proteins, known as bacterial enhancer binding proteins (bEBPs) to initiate transcription (Shingler, 2011; Wigneshweraraj et al., 2008).

The *rpoN* mutant, AMH109, was identified as a translucent colony mutant in the random transposon mutagenesis screen described in Chapter 3. RP-PCR and sequencing found that the transposon was inserted 1,088 bp into the 1,434 bp gene. The genomic context of this mutant was interrogated and showed that the genes surrounding *rpoN* are highly conserved across Enterobacteriaceae and are homologous to those in *E. coli*, *Pectobacterium* and *Dickeya* species. As is typical for S39006, the species that share the highest level of amino acid similarity are mainly *Dickeya* species, however certain genes are most similar to the closely related *Lonsdalea* and *Brenneria* species (Tables 5.1 & 5.2). Based on similarity with *E. coli*, the *rpoN* gene is predicted to be the first gene of a five-gene transcriptional unit (Jones et al., 1994) (Figure 5.1A). RpoN itself is remarkably well conserved across *Dickeya* species, sharing over 90% identity and similarity of 96%. This trend remains throughout the entire *rpoN* to *npr* operon, the genes preceding *rpoN*, which encode LPS transport proteins *lptCAB* are also very well conserved sharing 75 – 90% identity with closely related species.

The S39006 σ^{54} protein is predicted to contain three domains: an activator interacting domain (AID), core binding domain, and DNA binding domain, the locations of which are shown in Figure 5.1B. These domains are consistent with those described for σ^{54} in other organisms including *E. coli* and *Pseudomonas* spp. The σ^{54} core binding domain contains four helices, and has a negative charge allowing for binding and direct interaction with core RNA polymerase (RNAP) prior to the initiation of transcription while the σ^{54} DNA binding domain contains a helix-turn-helix motif to bind DNA (Buck et al., 2000; Hong et al., 2009; Wong et

al., 1994). The activator interaction domain inhibits transcription initiation of the σ^{54} -RNAP holoenzyme before the activator has bound, at which point transcription can begin (Casaz & Buck, 1999; Chaney et al., 2001; Syed & Gralla, 1997).

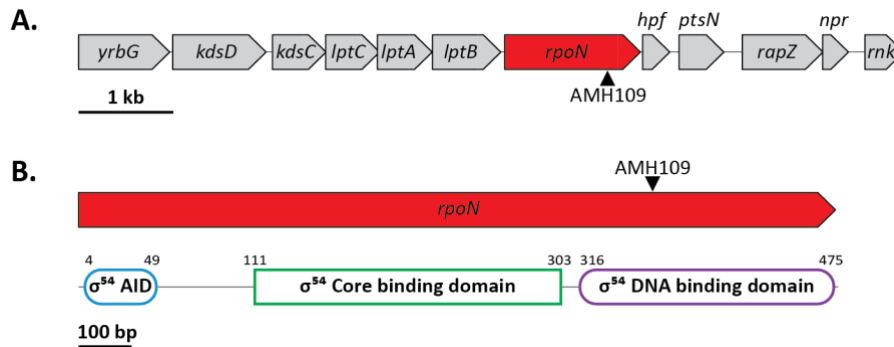


Figure 5.1 – Organisation of genes surrounding the AMH109 transposon insertion site.

(A) The transposon inserted in *rpoN*, highlighted in red, the location of the insertion is indicated by a black triangle. (B) The predicted protein domains of RpoN, the numbers above indicate the length of the protein in amino acids and the start and end of each domain, AID; activator interacting domain.

Table 5.1 – Amino acid sequence similarity search of RpoN using BLASTP.

Species	Identity (%)	Similarity (%)	Accession Number
<i>Dickeya zeae</i>	92	96	WP_012883034.1
<i>Dickeya lacustris</i>	91	96	WP_125257985.1
<i>Dickeya fangzhongdai</i>	91	96	WP_038663168.1
<i>Dickeya chrysanthemi</i>	91	96	WP_040002792.1
<i>Lonsdalea populi</i>	91	95	WP_123235863.1
<i>Lonsdalea britannica</i>	91	95	WP_085651064.1

Table 5.2 – Predicted function of genes surrounding *rpoN*.

ORF	Size (bp)	Predicted Function	Species/Strain	Identity (%)	Similarity (%)
<i>yrbG</i>	963	Calcium/sodium antiporter	<i>Dickeya paradisiaca</i>	86	91
<i>kdsD</i>	987	Arabinose-5-phosphate isomerase KdsD	<i>Dickeya</i> sp. Secpp 1600	89	95
<i>kdsC</i>	567	3-deoxy-manno- octulosonate-8-phosphatase KdsC	<i>Brenneria</i> sp. L3-3C-1	85	92
<i>lptC</i>	570	LPS export ABC transporter periplasmic protein LptC	<i>Lonsdalea iberica</i>	75	88
<i>lptA</i>	579	Lipopolysaccharide ABC transporter substrate-binding protein LptA	<i>Lonsdalea populi</i>	80	88
<i>lptB</i>	726	LPS export ABC transporter ATP-binding protein	<i>Brenneria</i> sp. CFCC 11842	95	98
<i>rpoN</i>	1434	RNA polymerase factor sigma-54	<i>Dickeya zeae</i>	92	96
<i>hpf</i>	288	Ribosome hibernation promoting factor	<i>Lonsdalea quercina</i>	94	100
<i>ptsN</i>	474	PTS IIA-like nitrogen regulatory protein PtsN	<i>Dickeya dadantii</i>	94	98
<i>rapZ</i>	855	RNase adapter RapZ	<i>Dickeya paradisiaca</i>	98	99
<i>npr</i>	273	PTS phosphocarrier protein NPr	<i>Dickeya paradisiaca</i>	89	96
<i>rnk</i>	411	Nucleoside diphosphate kinase regulator	<i>Pectobacterium punjabense</i>	82	87

5.2.2 The *rpoN* mutant shows reduced gas vesicle production

The original starting point for the random transposon mutagenesis screen was to find novel regulators of gas vesicle production in *S39006*. The *rpoN* transposon insertion mutant, AMH109, was originally identified as a translucent colony mutant. This suggested that the mutant was not making any gas vesicles which refract light and make wild type cells appear opaque. To determine whether this was the case, the strain was subjected to flotation assays and spot tests along with imaging using PCM and TEM. AMH109 showed a reduction in flotation ability and opacity compared to the wild type *S39006* (Figure 5.2A & C). PCM images taken from flotation assays and spot tests showed no phase bright structures in AMH109 cells, like those of the GV negative strain GPA1 (Figure 5.2B & D). Similarly, no individual GVs could be observed in AMH109 when cells were observed under TEM (Figure 5.2E). Further evidence that this strain was not making gas vesicles was the lack of any GvpC band on a western blot, similar to the gas vesicle negative control strain GPA1 (Figure 5.2F).

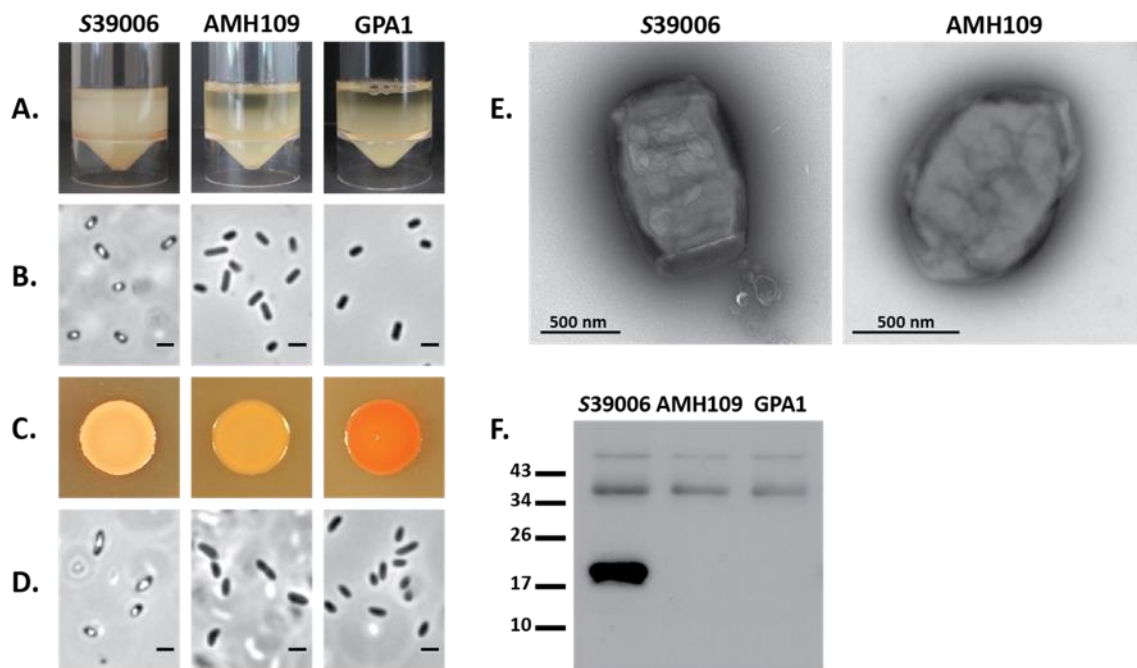


Figure 5.2 – Transposon insertion in *rpoN* reduces flotation and gas vesicle production.

(A) Flotation assays for *S39006*, *rpoN* transposon mutant AMH109, and gas vesicle negative control strain GPA1 after 48 h standing at room temperature. (B) PCM images from the flotation assay shown directly above, the scale bar indicates 1 μm . (C) Spot tests of each strain with normalised cell number, grown for 48 h at 30 $^{\circ}\text{C}$ and associated PCM images directly below (D). (E) Representative TEM images showing AMH109 is unable to make GVs. The *S39006* image is also shown in Figure 4.2 and Figure 6.2. (F) Western blot using an antibody raised against GvpC.

5.2.3 Transcription of *gvpA1-gvpY* is reduced in the *rpoN* mutant

Transcriptional fusions in *gvpA1* and *gvrA* were utilized to determine whether changes in the GV production of AMH109 were caused at a transcriptional or post-transcriptional level. The GV cluster of S39006 is comprised of two operons that begin with *gvpA1* and *gvrA* respectively. The first cluster is composed of mainly structural genes with the three known regulatory genes of the cluster (*gvrA*, *gvrB*, and *gvrC*) all found in the second operon. The strains GPA1 and GRA contain *uidA* gene fusions in *gvpA1* and *gvrA* respectively. By measuring the activity of the *uidA* gene product, β -glucuronidase, the level of transcription of each gene can be assessed. The transposon from AMH109 was transferred into GPA1 and GRA by transduction to give AMH111 and AMH112 respectively. The β -glucuronidase activity was measured in GPA1, AMH111, GRA, and AMH112 in aerobic and microaerophilic conditions every two hours over the course of a 14 or 16 hour growth curve. The OD₆₀₀ was also measured at each time point and all fluorescence values were normalised to the OD₆₀₀.

The *rpoN* transposon insertion mutant exhibited a slight difference in growth rate over the course of the growth curve in aerobic conditions but reached the same final culture density (Figure 5.3A & B, dotted lines). This difference in growth was oxygen dependent and no differences were observed under oxygen limited conditions (Figure 5.3C & D, dotted lines). There were significant differences in *gvpA1* expression under both aerobic and microaerophilic conditions with the *rpoN* mutant showing either very low (aerobic) or no activity (microaerophilic) (Figure 5.3A & C, solid lines). In previous gas vesicle mutants that have been described by other lab members (e.g. *rbsR*), this drop in *gvpA1* expression could be attributed to a concomitant drop in *gvrA* expression (Lee et al., 2017; Ramsay et al., 2011). However, in this case, the *rpoN* mutant showed no significant difference in *gvrA* expression in either aerobic or microaerophilic conditions (Figure 5.3B & D, solid lines). There was one time point in aerobic conditions (10 h) where *gvrA* expression appeared upregulated in the *rpoN* mutant however this was not statistically significant. This suggests that there may be an issue transducing a signal from the *gvrA* operon, and as such *gvpA1* transcription cannot occur.

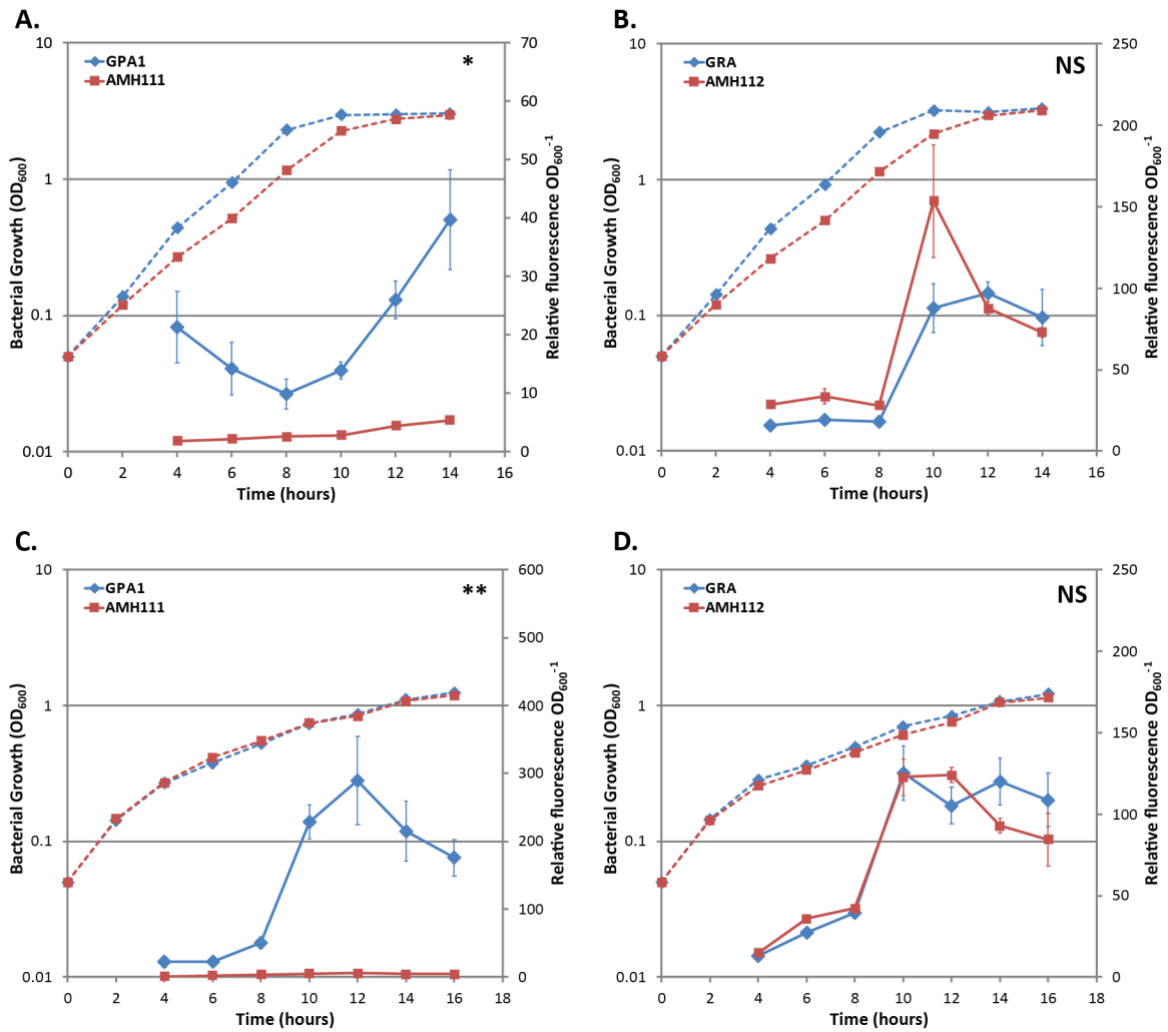


Figure 5.3 – *gvpA1* and *gvrA* expression in wild type and the *rpoN* mutant under aerobic and microaerophilic conditions.

β -glucuronidase activity from a chromosomal *gvpA1::uidA* fusion was assayed in wild type (GPA1, blue) and *rpoN* transposon mutant backgrounds (AMH111, red) under aerobic (A) and microaerophilic (C) conditions. β -glucuronidase activity from a chromosomal *gvrA::uidA* fusion was assayed in wild type (GRA, blue) and *rpoN* transposon mutant backgrounds (AMH112, red) under aerobic (B) and microaerophilic (D) conditions. Solid lines indicate β -glu activity while dashed lines show OD₆₀₀ measurements. Data shown are the mean values \pm SD (n = 3), asterisks indicate p-values comparing β -glu activity: *, p < 0.05; **, p < 0.01; ***, p < 0.001; NS, not significant.

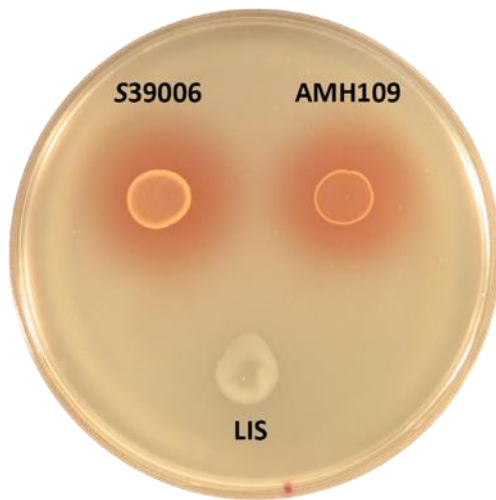
5.2.4 Mutation in *rpoN* causes diverse phenotypic impacts in S39006

Studies in other organisms have shown that disruption of *rpoN* causes pleiotropic effects including disrupted motility (Lilley & Bassler, 2000; Totten et al., 1990), cell adhesion (Plotkowski et al., 1994) and virulence (Hendrickson et al., 2001). To see if the transposon insertion in *rpoN* had wider effects than simply disrupting flotation and GV production, a series of phenotype assays were performed. As a basic screen, the effect of the transposon insertion in *rpoN* on QS molecule, antibiotic, and PCWDE production was measured using plate assays, along with the utilization of specific low-concentration agars to measure swimming and swarming motility.

In a plate assay, similar levels of the QS molecule BHL were detected in AMH109 and wild type S39006 (Figure 5.4A). Production of the carbapenem antibiotic was increased in AMH109 compared to the wild type strain (Figure 5.4B). To quantify this increase, a growth curve was performed with samples taken from both strains every two hours and the activity of carbapenem determined (Figure 5.5A). The carbapenem levels were normalized based on OD₆₀₀ and corroborated the initial observations that carbapenem antibiotic production is increased in the *rpoN* mutant. At the peak of production (8 h), the *rpoN* mutant produced double the amount of carbapenem compared to the wild type. Production of the carbapenem antibiotic was also induced two hours earlier in the mutant than the wild type (Figure 5.5A). The production of the other antibiotic, prodigiosin, was also quantified during a growth curve, however there was no statistically significant difference in pigment despite spots of AMH109 appearing less red on plates (Figure 5.5B).

AMH109 also showed a large drop in pectate lyase production, swimming motility and swarming motility although cellulase production was unaffected (Figure 5.4 C – F). Swarming motility was more strongly inhibited than swimming motility which, although diminished, was still possible in this strain. The virulence of AMH109 in a *C. elegans* model was also established. The *rpoN* mutant showed a slight, but significant, drop in virulence over the course of the survival curve (Figure 5.6).

A. BHL



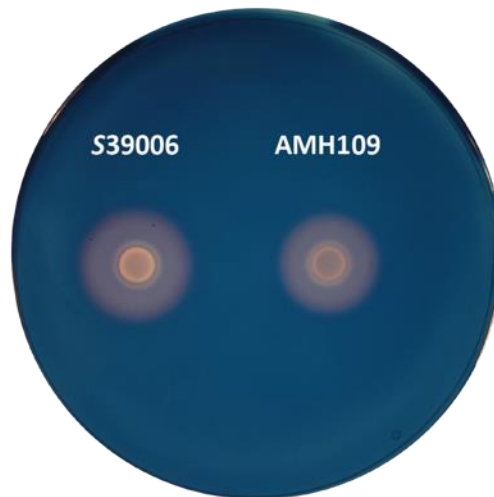
B. Carbapenem



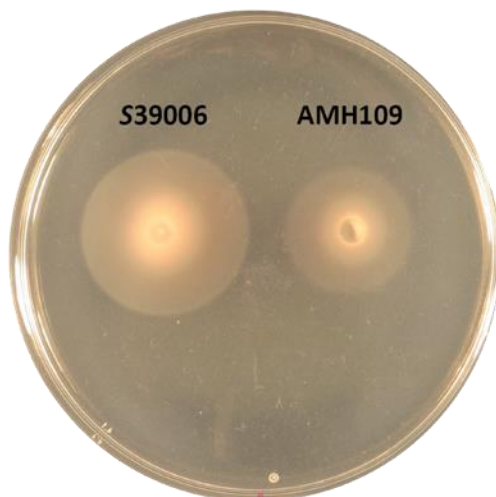
C. Pectate Lyase



D. Cellulase



E. Swimming



F. Swarming



Figure 5.4 – The transposon insertion in *rpoN* is pleiotropic.

Overnight cultures of the indicated strains were adjusted to an OD_{600} of 1 (A – D) or 0.2 (E and F) and spotted onto different agar plates to assay the production of BHL (A), carbapenem (B), pectate lyase (C) and cellulase (D). Swimming (E) and swarming (F) motility were also assayed.

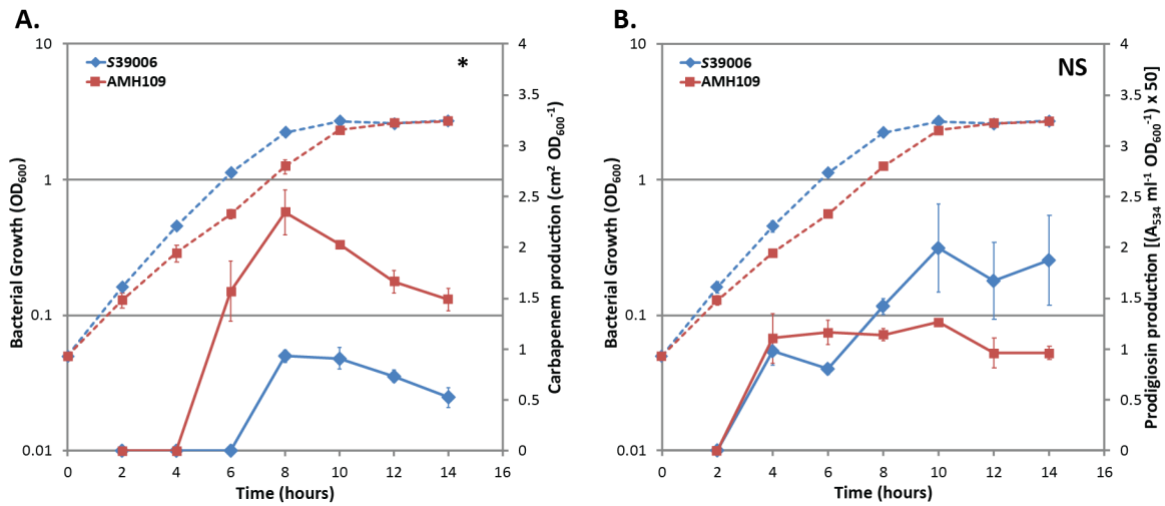


Figure 5.5 – Transposon insertion in *rpoN* increases carbapenem but not prodigiosin production. Production of the carbapenem (A) and prodigiosin (B) antibiotics were measured over the course of a growth curve for S39006 (blue) and *rpoN* transposon insertion mutant AMH109 (red). Solid lines indicate carbapenem/prodigiosin production while dashed lines show OD₆₀₀ measurements. Data shown are the mean values \pm SD (n = 3), asterisks indicate p-values comparing carbapenem/prodigiosin production between strains: *, p < 0.05; **, p < 0.01; ***, p < 0.001; NS, not significant

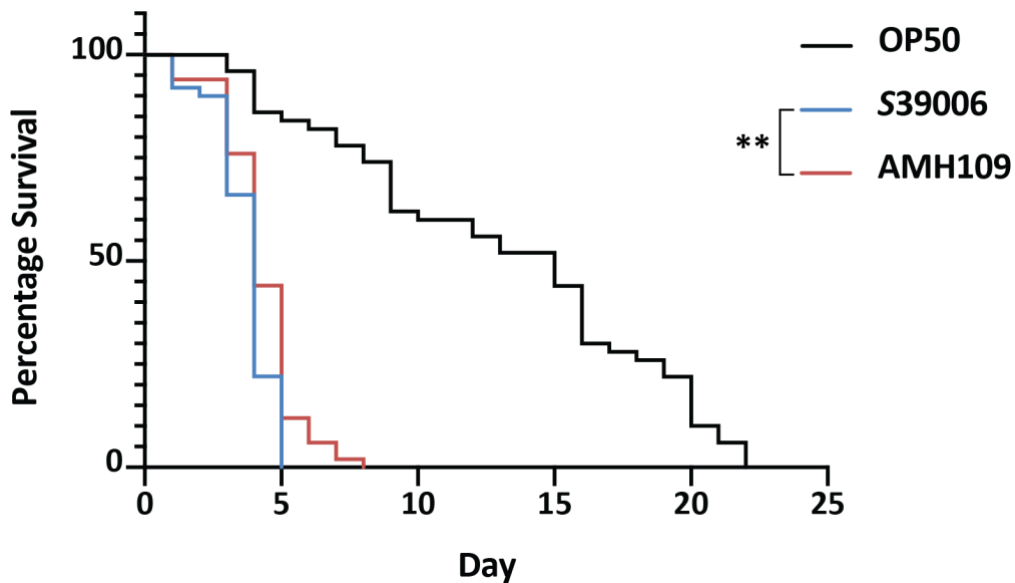


Figure 5.6 – Transposon insertion in *rpoN* attenuates virulence in a *C. elegans* model. Survival curves are shown for *C. elegans* fed S39006 (blue), AMH109 (red) and the control feeder strain *E. coli* OP50 (black). Fifty L4 stage worms were used for each bacterial strain, a log-rank test was used to determine if there was a significant difference in survival between S39006 and AMH109: *, p < 0.05; **, p < 0.01; ***, p < 0.001; NS, not significant.

5.2.5 The transposon insertion in *rpoN* can be complemented

A bioinformatic analysis of the genes surrounding *rpoN* suggested that it is the initial gene of a five gene operon. Therefore, the transposon insertion could have an effect on transcription of downstream genes as the transposon contains a transcriptional terminator (Monson et al., 2015). To determine whether it was *rpoN* or a downstream gene that was responsible for the pleiotropic phenotypes observed, various complementation assays were carried out. These assays were performed using wild type S39006 carrying the empty vector pQE80-*oriT* (pQE), AMH109 carrying the empty vector, and AMH109 carrying the complementation vector pAH1 (pQE80-*oriT* with the S39006 *rpoN* gene cloned between the *Bam*HI and *Sac*I restriction sites). Expression of genes within the multiple cloning site of this plasmid can be induced by IPTG, however a basal level of “leaky” expression will always be present as the repression is not as tight as in some other expression systems.

The basal level of *rpoN* expression provided by pAH1 was sufficient to restore GV production and flotation in AMH109 (Figure 5.7A & B). The AMH109 + pAH1 spot test colony also appeared opaque, and phase bright structures could once again be seen when cells were viewed under PCM (Figure 5.7C & D). Motility was restored by expression of *rpoN in trans* with AMH109 + pAH1 cells able to swim to the same distance as wild type cells while swarming motility was partially restored (Figure 5.7F & G). Pectate lyase production also returned to wild type levels (Figure 5.7H). A western blot using an antibody raised against GvpC was also performed and the GvpC band at 18 kDa was restored in the complemented mutant (Figure 5.7E). However, the band had a much greater density than the wild type carrying the empty vector suggesting that the uninduced level of *rpoN* expression from pAH1 is greater than the levels found in S39006 under normal conditions. This is likely due to the abundance of the plasmid with 20-30 copies estimated per cell. An assay of *gvpA1* transcription was also performed using the strains carrying either the empty vector or complementation vector pAH1 (Figure 5.8). By adding *rpoN* back into the system, the growth rate and transcription of *gvpA1* was returned to wild type levels, or higher.

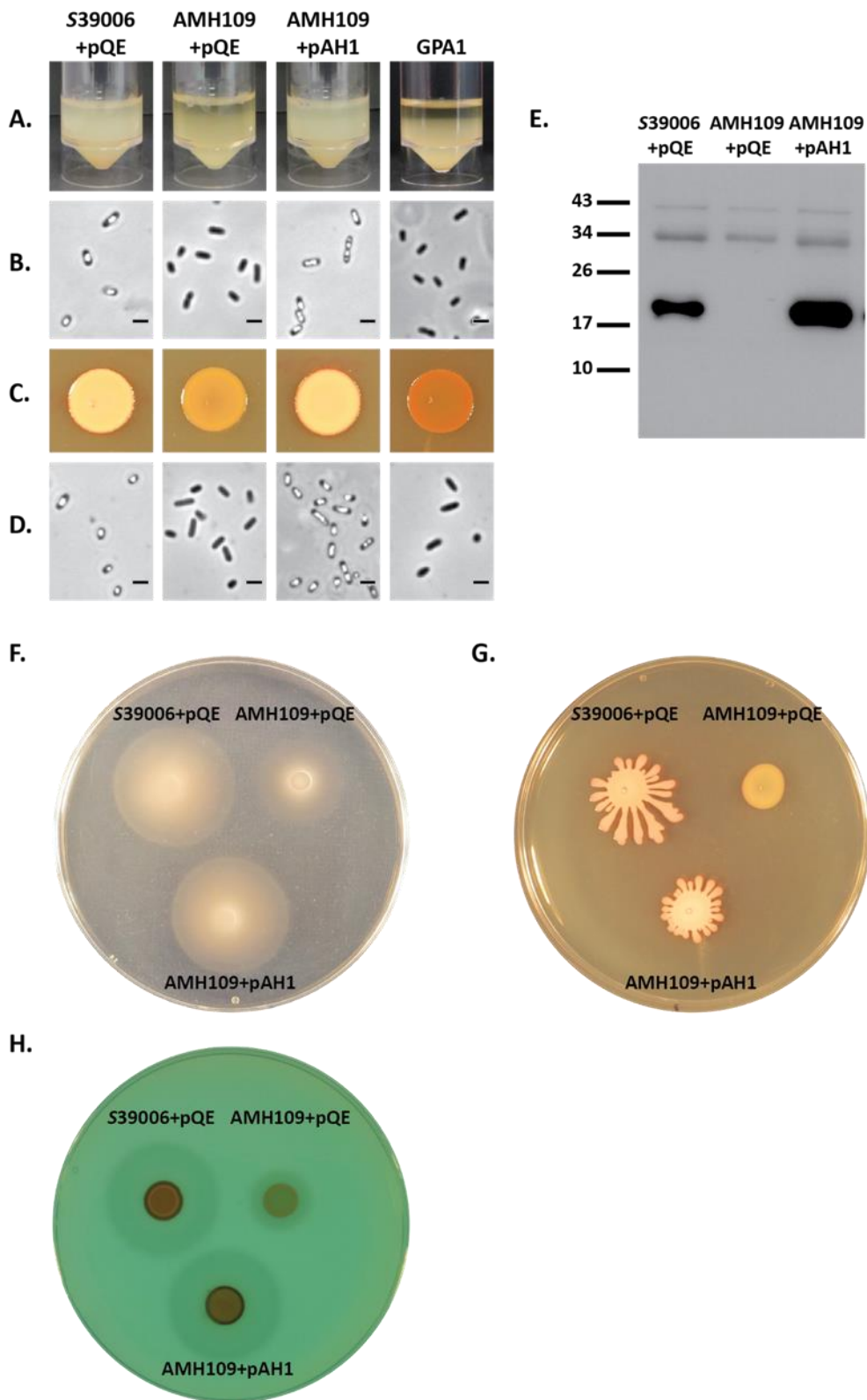


Figure 5.7 – Transposon insertion in *rpoN* can be complemented.

(A) Flotation assays and (C) Spot tests with associated PCM images shown directly below in (B) and (D) for wild type S39006 carrying empty vector (pQE), AMH109 (*rpoN* transposon mutant) carrying empty vector, and AMH109 with *rpoN* expressed *in trans* (pAH1). (E) A western blot against using an antibody raised against GvpC for the same strains. Assays to determine if expression of *rpoN* can complement swimming (F), swarming (G), and pectate lyase (H) phenotypes previously observed in AMH109.

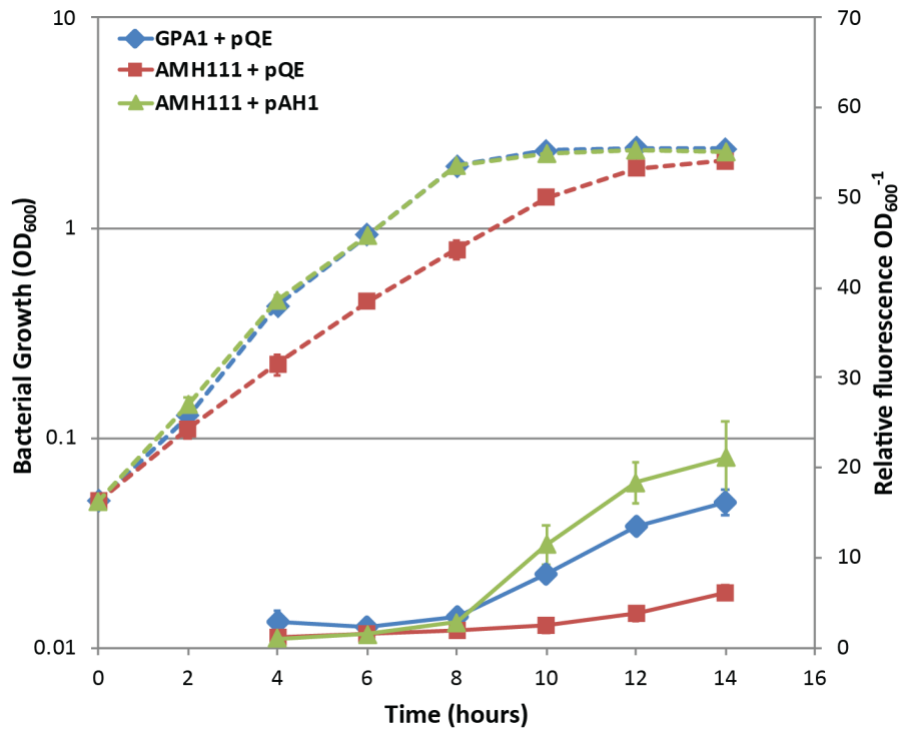


Figure 5.8 – Transcription of the *gvpA1* can be restored by expression of *rpoN* in trans. β -glucuronidase activity from a chromosomal *gvpA1::uidA* fusion was assayed in wild type with empty vector (GPA1 + pQE, blue), *rpoN* with empty vector (AMH111 + pQE, red), and *rpoN* with complementation vector (AMH111 + pAH1) strains. Solid lines indicate β -glu activity while dashed lines show OD₆₀₀ measurements. Data shown are the mean values \pm SD (n = 3).

5.2.6 A *rpoN* knockout has the same effect as the transposon insertion

As previously discussed, the *rpoN* gene is predicted to be part of an operon raising the possibility of polar effects due to the transposon insertion. To circumvent any potential polar effects a “clean” knockout strain was created using allelic exchange to remove the entire *rpoN* gene except for the first three and last three codons. This knockout strain, AMH31, was then used to perform various phenotype assays and its performance compared to wild type S39006 and the original transposon insertion mutant AMH109.

Figure 5.9 shows that the phenotypes of AMH31, the *rpoN* knockout strain, and AMH109, the *rpoN* transposon insertion strain, are indistinguishable. Both have reduced flotation ability and appear translucent in colony spot tests at normalized OD₆₀₀ (Figure 5.9A & C). This lack of flotation ability and opacity is the result of a failure to make gas vesicles, which is clear from both the PCM images where no phase bright structures (“gas vacuoles”) can be seen (Figure 5.9B & D). The western blot confirms that no GVs are being produced as no GvpC protein is detected for AMH31, AMH109 or the GV negative strain GPA1 (Figure 5.9E). The plate assays show there is no difference between the transposon mutant and the knockout mutant in terms of swimming motility, swarming motility, carbapenem antibiotic production or pectate lyase production (Figure 5.9 F – I).

The creation and testing of the *rpoN* knockout mutant provided confirmatory evidence that disruption of *rpoN* is the cause of the phenotypes observed and the downstream genes of the operon are not responsible for either the effects on GV production or the other pleiotropic effects seen in the *rpoN* transposon mutant. As a result, AMH109 was then used to perform a comparative proteomic analysis to determine if there were any unseen effects of the transposon insertion and further define any other genes under σ^{54} control in S39006.

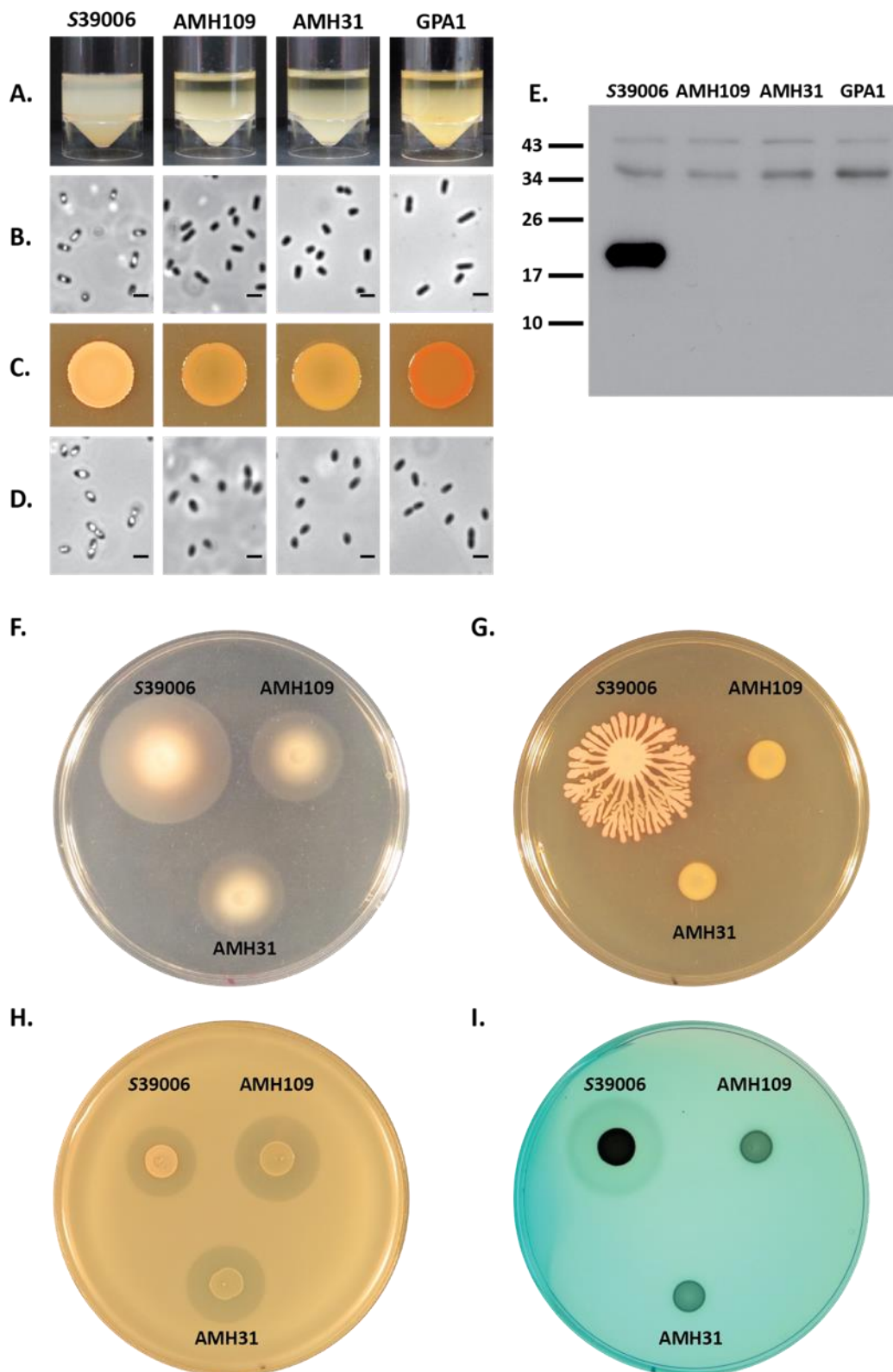


Figure 5.9 – The *rpoN* knockout strain AMH31 displays the same phenotypes as the *rpoN* transposon mutant AMH109.

(A) Flotation assays and (C) Spot tests with associated PCM images shown directly below in (B) and (D) for wild type S39006, AMH109 (*rpoN* transposon mutant), and AMH31 (*rpoN* knockout). (E) A western blot against using an antibody raised against GvpC for the same strains. The effect of *rpoN* knockout on swimming (F) and swarming motility (G), and carbapenem (H) and pectate lyase (I) production

5.2.7 Intracellular protein extraction and quantification in S39006 and the *rpoN* mutant

This chapter has identified and characterized the *rpoN* gene of S39006. It functions as a novel regulator of GV morphogenesis and has pleiotropic impacts on carbapenem production, pectate lyase production, swimming motility, swarming motility, and virulence in a *C. elegans* model. A quantitative comparative proteomic analysis was performed between AMH109 and S39006 to determine if any further pleiotropic effects were occurring because of disruption to the *rpoN* gene.

Bacterial growth conditions and protein sample preparation can have large impacts on the results of a quantitative proteomic analysis. Previous growth curves had shown a slight growth defect in the *rpoN* transposon mutant, AMH109, that was resolved by the time both AMH109 and wild type had reached stationary phase. A growth curve was performed, and protein samples extracted after at 12, 14 and 16 h to confirm that OD₆₀₀ and cell numbers were not significantly different between the two strains. The amount of GvpC that could be detected via a western blot was also determined (Figure 5.10). These time points were also chosen as transcription of the *gvpA1* operon (where the core GV structural proteins are located) is increased as cells enter stationary phase (Ramsay et al., 2011). The western blot confirmed that GvpC could be detected in wild type cells at all time points, while OD₆₀₀ measurements and colony counts showed no significant difference between wild type and AMH109.

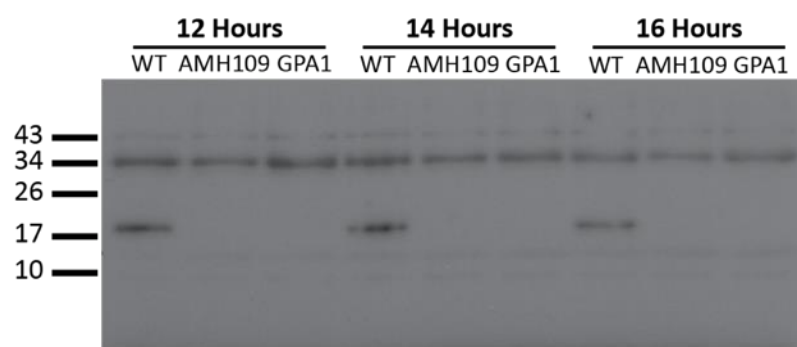


Figure 5.10 – Western blot for GvpC in wild type, AMH109, and GPA1 after 12, 14, and 16 hours growth.

GvpC bands are visible in the wild type columns at approximately 18 kDa, none are present in the AMH109 or GPA1 columns.

To be consistent with previous proteomics experiments carried out in S39006, the protein extractions were performed after 14 h growth in LB (Quintero-Yanes et al., 2020). Three replicates of wild type S39006 and AMH109 were grown in 25 mL LB in 250 mL flasks at 30 °C with shaking at 215 rpm. After 14 h growth each culture was normalised to an OD₆₀₀ of 2 and 25 mL of culture was used for each protein extraction. Proteins extracted from S39006 and AMH109 had similar concentrations and a sample of each extract was separated by SDS-PAGE to determine the protein profile (Figure 5.11A). The profiles appeared similar across replicates and between the two strains. A western blot for GvpC was also performed as previous experiments have shown clear differences in production of this protein at 14 hours (Figure 5.10B). The band density was similar across S39006 samples and there was no GvpC protein detected in AMH109 samples, consistent with previous western blots and the transcriptional data presented earlier in the chapter (Figures 5.2 & 5.3). After these quality control checks were performed, samples were analysed by LC-MS/MS to quantify the intracellular proteome of each sample.

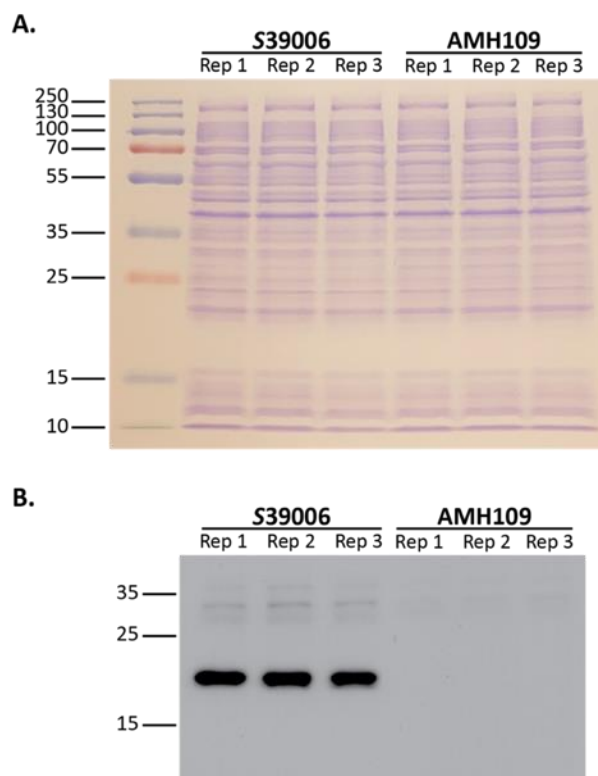


Figure 5.11 – Intracellular protein samples extracted from S39006 and AMH109.

(A) SDS-PAGE analysis of the intracellular protein extracts for three replicates each of S39006 and AMH109. The first lane shows Thermo Scientific™ PageRuler™ Prestained Protein Ladder with sizes indicated beside. (B) A western blot using an antibody raised against GvpC (~18 kDa) for the three replicates of S39006 and AMH109.

The purified protein samples were sent to the CCP where tandem mass tagging with 16 isobaric reporters (TMT-16plex) was performed. This procedure was performed in collaboration with Carlo Sandoval, a PhD student also studying the regulation of GVs in S39006. The tagged samples represented three replicates each of wild type S39006, AMH109, AMH141 (to be discussed in chapter 6), two mutants currently under investigation by Carlo Sandoval, and a final pooled sample to fully utilize the 16 reporters provided in the TMT-16plex analysis. The TMT labelling, LC-MS/MS analysis and proteomic data analysis was performed in collaboration with the Cambridge Centre for Proteomics, University of Cambridge (<https://proteomics.bio.cam.ac.uk>).

Previous bioinformatic analysis of the S39006 genome found 4,413 protein-encoding genes (Fineran et al., 2013) and the complete genome sequence of S39006 has been uploaded for public access in the NCBI database (www.ncbi.nlm.nih.gov). The amino acid sequences of predicted proteins are also available, which allowed for comparative analysis of the TMT-labelled peptides to determine their relative abundance between S39006 and AMH109. In this experiment, the TMT labelling efficiency was 95.7 % and the raw data contained 2986 proteins. After removing any proteins that contained missing values and proteins belonging to the cRAP (Mellacheruvu et al., 2013), 2959 proteins remained. This represented 67% of the predicted proteins of S39006.

The correlation coefficient of each biological replicate was determined for both strains to confirm that protein samples were reproducible. The correlation coefficients between replicates of the same strain were between 0.99 and 1, while coefficients between replicates of different strains were lower, at 0.96 to 0.97 (Figure 5.12). Additionally, a boxplot (performed after sample normalization with the median) showed a normal distribution of protein quantification and replicates of each strain had similar distributions (Figure 5.13). A differential expression analysis (DEA) was carried out using the limma package (Ritchie et al., 2015), which permitted a principal component analysis (PCA) between samples (Figure 5.14). The PCA plot shows samples of the *rpoN* mutant (AMH109) are clearly separated from wild type S39006 samples, while replicates are closer together (Figure 5.14). A histogram visualising the p-values after the DEA shows that the majority of the data were significantly different, with a high peak near zero (Figure 5.15).

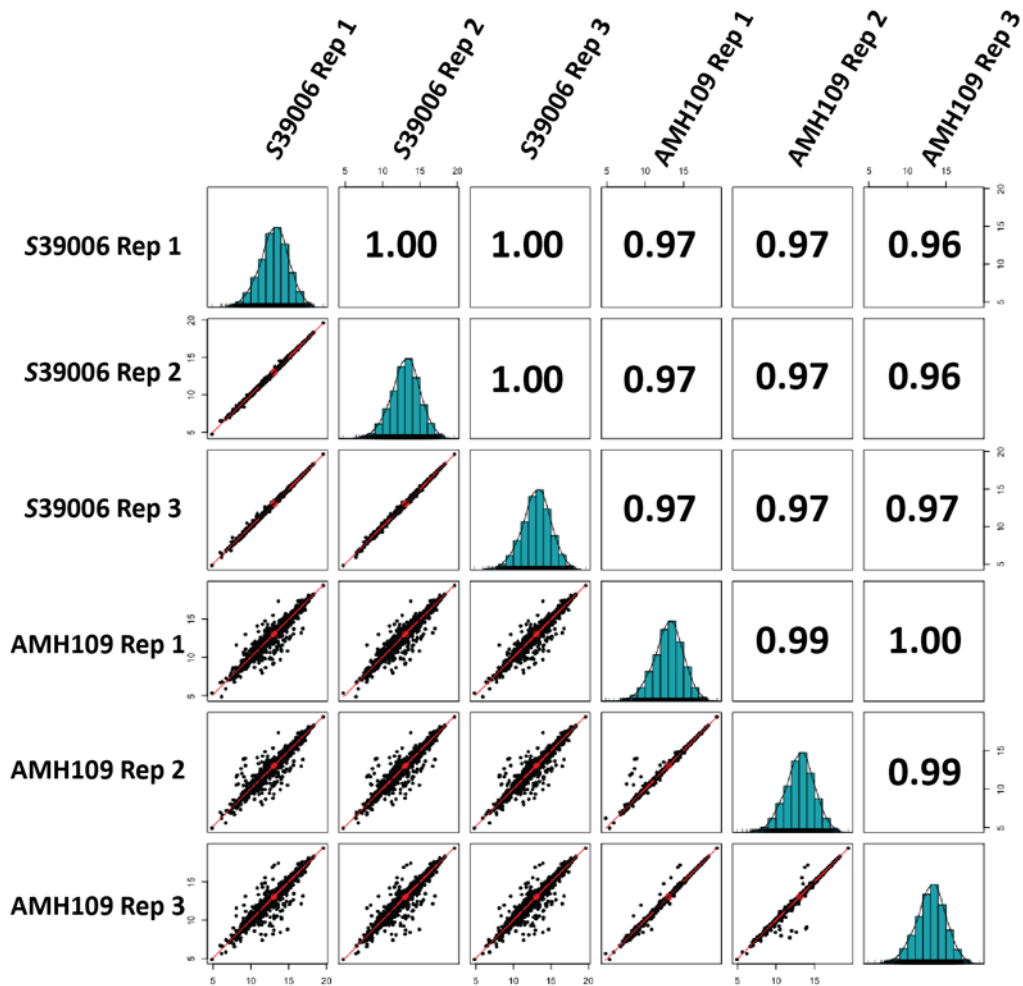


Figure 5.12 – Pearson correlation coefficients between replicates of S39006 and AMH109. Three replicates of each strain were used for the quantitative proteomic analysis. The correlation coefficient varied from 0.96 to 0.97 between S39006 and AMH109 while coefficients were between 0.99 and 1 within biological replicates.

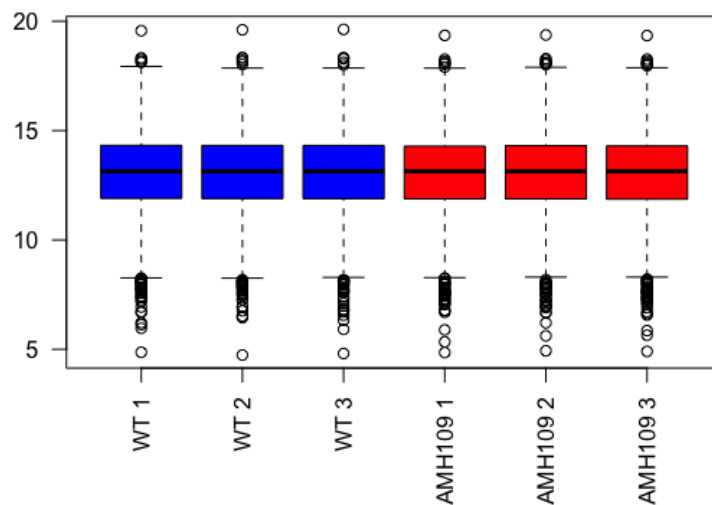


Figure 5.13 – Boxplot of protein abundances in S39006 and AMH109. The raw data was normally distributed and was normalised using the median of each channel. Each strain had similar distributions across biological replicates.

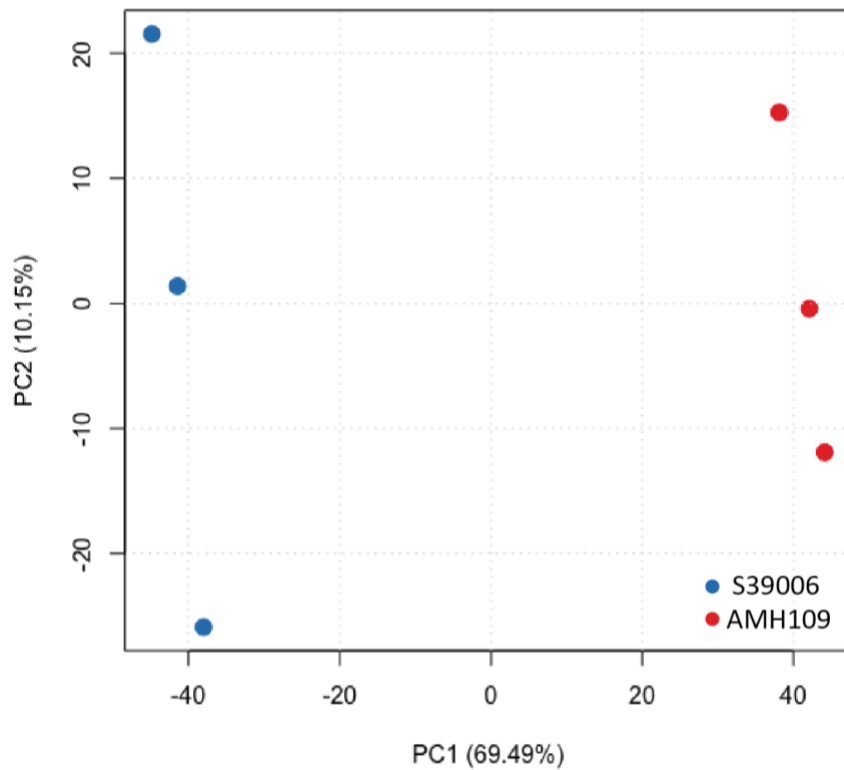


Figure 5.14 – The PCA of the protein quantification in S39006 and AMH109. Blue dots represent wild type S39006 while red dots represent the *rpoN* transposon mutant AMH109. The protein quantification values have been \log_2 transformed and the PCA indicates the two samples were well separated and group based on biological replicates.

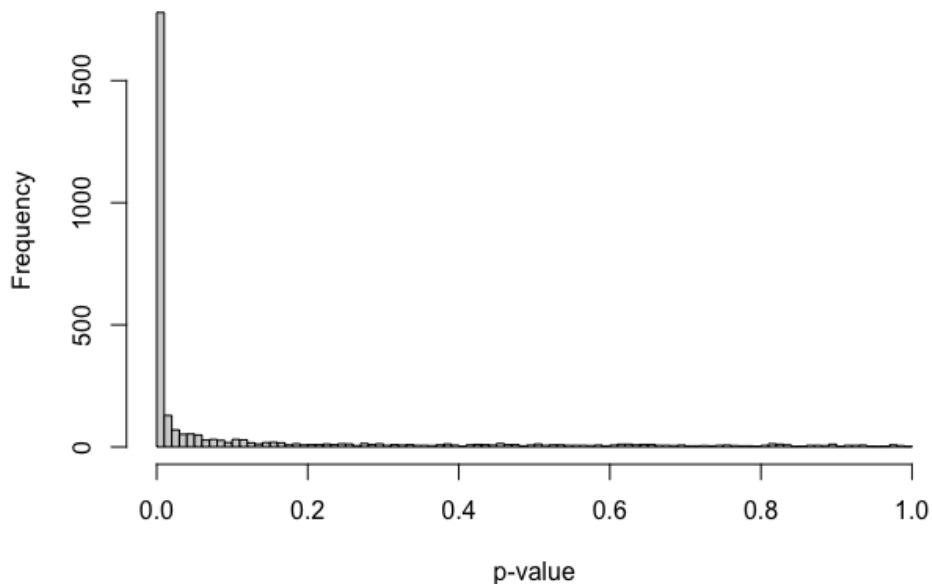


Figure 5.15 – p-value distribution of proteome quantitation in AMH109. Bars represent the frequency of adjusted p-values for the fold change of protein abundance between wild type and AMH109 (the *rpoN* transposon insertion mutant).

The top 30 most upregulated proteins are shown in Table 5.3. Three proteins encoded by the carbapenem operon were upregulated; CarD, CarH and CarC, with fold changes of between 1.22 and 0.96, representing approximately double the amount of protein seen in wild type S39006. This observation is consistent with the increased production of carbapenem observed in the *rpoN* mutant in earlier assays. Figure 5.18B shows the changes in protein production across the entire carbapenem cluster with all proteins that were detected showing significant increases in abundance, although CarA, CarB, CarF and CarG were not among the top 30 proteins shown in Table 5.3. CarR and CarE were not detected in this proteomic analysis.

Other upregulated proteins had a diverse range of functions including transcriptional regulators, transporters, a creatininase and a monooxygenase. Where no specified protein name was annotated the proteins have been named after their respective cognate open reading frame e.g. *orf6740* encodes the Creatininase Orf6740. Among the most highly upregulated proteins, two groups emerged, those encoded by *orf6745* to *orf6720*, and *orf7530* to *orf7540*. An analysis of the genomic context of each region revealed a seven gene operon encompassing *orf6750* to *orf6720* and a three gene operon including *orf7530*, *orf7535* and *orf7540*. While the proteomic analysis did not identify any protein predicted to be encoded by Orf6750 or Orf6725, the remaining five proteins, Orf6745, Orf6740, Orf6735, Orf6730 and Orf6720 were detected. These five proteins were among the most highly upregulated of the entire *rpoN* mutant, with a fold change in abundance ranging from 1.72 to 3.58. This provides strong evidence that RpoN is involved in the repression of this operon, either directly or indirectly through another regulator. The proteins encoded by this operon appear to be involved in the production of an ABC transporter system, and include a substrate-binding protein, a permease, and an ATP binding protein. The second highly upregulated operon, *orf7530* to *orf7540*, contains a GntR family transcriptional regulator (*orf7530*), an aspartate/glutamate racemase (*orf7535*), and an allantoinase homologous to PuuE (*orf7540*). Orf7535 was not detected in this proteomics analysis, but the other two proteins encoded by the operon are upregulated by a fold change of 2.01 and 1.59 respectively, representing two to four times the amount of protein in the *rpoN* mutant compared to the wild type S39006.

Table 5.3 – The top thirty most upregulated proteins quantified AMH109.

Protein ID	Description	Log₂ FC	Adjusted p-value
A0A2I5T4P5	Creatininase, Orf6740	3.58	5.28E-10
A0A2I5T4Q2	Monooxygenase, Orf6810	3.20	2.45E-10
A0A2I5TH49	ABC transporter substrate-binding protein, Orf6735	2.89	1.26E-12
A0A2I5T4P8	ABC transporter ATP-binding protein, Orf6730	2.67	9.56E-13
A0A2I5TM90	Ornithine decarboxylase, SpeF	2.44	6.11E-09
A0A2I5T4Q6	FAD-binding oxidoreductase, Orf6720	2.27	1.71E-13
A0A2I5THF2	GntR family transcriptional regulator, Orf7530	2.01	1.71E-13
A0A2I5TH26	RidA family protein, Orf6745	1.72	3.57E-12
A0A2I5THS3	ABC transporter substrate-binding protein, Orf8140	1.66	2.44E-13
A0A2I5TQC3	Allantoinase, Orf7540	1.59	4.42E-13
A0A2I5TII5	Histidine ammonia-lyase, Orf9705	1.53	9.56E-13
A0A2I5TM24	D-alanyl-D-alanine endopeptidase, Orf16610	1.31	4.05E-09
A0A2I5TFS3	UPF0597 protein, Orf4245	1.28	1.31E-07
A0A2I5TIL3	Carbapenem biosynthesis protein, CarD	1.22	1.75E-07
A0A2I5T664	ABC transporter substrate-binding protein, Orf9685	1.22	1.71E-13
A0A2I5T388	NUDIX domain-containing protein, Orf3920	1.21	1.82E-10
A0A2I5TC92	RNA chaperone/antiterminator, CspA	1.19	1.77E-07
A0A2I5T6L2	Uncharacterized protein, Orf10590	1.12	2.91E-10
A0A2I5T6A9	Carbapenem biosynthesis protein, CarH	1.12	6.22E-11
A0A2I5T7P1	Spermidine/putrescine ABC transporter substrate-binding protein, Orf12705	1.06	4.94E-11
A0A2I5TEU6	Phosphomethylpyrimidine synthase ThiC	1.06	4.79E-10
A0A2I5TCD9	ATP-dependent RNA helicase, DeaD	1.05	2.73E-08
A0A2I5TIZ1	NiFe hydrogenase, Orf10620	1.02	6.64E-07
A0A2I5TIG5	HAAAP family serine/threonine permease, Orf9620	1.00	1.06E-07
A0A2I5T8J1	UPF0260 protein, Orf14435	0.99	1.50E-08
A0A2I5TKF6	Uncharacterized protein Orf13555	0.99	2.93E-10
A0A2I5TG97	Miniconductance mechanosensitive channel, Orf5240	0.98	0.0054
A0A2I5TJH2	Oxidoreductase, Orf11645	0.98	4.90E-12
A0A2I5TIM8	DUF1933 domain-containing protein Orf9920	0.97	1.00E-06
A0A2I5TIN1	Carbapenem-3-carboxylate synthase, CarC	0.96	2.52E-06

An analysis of proteins with decreased abundance in the *rpoN* mutant compared to wild type S39006 showed 169 proteins with a $\log_2(\text{Fold Change})$ of greater magnitude than -0.5. The thirty proteins with the greatest decrease in abundance are shown in Table 5.4. Unsurprisingly, multiple proteins from the gas vesicle cluster were highly down regulated with GvpA1, GvpN, GvpV, GvpF1, and GvpW all found in the top 30 with fold changes ranging from -4.19 to -2.04. This is consistent with the observed changes in opacity in the *rpoN* mutant and the reduction in transcription of the *gvpA1* operon seen in transcriptional fusions (Figure 5.3A). An analysis of the change in abundance of all proteins encoded by the *gvpA1* and *gvrA* operons is shown in Figure 5.16A & B. The *gvpA1* operon shows the most dramatic changes with highly downregulated proteins in the first half of the operon. The proteins encoded by later genes, *gvpA2* to *gvpY* show smaller changes in abundance, from -0.9 (GvpX) to -0.26 (GvpA3), raising the possibility of another promoter within the operon. In contrast, proteins encoded by the *gvrA* operon were upregulated relative to wild type, although the fold changes in abundance were much smaller compared to the levels of downregulation seen from the first operon. All of these changes were statistically significant, but it is difficult to determine the biological significance of small changes in protein abundance from a proteomics experiment alone.

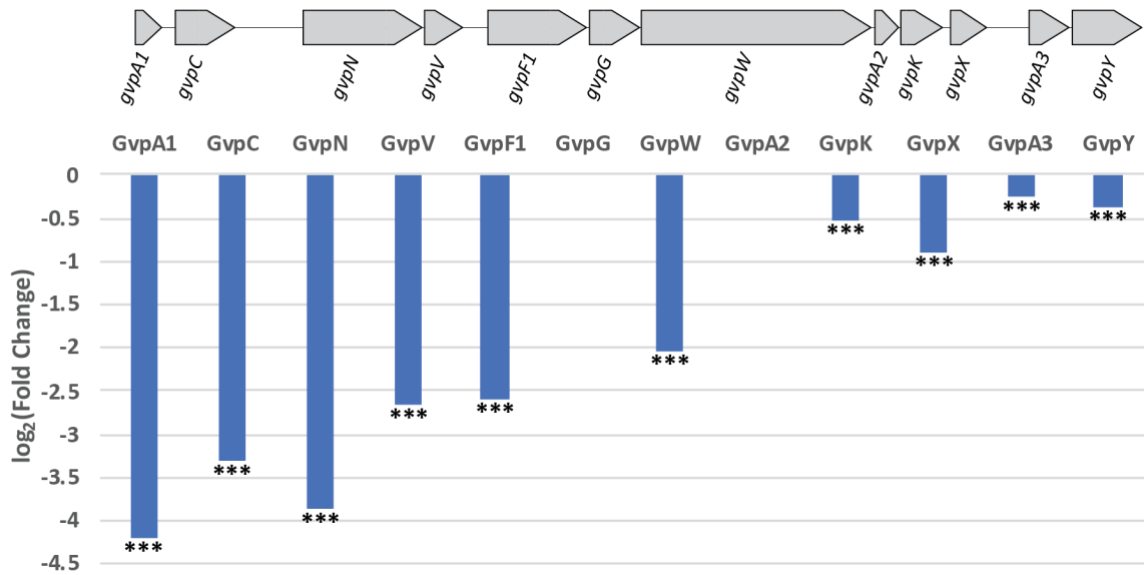
In experiments to quantify the production of prodigiosin, the *rpoN* mutant showed lower levels of pigment production, however these differences were not statistically significant (Figure 5.5B). In the proteomics analysis, 13 of the 15 proteins from the genes of the prodigiosin biosynthetic operon were detected; only PigL and PigM were not detected. The fold change in abundance of the proteins encoded by the prodigiosin gene cluster ranged from 0.10 to -1.13 (Figure 5.17A). Although the changes in some genes are less than the fold change threshold of 0.5, they are statistically significant. PigO was the only protein detected with a non-significant fold change. These changes suggest that *rpoN* does play a role in the regulation of prodigiosin production, however these changes are not as dramatic as those observed for other regulators of prodigiosin. During phenotype assays, it was also noted that the *rpoN* mutant showed a reduction in swimming motility and was unable to swarm (Figure 5.4E & F). An analysis of proteins involved in flagellar synthesis and chemotaxis has found 29 proteins that were significantly downregulated with a fold change

below -0.5 (Table 5.5). Several other proteins predicted to be involved in motility were also identified with smaller fold changes.

Table 5.4 – The top thirty most downregulated proteins quantified AMH109.

Protein ID	Description	Log₂ FC	Adjusted p-value
A0A2I5TMG5	Effector protein, Orf17400	-4.48	1.57E-08
M9WML5	Gas vesicle structural protein, GvpA1	-4.19	2.91E-10
A0A2I5T9H4	Acyl carrier protein, 16240	-3.92	2.14E-11
M9WR86	Gas vesicle protein, GvpN	-3.86	1.54E-09
A0A2I5TLW3	Uncharacterized protein, Orf16225	-3.64	3.94E-11
A0A2I5TDG0	Acyl-CoA dehydrogenase, Orf16180	-3.46	3.85E-11
A0A2I5TME6	Hydrogenase 4 subunit H, Orf17295	-3.45	1.77E-10
M9WV25	Gas vesicle structural protein, GvpC	-3.30	3.58E-10
A0A2I5TME0	NADH-quinone oxidoreductase subunit, NuoB	-3.11	2.16E-09
A0A2I5TMD4	Formate hydrogenlyase maturation protein, HycH	-3.00	1.00E-12
A0A2I5TCN3	Acetoin catabolism protein X, Orf22445	-2.97	3.09E-08
A0A2I5TLX4	HlyD_D23 domain-containing protein, Orf16280	-2.87	8.12E-11
A0A2I5TPZ3	ABC transporter substrate-binding protein, Orf22440	-2.81	3.78E-12
A0A2I5TDH0	Electron transporter, Orf17260	-2.66	2.10E-11
A0A2I5TM3	Formate dehydrogenase subunit alpha, Orf17405	-2.66	7.80E-11
M9WV41	Gas vesicle protein, GvpV	-2.65	3.57E-12
A0A2I5TLX0	Diaminopimelate decarboxylase, Orf16230	-2.63	7.35E-12
A0A2I5TCK9	Alpha-ketoacid dehydrogenase subunit beta, Orf22435	-2.59	6.85E-12
M9WV12	Gas vesicle protein, GvpF1	-2.59	2.41E-11
A0A2I5T9G0	Alanine-phosphoribitol ligase, Orf16200	-2.58	5.89E-12
A0A2I5TLU8	Uncharacterized protein, Orf16175	-2.58	8.22E-13
A0A2I5TD67	Phage shock protein, PspA	-2.55	5.89E-12
A0A2I5TPX7	Acetoin dehydrogenase dihydrolipoyllysine-residue acetyltransferase, Orf22430	-2.44	3.85E-11
A0A2I5TLU7	DUF2807 domain-containing protein, Orf16160	-2.31	3.37E-12
A0A2I5T9I0	Acyl-CoA dehydrogenase, Orf16195	-2.24	2.00E-12
A0A2I5T9J1	Cytochrome P450, Orf16165	-2.13	1.71E-13
M9WMK5	Gas vesicle protein, GvpW	-2.04	1.02E-11
A0A2I5TDX7	Ribosome hibernation promoting factor, Hpf	-2.03	4.83E-11
A0A2I5TME7	Hydrogenase large subunit, HycE	-2.01	3.01E-11
A0A2I5TME2	Hydrogenase 4 subunit, Orf17265	-1.97	3.60E-11

A.



B.

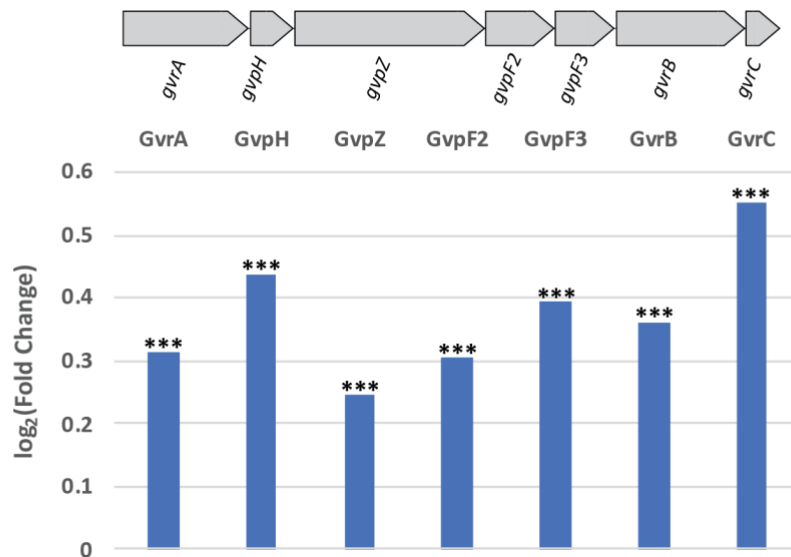
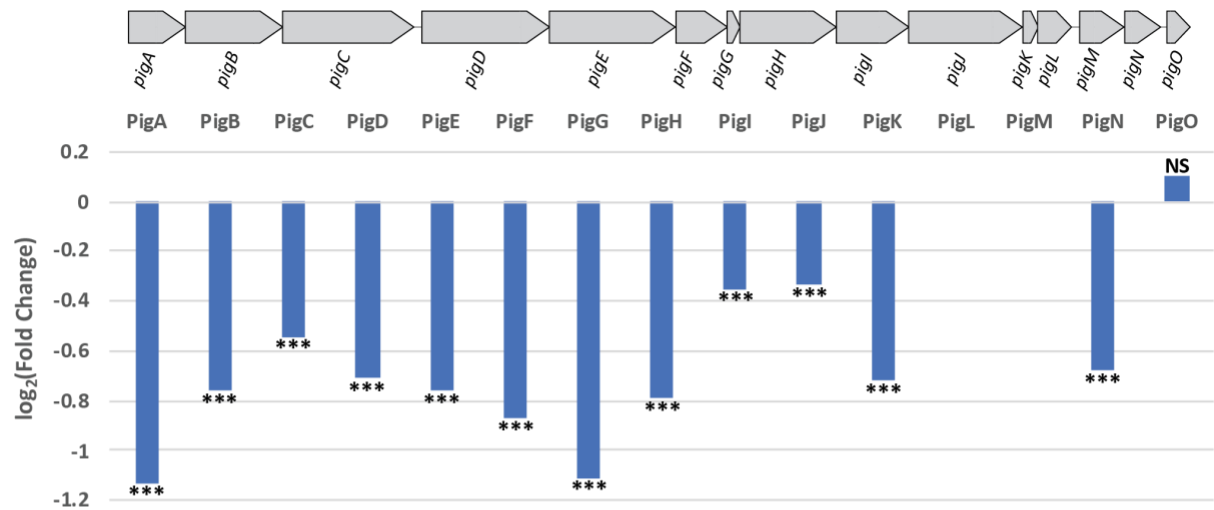


Figure 5.17 – RpoN modulates proteins of the *gvpA1* and *gvrA* operons.

Bars represent the difference in production of the indicated protein in AMH109 compared to S39006. Stars represent the adjusted p-values: ***, $p < 0.001$. Proteins not detected in the proteomic analysis are represented by spaces without bars.

A.



B.

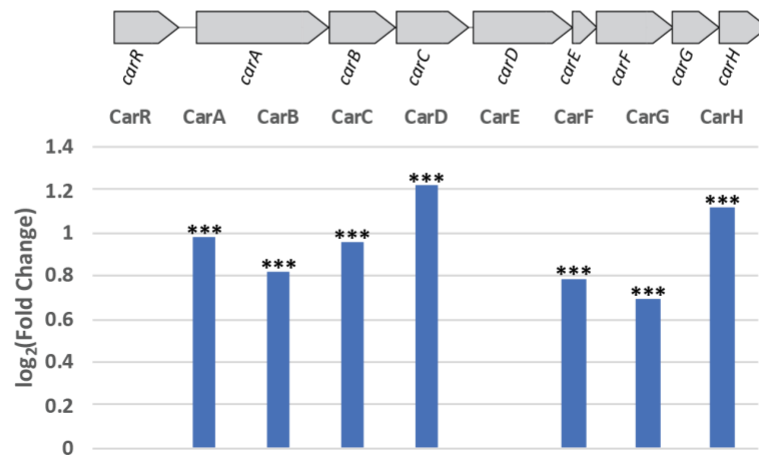


Figure 5.18 – RpoN modulates the expression of the prodiginosin and carbapenem operons. Bars represent the difference in production of the indicated protein in AMH109 compared to S39006. Stars represent the adjusted p-values: ***, $p < 0.001$. Proteins not detected in the proteomic analysis are represented by spaces without bars.

Table 5.5 – The fold change of proteins involved in flagellar biosynthesis and chemotaxis in AMH109.

Protein ID	Description	Log₂ FC	Adjusted p-value
A0A2I5TNH2	Methyl-accepting chemotaxis protein	-1.75	2.40E-10
A0A2I5T731	Basal-body rod modification protein, FlgD	-1.71	1.02E-10
A0A2I5TQV1	Chemotaxis protein	-1.43	7.43E-09
A0A2I5T7L5	Chemotaxis protein	-1.31	4.14E-10
A0A2I5T704	Flagellar motor stator protein, MotA	-1.28	3.21E-09
A0A2I5T2Y6	Methyl-accepting chemotaxis protein	-1.28	2.73E-10
A0A2I5T751	Methyl-accepting chemotaxis protein II	-1.17	1.48E-08
A0A2I5T6Z9	Motility protein, MotB	-1.12	1.94E-10
A0A2I5T4U2	Methyl-accepting chemotaxis protein	-1.10	8.55E-09
A0A2I5T734	Flagellar assembly protein, FliH	-1.05	5.59E-10
A0A2I5TJ11	Flagellin	-1.00	5.00E-10
A0A2I5TJF3	Flagellar motor switch protein, FliG	-1.00	2.14E-11
A0A2I5TL40	Methyl-accepting chemotaxis protein	-0.98	4.05E-09
A0A2I5T6Z1	Chemotaxis protein, CheA	-0.95	6.27E-10
A0A2I5TCN4	Methyl-accepting chemotaxis protein	-0.92	4.36E-08
A0A2I5TJC4	Methyl-accepting chemotaxis protein	-0.87	1.39E-08
A0A2I5T745	Flagellar M-ring protein	-0.83	4.48E-09
A0A2I5T7J5	Chemotaxis protein	-0.79	5.74E-09
A0A2I5TJE5	Chemotaxis protein, CheW	-0.73	1.10E-09
A0A2I5T773	Flagellar hook-filament junction protein, FlgL	-0.67	1.99E-05
A0A2I5TMV9	Methyl-accepting chemotaxis protein	-0.64	2.01E-07
A0A2I5T707	Chemotaxis protein methyltransferase	-0.64	5.43E-11
A0A2I5T9J2	Methyl-accepting chemotaxis protein	-0.62	1.58E-06
A0A2I5T787	Flagellum-specific ATP synthase, FliI	-0.62	1.61E-08
A0A2I5TDL0	Methyl-accepting chemotaxis protein	-0.62	2.01E-09
A0A2I5T713	Flagellar hook-associated protein 1	-0.62	1.84E-06
A0A2I5T4V5	Methyl-accepting chemotaxis protein	-0.56	1.68E-07
A0A2I5T4L4	Methyl-accepting chemotaxis protein	-0.54	2.23E-07
A0A2I5T4A0	Methyl-accepting chemotaxis protein	-0.50	4.31E-07
A0A2I5TJG3	Flagellar hook-associated protein 2	-0.47	0.001344
A0A2I5TJD2	Chemotaxis protein, CheY	-0.47	4.99E-08
A0A2I5T727	Flagellar protein, FliL	-0.45	2.65E-06
A0A2I5T716	Flagellar biosynthetic protein, FlhB	-0.41	6.93E-07
A0A2I5TEC6	Methyl-accepting chemotaxis protein	-0.41	3.77E-05

In addition to proteins that were expected to be down regulated in the *rpoN* mutant based on phenotype assays: GV proteins, prodigiosin biosynthesis proteins and flagellar proteins; several other proteins were identified by the proteomics analysis. The proteins with the greatest fold changes in abundance are shown in Table 5.4 and a genomic analysis of the genes predicted to encode them was performed. Two particularly heavily downregulated proteins, encoded by genes *orf17400* and *orf17405* had a fold change of -4.48 and -2.66. These genes are predicted to encode an effector protein and formate dehydrogenase subunit respectively. Two other key regions were those encoded by genes *orf22450* to *orf22430* and *orf16280* to *orf16160*. In addition to showing some of the strongest decreases in protein abundance, both regions contain a predicted σ^{54} -dependent transcriptional regulator, similar to that encoded by *gvrA*. The genomic organization of these regions, fold changes in abundance and the predicted function of each protein is shown in Figures 5.19 & 5.20 and Tables 5.6 & 5.7.

The cluster of genes shown in Figure 5.19 is predicted to be involved in the utilisation of acetoin as a carbon source. The protein products encoded by *orf22445*, *orf22440*, *orf22435*, and *orf22430* were four of the most highly downregulated proteins found in the quantitative proteomic analysis of AMH109. The protein encoded by *orf22425* was not detected in this analysis. This provides strong evidence that σ^{54} is responsible, either directly or indirectly for expression of these genes. The gene directly upstream of the predicted acetoin catabolism operon, *orf22450* encodes a σ^{54} -dependent transcriptional regulator, which was only very slightly downregulated compared to the downstream genes.

The second cluster of genes that showed strong downregulation in many of the predicted protein products was the 25 gene region spanning *orf16280* to *orf16160* (Figure 5.20). Of these 25 genes, five were not detected in the proteomic analysis (the proteins encoded by *orf16255*, *orf16250*, *orf16245*, *orf16220*, and *orf16190*). One protein showed no significant difference (Orf16260), while the other 19 proteins of the cluster were all significantly downregulated, although the magnitude of the downregulation varied with \log_2 Fold Changes of -0.39 to -3.64. This region is homologous to the Virulence Factor Modulating (*vfm*) cluster first characterised in *Dickeya dadantii* (Duprey et al., 2019; Nasser et al., 2013). This cluster contains a σ^{54} -dependent transcriptional regulator, which shows only a slight

change in abundance, similar to that encoded by *orf22450* in the previously discussed operon. A wide range of changes in protein abundance were observed, indicating that not all genes are under the control of σ^{54} and that there are other factors in play that govern the regulation of this cluster in S39006. This is not a surprising finding given the complex and overlapping nature of gene regulation that has previously been described in this bacterium. Taken together, this suggests that σ^{54} modulates expression of the *vfm* cluster in S39006, possibly using the product of *orf16265* as an enhancer binding protein.

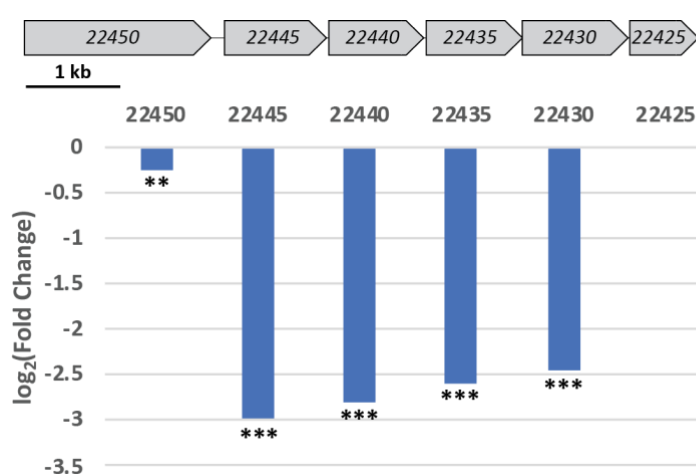


Figure 5.19 – Genomic organisation and changes in protein abundance of Orf22450 to Orf22425. Bars represent the difference in production of the indicated protein in AMH109 compared to S39006. Stars represent the adjusted p-values: **, $p < 0.01$; ***, $p < 0.001$. Proteins not detected in the proteomic analysis are represented by spaces without bars.

Table 5.6 – Predicted functions of proteins encoded by *orf22450* to *orf22425*.

Gene Name	Predicted Function	Log ₂ FC	Adjusted p-value
<i>orf22450</i>	σ^{54} -dependent Fis family transcriptional regulator	-0.24	0.0019
<i>orf22445</i>	Acetoin catabolism protein X	-2.97	3.09E-08
<i>orf22440</i>	ABC transporter substrate binding protein	-2.81	3.78E-12
<i>orf22435</i>	Alpha-ketoacid dehydrogenase subunit beta	-2.59	6.85E-12
<i>orf22430</i>	Acetoin dehydrogenase dihydrolipoyllysine-residue acetyltransferase subunit	-2.44	3.85E-11
<i>orf22425</i>	Lipoate-protein ligase A	Not Detected	

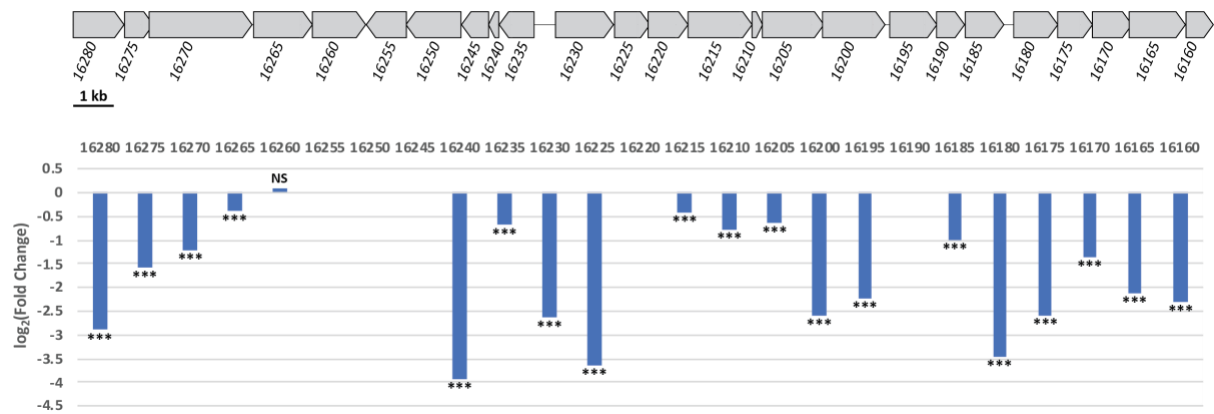


Figure 5.20 – Genomic organisation and changes in protein abundance of Orf16280 to Orf16160. Bars represent the difference in production of the indicated protein in AMH109 compared to S39006. Stars represent the adjusted p-values: ***, $p < 0.001$; NS, not significant. Proteins not detected in the proteomic analysis are represented by spaces without bars.

Table 5.7 – Predicted functions of proteins encoded by *orf16280* to *orf16160*.

Gene Name	Predicted Function	Log ₂ FC	Adjusted p-value
<i>orf16280</i>	Uncharacterised protein	-2.87	8.12E-11
<i>orf16275</i>	ABC transporter ATP-binding protein	-1.56	5.74E-09
<i>orf16270</i>	Peptide ABC transporter permease	-1.23	8.03E-11
<i>orf16265</i>	σ^{54} -dependent Fis family transcriptional regulator	-0.39	5.05E-09
<i>orf16260</i>	PAS domain-containing sensor histidine kinase	0.08	0.162
<i>orf16255</i>	Alpha/beta hydrolase	Not Detected	
<i>orf16250</i>	Uncharacterised protein	Not Detected	
<i>orf16245</i>	VfmB protein	Not Detected	
<i>orf16240</i>	Acyl carrier protein	-3.92	2.14E-11
<i>orf16235</i>	Uncharacterised protein	-0.68	1.89E-04
<i>orf16230</i>	Diaminopimelate decarboxylase	-2.63	7.35E-12
<i>orf16225</i>	Uncharacterised protein	-3.64	3.94E-11
<i>orf16220</i>	3-oxoacyl-ACP synthase	Not Detected	
<i>orf16215</i>	Long-chain fatty acid-CoA ligase	-0.41	1.15E-07
<i>orf16210</i>	Phosphopantetheine-containing protein	-0.79	1.93E-09
<i>orf16205</i>	Alanine-phosphoribitol ligase	-0.62	2.46E-04
<i>orf16200</i>	Alanine-phosphoribitol ligase	-2.58	5.89E-12
<i>orf16195</i>	Acyl-CoA dehydrogenase	-2.24	2.00E-12
<i>orf16190</i>	Uncharacterised protein	Not Detected	
<i>orf16185</i>	3-oxoacyl-ACP synthase	-1.01	7.45E-13
<i>orf16180</i>	Acyl-CoA dehydrogenase	-3.46	3.85E-11
<i>orf16175</i>	Uncharacterised protein	-2.58	8.22E-13
<i>orf16170</i>	3-oxoacyl-ACP synthase	-1.35	4.25E-12
<i>orf16165</i>	Cytochrome P450	-2.13	1.71E-13
<i>orf16160</i>	Uncharacterised protein	-2.31	3.37E-12

σ^{54} was originally identified as a regulator of nitrogen metabolism and fixation. To determine if this sigma factor was carrying out a similar function in S39006 the proteomic data was screened for any proteins known to be involved in nitrogen regulation or nitrogen fixation. S39006 has a complete set of *nif* genes, which encode a nitrogenase complex to convert atmospheric nitrogen into a usable form. However, it has not been shown to fix atmospheric nitrogen thus far. Given that the proteome extraction was carried out in a rich medium and under aeration, there is unlikely to be any significant expression of the *nif* cluster. Two proteins encoded by the *nif* cluster were identified, NifK and NifY, both of which were slightly upregulated (\log_2FC of 0.27 and 0.18 respectively). The other proteins encoded by the *nif* cluster were not detected in the proteomic analysis. One protein that was significantly downregulated in the *rpoN* mutant was the nitrogen regulatory protein PtsN, which had a \log_2FC of -0.80.

A search for other known regulators in S39006 revealed that Hfq was significantly upregulated ($\log_2FC = 0.79$) in the *rpoN* mutant compared to wild type S39006 while RhIA and PigT were significantly down regulated. The decrease in abundance of RhIA could explain the inability of the *rpoN* mutant to swarm. Other previously described regulators of motility or antibiotic production were detected in the proteomic analysis but were only slightly altered in abundance implying that they are unlikely to be the mechanism through which RpoN is acting to alter the various pleiotropic phenotypes described (Table 5.8).

Table 5.8 – Fold change in abundance of known regulators in the *rpoN* mutant.

Protein ID	Description	Log ₂ FC	Adjusted p-value
A0A2I5TGF0	RNA-binding protein Hfq	0.79	0.00124
A0A2I5TBT4	XRE family transcriptional regulator, PigP	-0.19	1.71E-05
A0A2I5TQV6	ArsR family transcriptional regulator, PigS	-0.28	1.64E-04
A0A2I5TCX5	GntR family transcriptional regulator, PigT	-0.56	1.38E-10
A0A2I5TIV4	LysR family transcriptional regulator, PigU	0.17	3.56E-04
A0A2I5TEY7	Phosphate transport system permease protein, PstA	0.19	0.002
A0A2I5TEY8	Phosphate-binding protein, PstS	0.30	0.0815
A0A2I5T5K2	RNA-binding protein, RsmA	-0.03	0.29
A0A2I5T515	Stationary phase sigma factor, RpoS (σ^{38})	-0.16	0.012
Q9RA96	SylA-like transcriptional regulator, Rap	0.28	1.19E-06
A0A2I5T9G2	Alpha/beta hydrolase, RhIA	-0.88	5.76E-09

5.2.9 Prediction of RpoN binding sites in S39006

The regulon of σ^{54} has been well studied and as a result consensus sequences for the σ^{54} binding site have been determined (Barrios et al., 1999; Cases et al., 2003; Dombrecht et al., 2002; Studholme, 2002). The σ^{54} binding site consensus sequence in *E. coli* was used as a starting point for a bioinformatic screen of potential binding sites in S39006 (Barrios et al., 1999; Bonocora et al., 2015; Hunt & Magasanik, 1985). Using MEME suite, putative σ^{54} binding sites were determined and a S39006 specific consensus sequence was built (Figure 5.21). A table of the top hits for putative σ^{54} binding sites in S39006 and the genes they are found upstream of is shown in Table 5.9. The genes that are predicted to be downstream of a *rpoN* binding site encode proteins with a wide variety of functions. More experiments are needed to fully validate these putative σ^{54} binding sites in S39006, however many of the predicted sites are consistent with the proteomic analysis presented in this chapter.

For instance, the acetoin catabolism operon shown in Figure 5.19 and encoded by *orf22445* to *orf22425* is predicted to have a σ^{54} binding site located upstream of the first gene in the operon, *orf22445*, immediately downstream of *orf22450* which encodes a σ^{54} -dependent transcriptional activator. Similarly, there is a σ^{54} binding site located upstream of *orf16280*, the first gene of the putative S39006 *vfm* cluster. This cluster was highlighted from the proteomics analysis as encoding proteins that were extremely reduced in abundance in the *rpoN* mutant. A σ^{54} binding site upstream of *gvpA1* was also detected in this analysis, consistent with the previous identification by Tashiro et al. (2016). Another binding site was found upstream of *glnK*, consistent with previous findings in *E. coli* (Reitzer & Schneider, 2001).

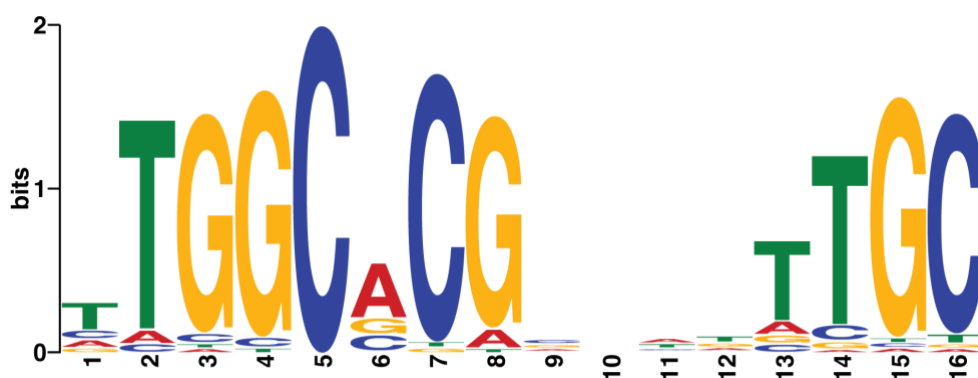


Figure 5.21 – Predicted binding site of RpoN in S39006 generated by MEME.

Table 5.9 – The location of predicted RpoN binding sites in S39006.

Name	Predicted Function	p-value	Binding Site
<i>orf6980</i>	Cytosine permease	8.67E-07	CATACAAAAATAGGCACGCTTA TTGCTCTATCCCT
<i>orf22445</i>	Acetoin catabolism protein X	1.33E-06	ATAATAACACTTGGCCCCGAAAT TTGCCATAGAGATT
<i>orf12705</i>	Spermidine/putrescine ABC transporter substrate binding protein	1.33E-06	TTATCAGATATTGGCACGAAAT ATGCTTTATATAAA
<i>orf7240</i>	Glycerate kinase	7.23E-06	CACTCGGTAGTTGGCAGGGCTG GTGCCCTGCGTCTA
<i>orf12805</i>	RNA polymerase sigma factor	7.23E-06	CATTAAGGGTGTGGCACACGCT TTGCTATCTCGCTC
<i>orf16805</i>	LysR family transcriptional regulator	8.65E-06	TAAAAGGAATATGGCGCGGTTT TTGCTACCTGTAGA
<i>orf6480</i>	GntR family transcriptional regulator	8.65E-06	CTAGGTAAAATGGCACGAGAA GTGCTTTGATTTAA
<i>orf7570</i>	Gamma-glutamyltransferase	1.40E-05	GTGGAAAAGATGGAACGGGT TTTGCTTTACCCCGG
<i>orf9715</i>	ABC transporter permease	1.40E-05	CTAAAGAAAGCTGGCACAACCA TTGCTTGTATAGAC
<i>uraD</i>	OHCU decarboxylase	1.40E-05	CTCGATATAAATGGCATGCTAG TTGCAGATCTCTTA
<i>atzF</i>	Allophanate hydrolase	1.40E-05	AATTA AAAATATGGCACGGTGT TTGTATGAATGGAC
<i>glnK</i>	Nitrogen regulatory protein GlnK	1.40E-05	AAATCATTTTATGGCACACCATT TGCTTTATTGATG
<i>orf16945</i>	LuxR family transcriptional regulator	1.40E-05	AATGAGGAAGCTGGCACCGTGT TTGCATGGTGTCTG
<i>gvpA1</i>	Gas vesicle structural protein	1.40E-05	TGCCTATAGGTTGGCGCATGAG TTGCATTCTACATG
<i>modA</i>	Molybdate ABC transporter substrate binding protein	1.63E-05	ACGCTCAATGTTGGCATGACGG TTGTGTATTCTGAC
<i>orf14070</i>	PrkA family serine protein kinase	1.63E-05	GCACCACAAGTTGGCATAAGGG TTGCTGTA CTGACA
<i>orf21080</i>	Integrase	1.63E-05	CTAAGCCCGCTTGGAAACCAGCC TTGCGGGCTTTTTT
<i>orf16280</i>	Hypothetical protein	2.10E-05	GAGATGATAATTGGCATGAATG CTGCTTGATGCTGG

5.3 Discussion

The production of gas vesicles in *S39006* is controlled by a complex regulatory network. Regulatory inputs include proteins encoded by the GV cluster (*GvrA*, *GvrB*, and *GvrC*), quorum sensing, and the Rsm system (a homologue of the Csr system in *E. coli*) (Ramsay et al., 2011). Further elements of the regulatory have been identified through random transposon mutagenesis screens. Proteins that perform a broad range of functions have been linked to GV production in *S39006* including *PigX*, *PigP*, *RbsR*, *TopA*, *FloR*, and *TrkH* (Lee, 2019; Lee et al., 2017; Quintero-Yanes et al., 2020, 2019; Ramsay et al., 2011). *RbsR* acts as a repressor of the ribose operon and is a LacI family transcriptional regulator that is predicted to bind upstream of *gvrA* to activate production of GVs (Lee et al., 2017). It is likely that there are other factors affecting binding of *RbsR* at the *gvrA* site as an electrophoretic mobility shift assay (EMSA) could not prove binding at this site, only at a site upstream of *rbsD* (the first gene of the ribose operon) (Lee et al., 2017). The binding of *RbsR* was reduced in the presence of ribose indicating that the availability of this carbon source could affect when GVs are produced.

The availability of oxygen also affects GV production, with expression of the GV cluster significantly upregulated in low oxygen environments (Ramsay et al., 2011). Environmental potassium levels have also been shown to affect GV production. A mutant with a transposon insertion in *trkH*, encoding a low-affinity potassium uptake transporter, showed a hyper opaque phenotype and overproduced GVs (Quintero-Yanes et al., 2019). Expression of the *gvpA1* operon and flotation was reduced in wild type *S39006* at high concentrations of potassium indicating that potassium, imported via *TrkH*, is a key environmental signal regulating cell buoyancy in *S39006* (Quintero-Yanes et al., 2019). *FloR*, a DeoR family transcription factor, has also been described as a global regulator in *S39006*, controlling GV and antibiotic production, motility and virulence (Quintero-Yanes et al., 2020). GV, carbapenem and prodigiosin antibiotic production, and virulence in a *C. elegans* model were all reduced in a *floR* mutant while swimming and swarming motility was upregulated (Quintero-Yanes et al., 2020). A proteomic analysis of a *floR* transposon insertion mutant indicated that *FloR* regulates these varied phenotypes by controlling the transcription of regulatory genes including *rsmA*, *rpoS*, and *pigU* (Quintero-Yanes et al., 2020).

In this chapter a comprehensive analysis was performed to determine the effect of a transposon insertion in *rpoN*. RpoN (also called σ^{54} or σ^N) has been widely studied in various systems but it has not been characterised in S39006 until now. The *rpoN* mutant was found to have decreased flotation ability and production of GVs. This was due to a reduction in transcription of the *gvpA1* operon (which encodes the GV structural genes) but no significant changes in transcription of the *gvrA* operon were observed (Figure 5.3). The *gvrA-gvrC* operon encodes three regulators of GV production: GvrA, GvrB and GvrC. In a study of single gene knockouts for each gene of the GV cluster, knockouts of *gvrA* and *gvrB* were unable to produce GVs while in the *gvrC* knockout a few GVs could be observed in cells taken from a colony on a plate – but none in planktonic cells (Tashiro et al., 2016). This showed that GvrA, GvrB, and GvrC are all required independently for full GV production in S39006. It was suggested that these regulators could be integrating different physiological or environmental cues into the GV production pathway (Tashiro et al., 2016). GvrA contains three domains: a response regulator domain, an AAA+ ATPase domain (characteristic of a σ^{54} interaction domain), and a helix turn helix domain (characteristic of other bacterial regulatory proteins including Fis) (Monson et al., 2016; Ramsay et al., 2011). GvrB contains a PAS domain, a histidine sensor kinase domain and a histidine kinase-like ATPase domain (Monson et al., 2016; Ramsay et al., 2011). GvrA and GvrB show similarity to two-component regulatory system proteins NtrC and NtrB respectively (Monson et al., 2016; Ramsay et al., 2011). GvrC is similar to the single-domain response regulator protein CheY (Monson et al., 2016; Ramsay et al., 2011).

The NtrBC two component system was originally described in *E. coli* whereby NtrB autophosphorylates under nitrogen-limiting conditions and transfers a phosphate to the response regulator NtrC, a bacterial enhancer binding protein, that activates σ^{54} -dependent transcription (Ninfa & Magasanik, 1986; Reitzer & Magasanik, 1985; Weiss & Magasanik, 1988). Bacteria utilize various sigma factors to co-ordinate expression of different groups of genes, due to the ability of sigma factors to enable promoter-specific transcription initiation of RNAP. These sigma factors fall into two distinct families, σ^{70} and σ^{54} (Merrick, 1993). In σ^{54} -dependent transcription, σ^{54} directs the RNA polymerase holoenzyme to bind DNA at the -12 and -24 promoter elements. The bEBP then binds to an upstream activator sequence and DNA looping allows interactions between the bEBP and σ^{54} to occur which

enables RNAP to form an open complex and transcription can occur (Buck et al., 2000; Bush & Dixon, 2012). In contrast, σ^{70} family sigma factors bind at -10 and -35 sequences with RNAP forming a closed complex that is readily converted to an open complex without the need for a bEBP (Bush & Dixon, 2012).

Given that there was no change in transcription of the *gvrA* operon in the *rpoN* mutant but a significant decrease in *gvpA1* transcription it is likely that σ^{54} acts directly to change transcription of the *gvpA1* operon and alter GV production. Previous analysis has identified a putative σ^{54} -binding site upstream of *gvpA1* and determined that *gvrA* is predicted to encode an NtrC-family bEBP (Ramsay et al., 2011; Tashiro et al., 2016). Therefore, the proposed mechanism through which σ^{54} activates GV production is through binding at the -12 and -24 sites with RNAP, which is then converted to an open complex by the binding of GvrA upstream, allowing transcription of the GV structural genes (Figure 5.22). This signal may be transduced via phosphorylation by GvrB, an NtrB-family protein and other external signals such as low oxygen concentration, high potassium concentration or nitrogen limitation. Further experiments are required to determine what signal might be transduced by the GvrB/GvrA system.

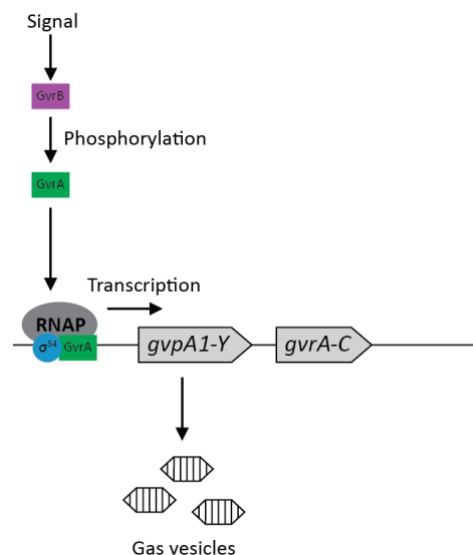


Figure 5.22 – Schematic diagram of the proposed method of σ^{54} regulation of GV production. GvrB transduces an unknown signal to GvrA via phosphorylation. This activates GvrA, facilitating binding to σ^{54} and allowing the conversion of RNAP to an open complex. This enables transcription of the *gvpA1* to *gvpY* operon, and the subsequent formation of mature GVs. In the absence of σ^{54} RNAP cannot form an open complex and no transcription of the *gvpA1* to *gvpY* operon can occur.

The quantitative proteomic analysis comparing wild type S39006 and the *rpoN* mutant revealed many proteins with significant increases and decreases in abundance. Many of these findings were reassuringly consistent with the phenotype assays already performed. For instance, the carbapenem biosynthetic proteins were strongly upregulated, and this is consistent with experimental data showing the *rpoN* mutant making twice as much carbapenem antibiotic as the wild type (Figures 5.18B & 5.5A). The reduction in prodigiosin production seen in the *rpoN* mutant was not statistically significant when quantified over the course of a growth curve, however the proteins encoded by the *pig* gene cluster were significantly reduced in abundance in the proteomics experiment. This is consistent with the greater differences in prodigiosin production seen at the 14 h time point of the growth curve, the point at which proteins were extracted for proteomic analysis (Figures 5.18A & 5.5B).

The *rpoN* mutant also showed a reduction in swimming motility and was unable to swarm (Figure 5.4E & F). An analysis of the proteomic data identified 29 proteins involved in flagellar motility and chemotaxis that were significantly downregulated in the *rpoN* mutant (Table 5.5). RhIA, which is required for surfactant biosynthesis and swarming motility in S39006 (Williamson et al., 2008), was also significantly downregulated with a fold change in abundance of -0.88. σ^{54} has been shown to regulate expression of flagellar structural and regulatory genes in *P. aeruginosa* (Dasgupta et al., 2003; Totten et al., 1990), *Helicobacter pylori* (Niehus et al., 2004), *Campylobacter jejuni* (Jagannathan et al., 2001), *Vibrio cholerae* (Prouty et al., 2001), *Labrenzia aggregata* (Xu et al., 2019), and *Bacillus cereus* (Hayrapetyan et al., 2015). This reduction in motility and flagellar synthesis could, at least in part, explain the attenuation in virulence the *rpoN* mutant displayed in a *C. elegans* model (Figure 5.6). Similar effects have been seen in *P. aeruginosa* where a *rpoN* mutant was impaired in its ability to kill *C. elegans*, exhibited reduced virulence in a mouse thermal injury model, and displayed reduced attachment and slower proliferation in an *Arabidopsis thaliana* leaf infectivity assay (Hendrickson et al., 2001). As S39006 is also capable of infecting plants, it would be interesting to determine if there was any reduction in virulence of the *rpoN* mutant in an *Arabidopsis*, tobacco, or potato model.

The proteomic analysis identified several significantly downregulated proteins in the *rpoN* mutant, including proteins predicted to be involved in the catabolism of acetoin. Acetoin (also called 3-hydroxy-2-butanone) is a metabolic product produced by a range of bacteria when grown on media containing glucose or other fermentable carbon sources (López et al., 1975; Xiao & Xu, 2007). The production of acetoin helps to prevent over-acidification of the cell as pyruvate is converted to acetoin (Tsau et al., 1992). Acetoin production also acts as an energy storing strategy as it can later be utilized during stationary growth when glucose has been depleted and acetoin also plays a role in the regulation of the NAD/NADH ratio (Grundy et al., 1993; Johansen et al., 1975; Xiao & Xu, 2007).

The genes responsible for the breakdown of acetoin are encoded by the *aco* gene cluster which has been investigated in a range of bacteria including *Bacillus subtilis* (Huang et al., 1999), *Clostridium magnum* (Kruger et al., 1994), *Klebsiella pneumoniae* (Deng et al., 1994), *Pelobacter carinolicus* (Oppermann & Steinbuchel, 1994), and *Pseudomonas putida* (Huang et al., 1994). The *aco* gene clusters from *B. subtilis*, *C. magnum*, and *P. putida* were all predicted to be preceded by a σ^{54} binding site (Xiao & Xu, 2007). The operon structure of S39006 shows the greatest similarity to that of *P. putida*. Bioinformatic analysis suggested a σ^{54} binding site was located upstream of *orf22445*. The gene directly upstream of *orf22445*, *orf22450*, is predicted to encode a σ^{54} -dependent transcriptional regulator. Based on the bioinformatic analysis and proteomics findings that proteins involved in the catabolism of acetoin were severely downregulated, it is highly likely that σ^{54} regulates acetoin catabolism by binding to the promoter sequence upstream of *orf22445* and is subsequently activated by the regulator encoded by *orf22450* to allow transcription of these genes to occur. This is very similar to the proposed mechanism through which σ^{54} controls transcription of the *gvpA1* operon following activation by GvrA. Further experiments need to be performed to test these hypotheses, for example ChIP-Seq could be used to determine where σ^{54} and bEBPs are binding to DNA. An EMSA using predicted binding sites as a probe and σ^{54} with or without the predicted bEBPs could also be performed.

Another region that was heavily downregulated in the *rpoN* mutant encoded a homologue of the *vfm* cluster found in many *Dickeya* species (Duprey et al., 2019; Nasser et al., 2013). This cluster encodes a second, AHL-independent, quorum sensing system in *Dickeya* and

function of this system in S39006 has not been fully investigated. The *vfm* cluster is required for virulence and PCWDE production in *D. dadantii* and the production of zeamines in *D. zea* (Lv et al., 2019; Nasser et al., 2013). If this region performs a similar function in S39006, it could also explain why pectate lyase production and virulence in *C. elegans* was reduced in the *rpoN* mutant. The two proteins of this cluster that showed the lowest change in abundance were the predicted σ^{54} -dependent transcriptional regulator encoded by *orf16265* (a homologue of *vfmH*) and the PAS domain-containing sensor histidine kinase encoded by *orf16260* (a homologue of *vfmI*). In *Dickeya* species, VfmH and VfmI form a two-component system that leads to VfmH regulating the expression of other *vfm* genes, including *vfmE* which encodes an AraC-type transcriptional regulator, VfmE, which itself regulates other *vfm* genes and genes encoding PCWDEs (Lv et al., 2019; Nasser et al., 2013). It is likely in S39006 that σ^{54} requires the presence of Orf16265 to initiate transcription of the genes in the *orf16280* – *orf16160* cluster. A putative σ^{54} binding site was identified upstream of *orf16280* however further experiments are required to determine the exact method of σ^{54} regulation of the S39006 *vfm* cluster and precisely what phenotypes are regulated by this system in S39006.

Several known regulators of secondary metabolite production, motility and virulence were identified in the proteomic analysis but few showed strong changes in abundance (Table 5.8). One protein that showed a significant increase in abundance was the RNA binding protein Hfq which has been previously characterized in S39006 (Wilf et al., 2013, 2011). An *hfq* mutant was unable to produce carbapenem or prodigiosin, had decreased PCWDE production and motility, and reduced virulence in *C. elegans* and potato models (Wilf et al., 2011). An *hfq* mutant was also shown to be unable to produce GVs in Chapter 3 of this work. Hfq regulates secondary metabolism in S39006 through positive regulation of the QS response regulators CarR and SmaR (Wilf et al., 2011). An increase in Hfq could therefore be responsible for the increased carbapenem production in the *rpoN* mutant. However, the increase in Hfq abundance does not explain the decrease in prodigiosin production and motility seen in the *rpoN* mutant. A potential reason for the decreased motility seen in the *rpoN* mutant could be due to an increase in RpoS (also called σ^S or σ^{38}) activity due to a lack of competition from RpoN. RpoS levels are increased during stationary phase and in S39006 RpoS acts as a repressor of antibiotic production and motility (Wilf & Salmond, 2012).

Analysis in *E. coli* has shown that 60 % of genes in the RpoN regulon are under reciprocal RpoS control, including flagellar genes (Dong et al., 2011). While there was no significant change in RpoS abundance in the *rpoN* mutant (Table 5.8), it is possible that the lack of RpoN allowed RpoS greater access to core RNA polymerase and therefore greater repression of genes involved in motility and prodigiosin production. RpoS has also been shown to be more stable in an *E. coli rpoN* mutant (Dong et al., 2011). Further experiments to determine the effects of competition between RpoS and RpoN in S39006 are required.

In addition to the proteomic analysis, a bioinformatic screen of putative σ^{54} binding sites in S39006 was carried out. Many of these sites were upstream of genes where the products showed decreased abundance in the proteomic analysis. Binding sites were also found proximal to putative bEBPs predicted to activate σ^{54} -mediated transcription and upstream of genes homologous to those under σ^{54} control in other systems, such as *glnK*. Further experimental work is required to validate these putative binding sites in S39006.

In summary, a random transposon mutagenesis screen identified a transposon insertion in *rpoN*, which is predicted to encode an alternative sigma factor, σ^{54} . The transposon insertion caused an increase in carbapenem production and a decrease in GV production, motility, pectate lyase production and virulence in *C. elegans*. A comparative quantitative proteomic analysis found 9.2 % of proteins identified were significantly altered in abundance with a $\log_2(\text{Fold Change})$ greater than ± 0.5 . The results of the proteomic analysis were consistent with the phenotype assays performed previously. The proteomic data also introduced novel avenues of investigation through the identification of significantly up and downregulated proteins that had not been linked to the *rpoN* mutant. These results show that σ^{54} is a highly pleiotropic regulator in S39006 and have suggested a mechanism through which σ^{54} affects GV production. Future experiments can be performed to further define the σ^{54} regulon in S39006 and determine if nitrogen availability is an important regulatory signal for flotation in this bacterium.

Chapter 6. The transcription factor DksA regulates production of gas vesicles and secondary metabolites in *Serratia* sp. ATCC 39006.

6.1 Introduction

The previous chapters of this dissertation described a random transposon mutagenesis screen carried out in S39006 to identify novel regulators of gas vesicle and secondary metabolite production. A wide range of putative regulators have been identified and characterized over the course of this study. Previously, in chapter 3, a transposon insertion in the gene *dksA* was identified that resulted in a loss of gas vesicles and flotation in S39006. This chapter describes the other pleiotropic impacts of this transposon insertion, using phenotypic characterisation and quantitative proteomic analysis.

DksA was originally identified as a DnaK suppressor when overexpression of DksA in *E. coli* enabled a *dnaK* mutant to overcome the temperature sensitive growth phenotype (Kang & Craig, 1990). DksA is a transcription factor that binds to the secondary channel of RNAP to potentiate the stringent response (Paul et al., 2004a). The stringent response is a method utilized by bacteria to respond to nutrient starvation conditions (Potrykus & Cashel, 2008). This response is induced by an accumulation of the alarmones ppGpp and pppGpp (guanosine tetraphosphate and guanosine pentaphosphate respectively), collectively referred to here as ppGpp (Potrykus & Cashel, 2008). DksA and ppGpp act synergistically to activate transcription of amino acid biosynthetic operons and repress transcription at rRNA promoters (Paul et al., 2004a, 2005). DksA is a virulence determinant in many bacteria and has been implicated in the production of fimbriae (Åberg et al., 2008), motility (Branny et al., 2001; Dalebroux et al., 2010b), and toxicity in various hosts (Mogull et al., 2001; Yun et al., 2008).

The DksA regulon has not been studied in S39006 nor has any link been made between this transcriptional regulator and flotation. This chapter aims to elucidate the effect of a mutation in *dksA* on a variety of phenotypes in S39006 and determine the pathways through which this regulation may be occurring.

6.2 Results

6.2.1 Sequence analysis and genomic context of *dksA*

During a random transposon mutagenesis screen, a translucent colony mutant was identified that did not appear to make any gas vesicles and was named AMH141. RP-PCR and sequencing determined that the transposon had inserted 265 bp into a 456 bp gene predicted to encode a homologue of DksA. The S39006 DksA homologue showed a very high degree of similarity to well characterised DksA proteins, with 96 % identity and 99 % similarity to *E. coli* DksA. As in *E. coli*, the S39006 version contains a C4-type zinc finger domain, where the transposon has inserted (Figure 6.1). The genetic context of *dksA* in S39006 is similar to other closely related strains, including *Dickeya*, *Pectobacterium* and *E. coli* strains. DksA itself is highly conserved across *Dickeya*, *Serratia*, *Citrobacter*, and *Brenneria* species with amino acid identity of 97 % and similarity of 98 – 100 % (Table 6.1). The genes surrounding *dksA* are predicted to encode proteins responsible for the biosynthesis of pantothenate (*panB-D*) and folate (*folK*), a tRNA synthetase (*gluQ*), and a polynucleotide adenyltransferase (*pcnB*) (Table 6.2). As usual in this *Serratia* strain, the gene products share the greatest identity with proteins from *Pectobacterium* or *Dickeya* species rather than other members of *Serratia*. *Brenneria* species belong to the Pectobacteriaceae family and were formerly placed in the *Erwinia* genus. In *E. coli*, *dksA* is predicted to be the first gene of a two gene operon, co-transcribed with *gluQ*, and it is likely that a similar operonic structure occurs in S39006.

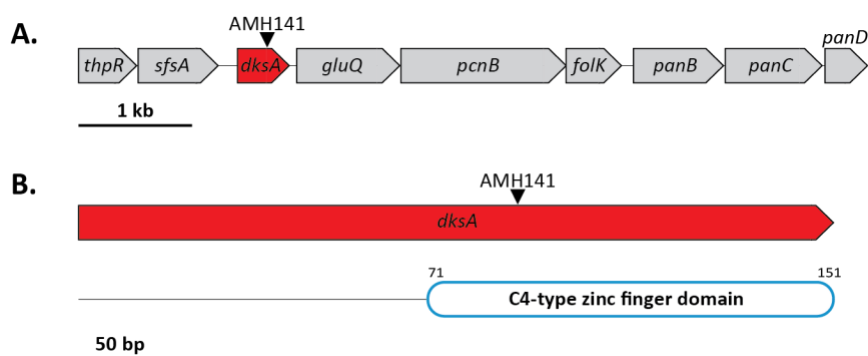


Figure 6.1 – Organisation of genes surrounding the AMH141 transposon insertion site.

(A) The transposon inserted in *dksA*, highlighted in red, the location of the insertion is indicated by a black triangle. (B) The predicted protein domains of DksA, the numbers above indicate the length of the protein in amino acids and the start and end of each domain.

Table 6.1 – Amino acid sequence similarity search of DksA using BLASTP.

Species	Identity (%)	Similarity (%)	Accession Number
<i>Dickeya lacustris</i>	99	100	WP_125260366.1
<i>Brenneria roseae</i>	97	100	WP_109055835.1
<i>Dickeya paradisiaca</i>	97	99	WP_015854501.1
<i>Gibbsiella quercinecans</i>	97	99	WP_095847315.1
<i>Serratia odorifera</i>	97	99	WP_004958885.1
<i>Citrobacter freundii</i>	97	98	WP_202580771.1

Table 6.2 – Predicted function of genes surrounding *dksA*.

ORF	Size (bp)	Predicted Function	Species/Strain	Identity (%)	Similarity (%)
<i>thpR</i>	531	RNA 2',3'-cyclic phosphodiesterase	<i>Brenneria roseae</i>	76	85
<i>sfsA</i>	723	DNA/RNA nuclease SfsA	<i>Pectobacterium aroidearum</i>	79	88
<i>dksA</i>	456	RNA-polymerase binding protein DksA	<i>Dickeya lacustris</i>	99	100
<i>gluQ</i>	909	tRNA glutamyl-Q(34) synthetase GluQRS	<i>Pectobacterium polonicum</i>	73	85
<i>pcnB</i>	1458	polynucleotide adenyltransferase PcnB	<i>Dickeya lacustris</i>	88	94
<i>folk</i>	498	2-amino-4-hydroxy-6-hydroxymethyldihydropteridine diphosphokinase	<i>Pectobacterium aquaticum</i>	82	88
<i>panB</i>	795	3-methyl-2-oxobutanoate hydroxymethyltransferase	<i>Brenneria</i> sp. CFCC 11842	86	94
<i>panC</i>	855	Pantoate--beta-alanine ligase	<i>Brenneria roseae</i>	82	94
<i>panD</i>	381	Aspartate 1-decarboxylase	<i>Brenneria alni</i>	93	96

6.2.2 The *dksA* mutant shows reduced GV production and flotation ability

The *dksA* transposon mutant, AMH141, was originally identified in a screen for novel regulators of GV production as a translucent colony mutant. This indicated that GVs were not produced to the same extent as wild type S39006 and therefore less light was refracted giving the colony a less opaque appearance. The production of GVs in this strain was investigated using PCM, TEM, flotation assays, spot tests and a western blot (Figure 6.2). The *dksA* transposon insertion mutant, AMH141, was subjected to a flotation assay with cells from the assay taken and viewed under PCM or TEM after 48 hours (Figure 6.2A, B & E). The flotation assay showed that AMH141 cells are not able to colonise the medium closest to the air liquid interface and stay suspended lower in the culture, similar to the GV negative control GPA1. This observation is supported by the lack of any bright spots within cells on PCM images and no (or very few) gas vesicles could be seen within cells in TEM samples (Figure 6.2B, D & E). Very occasionally, faint bright spots could be seen within some AMH141 cells under PCM, and some cells seen under TEM had a small number of GVs present. This suggested that although the AMH141 mutant is unable to float under some circumstances a small number GVs can be made in this strain.

AMH 141 cells viewed under PCM and TEM appeared to have a different shape than those of wild type or the gas vesicle negative control strain GPA1, in general appearing longer. AMH141 cells grown on solid media showed the same GV negative phenotype (Figure 6.2C & D). The AMH141 spot also appeared less pigmented than wild type or GPA1. However, it is difficult to properly assess changes in pigmentation when gas vesicle production has also changed, therefore the production of prodigiosin in AMH141 and wild type was quantified to determine if there were any significant changes in antibiotic production. A western blot using an antibody raised against GvpC (MW = 18 kDa) could not detect any protein in AMH141 or GPA1, while a strong band was seen in the gas vesicle producing wild type S39006 (Figure 6.2F).

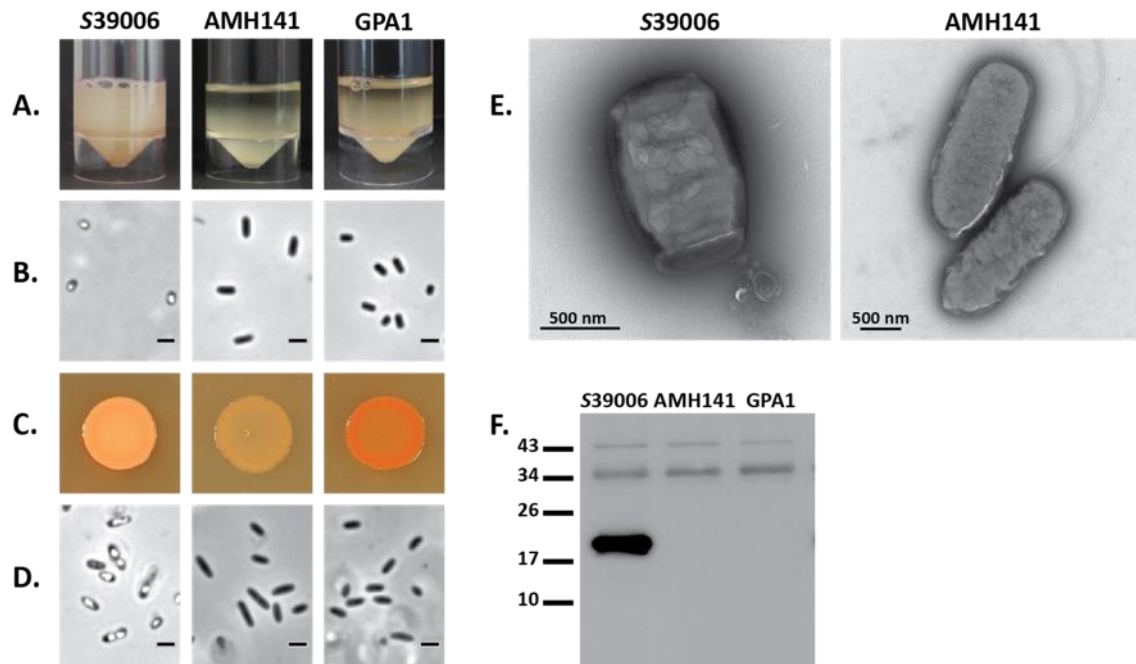


Figure 6.2 – Transposon insertion in *dksA* abolishes flotation and gas vesicle production.

(A) Flotation assays for S39006, *dksA* transposon mutant AMH141, and gas vesicle negative control strain GPA1 after 48 h standing at room temperature. (B) PCM images from the flotation assay shown directly above, the scale bar indicates 1 μm . (C) Spot tests of each strain with normalised cell number, grown for 48 h at 30 $^{\circ}\text{C}$ and associated PCM images directly below (D). (E) Representative TEM images showing AMH141 is unable to make GVs. The S39006 image is also shown in Figure 4.2 and Figure 5.2. (F) Western blot using an antibody raised against GvpC.

6.2.3 Transcription of the *gvpA1* and *gvrA* operons is reduced in the *dksA* mutant

The flotation assay, microscopy analysis, and western blot showed a clear reduction of gas vesicle production in AMH141. *uidA* gene fusions in *gvpA1* and *gvrA* were utilized to determine if GV production was affected at the transcriptional or post-transcriptional level. These fusions are in the first gene of each of the two operons of the gas vesicle cluster. By measuring the activity of the *uidA* gene product, β -glucuronidase, relative fluorescence can be used as a proxy for transcription. Measurements of fluorescence were carried out on samples taken every two hours over the course of a growth curve to determine how expression of *gvpA1* and *gvrA* changed in different growth phases of the *dksA* mutant. The assays were also carried out under microaerophilic conditions as oxygen depletion has been shown to be a key driver of transcription of the gas vesicle cluster (Ramsay et al., 2011). There was a significant reduction in transcription of the *gvpA1* and *gvrA* operons in aerobic and microaerophilic conditions (Figure 6.3). Previous work has found that reduced expression of genes in the *gvrA* operons, chiefly the regulatory genes *gvrA*, *gvrB*, and *gvrC* resulted in reduced *gvpA1* transcription (Ramsay et al., 2011; Tashiro et al., 2016). One hypothesis is that DksA acts only on transcription of the *gvrA* operon and that changes in abundance of GvrA, GvrB and GvrC cause the reduction in *gvpA1* transcription seen in the *dksA* mutant. However, it is also possible that DksA acts directly to change transcription of both operons. The reduction of *gvpA1* and *gvrA* expression is independent of oxygen with similar effects seen when mineral oil was overlaid on the cultures to produce microaerophilic conditions.

There is still some expression of the *gvpA1* operon, which contrasts with the other translucent mutant discussed in this work, *rpoN*, covered in Chapter 5. This gene encoded a sigma factor that required GvrA to activate transcription of *gvpA1*. In the *rpoN* mutant there was no change in *gvrA* expression while *gvpA1* expression was totally abolished. In contrast AMH141 showed decreased transcription of both operons but neither were completely abolished. This, along with the occasional GVs spotted when cells were viewed under the microscope, suggests that the reduction in gas vesicles in AMH141, although severe, is not absolute.

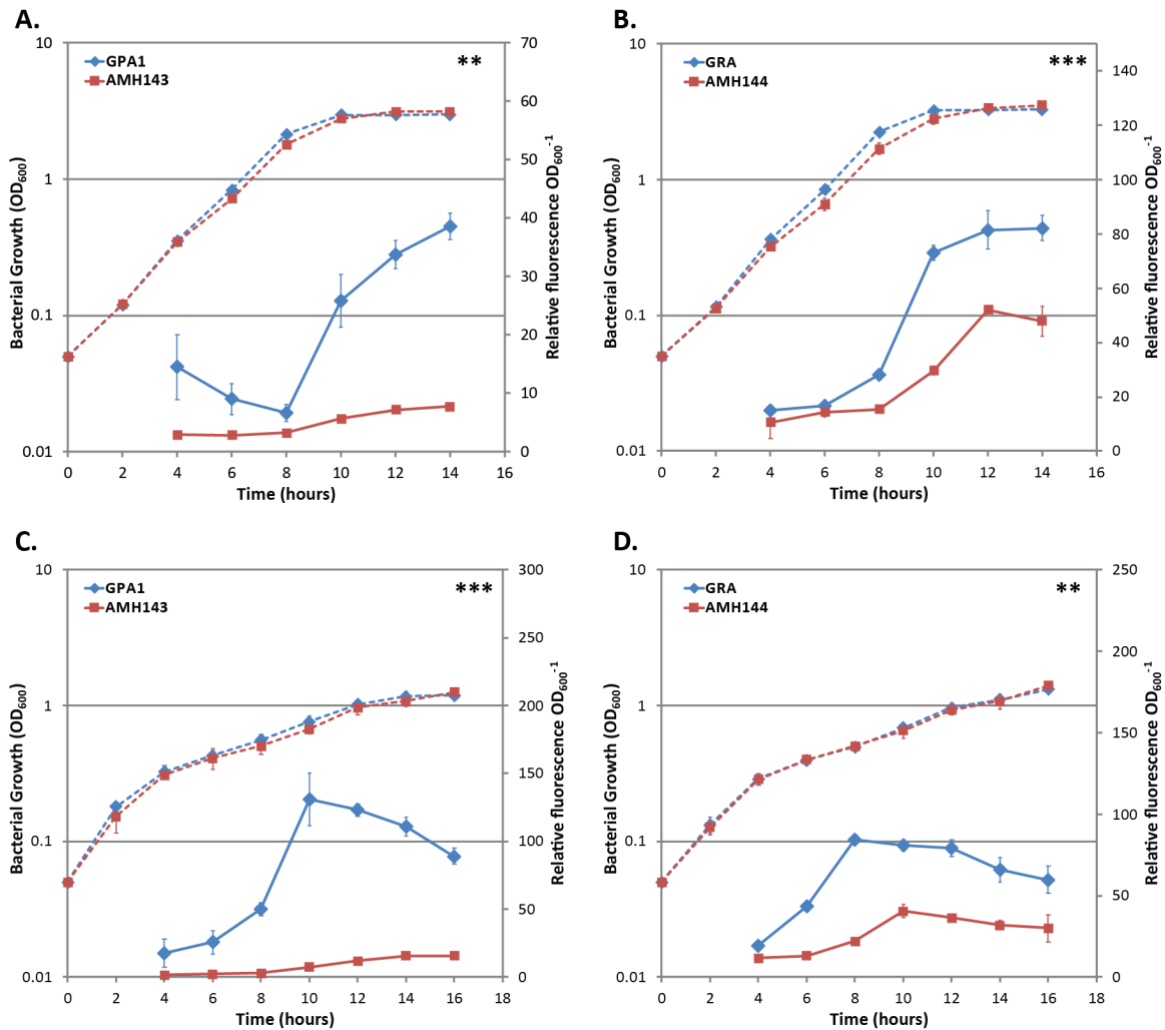


Figure 6.3 – *gvpA1* and *gvrA* expression in wild type and the *dksA* mutant under aerobic and microaerophilic conditions.

β -glucuronidase activity from a chromosomal *gvpA1::uidA* fusion was assayed in wild type (GPA1, blue) and *dksA* transposon mutant backgrounds (AMH142, red) under aerobic (A) and microaerophilic (C) conditions. β -glucuronidase activity from a chromosomal *gvrA::uidA* fusion was assayed in wild type (GRA, blue) and *dksA* transposon mutant backgrounds (AMH143, red) under aerobic (B) and microaerophilic (D) conditions. Solid lines indicate β -glu activity while dashed lines show OD₆₀₀ measurements. Data shown are the mean values \pm SD (n = 3), asterisks indicate p-values comparing β -glu activity: *, p < 0.05; **, p < 0.01; ***, p < 0.001; NS, not significant.

6.2.4 Mutation in *dksA* causes diverse phenotypic impacts in S39006

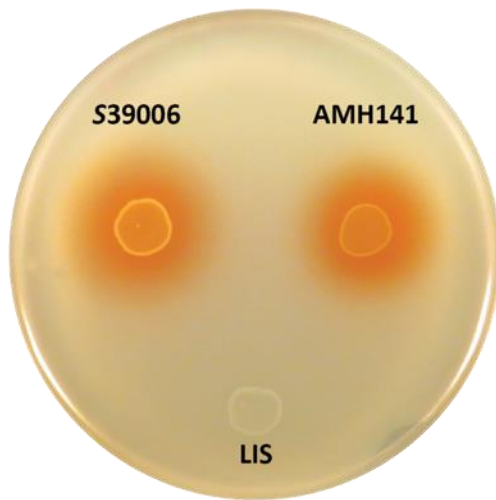
Following observations that the transposon insertion in *dksA* made colonies appear less pigmented and given previously described *dksA* mutants in different systems showed significant pleiotropy, a further phenotypic analysis of AMH141 was performed. Spot test assays were used with specific media and biosensor strains to test for any changes in the production of PCWDEs, QS molecules, antibiotic production, and changes in swimming and swarming motility. No difference was observed in the production of BHL, the main QS

signalling molecule in S39006, and no zone of inhibition was observed surrounding AMH141 when grown on ESS (Figure 6.4A & B). This indicates that AMH141 is not able to produce the carbapenem antibiotic. Assays to determine the amount of pectate lyase and cellulase produced showed no change in pectate lyase production but a reduction in cellulase production in the *dksA* mutant (Figure 6.4C & D). In addition to a reduction in the ability to float, the *dksA* mutant also showed reduced swimming and swarming motility, with swarming motility completely abolished (Figure 6.4E & F). This is a similar change in mobility to that seen in the *rpoN* mutant where flotation, swimming, and swarming were all reduced. This is also counter to previously published results where a reduction in gas vesicle production was linked to increased motility via swimming and swarming suggesting that they were oppositely regulated (Lee et al., 2017; Quintero-Yanes et al., 2020; Ramsay et al., 2011).

Tests were also performed to quantify antibiotic production over the course of a growth curve for the *dksA* mutant. This is a more sensitive method than the plate assays initially used for carbapenem production and visual observations of prodigiosin production. The quantification tests confirmed what was previously reported, a transposon insertion in *dksA* resulted in a complete elimination of carbapenem production (Figure 6.5A), and a severe reduction of prodigiosin production (Figure 6.5B). Although AMH141 no longer produced the carbapenem antibiotic it was still able to survive when grown on strains making the carbapenem indicating that the intrinsic resistance mechanism encoded by *carF* and *carG* was still functional.

As previous work has shown, genes that encode pleiotropic regulators in S39006 also often have an impact on virulence, particularly in a *C. elegans* model (Quintero-Yanes et al., 2020; Wilf et al., 2013, 2011). A killing curve was completed to determine the length of time *C. elegans* could survive when grown solely on wild type S39006, AMH141, or the preferred food source *E. coli* OP50 (Figure 6.6). There was a significant reduction in the virulence of AMH141 compared to wild type, with worms able to survive two days longer on average. These results confirmed that DksA acts as a global regulator in S39006 controlling gas vesicle, antibiotic, and cellulase production as well as motility and virulence in an animal model.

A. BHL



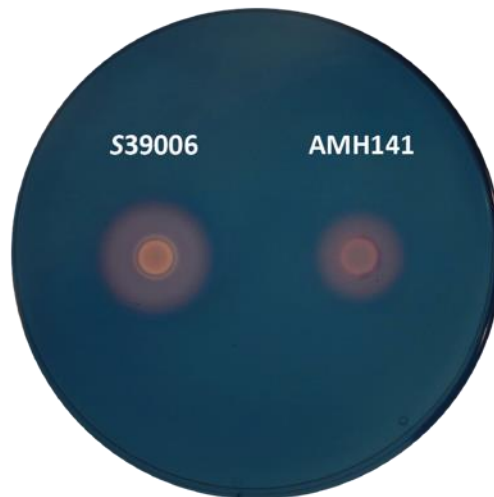
B. Carbapenem



C. Pectate Lyase



D. Cellulase



E. Swimming



F. Swarming

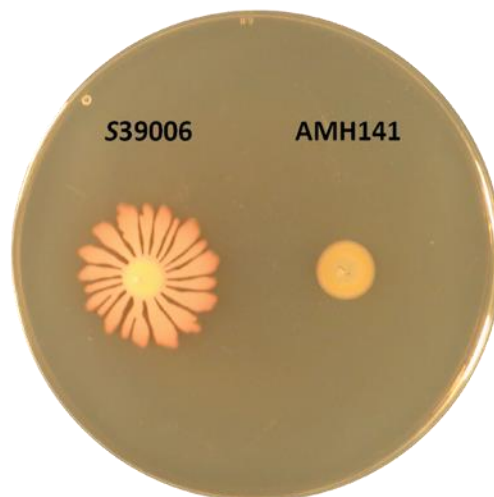


Figure 6.4 – The transposon insertion in *dksA* is pleiotropic.

Overnight cultures of the indicated strains were adjusted to an OD_{600} of 1 (A – D) or 0.2 (E and F) and spotted onto different agar plates to assay the production of BHL (A), carbapenem (B), pectate lyase (C) and cellulase (D). Swimming (E) and swarming (F) motility were also assayed.

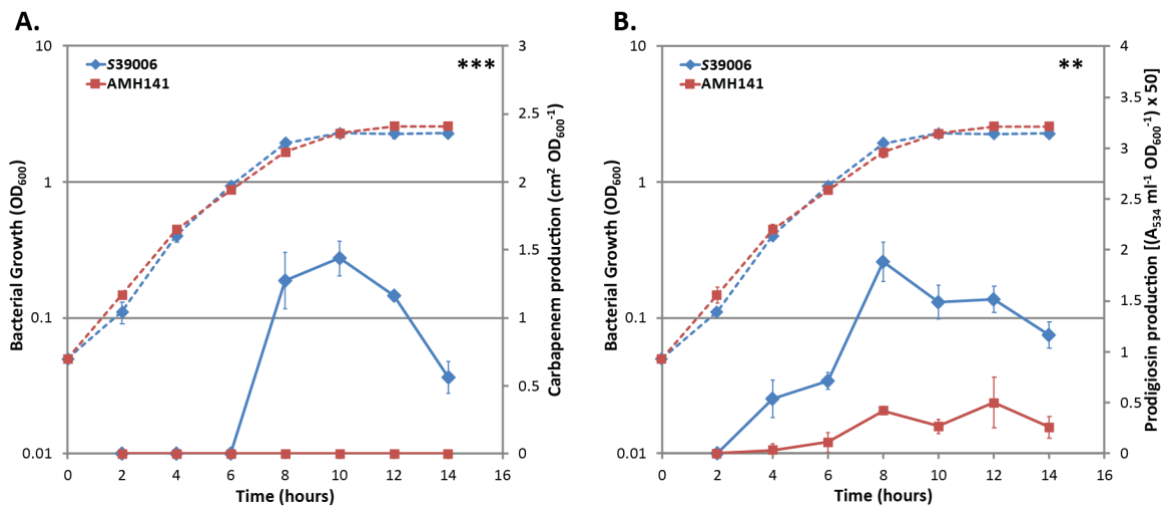


Figure 6.5 – Transposon insertion in *dksA* decreases carbapenem and prodigiosin production.

Carbapenem (A) and prodigiosin (B) production was measured over the course of a growth curve for S39006 (blue) and *dksA* transposon insertion mutant AMH141 (red). Solid lines indicate carbapenem/prodigiosin production while dashed lines show OD₆₀₀ measurements. Data shown are the mean values ± SD (n = 3), asterisks indicate p-values comparing carbapenem/prodigiosin production between strains: *, p < 0.05; **, p < 0.01; ***, p < 0.001; NS, not significant

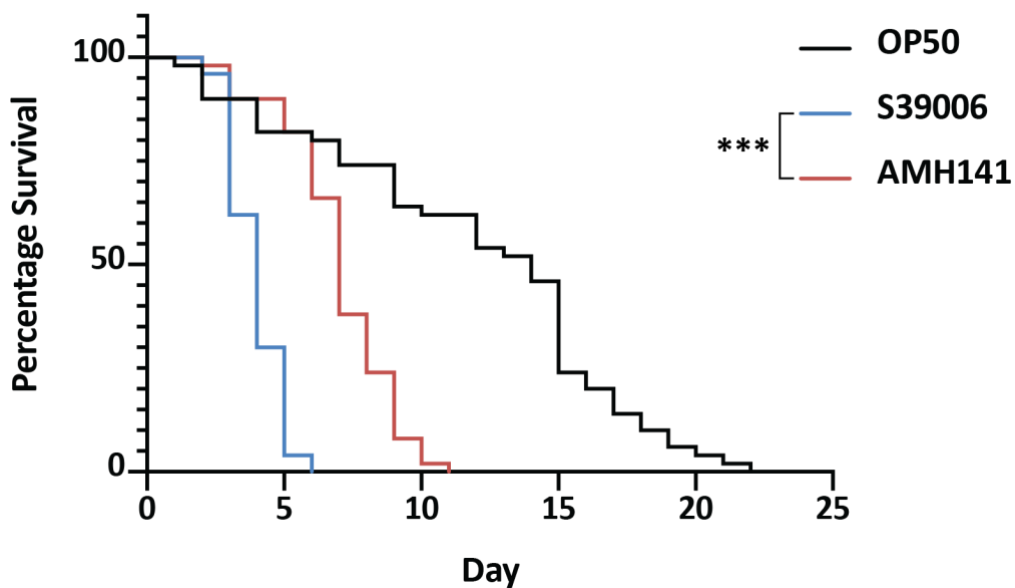


Figure 6.6 – Transposon insertion in *dksA* attenuates virulence in a *C. elegans* model.

Survival curves are shown for *C. elegans* fed S39006 (blue), AMH141 (red) and the control feeder strain *E. coli* OP50 (black). Fifty L4 stage worms were used for each bacterial strain, a log-rank test was used to determine if there was a significant difference in survival between S39006 and AMH141: *, p < 0.05; **, p < 0.01; ***, p < 0.001; NS, not significant. This experiment was also performed with AMH157 (shown in Figure 4.6); S39006 and OP50 controls are shared across the two figures.

6.2.5 Transposon insertion in *dksA* can be complemented

To confirm that the range of phenotypes observed in AMH141 was the result of disruption of *dksA* and not polar impacts on any downstream genes, *dksA* was cloned into the vector pQE80-*oriT* to be expressed *in trans*. This vector, named pAH4, was introduced into AMH141 via conjugation and the impact of reintroducing DksA was determined. All assays were carried out in comparison to wild type and AMH141 carrying the empty vector, pQE80-*oriT*, to account for any differences that were the result of the strains harbouring a plasmid. In flotation assays, colony spot tests and PCM images taken from samples of both (Figure 6.7A – D) the complemented strain, AMH141 + pAH4, regained the ability to float, produce gas vesicles and once again appeared opaque on a solid medium. The expression of *dksA* did not need to be induced with IPTG to see this complementation which indicated that the amount produced through leaky expression of the gene on pAH5 was sufficient to restore the flotation phenotypes. In the western blot, although a GvpC band could be seen in the complemented strain, it was not of the same density as the wild type + empty vector control (Figure 6.7E). This indicates that although leaky expression was sufficient to restore flotation, it does not increase total GvpC levels to the same as wild type. If this western blot were repeated with IPTG induction the detectable level of GvpC would be expected to be higher. There was a clear difference in the ability to detect GvpC in the AMH141 + pAH4 strain compared to the lack of any band seen in the AMH141 + pQE empty vector control.

Expression of *dksA in trans* restored the ability of AMH141 to swim, swarm, and produce cellulase (Figure 6.7F – H). Once again, these assays were carried out without any induction with IPTG and as a result some of the phenotypes observed did not return completely to wild type levels. Some assays, in particular the swarming assays, can vary significantly from plate to plate so all comparisons were made between strains on the same plate. The complemented mutant also appeared to return to wild type levels of prodigiosin production, although this has yet to be quantified. Taken together, these results suggest that *dksA* is responsible for the array of pleiotropic phenotypes seen in AMH141 and not any downstream genes that were disrupted by the presence of a transcriptional terminator within the transposon.

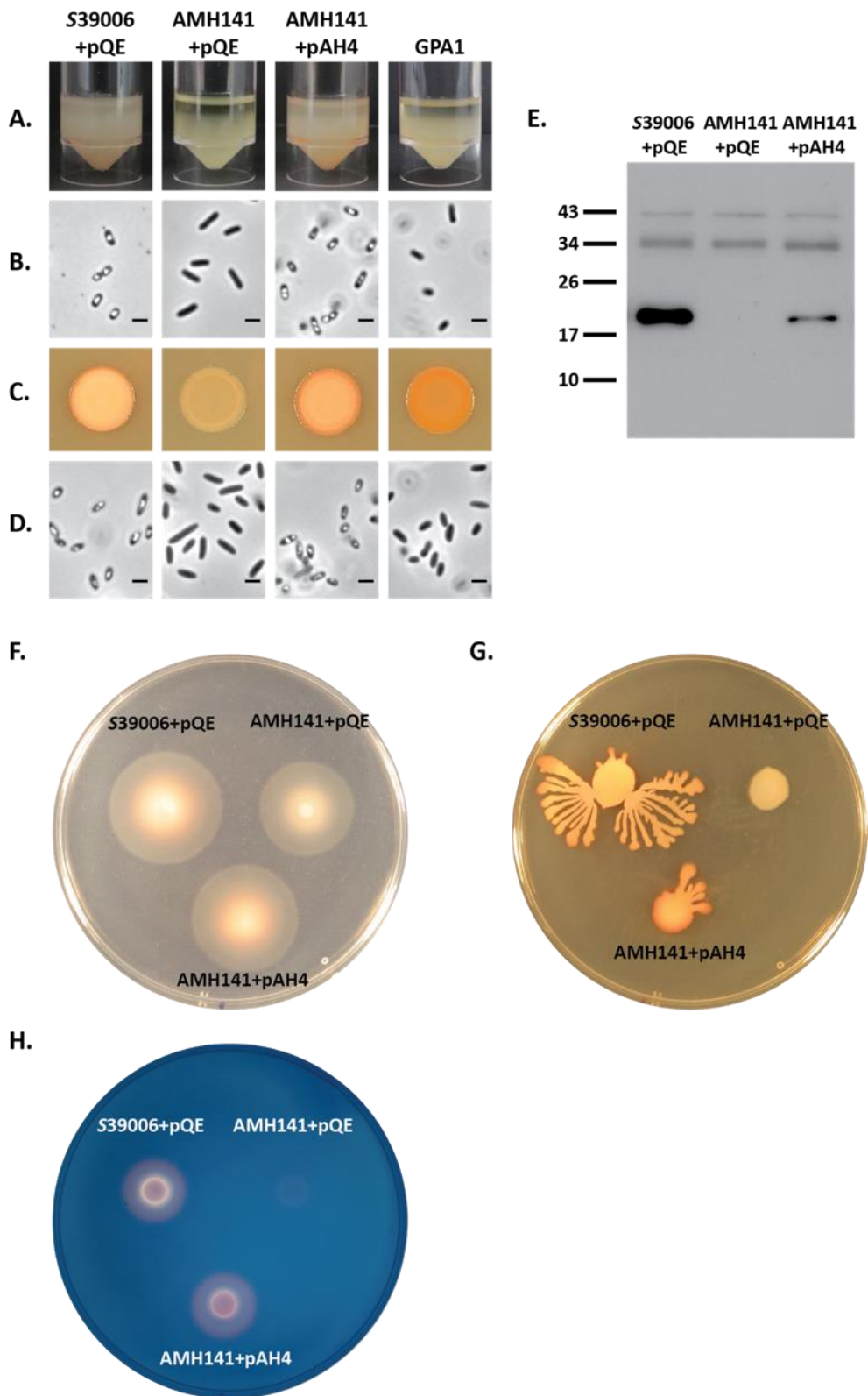


Figure 6.7 – Transposon insertion in *dksA* can be complemented.

(A) Flotation assays and (C) Spot tests with associated PCM images shown directly below in (B) and (D) for wild type S39006 carrying empty vector (pQE), AMH141 (*dksA* transposon mutant) carrying empty vector, and AMH141 with *dksA* expressed *in trans* (pAH4). (E) A western blot against using an antibody raised against GvpC for the same strains. Assays to determine if expression of *dksA* can complement swimming (F), swarming (G, and cellulase (H) phenotypes previously observed in AMH141.

6.2.6 A *dksA* knockout has the same effect as transposon insertion

As *dksA* is predicted to form part of an operon it is possible that the transposon insertion could have polar effects. To circumvent this a *dksA* knockout strain was created by allelic exchange, removing the entire *dksA* gene except for the first three and last three codons. This strain, called AMH32, was subjected to a similar phenotypic analysis as described earlier for AMH141 to determine if the same levels of disruption were seen. AMH32 cells were unable to float, similar to the GV negative control strain GPA1 and AMH141, and no bright spots were seen in cells viewed under PCM (Figure 6.8A & B), Similarly spot patches appeared translucent and showed no bright spots in PCM images (Figure 6.8C & D). No GvpC could be detected in a western blot and swimming motility and cellulase production was reduced in AMH32, as in AMH141 (Figure 6.8E – G). Carbapenem production and swarming motility were also abolished in the *dksA* knockout strain (Figure 6.8H & I). These data provided confirmation that the differences seen in AMH141 were the result of interruption to *dksA* and not any downstream effects.

6.2.7 The mutation of *dksA* can be partially bypassed by the disruption of *guaBA*

When AMH141 cells were viewed under the TEM, occasional cells contained a small number of gas vesicles. This indicated that, although colonies appeared translucent, there may be some low level of gas vesicle production in this mutant, a hypothesis that was supported by the transcriptional data (Figure 6.3). To explore these observations in greater detail, a bypass mutagenesis screen was carried out to determine if gas vesicle production could be restored. This screen was carried out using a second plasposon system, pDS1028; a plasmid that cannot replicate in S39006 but carried a transposon that contained a chloramphenicol resistance cassette (Monson et al., 2015). The second transposon was introduced into AMH141 cells by conjugation and putative double transposon insertion mutants were selected on agar plates that contained chloramphenicol and kanamycin. A total of 56,548 insertion mutants from 10 independent conjugation patches were screened in a search for colonies that showed increased opacity compared to AMH141. Putative bypass mutants were streaked out to single colonies, then the chloramphenicol resistance transposon insertion was transduced back into AMH141 to ensure that the observed changes in opacity were the result of the transposon insertion and not any other random mutation. Strains that still showed changes in opacity following transduction into a clean background were then subjected to RP-PCR to identify the transposon insertion site.

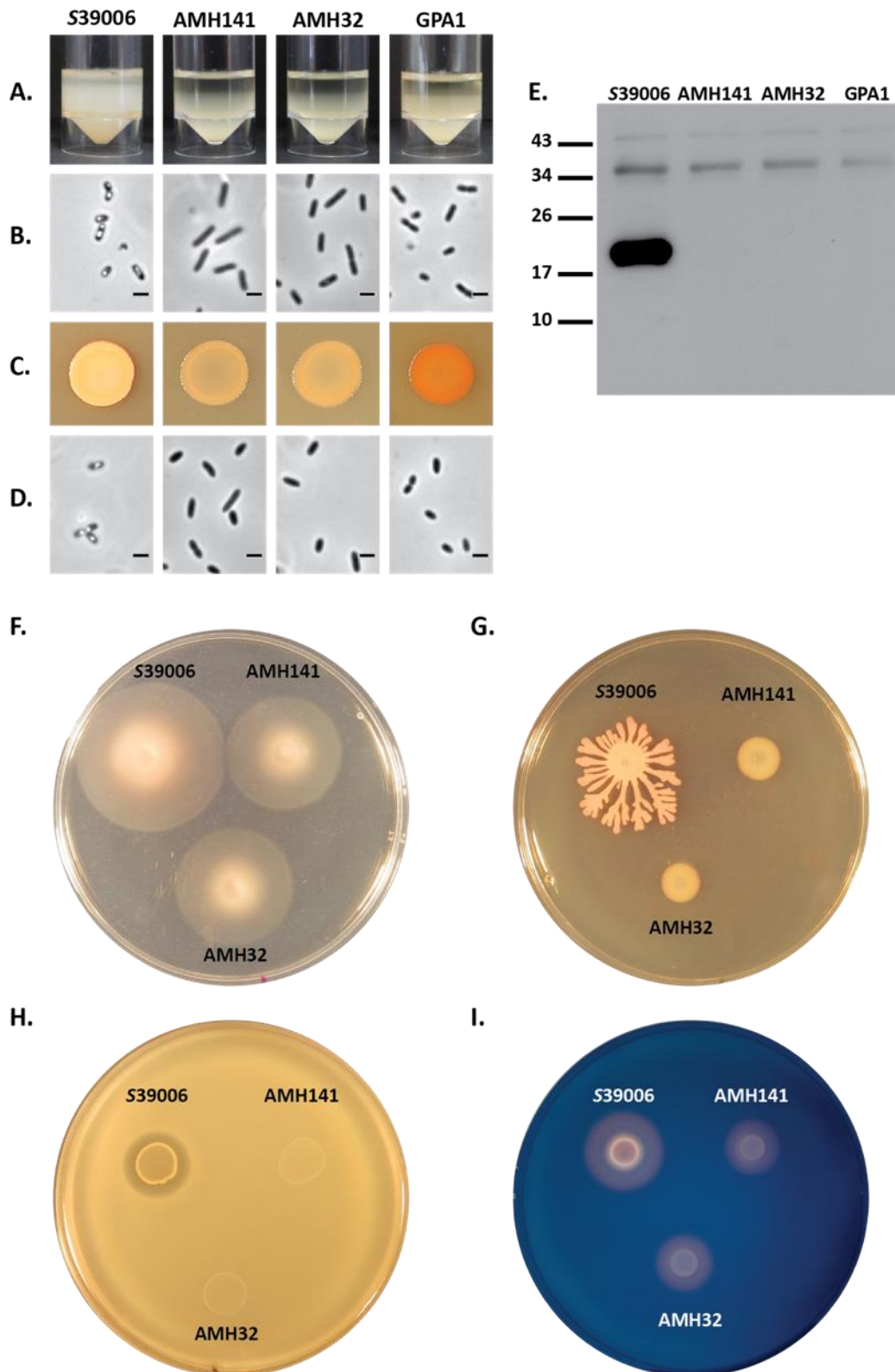


Figure 6.8 – The *dksA* knockout strain AMH32 displays the same phenotypes as the *dksA* transposon mutant AMH141.

(A) Flotation assays and (C) Spot tests with associated PCM images shown directly below in (B) and (D) for wild type S39006, AMH141 (*dksA* transposon mutant), AMH32 (*dksA* knockout), and GPA1 (GV negative control strain). (E) A western blot using an antibody raised against GvpC for the same strains. The effect of *dksA* knockout on swimming motility (F), swarming motility (G), carbapenem antibiotic production (H), and cellulase production (I).

After these quality control checks were performed, only one double transposon mutant remained that showed an increased opacity compared to AMH141, indicating that this mutation is only rarely capable of genetic bypass. This double mutant, AMH33, had a transposon insertion in the *guaB* gene, in addition to the previously characterized insertion in *dksA*. This strain showed severe growth defects and as such incubation times for liquid cultures were increased from 24 to 48 hours and growth on a solid medium was assessed after 96 hours instead of the usual 48 hours (Figure 6.9). To assess the impact of the transposon insertion in *guaB* on GVs the transposon was also transduced into wild type S39006 to give a single *guaB* mutant, named AMH35. The double transposon mutant, AMH33, was able to float more successfully than the *dksA* transposon mutant AMH141 and bright spots could be seen in PCM images (Figure 6.9). In PCM images, AMH33 cells were far larger than wild type or AMH141 indicating that normal cell division is disrupted in this strain. The *guaB* single transposon mutant was hyper opaque and cells showed a stronger flotation phenotype than wild type with a white pellicle forming at the air-liquid interface. AMH35 cells also appeared larger than wild type and the growth defects seen in AMH33 was also observed for this strain indicating that *guaB*, although not essential for S39006 survival in LB is very important.

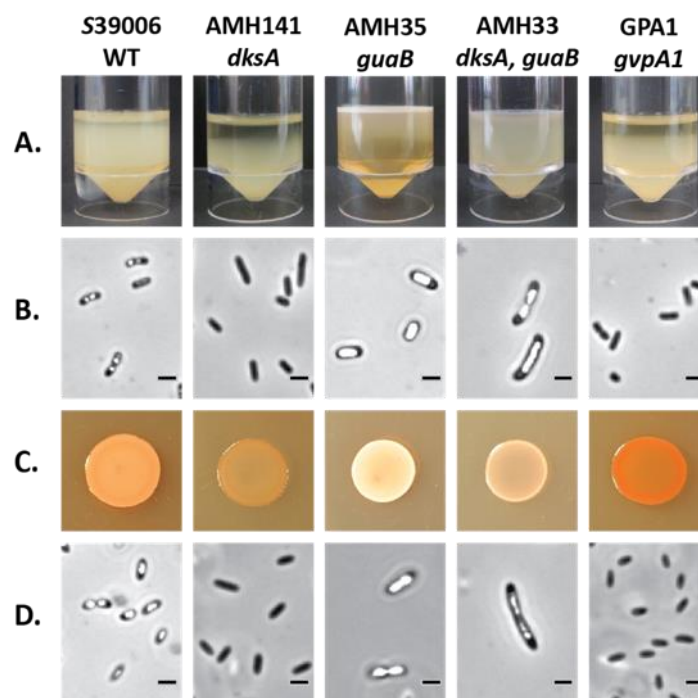


Figure 6.9 – A second transposon insertion in *guaB* can bypass the *dksA* gas vesicle phenotype. (A) Flotation assays and (C) Spot tests with associated PCM images shown directly below in (B) and (D) for wild type S39006, AMH141 (*dksA* transposon mutant), and AMH35 (*guaB* transposon mutant), AMH33 (*dksA*, *guaB* double transposon mutant), and GPA1 (GV negative control strain).

6.2.8 Intracellular protein extraction and quantification in S39006 and the *dksA* mutant

The transposon insertion in *dksA* has been shown to have pleiotropic impacts on S39006 physiology with changes in antibiotic production, virulence and motility observed. A quantitative comparative proteomic analysis was carried out between AMH141 and wild type S39006 to determine if any further pleiotropic effects had occurred due to the disruption in *dksA*. This analysis was also performed to provide further information about the DksA regulon in S39006 and identify potential pathways through which various phenotypic changes might have occurred.

This proteomic analysis was carried out in conjunction with that described in chapter 5 for the *rpoN* mutant, AMH109. A growth curve was performed prior to the protein extraction to ensure that cell numbers and OD₆₀₀ were not significantly different between the strains, this was important as previous analysis had suggested that AMH109 cells may be longer than wild type. No significant difference in cell numbers or OD₆₀₀ was observed in samples taken after 12, 14 or 16 h growth in LB. A western blot was performed to determine whether detectable levels of GvpC was present in wild type cells at these time points and to confirm that no GvpC could be detected in AMH141 samples (Figure 6.10).

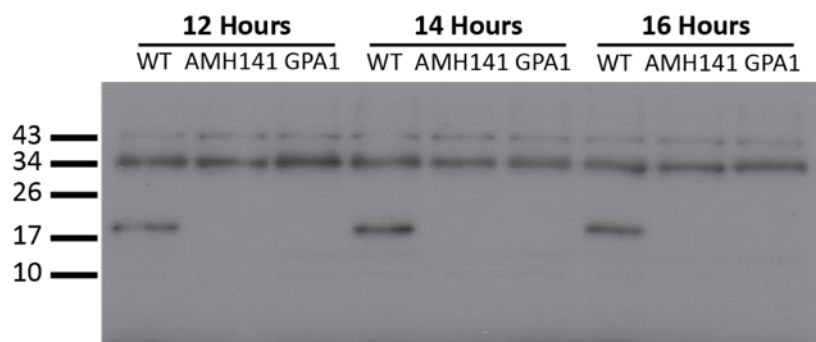


Figure 6.10 – Western blot for GvpC in wild type, AMH141 and GPA1 after 12, 14, and 16 hours growth.

GvpC bands are visible in the wild type columns at approximately 18 kDa, none are present in the AMH141 or GPA1 columns.

The protein extractions were performed after 14 h growth in LB, with three replicates of each strain used. The wild type samples are shared across the two analyses presented in this chapter and chapter 5. Proteins extracted from wild type and AMH141 cultures had similar concentrations and a sample of each extract was separated by SDS-PAGE to determine the protein profile (Figure 6.11A). A western blot against GvpC was also performed and showed similar band densities across wild type samples and no GvpC production in AMH141, consistent with previous observations (Figure 6.11B). After these quality control checks had been performed, samples were analysed by LC-MS/MS as previously described. Purified protein samples were sent to the CCP where tandem mass tagging with 16 isobaric reporters was performed. As mentioned in chapter 5, these experiments were carried out in collaboration with Carlo Sandoval.

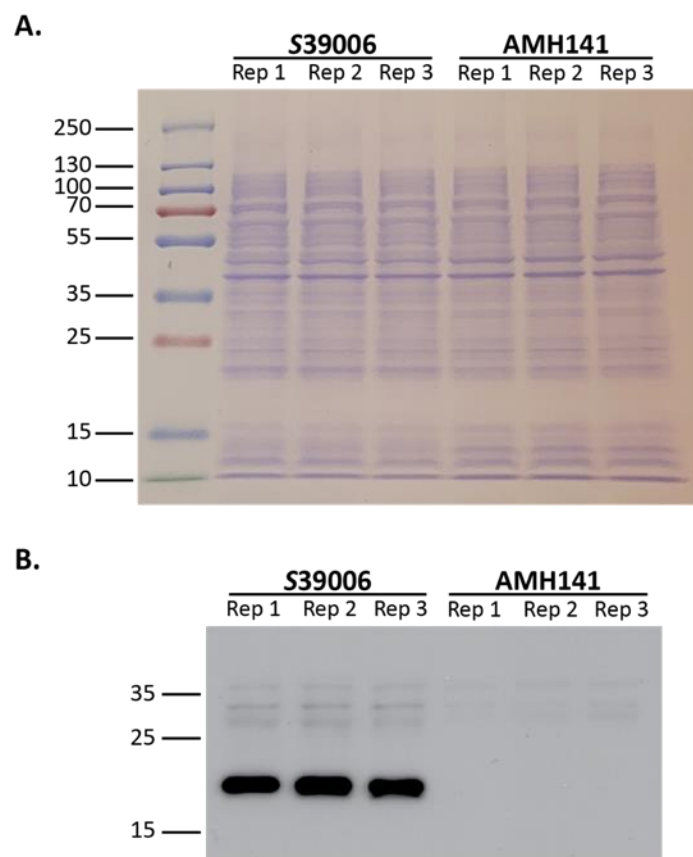


Figure 6.11 – Intracellular protein samples extracted from S39006 and AMH141.

(A) SDS-PAGE analysis of the intracellular protein extracts for three replicates each of S39006 and AMH141. The first lane shows Thermo Scientific™ PageRuler™ Prestained Protein Ladder with sizes indicated beside. (B) A western blot using an antibody raised against GvpC (~18 kDa) for the three replicates of S39006 and AMH141.

Previous analysis of the S39006 genome identified 4,413 protein-encoding genes (Fineran et al., 2013), and the whole genome sequence of S39006 is publicly available (www.ncbi.nlm.nih.gov). The amino acid sequences of predicted proteins were used in the comparative analysis of TMT-labelled peptides to determine the relative abundance of each protein identified between S39006 wild type and the *dksA* mutant AMH141. As with the previous proteomic analysis, TMT labelling efficiency was 95.7 % and 2986 proteins were identified. After removing any proteins that had missing values for some samples and proteins belonging to the common Repository of Adventitious Proteins (cRAP) (Mellacheruvu et al., 2013) 2959 proteins remained, representing 67 % of the predicted proteins in S39006.

Correlation coefficients between each biological replicate were determined for each strain to confirm protein samples were extracted in a reproducible manner. The correlation coefficients across replicates of the same strain were 1.00 indicating they are highly correlated while coefficients between replicates from different strains were lower at 0.95 (Figure 6.12). A boxplot performed after sample normalization with the median which showed that protein quantification was normally distributed and replicates within each strain had similar distributions (Figure 6.13). As for the *rpoN* analysis, a DEA was carried out using the limma package in R (R Core Team, 2020; Ritchie et al., 2015). This allowed a PCA to be performed between samples which showed a clear separation between wild type S39006 and AMH141 replicates (Figure 5.14). A histogram visualising the p-values after the DEA shows a high peak near zero, indicating that the majority of the data were significantly different (Figure 5.15).

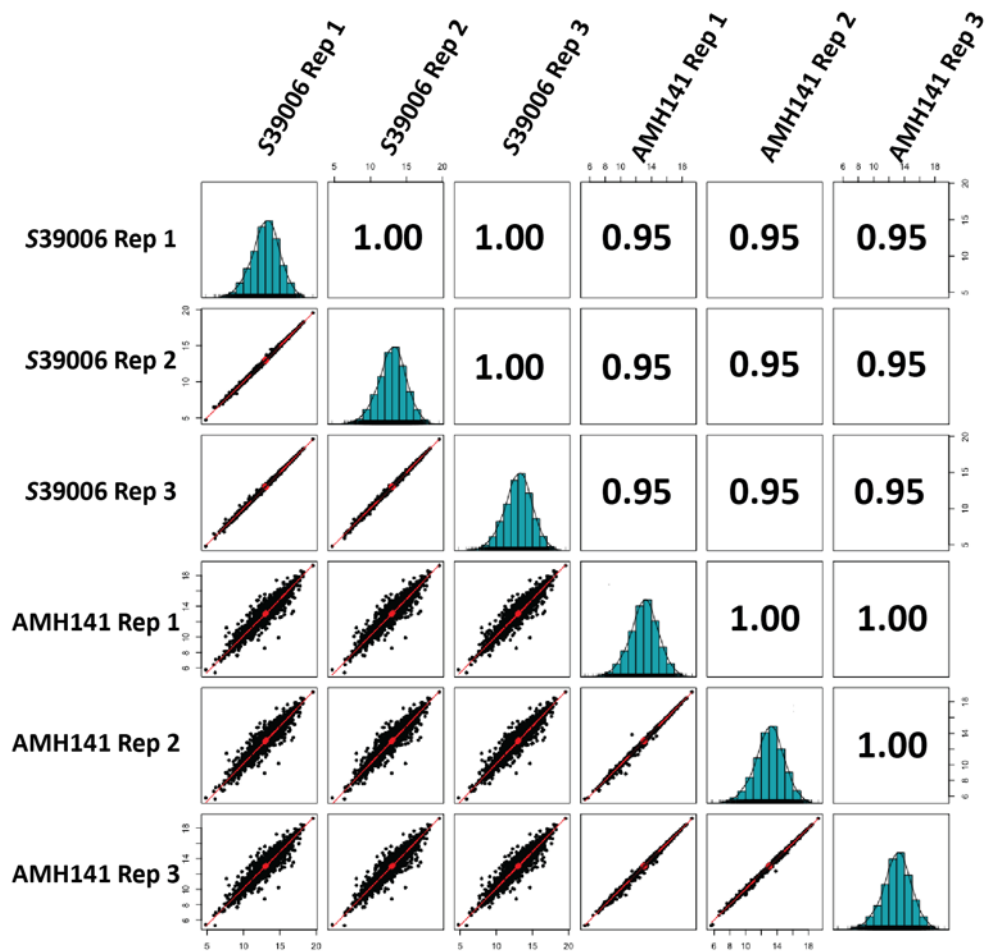


Figure 6.12 – Pearson correlation coefficients between replicates of S39006 and AMH141. Three replicates of each strain were used for the quantitative proteomic analysis. The correlation coefficient was 0.95 between S39006 and AMH141 while coefficients were 1.00 within biological replicates.

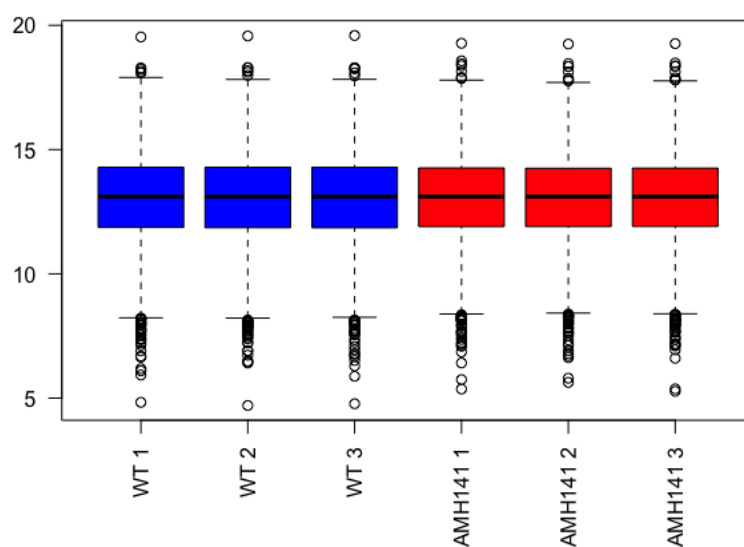


Figure 6.13 – Boxplot of protein abundances in S39006 and AMH141. The raw data was normally distributed and was normalised using the median of each channel. Each strain had similar distributions across biological replicates.

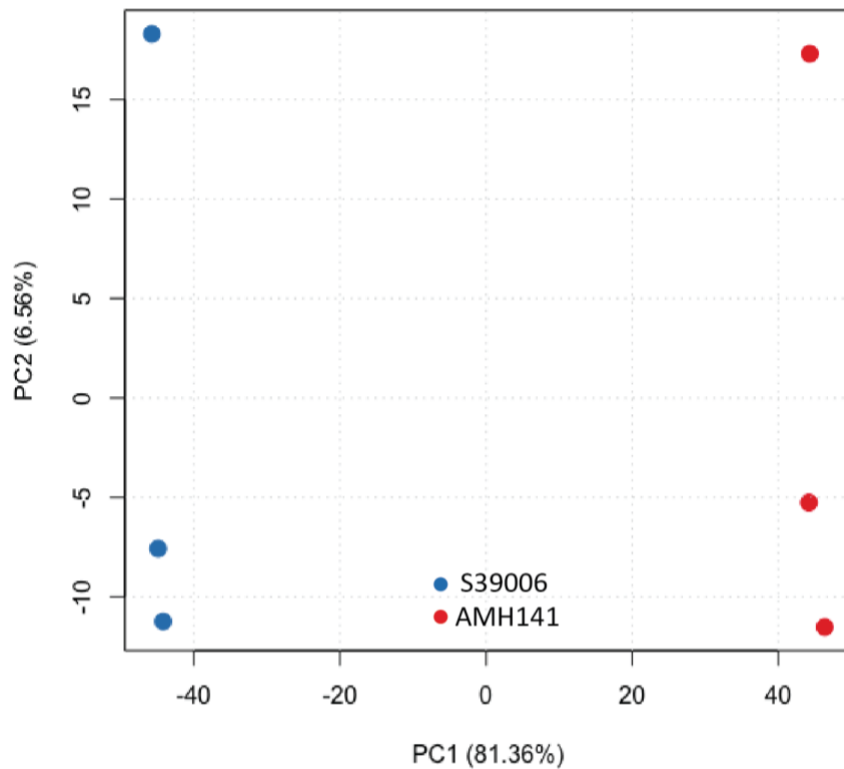


Figure 6.14 – The PCA of the protein quantification in S39006 and AMH141. Blue dots represent wild type S39006 while red dots represent the *dksA* transposon mutant AMH141. The protein quantification values have been \log_2 transformed and the PCA indicates the two samples were well separated and group based on biological replicates.

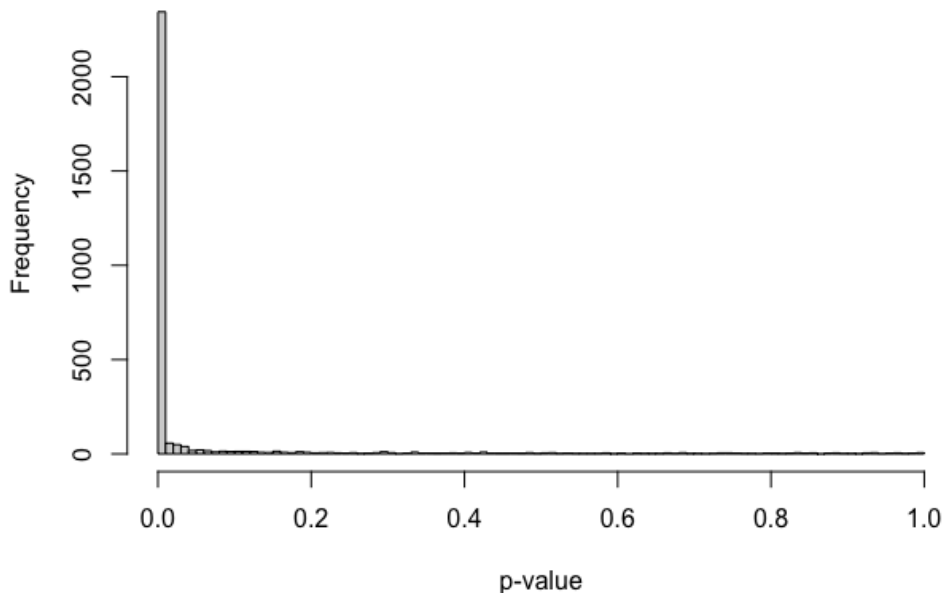


Figure 6.15 – p-value distribution of proteome quantitation in AMH141. Bars represent the frequency of adjusted p-values for the fold change of protein abundance between wild type and AMH141 (the *dksA* transposon insertion mutant).

6.2.9 Proteins showed differential abundance between S39006 and the *dksA* mutant

To maintain consistency with previously reported proteomic data (Chapter 5), the proteomic analysis here is also focused on proteins with an adjusted p-value of less than 0.01 and a fold change cut off of 0.5. Using these conditions, 771 proteins were identified with significantly altered abundance in the *dksA* mutant compared to wild type. This was comprised of 422 proteins that were significantly upregulated (54.7 %) and 349 proteins that were significantly downregulated (45.3 %). There were many other proteins that had a significant adjusted p-value ($p < 0.01$) with a fold change of less than ± 0.5 . It is possible that these smaller changes still have an important physiological effect on S39006 however, for the purpose of this analysis only the largest changes in abundance will be discussed.

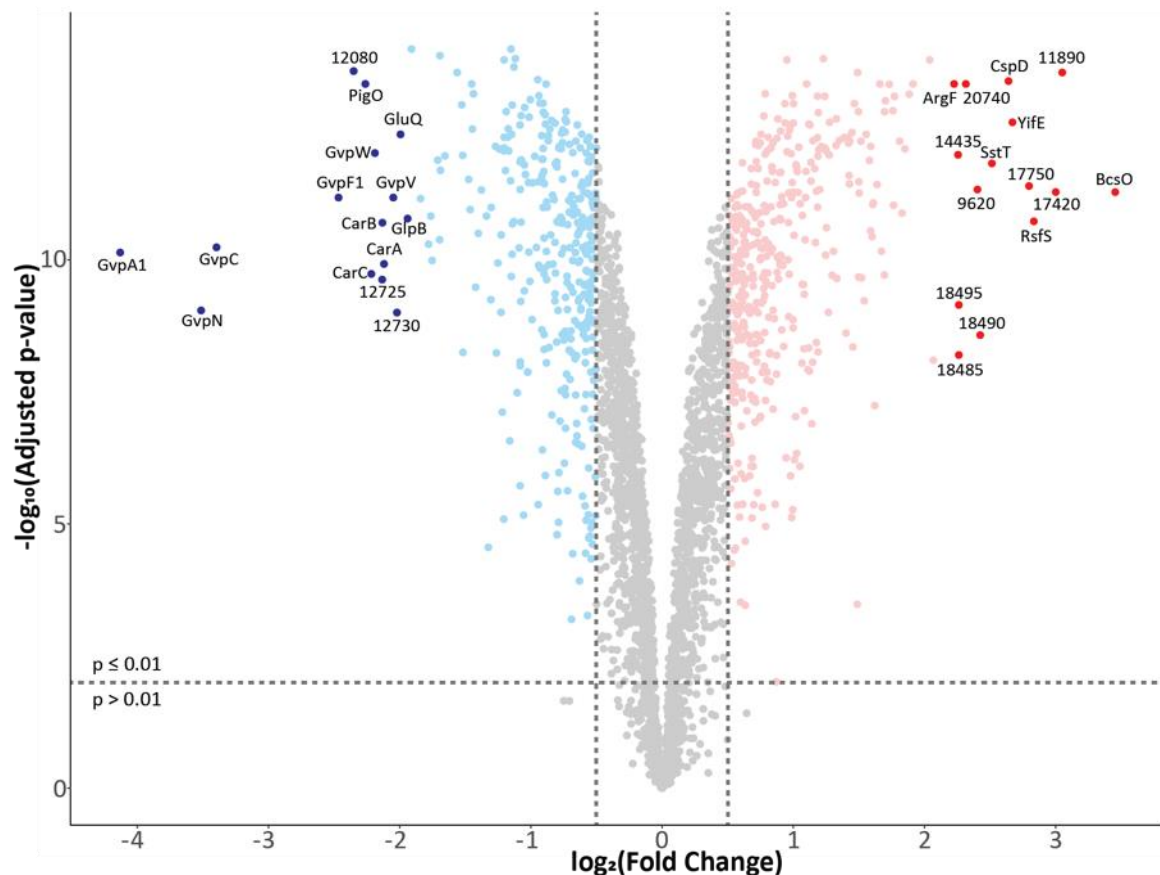


Figure 6.16 – Volcano plot of differential protein abundances in AMH141.

The volcano plot shows the relationship between the fold change and adjusted p-values of the 2959 proteins identified and quantified by TMT and LC-MS/MS. Blue coloured points show downregulated proteins and red coloured points show upregulated proteins ($p < 0.01$ and fold change > 0.5). Grey coloured points indicate proteins with no significant changes or changes of insufficient magnitude. The 15 most highly up or downregulated proteins are highlighted in darker red/blue dots respectively and labelled with their protein name or gene number where proteins were unnamed.

The top 30 most highly upregulated proteins in the *dksA* mutant are shown in Table 5.3. The fact that these proteins are found in such high abundance indicates that DksA plays some role in repressing their transcription in wild type S39006. This may be a direct inhibition of transcription or could be through changes in the transcription of other regulators. The most highly upregulated protein, BcsO, was predicted to be involved in the synthesis of cellulose and had a Log₂FC of 3.45. S39006 contains a type Ib cellulose synthase operon homologous to those found in closely related *Dickeya* and *Erwinia* species (Römling & Galperin, 2015). The S39006 operon contains *bcsO*, *bcsQ*, *bcsA*, *bcsB*, *bcsC*, *bcsD*, and *bcsZ*, genes which are predicted to encode a cellulose synthase (*bcsA*, *bcsB*, *bcsC* and *bcsD*), an endoglucanase (*bcsZ*), and a ParA/MinD-related NTPase (*bcsQ*). The function of BcsO is unknown and is specific to enterobacterial type Ib cellulose operons (Römling & Galperin, 2015). The BcsQ, BcsA and BcsB proteins were not detected in this proteomic analysis however, BcsC and BcsD were detected and were significantly upregulated (Log₂FC of 0.87 and 1.66 respectively). BcsZ was detected and had a change in abundance of 0.38, however the adjusted p-value was above the 0.01 significance threshold (p = 0.0399).

Another highly upregulated protein in the *dksA* mutant was a molecular chaperone encoded by *orf11890*. This protein shares 72 % identity and 82 % similarity with YegD from *E. coli* K12. YegD belongs to the Hsp70 protein superfamily but does not contain the C-terminal substrate binding domain of other Hsp70 family proteins such as DnaK (Itoh et al., 1999). DksA was originally identified as a suppressor of DnaKJ as overproduction of DksA restores the ability of a *dnaKJ* mutant to grow at high temperatures, however the exact mechanism of this suppression remains unknown (Chandrangsu et al., 2012; Kang & Craig, 1990). A bioinformatic search identified DnaK and DnaJ homologues in S39006 and both proteins were downregulated with a fold change of -0.37 in the *dksA* mutant. It is possible that in wild type S39006 expression of *orf11890* is induced by increases in temperature, based on the similarity of Orf11890 to other heat shock proteins. It was interesting to see a cold shock-like protein, CspD also strongly upregulated in the *dksA* mutant (Log₂FC = 2.64). This suggests that DksA is partly responsible for regulating responses to temperature stress in S39006.

DksA potentiates ppGpp-mediated expression of amino acid biosynthesis operons and repression of rRNA promoters (Paul et al., 2004a, 2005). Production of ppGpp is increased rapidly in response to various stressors including amino acid starvation, fatty acid synthesis limitation, and phosphate starvation (Battesti & Bouveret, 2006; Bougdour & Gottesman, 2007; Haseltine & Block, 1973). DksA can also function independently of ppGpp and sometimes in opposition to ppGpp (Magnusson et al., 2007). Disruption of *dksA* has been shown to affect the ability of strains to respond to nutrient limitation and activate the correct genes. Many of the proteins that were significantly upregulated in the *dksA* mutant were transporters or permeases, which would aid the cell in surviving stressful conditions. It is possible that these genes are normally repressed in non-nutrient limited conditions by DksA directly or through another regulator, to be initiated under nutrient stress. However, in the *dksA* mutant these genes are expressed regardless of nutrient availability.

Two of the most highly upregulated proteins in AMH141 are predicted to be involved in the arginine deiminase pathway, ArcA and ArcB. A third protein of this pathway, ArcC, a carbamate kinase was also identified and showed only a small change in abundance ($\text{Log}_2\text{FC} = 0.25$). This is surprising given the gene encoding ArcC is located in between *arcA* and *arcB* in S39006. It is possible that there are multiple promoters for these genes, ribosome binding sites of varying affinities, or that other post-transcriptional regulation is occurring. The arginine deiminase pathway catalyses the conversion of arginine into ornithine, ammonia and carbon dioxide while producing ATP (Cunin et al., 1986). The ornithine decarboxylase SpeF was also highly upregulated (Table 6.3), this enzyme is expressed under high ornithine levels in *E. coli* and is repressed strongly under normal conditions (Kashiwagi et al., 1991; Valle et al., 2020). It is possible that increased ornithine production by ArcA and ArcB lead to increased expression of *speF* in the *dksA* mutant.

DksA is a highly pleiotropic transcriptional regulator and the mutation of this gene in S39006 has caused wide ranging effects on protein abundances. These changes in transcription and subsequent protein abundance are likely to be at least partially the result of changes to transcriptional regulators such as the XRE family transcriptional regulator Orf9605, which had a Log_2FC of 1.69. This protein shows some homology to the *E. coli* RodZ (33.7 % identity, 55.3 % similarity) and may play a similar role in the maintenance of cell shape.

Table 6.3 – The top thirty most upregulated proteins quantified AMH141.

Protein ID	Description	Log₂ FC	Adjusted p-value
A0A2I5TF72	Cellulose biosynthesis protein, BcsO	3.45	5.24E-12
A0A2I5T788	Molecular chaperone, Orf11890	3.05	2.85E-14
A0A2I5TMG7	Dicarboxylate/amino acid:cation symporter, Orf17420	3.00	5.22E-12
A0A2I5TMY3	Ribosomal silencing factor, RsfS	2.83	1.87E-11
A0A2I5TMM6	Chlorinating enzyme, Orf17750	2.80	4.02E-12
A0A2I5T355	UPF0438 protein, YifE	2.67	2.50E-13
A0A2I5TLP5	Cold shock-like protein, CspD	2.64	4.15E-14
A0A2I5TCL0	Serine/threonine transporter, SstT	2.51	1.50E-12
A0A2I5TDJ0	Uncharacterized protein, Orf18490	2.42	2.66E-09
A0A2I5TIG5	HAAAP family serine/threonine permease, Orf9620	2.40	4.68E-12
A0A2I5TBS6	Cytosine permease, Orf20740	2.32	4.70E-14
A0A2I5TAM9	DUF1446 domain-containing protein, Orf18485	2.26	6.34E-09
A0A2I5TAL9	Acetate CoA-transferase subunit alpha, Orf18495	2.26	7.16E-10
A0A2I5T8J1	UPF0260 protein, Orf14435	2.26	1.03E-12
A0A2I5TM77	Ornithine carbamoyltransferase, ArcB	2.23	4.70E-14
A0A2I5TM90	Ornithine decarboxylase, SpeF	2.07	7.94E-09
A0A2I5TH56	Bifunctional protein, Aas	2.04	1.65E-14
V3TWJ7	DNA polymerase III subunit theta, HolE	1.91	4.70E-14
A0A2I5TMZ0	Hydrolase, Orf18415	1.88	7.36E-14
A0A2I5TM92	Arginine deiminase, ArcA	1.85	7.98E-13
A0A2I5TF18	TetR family transcriptional regulator, Orf2710	1.83	1.31E-11
A0A2I5TNE9	ABC transporter ATP-binding protein, Orf19345	1.81	5.70E-13
A0A2I5T7L6	FMN-dependent NADH-azoreductase, Azor	1.77	8.07E-14
A0A2I5T9C5	Citrate lyase acyl carrier protein, CitD	1.76	9.27E-12
A0A2I5TCS3	Der GTPase-activating protein, YihI	1.76	1.51E-13
A0A2I5TP28	N-acetyltransferase, Orf20730	1.73	4.77E-14
A0A2I5T245	DUF1611 domain-containing protein, Orf1735	1.70	9.78E-14
A0A2I5T4G9	Hydrolase, Orf6305	1.70	1.57E-13
A0A2I5T649	XRE family transcriptional regulator, Orf9605	1.69	1.94E-10
A0A2I5TQ50	Uncharacterized protein, Orf1400	1.67	6.90E-11

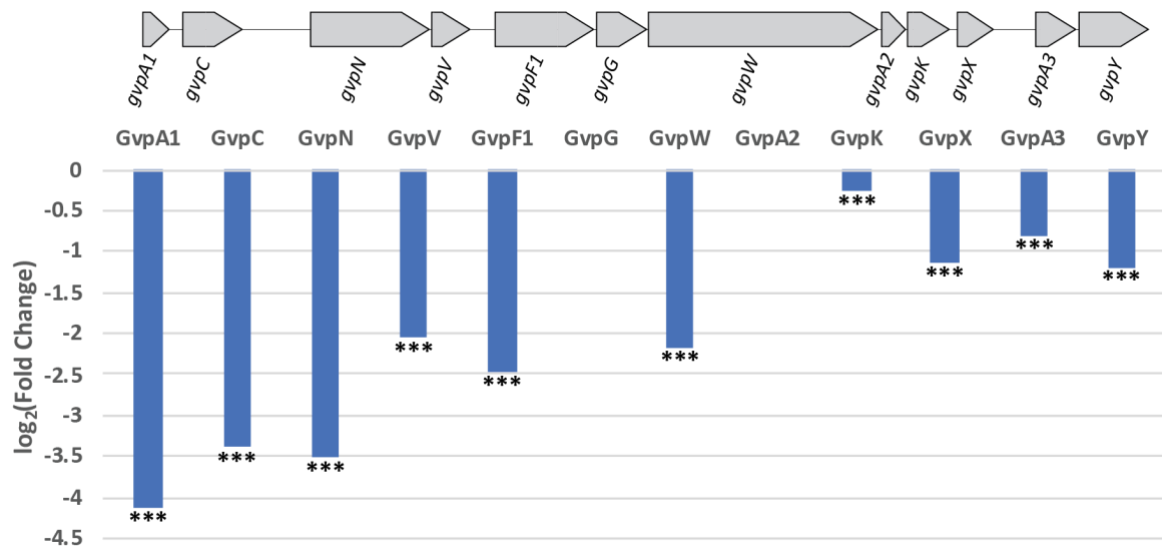
In addition to many significantly upregulated proteins found in the comparative proteomic analysis of AMH141, a wide range of significantly downregulated proteins were also observed. As previous assays have shown, many key phenotypes such as motility, flotation and antibiotic production were reduced in the *dksA* mutant. This pattern was continued in the proteomic analysis. The key phenotype used to initially identify the *dksA* mutant was the inability to product gas vesicles. The proteins of the GV cluster showed a large reduction in abundance with GvpA1, GvpN, GvpC and GvpF1 the four most downregulated proteins identified (Table 6.4). 17 of the 19 proteins encoded by the GV cluster were identified in this proteomic analysis with all but two (GvpH and GvrC) showing significant reductions in abundance (Figure 6.17). However, the changes of the greatest magnitude occurred in proteins encoded by the first half of the *gvpA1* operon.

The *dksA* mutant, AMH141, was found to have significantly decreased production of prodigiosin relative to wild type S39006 which gave it a less pigmented appearance. The change in prodigiosin production in this strain was not as dramatic as the change in carbapenem production observed (Figure 6.5). Only one protein encoded by the *pig* gene cluster was identified in the top 30 most highly downregulated proteins, PigO; a protein that is not essential for prodigiosin production. 12 of the 14 other proteins encoded by the prodigiosin cluster were identified in this proteomic analysis, with PigL and PigM the only proteins not identified. The change in abundance of most proteins encoded by the *pig* cluster was very similar with Log₂FC values ranging from -0.61 to -1.08 (Figure 6.18A). PigK and PigN had slightly smaller Log₂FC of -0.38 and -0.48 respectively (Figure 6.18A). Of the 30 proteins with the greatest reduction in abundance in AMH141 compared to S39006, four of them are involved in biosynthesis of or intrinsic resistance to the carbapenem antibiotic (CarA, CarB, CarC, and CarF). Three other proteins encoded by the carbapenem gene cluster were also identified in the proteomic analysis: CarD, CarG and CarH. These three proteins were significantly reduced in abundance although to a lesser extent (Figure 6.18B). CarR and CarE were not detected in this analysis. This is consistent with the previously reported findings that AMH141 does not produce the carbapenem antibiotic (Figure 6.5A).

Table 6.4 – The top thirty most downregulated proteins quantified AMH141.

Protein ID	Description	Log₂ FC	Adjusted p-value
M9WML5	Gas vesicle structural protein, GvpA1	-4.13	7.29E-11
M9WR86	Gas vesicle protein, GvpN	-3.51	9.10E-10
M9WV25	Gas vesicle structural protein, GvpC	-3.40	5.81E-11
M9WVI2	Gas vesicle protein, GvpF1	-2.47	6.65E-12
A0A2I5TJS4	FAD-binding oxidoreductase, Orf12080	-2.35	2.68E-14
A0A2I5TP08	tRNA (N6-threonylcarbamoyladenine(37)-N6)-methyltransferase, PigO	-2.26	4.70E-14
A0A2I5TIN1	Carbapenem-3-carboxylate synthase, CarC	-2.22	1.85E-10
M9WMK5	Gas vesicle protein, GvpW	-2.19	9.55E-13
A0A2I5TQI9	Uncharacterized protein, Orf12725	-2.13	2.37E-10
A0A2I5TIP9	Carbamoyl-phosphate synthase large chain, CarB	-2.13	1.99E-11
A0A2I5TIM8	Carbapenem-3-carboxylate synthetase, CarA	-2.12	1.20E-10
M9WV41	Gas vesicle protein, GvpV	-2.05	6.65E-12
A0A2I5TK25	Uncharacterized protein, Orf12730	-2.02	9.98E-10
A0A2I5T5M0	Glutamyl-Q tRNA(Asp) synthetase, GluQ	-1.99	4.23E-13
A0A2I5TFS0	Anaerobic glycerol-3-phosphate dehydrogenase subunit B, GlpB	-1.94	1.66E-11
A0A2I5T651	Endopeptidase, Orf9560	-1.91	1.03E-14
A0A2I5T5L6	Ribosomal associated inhibitor protein, RaiA	-1.84	6.95E-12
A0A2I5T3D9	Anaerobic glycerol-3-phosphate dehydrogenase subunit A, GlpA	-1.78	5.08E-11
A0A2I5T3E9	Anaerobic glycerol-3-phosphate dehydrogenase subunit C, GlpC	-1.76	1.49E-11
A0A2I5T8V4	Uncharacterized protein, Orf15000	-1.75	1.03E-10
A0A2I5TIY6	Uncharacterized protein, Orf10555	-1.71	1.30E-12
A0A2I5TPU6	ATP-independent periplasmic protein-refolding chaperone, Orf22230	-1.70	4.17E-11
A0A2I5TA03	Putrescine aminotransferase, YgjG	-1.69	1.37E-14
A0A2I5TIN5	Carbapenem resistance protein, CarF	-1.69	2.03E-12
A0A2I5T3Z7	Glycoside hydrolase family 68 protein, Orf5400	-1.66	1.08E-12
A0A2I5TIZ8	3-hydroxybutyryl-CoA dehydrogenase, Orf10600	-1.56	2.85E-14
A0A2I5T9L7	Heat-shock protein, Orf16490	-1.53	1.17E-13
A0A2I5TIX7	Uncharacterized protein, Orf10565	-1.52	1.06E-12
A0A2I5T9M6	Outer membrane protein, OmpX	-1.52	5.67E-09
A0A2I5TIX8	Acyl-CoA dehydrogenase, Orf10530	-1.47	3.01E-12

A.



B.

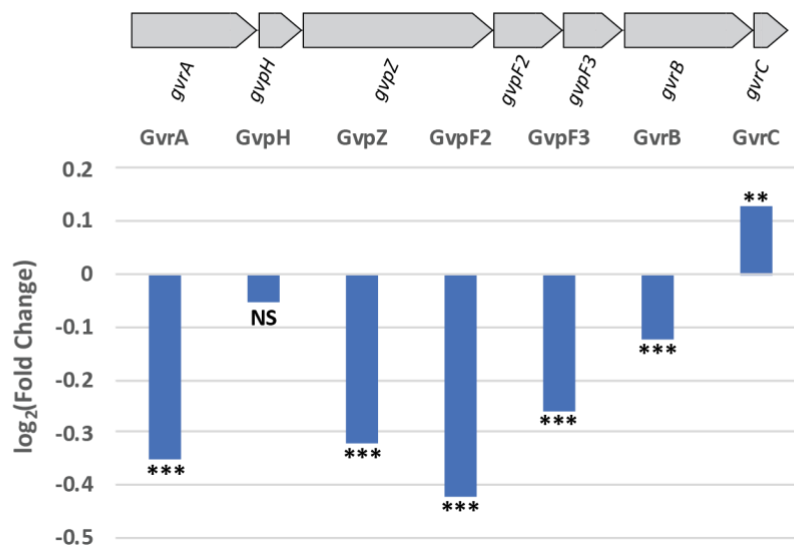


Figure 6.17 – DksA modulates proteins of the *gvpA1* and *gvrA* operons.

Bars represent the difference in production of the indicated protein in AMH141 compared to S39006. Stars represent the adjusted p-values: **, $p < 0.01$; ***, $p < 0.001$; NS, not significant. Proteins not detected in the proteomic analysis are represented by spaces without bars.

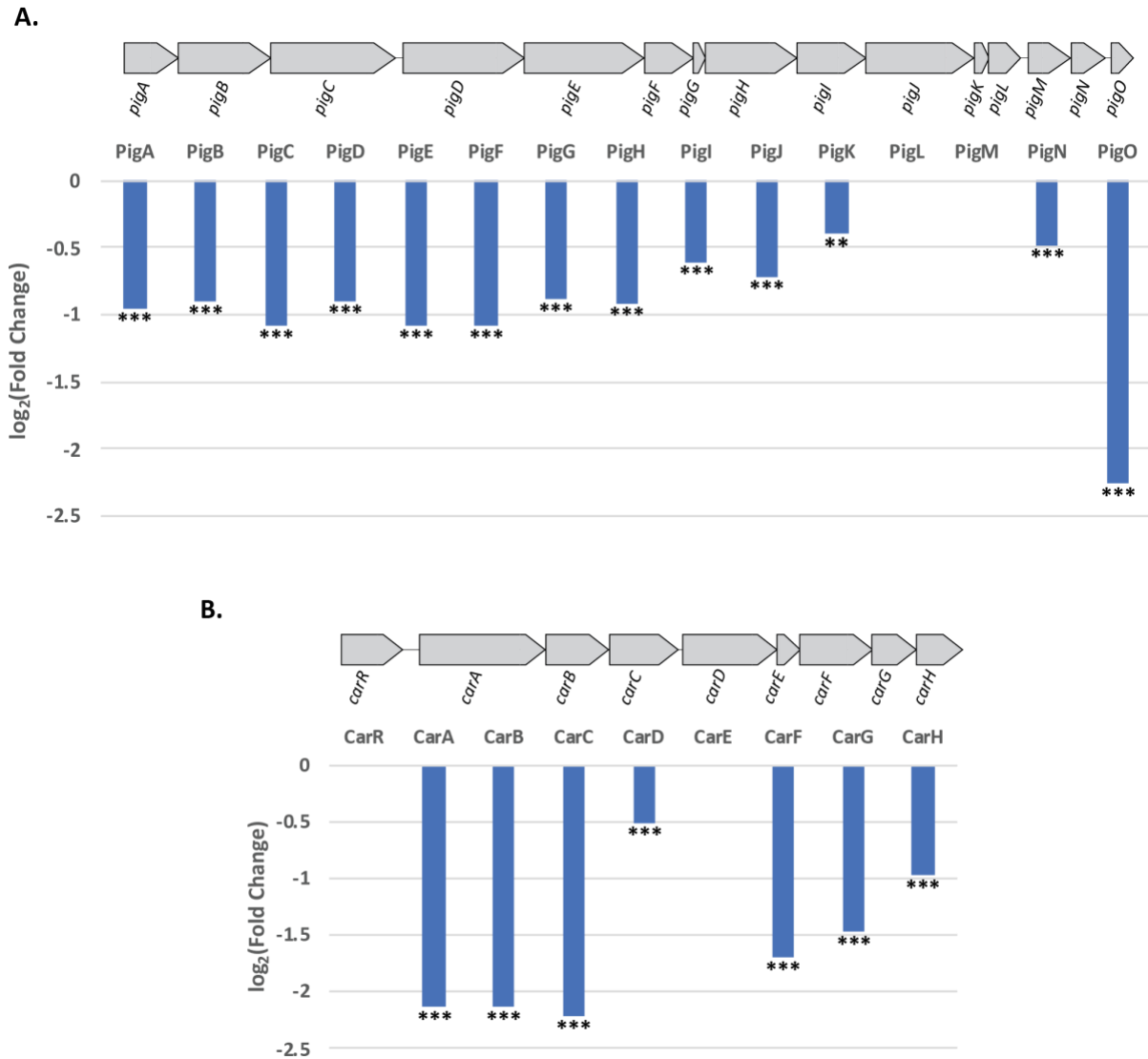


Figure 6.18 – DksA modulates the expression of the prodigiosin and carbapenem operons. Bars represent the difference in production of the indicated protein in AMH141 compared to S39006. Stars represent the adjusted p-values: **, $p < 0.01$; ***, $p < 0.001$; NS, not significant. Proteins not detected in the proteomic analysis are represented by spaces without bars.

In addition to proteins involved in the production of GVs and antibiotics, the *dksA* mutant had many other significantly downregulated proteins indicating that DksA is involved in the regulation of more phenotypes than can be easily detected in S39006. Three proteins that were highly reduced in abundance in AMH141 compared to wild type were GlpA, GlpB, and GlpC. These proteins represent the three subunits of glycerol-3-phosphate dehydrogenase, a respiratory enzyme that converts glycerol-3-phosphate to dihydroxyacetone phosphate. Each of these proteins showed a similar reduction in abundance ranging from -1.76 to -1.94. Other heavily downregulated proteins in the *dksA* mutant include an endopeptidase (Orf9560), an outer membrane protein (OmpX), and an acyl-CoA dehydrogenase (Orf10530). There was also a region encoded by genes *orf10555* to *orf10575* where all proteins were heavily downregulated (Log₂FC of -1.00 to -1.71) that were all uncharacterised proteins. A bioinformatic analysis has failed to identify a function for these proteins, however the proteins encoded by *orf10560*, *orf10565*, *orf10570*, and *orf10575* all showed the greatest degree of similarity to proteins encoded by *Desulfotomaculum acetoxidans*, with 33 to 56 % identity. *D. acetoxidans* is an obligate anaerobe, that is capable of reducing sulphate and forming spores (Watanabe et al., 2018; Widdel & Pfennig, 1977). It was originally isolated from mud samples from piggery waste and cells from an agar colony produce bright spots when viewed under PCM that appear very similar to gas vacuoles (Watanabe et al., 2018; Widdel & Pfennig, 1977).

As one of the key phenotypes of the *dksA* mutant was a reduction in swimming motility and the abolition of swarming motility, a search of the proteomic data was performed for proteins predicted to be involved in motility and chemotaxis. In contrast to the *rpoN* mutant proteomic data, the *dksA* mutant saw a mixture of up and downregulated motility proteins (Table 6.5). The proteins with a significant adjusted p-value are shown in Table 6.5 below, however there were other proteins identified with small changes in abundance that were not viewed as statistically significant and as such have not been included. There are regulatory proteins that are downregulated (such as the flagellar sigma factor FliA) and upregulated (such as the transcriptional regulator FlhD), as well as similar responses for structural proteins. This range of responses highlights the complex nature of motility regulation in S39006 and makes it difficult to determine the exact targets through which DksA is affecting motility.

Table 6.5 – The fold change of proteins involved in flagellar biosynthesis and chemotaxis in AMH141.

Protein ID	Description	Log₂ FC	Adjusted p-value
A0A2I5T758	Methyl-accepting chemotaxis protein	-1.08	6.12E-10
A0A2I5T751	Methyl-accepting chemotaxis protein II	-1.03	1.33E-08
A0A2I5TIT9	Flagella biosynthesis regulator, Flk	-0.84	2.30E-13
A0A2I5T753	RNA polymerase sigma factor, FliA	-0.64	1.98E-11
A0A2I5T4L4	Methyl-accepting chemotaxis protein	-0.49	2.25E-07
A0A2I5T707	Chemotaxis protein methyltransferase	-0.38	1.91E-09
A0A2I5TMV9	Methyl-accepting chemotaxis protein	-0.37	1.73E-05
A0A2I5T4U2	Methyl-accepting chemotaxis protein	-0.33	3.51E-04
A0A2I5TD97	Flagellar brake protein, YcgR	-0.32	5.67E-08
A0A2I5T6Z1	Chemotaxis protein, CheA	-0.30	1.77E-05
A0A2I5TJI1	Flagellin	-0.29	3.08E-05
A0A2I5TNH2	Methyl-accepting chemotaxis protein	-0.26	3.56E-03
A0A2I5TJD2	Chemotaxis protein, CheY	-0.23	1.46E-05
A0A2I5TJE5	Chemotaxis protein, CheW	-0.22	4.37E-05
A0A2I5T721	Flagellar protein, FliJ	0.22	1.02E-06
A0A2I5TJF8	Flagellar motor switch protein, FliM	0.25	4.95E-08
A0A2I5T727	Flagellar protein, FliL	0.26	2.08E-04
A0A2I5TJF3	Flagellar motor switch protein, FliG	0.27	2.56E-06
A0A2I5T4V5	Methyl-accepting chemotaxis protein	0.28	4.85E-05
A0A2I5TEC6	Methyl-accepting chemotaxis protein	0.31	2.04E-04
A0A2I5T745	Flagellar M-ring protein	0.33	1.33E-05
A0A2I5TQH5	Flagellar L-ring protein, FlgH	0.34	1.07E-06
A0A2I5T732	Flagellar motor switch protein, FliN	0.40	2.37E-08
A0A2I5T9J2	Methyl-accepting chemotaxis protein	0.40	4.62E-05
A0A2I5TQV1	Chemotaxis protein	0.42	3.02E-04
A0A2I5T2Y6	Methyl-accepting chemotaxis protein	0.44	3.17E-06
C5J9G8	Flagellar biosynthesis protein, FlhA	0.46	3.56E-07
A0A2I5T716	Flagellar biosynthetic protein, FlhB	0.51	2.57E-08
A0A2I5T763	Flagella basal body P-ring formation protein, FlgA	0.51	2.43E-07
A0A2I5T743	Flagellar secretion chaperone, FliS	0.54	6.49E-10
A0A2I5T7J5	Chemotaxis protein	0.56	5.04E-08
A0A2I5TJD3	Flagellar transcriptional regulator, FlhD	0.56	2.86E-05
A0A2I5TJE0	Flagellar P-ring protein, FlgI	0.56	3.22E-08
A0A2I5T725	Flagellar hook-length control protein, FliK	0.57	1.50E-08
A0A2I5TJF1	Flagella biosynthesis regulatory protein, FliT	0.57	9.43E-10
A0A2I5TL40	Methyl-accepting chemotaxis protein	0.65	7.23E-08
A0A2I5TB03	Methyl-accepting chemotaxis protein	0.79	1.11E-05
A0A2I5TJG3	Flagellar hook-associated protein 2	0.86	4.23E-06

DksA is a highly pleiotropic regulator that has been shown to act by altering transcription of other regulators. To investigate if DksA may be acting through a similar mechanism in S39006, the proteomic data was searched for known regulators of GV production, antibiotic production, and motility. Table 6.6 shows the identified regulators, the change in abundance, and the adjusted p-value. Four regulators showed a Log₂FC of greater magnitude than ± 0.5, the phosphate-binding protein PstS (-0.69), the stationary phase sigma factor RpoS (-0.73), the FAD assembly factor SdhE (0.55), and the LuxR family transcriptional regulator SmrR (-0.88). Several other regulators show changes in abundance that are close to the cut-off of 0.5 and may have significant effects on the cell. S39006 *rpoS* mutants are hyper motile and hyper producers of prodigiosin and carbapenem, opposite phenotypes from those observed in the *dksA* mutant, a surprising finding given the drop in RpoS abundance in this mutant. These data show that DksA is a master regulator in S39006, affecting GV, antibiotic production, motility, and virulence through a wide variety of other regulators.

Table 6.6 – Fold change in abundance of known regulators in the *dksA* mutant.

Protein ID	Description	Log₂ FC	Adjusted p-value
A0A2I5TGF0	RNA-binding protein Hfq	0.40	4.27E-02
A0A2I5TBT4	XRE family transcriptional regulator, PigP	0.22	2.29E-06
A0A2I5TQV6	ArsR family transcriptional regulator, PigS	-0.35	9.91E-06
A0A2I5TCX5	GntR family transcriptional regulator, PigT	0.25	1.37E-07
A0A2I5TIV4	LysR family transcriptional regulator, PigU	0.49	4.74E-09
A0A2I5T9R8	Two-component system response regulator, PigQ	0.35	2.67E-07
A0A2I5T502	Histidine kinase, PigW	0.49	3.20E-07
A8YPB0	GGDEF/EAL domain protein, PigX	0.37	5.08E-09
B6ETQ0	TetR family transcriptional repressor, PigZ	0.25	1.94E-05
A0A2I5TEY7	Phosphate transport system permease protein, PstA	0.19	0.002
A0A2I5TEY8	Phosphate-binding protein, PstS	-0.69	6.36E-04
B6ZCE8	Phosphate transport system permease protein, PtsC	0.30	2.30E-05
B6ZCF2	Phosphate regulon transcriptional regulatory protein, PhoB	-0.43	1.24E-08
A0A2I5T5K2	RNA-binding protein, RsmA	-0.08	3.46E-03
A0A2I5T515	Stationary phase sigma factor, RpoS (σ^{38})	-0.73	1.46E-08
Q9RA96	SylA-like transcriptional regulator, Rap	-0.44	3.53E-09
A0A2I5T9G2	Alpha/beta hydrolase, RhlA	-0.07	1.85E-01
G4V4G2	FAD assembly factor SdhE	0.55	1.62E-09
Q9L3I8	LuxR family transcriptional regulator, SmrR	-0.88	4.73E-14

6.3 Discussion

This chapter has outlined the pleiotropic effects of a transposon insertion in the *dksA* gene of S39006. The *dksA* mutant (AMH141) showed reduced ability to produce gas vesicles and float, as well as a reduction in swimming motility and the inability to swarm on Eiken agar. This strain was also unable to produce the carbapenem antibiotic, showed significantly reduced production of prodigiosin, and had significantly reduced virulence in a *C. elegans* model. A quantitative proteomic analysis comparing the wild type S39006 with AMH141 confirmed the observations from phenotypic assays with proteins involved in antibiotic synthesis and GV structural proteins significantly downregulated. Many regulatory proteins were identified in the proteomic analysis and showed significant changes in abundance providing potential pathways through which DksA activates GV production, antibiotic production, and virulence.

DksA is a fundamental element of the stringent response in Gram-negative bacteria, increasing the effect of the alarmones ppGpp and pppGpp (collectively referred to here as ppGpp) (Paul et al., 2004a). The stringent response helps bacteria to adapt to nutritional starvation, heat shock and oxidative stress (Potrykus & Cashel, 2008). In *E. coli*, ppGpp is synthesised by RelA and SpoT from GDP (to make ppGpp) or GTP (to make pppGpp) and ATP (Dalebroux et al., 2010a). Most Gram-negative gammaproteobacteria encode homologues of RelA and SpoT including S39006. The synthetase activity of RelA is triggered at the ribosome by the accumulation of uncharged tRNAs that occurs during amino acid starvation (Haseltine & Block, 1973). The bifunctional synthetase-hydrolase SpoT enzyme responds to a wider range of nutrient stresses including phosphate, carbon, iron and fatty acid starvation (Dalebroux & Swanson, 2012). ppGpp can then bind RNA polymerase at two sites; at the interface between the β' and ω subunits or the interface between the β' subunit and DksA (Ross et al., 2016, 2013). The most well described effects of ppGpp and DksA are the repression of rRNA operons, a reduction in DNA replication, and activation of amino acid biosynthetic operons (Ferullo & Lovett, 2008; Potrykus & Cashel, 2008; Schreiber et al., 1995). DksA is likely to perform a similar function in S39006 with several amino acid biosynthesis genes downregulated in the *dksA* mutant (Table 6.4).

ppGpp and DksA can act positively or negatively on transcription by RNAP depending on properties of the individual promoters that RNAP binds (Haugen et al., 2008). In *E. coli*, DksA mediates the effect of ppGpp on transcription of σ^{70} -dependent rRNA promoters. A two to three-fold decrease in transcription of rRNA promoters by ppGpp was observed *in vitro* while ~20-fold inhibition was observed in cells (Barker et al., 2001b; Paul et al., 2004a). Inactivation of *dksA* almost abolishes the inhibition of rRNA promoters by ppGpp, preventing the regulation of ribosome synthesis (Paul et al., 2004a). This inhibition occurs through reduction in the lifetime of rRNA promoter open complexes by DksA even in the absence of ppGpp (Paul et al., 2004a). DksA and ppGpp work together to increase transcription from a range of promoters at least partly through indirect mechanisms such as increased free RNAP concentration as a result of the reduced rRNA operon transcription (Barker et al., 2001a; Haugen et al., 2008). Further experiments are required to determine how disruption of *dksA* affects transcription of rRNA promoters in S39006.

DksA can act independently of ppGpp; it reduces the lifetimes of rRNA promoter open complexes and increases the concentration of initiating nucleoside triphosphate required for transcription to occur (Paul et al., 2004a). This increases the probability of DNA-strand collapse before NTP incorporation can occur (Paul et al., 2004a, 2004b). Overexpression of DksA can compensate for some ppGpp⁰ phenotypes including the induction of *rpoS* transcription and overcoming sedimentation and motility defects (Brown et al., 2002; Magnusson et al., 2007). Together with ppGpp, DksA is required for adherence of enterohaemorrhagic *E. coli* to intestinal epithelial cells by activating transcription of the regulatory genes *ler* and *pch* (Nakanishi et al., 2006). DksA plays a contrasting role to ppGpp in the regulation of the *fimB* promoter, governing the production of fimbriae in *E. coli* (Åberg et al., 2008). The production of type I fimbriae was downregulated in ppGpp-deficient strains of *E. coli* while DksA-deficient strains showed hyperfimbriation (Åberg et al., 2006, 2008). This is thought to be due to increased access of GreA and GreB (which are structural homologues of DksA) to the secondary channel of RNAP (Åberg et al., 2008). DksA is also implicated in the virulence of *Salmonella enterica* serovar Typhimurium during the infection of chickens with *dksA* mutants less lethal in 1-day old chicks and poor colonisers of the intestines of 3-week old animals (Turner et al., 1998). *S. Typhimurium dksA* mutants also showed reduced virulence in mice, which was attributed to reduced

expression of *rpoS* and an inability to accumulate RpoS in stationary phase (Webb et al., 1999). The S39006 *dksA* mutant showed a reduction in virulence in a *C. elegans* model with worms surviving two days longer on average compared to wild type. The proteomic analysis identified RpoS as being significantly downregulated in the *dksA* mutant and previous work has shown that an *rpoS* mutant had reduced virulence in *C. elegans* (Wilf & Salmond, 2012). The reduction of RpoS abundance represents a potential pathway through which the *dksA* mutant is attenuated in virulence in *C. elegans*.

Another factor that may be partly responsible for the decreased virulence of the *dksA* mutant was the upregulation of the cellulose biosynthesis operon identified in the proteomic analysis. This suggests that DksA is responsible for repressing the expression of these genes in wild type S39006. Enhanced cellulose production led to a decrease in the virulence of *Salmonella enterica* in a mouse model, and decreased replication inside macrophages (Pontes et al., 2015). However, cellulose has also been identified as a major component of the extracellular matrix of biofilms, with acetylated cellulose required for colonisation of the air-liquid interface in *Pseudomonas fluorescens* (Spiers et al., 2003). Cellulose is also required for pellicle-biofilm formation in *Dickeya dadantii* and enhances plant surface colonisation (Prigent-Combaret et al., 2012). Further experiments are required to determine if there is any change to the virulence of S39006 in a plant model when *dksA* is disrupted.

The proteomic analysis also identified two other proteins of interest, the ribosome silencing factor RsfS and the ribosome associated inhibitor protein RaiA (Log₂FC of 2.83 and -1.84 respectively). RaiA has been shown to stabilize vacant 70S ribosomes in an inactive state and was induced by ppGpp in microarray data from *E. coli* (Agafonov et al., 1999; Durfee et al., 2008; Prossliner et al., 2015; Traxler et al., 2008). Given the importance of DksA in potentiating ppGpp regulation, it makes sense that this protein is so highly downregulated in the *dksA* mutant. RsfS binds to the 50S ribosomal subunit and although it is not necessary for rapid growth initially, *rsfS* mutants showed arrested growth in mid-exponential phase (Häuser et al., 2012; Li et al., 2015). *rsfS* mutants also showed increased protein synthesis in the transition to stationary phase, indicating that RsfS plays a role in reducing translation in stressful conditions (Häuser et al., 2012; Prossliner et al., 2015). DksA performs a similar

role in bacteria, there may be some form of inhibition between these two pathways which could explain why RsfS was so highly upregulated in the proteomic analysis of the *dksA* mutant.

As DksA is such a physiologically wide-ranging transcription factor, it was hypothesised that it could be acting through other regulators that have been previously described in S39006. One well characterised regulator that was hypothesised to be potentiating the phenotypic changes seen in the *dksA* mutant was Hfq. A previously described Hfq mutant showed reduced swimming motility, swarming motility, antibiotic production and virulence in a *C. elegans* model (Wilf et al., 2011). In addition to this, DksA was required for efficient transcription of *hfq* in *Shigella flexneri* and expression of *hfq* in a *dksA* mutant could restore some virulence phenotypes (Sharma & Payne, 2006). A slight increase in Hfq abundance ($\text{Log}_2\text{FC} = 0.40$) was observed in the proteomic analysis of the *dksA* mutant. If DksA was required for transcription of Hfq, a reduction in abundance would be expected in the proteomic analysis. DksA does not appear to activate transcription of *hfq* in S39006 and the phenotypes observed in the *dksA* mutant are not the result of low *hfq* levels.

The stringent response has also been linked to the carbon storage regulator (CsrA) regulatory pathway, where ppGpp induces expression of non-coding regulatory RNAs (Edwards et al., 2011). In *E. coli* *relA*, *spoT*, and *dksA* transcripts were identified as direct targets of CsrA regulation (Edwards et al., 2011; Potts et al., 2017). A feedback loop was discovered whereby CsrA was found to activate *dksA* expression while DksA and ppGpp activated *csrA* expression (Edwards et al., 2011). This DksA-mediated activation of *csrA* expression was partly dependent on RpoS (Edwards et al., 2011). Furthermore, DksA and ppGpp were also found to activate transcription of *csrB* and *csrC*, with RNA levels of CsrB and CsrC reduced 10-fold in *dksA* and ppGpp⁰ strains. The positive effects of DksA on CsrA levels were less than the effects on *csrB* and *csrC* transcription indicating that DksA and ppGpp are net antagonists of CsrA activity in *E. coli* (Edwards et al., 2011). A homologue of the Csr system is present in S39006 where it is called the Rsm system (Williamson et al., 2008). RsmA (a CsrA homologue) negatively regulates swarming motility through repression of *rhIA* and *flhC*; a *rsmA* mutant also overproduces prodigiosin (Williamson et al., 2008). The proteomic analysis found no significant change in RsmA abundance in AMH141 ($\text{Log}_2\text{FC} = -$

0.08), indicating that DksA on its own does not activate *rsmA* expression in S39006. This is consistent with the phenotypic data where the *dksA* mutant shows reduced swarming motility and prodigiosin production, the opposite of a *rsmA* mutant.

An indirect mechanism through which ppGpp and DksA regulate transcription is through σ -factor competition. High concentrations of ppGpp inhibit RNAP from binding to strong σ^{70} -dependent promoters such as promoters for rRNA and tRNA genes; as such more core RNAP is available to bind alternative σ -factors that accumulate due to various stresses (Dalebroux & Swanson, 2012; Österberg et al., 2011). ppGpp also increases the stability of alternative sigma factors such as the stationary phase sigma factor RpoS (σ^S). In *E. coli*, ppGpp promotes RpoS stability by inducing expression of the anti-adaptor proteins IraP and IraD which bind to the adaptor protein RssB, which otherwise targets RpoS for degradation (Bougdour & Gottesman, 2007; Merrikkh et al., 2009). ppGpp mutants fail to induce the RpoS regulon and ppGpp is required for the production of RpoS (Kvint et al., 2000). Similar responses have been observed for RpoN (σ^{54}). DksA and ppGpp are required for σ^{54} transcription in *E. coli* however when σ^{70} mutants that show poor binding with RNAP in competition assays were present, DksA was no longer necessary for σ^{54} transcription to occur (Bernardo et al., 2006).

In the proteomic analysis, RpoS was significantly downregulated in the *dksA* mutant ($\text{Log}_2\text{FC} = -0.73$). Previous analysis has shown that an *rpoS* mutant was unable to make GVs, however this mutant was also a hyper producer of prodigiosin and carbapenem (Quintero-Yanes et al., 2020; Wilf & Salmond, 2012). The DksA mutant was unable to make the carbapenem antibiotic and showed significantly reduced prodigiosin production indicating that reduction in RpoS cannot be the only mechanism through which DksA is regulating flotation and secondary metabolite production in S39006. In transcription assays the *gvpA1* and *gvrA* operons were both downregulated in the *dksA* mutant compared to the wild type. Reduced expression of GvrA, GvrB, and GvrC could result in decreased transcription of the *gvpA1* operon (Ramsay et al., 2011; Tashiro et al., 2016). However, the proteomic analysis only showed slight decreases in abundance of GvrA and GvrB (Log_2FC of -0.35 and -0.12 respectively) and a surprising increase in GvrC abundance (Log_2FC of 0.12). It is possible

that other small changes such as a decrease in RpoN (Log₂FC of -0.24), which was shown in chapter 5 to be essential for GV production are partly responsible for the lack of GVs seen in the *dksA* mutant. Previous studies have shown the importance of DksA and ppGpp in potentiating the responses of RpoN and RpoS, so it is possible that the reason the *DksA* mutant was unable to make GVs is due to the alternative sigma factors such as RpoN and RpoS not being able to activate transcription as they normally would.

In *Streptomyces coelicolor* A3(2) cells that are starved for nitrogen, RelA is required for ppGpp synthesis, expression of the activator *redD* and subsequent undecylprodigiosin production (Chakraborty & Bibb, 1997; Martínez-Costa et al., 1996). This phenotype can be bypassed by phosphate limitation or overexpression of *rshA* (RelA/SpoT homologue) (Sun et al., 2001). Although S39006 does not have a homologue of RedD, it is possible that ppGpp and its common partner DksA act through another transcriptional regulator to control prodigiosin production. In quantitative assays for prodigiosin production, the *DksA* mutant AMH141 produced significantly less prodigiosin than wild type with production over the course of a growth curve approximately one third that of wild type (Figure 6.5B). This trend was also seen in the quantitative proteomic analysis of AMH141 wherein most detected proteins encoded by the prodigiosin cluster had a Log₂FC of between -0.5 and -1 (Figure 6.18A). It is possible that DksA acts directly to regulate transcription of this operon by altering promoter stability as it has been shown to do in other systems. Another possibility is that DksA acts through one of the many previously described regulators of prodigiosin in S39006 or through an undiscovered mechanism. Several previously described regulators of prodigiosin were significantly altered in abundance in the *DksA* mutant including PstS (Log₂FC = -0.69), Rap (-0.44), SmaR (-0.88), RpoS (-0.73), Hfq (0.40), RbsR (0.56), PigU (0.49), PigW (0.49), PigX (0.37) and SdhE (0.55). There is no obvious pattern to these changes with some repressors of prodigiosin production decreased in abundance (e.g. RpoS and SmaR), and others increased in abundance (e.g. PigX). Similarly, some known activators are increased in abundance (e.g. PigW and RbsR) while others are decreased (e.g. Rap). Some of the changes in abundance are small but still statistically significant, so further experiments will be required to determine the physiological significance of any individual changes. It is therefore difficult to pinpoint any one pathway through which DksA is affecting prodigiosin production as it is likely to be the result of many small changes

throughout the complex, interconnected regulatory network of S39006 resulting in the net reduction of prodigiosin production in this mutant.

In a bypass mutagenesis of AMH141, a double mutant was identified with restored ability to produce gas vesicles, albeit with a large growth defect. This mutant, AMH33, had a transposon insertion in *guaB*, which encodes an inosine 5'-monophosphate (IMP) dehydrogenase. The *guaB* gene is located upstream of *guaA*, encoding a guanosine 5'-monophosphate (GMP) synthetase, this gene is also likely disrupted in AMH33 as the transposon contains a transcriptional terminator. GuaA and GuaB are required for the biosynthesis of GMP, a precursor for synthesis of guanine nucleoside triphosphates, from IMP, a common nucleotide precursor (Mehra & Drabble, 1981). GuaB is utilised in both *de novo* and salvage nucleotide synthesis pathways and is inhibited by ppGpp in *E. coli* and *Bacillus subtilis* (Gallant et al., 1971; Irving et al., 2021; Kriel et al., 2012). Further investigations are needed to determine the exact mechanism through which the disruption of the *guaBA* operon enables GV production to resume. It is possible that the disruption of *guaB* may affect ppGpp production as it usually requires GTP or GDP, both of which require the products of GuaB and GuaA reactions (GMP). A mutant with a transposon in *guaB* only shows a hyper opaque phenotype and overproduces GVs compared to wild type S39006. These strains still show severe growth defects and are unable to grow on a minimal medium as is expected.

The impact of ppGpp on GV biogenesis in S39006 has yet to be investigated. Future experiments could include the creation of ppGpp⁰ strains of S39006 through *relA* and *spoT* knockouts to determine the phenotypes under stringent control in this strain. This could also provide clarity over the circumstances in which ppGpp and DksA work together and oppositely in S39006. Other investigations into the regulation of GV production in S39006 have revealed the role of a range of environmental factors including oxygen concentration, where low oxygen concentrations increase GV production, and ribose, which affects the DNA binding ability of RbsR, an activator of GV production (Lee et al., 2017; Ramsay et al., 2011). Environmental potassium has also been shown to be an input into GV production through the potassium transporter TrkH with high environmental potassium concentrations suppressing GV production (Quintero-Yanes et al., 2019). Furthermore, in Chapter 5 the

alternative sigma factor, RpoN, was shown to be required for GV production; while the exact inputs that govern the RpoN regulon in *S39006* remain unknown, in other systems it is a key part of the response to nitrogen starvation. GVs are also under quorum sensing control, indicating that population density affects this form of movement (Ramsay et al., 2011). This chapter adds another key environmental input to the regulatory network governing GV production with the transcriptional regulator DksA shown to be required for GV production in *S39006*. DksA is a key potentiator of the stringent response in many bacteria and it is likely that amino acid starvation and other nutrient limitations that normally control entry into the stringent response cause *S39006* to produce GVs. This adds further evidence to previous assertions that *S39006* produces GVs as an energetically favourable method to move to more nutrient rich habitats (Ramsay et al., 2011).

Chapter 7. Final Discussion

Bacteria have adapted to improve their survival in a wide range of environments. For many bacteria a key component of these survival strategies is mobility, for example swimming, swarming, floating, gliding or twitching (Jarrell & McBride, 2008). The regulation of mobility is multifaceted and coordinated in response to various environmental stimuli. *S39006* is capable of swimming and swarming motility in addition to flotation through the production of GVs. Work over the past decade in this laboratory has shown that the regulatory network governing these phenotypes is highly complicated and overlapping, with flagellar motility often oppositely regulated compared to flotation (Ramsay et al., 2011). Regulators of motility in *S39006* have also frequently been found to co-regulate the production of secondary metabolites and PCWDEs as well as virulence in both plant and animal models. Furthermore, some regulators appear to have opposite impacts on these different phenotypes. For example, RsmA is a negative regulator of prodigiosin production, swarming motility and virulence but a positive regulator of GV production (Ramsay et al., 2011; Wilf et al., 2013; Williamson et al., 2008). Screens for regulators of GV production have discovered other pleiotropic regulators, such as RbsR, a LacI family transcriptional regulator that positively regulates GV, antibiotic, and PCWDE production while negatively regulating flagellar motility (Lee et al., 2017). These screens have also identified roles for environmental inputs that can affect flotation in *S39006*, such as potassium availability (Quintero-Yanes et al., 2019). So, prior to this study, it was clear that there were various environmental and physiological cues impacting on GV regulation (Figure 7.1). However, it seemed unlikely that this repertoire of known regulators represented a comprehensive set of inputs to GV regulation. Therefore, this project aimed to search for, identify, and define any novel regulatory inputs to GV biogenesis in *S39006*.

A random transposon mutagenesis screen was performed to identify novel regulators of GV production in *S39006* (Chapter 3). The regulators identified included an IclR-family transcriptional regulator (*orf6410*), a putative antitoxin (*ratB*), and a 4'-phosphopantetheinyl transferase (*orf2785*). Disruption of each of these genes had pleiotropic impacts on *S39006*, the exact mechanism of which are an avenue for further

study. Orf6410 was a positive regulator of carbapenem production and a negative regulator of swimming and swarming motility while RatB was the opposite; a negative regulator of carbapenem production and a positive regulator of motility. A transposon insertion was also identified in the previously described regulator *hfq*; this mutant shared the same characteristics as a *hfq* knockout strain. This work showed that Hfq affects GV production with no GVs observed in the *hfq* transposon insertion mutant. The *orf2785* mutant, AMH105, showed the most striking pleiotropy, overproducing prodigiosin and surfactant with increased flagellar motility, compared to wild type S39006. It would be interesting to determine if the transposon insertion in *orf2785* resulted in any transcriptional changes to *rhIA* (which encodes an enzyme necessary for rhamnolipid biosynthesis) and the *pigA-O* operon or whether the changes are post-transcriptional. Future work could also be performed to determine whether *ratAB* encodes a functional toxin-antitoxin (TA) system in S39006 and the conditions that activate this system. Moreover, it would be interesting to know what physiological benefit S39006 might derive from linking expression of a TA system to GV biogenesis.

Three GV mutants identified in the initial screen were chosen for study in greater depth: AMH157, which contained a transposon insertion in the O-antigen ligase encoding gene *waaL* (Chapter 4); AMH109, which contained a transposon insertion in *rpoN* encoding an alternative sigma factor (Chapter 5); and AMH141, which contained a transposon insertion in *dksA*, an RNA-polymerase binding transcription factor (Chapter 6). A transposon insertion in *waaL* had been reported previously by a former lab member but had not been investigated in any detail. Here, it was reported that the transposon insertion in *waaL* resulted in a complete loss of flotation in S39006 and yet gas vesicle production was clearly increased compared to wild type. Furthermore, this mutant also showed increased carbapenem production, decreased virulence in a *C. elegans* model, and an inability to swim or swarm. Study of this mutant proved that the production of GVs is necessary but not sufficient for flotation to occur in S39006. An LPS stain showed that the outer surface of AMH157 was altered, and cells viewed under phase contrast microscopy showed increased clumping compared to wild type. These observations proved that the changes in flotation must be the result of changes in the way cells interact with each other rather than simply being attributable exclusively to a lack of GVs within the cells. This LPS impact is also likely

to be the reason why cells are unable to carry out the cooperative movements required for swarming motility. Studies of LPS mutants in other systems have shown similar reductions in motility and it is possible that the transcriptional changes seen in the GV cluster are the result of an unknown feedback mechanism from the cell surface. There is evidence from *Proteus mirabilis* that disruption of *waaL* prevented activation of the *flhDC* operon (Morgenstein et al., 2010). The activity of *flhDC* and *rsmA*, a known regulator of *flhC*, would be an avenue for future exploration in this strain. A proteomic or transcriptomic analysis of AMH157 might also help to elucidate the regulators that are part of the putative feedback system from the cell surface to transcription of the GV cluster.

The transposon insertion in *rpoN* was similarly pleiotropic with the mutant AMH109 showing increased carbapenem production, reduced pectate lyase production, swimming motility, swarming motility, and slightly reduced virulence in a *C. elegans* model. Gas vesicle production was greatly reduced in this mutant, an unusual result as most other mutants with reduced GV production showed increased flagellar motility (Lee et al., 2017; Quintero-Yanes et al., 2020; Ramsay et al., 2011). Using transcriptional fusions in the two operons of the GV cluster it was shown that the decrease in GV production was the result of decreased transcription of the *gvpA1* operon, but no concomitant decrease in transcription of the *gvrA* operon was observed. Subsequent proteomic analysis also identified proteins that were significantly up- and downregulated in abundance in AMH109 compared to wild type S39006. As was expected based on previous assays, carbapenem biosynthesis proteins were highly upregulated while proteins encoded by the GV cluster and those involved in motility were significantly reduced in abundance. In addition, some surprising proteins were identified that were strongly downregulated in abundance, including those encoded by the S39006 version of the *vfm* cluster – a curious quorum sensing system first described in *Dickeya dadantii* (Nasser et al., 2013). Putative RpoN (σ^{54}) binding sites were identified upstream of several genes that encoded proteins that were strongly reduced in abundance compared to wild type. This, coupled with the presence of σ^{54} -dependent transcriptional regulator genes near these binding sites, provides evidence that σ^{54} may be binding to these regulators to direct RNAP to express downstream genes. Further work is needed to determine the exact environmental inputs that activate σ^{54} in S39006. RpoN is most well characterised as a potentiator of the nitrogen starvation response in *E. coli* (Hunt &

Magasanik, 1985). Further study is required to determine if nitrogen limitation is another input into the regulatory network governing GV production in S39006. A ChIP-Seq analysis could also be performed to determine the σ^{54} binding sites in S39006 and validate those found in the bioinformatic analysis.

The final GV mutant detailed in this study was AMH141 which contained a transposon insertion in *dksA*. In *E. coli*, DksA is a key potentiator of the stringent response acting with ppGpp to activate transcription of amino acid biosynthetic operons and repress transcription at rRNA promoters under nutrient starvation conditions (Paul et al., 2004a, 2005). Disruption of *dksA* in S39006 caused a reduction in GV production, swimming and swarming motility, antibiotic production, cellulase production and virulence in *C. elegans*. The changes in GV production were the result of a reduction in transcription of the *gvpA1* and *gvrA* operons. While transcription of the GV cluster was significantly lowered in the *dksA* mutant it was not completely abolished, leading to the hypothesis that this reduction in GV production might somehow be bypassed. A mutant was identified with transposon insertions in both *dksA* and *guaB* that regained the ability to make GVs. However, this double mutant also exhibited a significant growth defect due to the *guaB* mutation. Given the highly pleiotropic effect of the transposon insertion in *dksA*, a proteomic analysis was carried out in AMH141 to determine a wider cohort of proteins in the DksA regulon in S39006. This analysis found 771 (26 %) proteins significantly up or downregulated in AMH141 compared to wild type. Many of the most highly downregulated proteins were those involved in carbapenem, prodigiosin, or GV production, as expected. Proteins involved in chemotaxis and motility showed significant up and downregulation depending on the protein, which was unexpected given the reduced swimming motility and abolished swarming motility seen in this strain. This analysis also identified a series of proteins predicted to be involved in cellulose biosynthesis that were strongly upregulated in AMH141. It is difficult to pinpoint the exact mechanism through which DksA is regulating any of these responses in wild type S39006 because of the significant changes that were observed in expression of many known regulatory proteins, such as PigU, PigW, PstS, RpoS and SmaR. Further work should also be performed to determine the functionality of the stringent response in S39006, including the creation of *relA* and *spoT* knockouts to provide an indication of whether DksA is affecting these phenotypes in conjunction with, or

independently of ppGpp. However, based on these results, it is likely that nutrient starvation and the induction of the stringent response is a key signal used to trigger GV production. This is consistent with previous hypotheses that S39006 produces GVs as an energetically inexpensive means to explore new favourable environments through simple flotation (Ramsay et al., 2011).

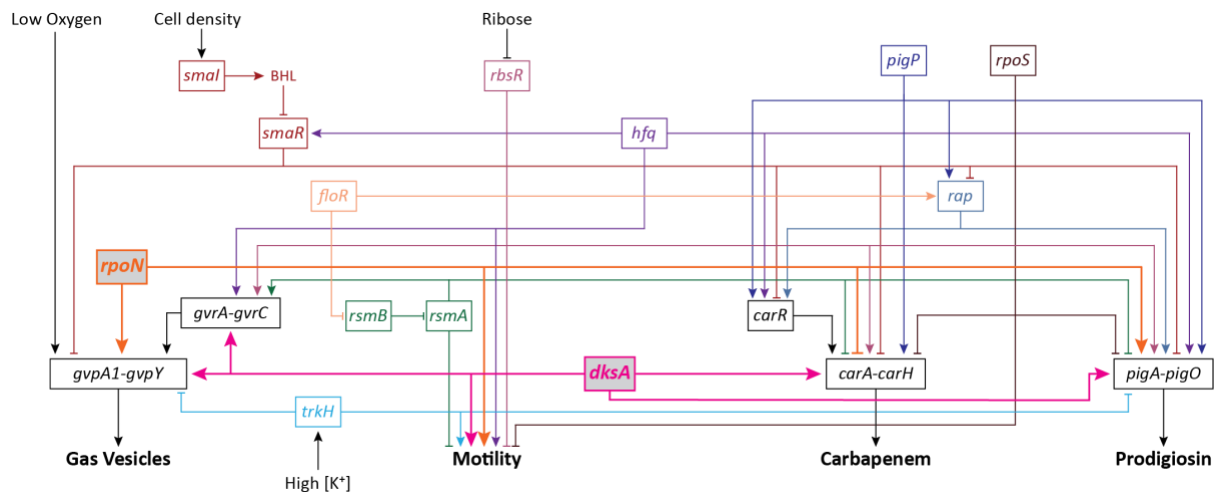


Figure 7.1 – Model of the regulatory network in S39006 for GV production, motility, and secondary metabolite production in S39006.

Grey boxes indicate regulatory genes identified in the present study (*rpoN* and *dksA*). Pointed arrowheads indicate activation while flat arrowheads indicate inactivation.

The present study has described in detail three genes that regulate the production of GVs in S39006 (*waal*, *rpoN*, and *dksA*). Each of these regulators had strongly pleiotropic impacts on the physiology of S39006 affecting the production of secondary metabolites and PCWDEs, motility, and virulence. A proteomic study of the *rpoN* and *dksA* mutants provided greater insight into the respective regulons of RpoN and DksA in S39006 and has identified several potential avenues for further investigation. As *rpoN* and *dksA* mutations both affect the production of PCWDEs and impact virulence in an animal model, it would be interesting to determine if there were also changes in virulence in a plant (potato) model for these mutants. The studies reported in this thesis have provided some important information on the mechanisms through which these new regulators act to modulate GV production. In defining several novel and highly pleiotropic regulatory genes that affect GV biogenesis, this study has confirmed that the regulatory networks of S39006 are extremely complex and overlapping (Figure 7.1). Consequently, functional dissection of individual regulatory pathways is possible, but demanding, and necessitates integrated analyses exploiting the

combined power of all the 'omics technologies to develop holistic views of the physiology of this bacterial strain. S39006 was originally isolated in New Jersey, USA, in a search for environmental bacteria that made new antibiotics – in this case a simple carbapenem. The discovery of GV production in this strain was reported many years after carbapenem antibiotic production had been described (Parker et al., 1982; Ramsay et al., 2011). Given the diversity of phenotypes expressed by this strain and the sheer genetic and physiological complexity of how these phenotypes are modulated, it is obvious that future studies of S39006 will continue to uncover fascinating insights into the intriguing physiology of this bacterium.

References

- Aballay, A., Drenkard, E., Hilbun, L. R., & Ausubel, F. M. (2003). *Caenorhabditis elegans* innate immune response triggered by *Salmonella enterica* requires intact LPS and is mediated by a MAPK signaling pathway. *Current Biology*, *13*(1), 47–52.
[https://doi.org/10.1016/S0960-9822\(02\)01396-9](https://doi.org/10.1016/S0960-9822(02)01396-9)
- Åberg, A., Shingler, V., & Balsalobre, C. (2006). (p)ppGpp regulates type 1 fimbriation of *Escherichia coli* by modulating the expression of the site-specific recombinase FimB. *Molecular Microbiology*, *60*(6), 1520–1533. <https://doi.org/10.1111/J.1365-2958.2006.05191.X>
- Åberg, A., Shingler, V., & Balsalobre, C. (2008). Regulation of the *fimB* promoter: a case of differential regulation by ppGpp and DksA *in vivo*. *Molecular Microbiology*, *67*(6), 1223–1241. <https://doi.org/10.1111/J.1365-2958.2008.06115.X>
- Abeyrathne, P. D., Daniels, C., Poon, K. K. H., Matewish, M. J., & Lam, J. S. (2005). Functional characterization of WaaL, a ligase associated with linking O-antigen polysaccharide to the core of *Pseudomonas aeruginosa* lipopolysaccharide. *Journal of Bacteriology*, *187*(9), 3002–3012. <https://doi.org/10.1128/JB.187.9.3002-3012.2005>
- Agafonov, D. E., Kolb, V. A., Nazimov, I. V., & Spirin, A. S. (1999). A protein residing at the subunit interface of the bacterial ribosome. *Proceedings of the National Academy of Sciences*, *96*(22), 12345–12349. <https://doi.org/10.1073/PNAS.96.22.12345>
- Alba, B. M., & Gross, C. A. (2004). Regulation of the *Escherichia coli* σ^E -dependent envelope stress response. *Molecular Microbiology*, *52*(3), 613–619.
<https://doi.org/10.1111/j.1365-2958.2003.03982.x>
- Alberti, L., & Harshey, R. M. (1990). Differentiation of *Serratia marcescens* 274 into swimmer and swarmer cells. *Journal of Bacteriology*, *172*(8), 4322–4328.
<https://doi.org/10.1128/JB.172.8.4322-4328.1990>
- Alting-Mees, M. A., & Short, J. M. (1989). pBluescript II: gene mapping vectors. *Nucleic Acids Research*, *17*(22), 9494. <https://doi.org/10.1093/nar/17.22.9494>
- Altschul, S. F., Gish, W., Miller, W., Myers, E. W., & Lipman, D. J. (1990). Basic Local Alignment Search Tool. *Journal of Molecular Biology*, *215*(3), 403–410.
[https://doi.org/10.1016/S0022-2836\(05\)80360-2](https://doi.org/10.1016/S0022-2836(05)80360-2)
- Andro, T., Chambost, J. P., Kotoujansky, A., Cattaneo, J., Bertheau, Y., Barras, F., ... Coleno, A.

- (1984). Mutants of *Erwinia chrysanthemi* defective in secretion of pectinase and cellulase. *Journal of Bacteriology*, *160*(3), 1199–1203.
<https://doi.org/10.1128/jb.160.3.1199-1203.1984>
- Baba, T., Ara, T., Hasegawa, M., Takai, Y., Okumura, Y., Baba, M., ... Mori, H. (2006). Construction of *Escherichia coli* K-12 in-frame, single-gene knockout mutants: the Keio collection. *Molecular Systems Biology*, *2*(1).
- Babitzke, P., & Romeo, T. (2007). CsrB sRNA family: sequestration of RNA-binding regulatory proteins. *Current Opinion in Microbiology*, *10*(2), 156–163.
<https://doi.org/10.1016/J.MIB.2007.03.007>
- Bailey, T. L., Johnson, J., Grant, C. E., & Noble, W. S. (2015). The MEME Suite. *Nucleic Acids Research*, *43*(W1), W39–W49. <https://doi.org/10.1093/NAR/GKV416>
- Bainton, N. J., Stead, P., Chhabra, S. R., Bycroft, B. W., Salmond, G. P. C., Stewart, G. S. A. B., & Williams, P. (1992). N-(3-oxohexanoyl)-L-homoserine lactone regulates carbapenem antibiotic production in *Erwinia carotovora*. *Biochemical Journal*, *288*(3), 997–1004.
- Barker, M. M., Gaal, T., & Gourse, R. L. (2001a). Mechanism of regulation of transcription initiation by ppGpp. II. Models for positive control based on properties of RNAP mutants and competition for RNAP. *Journal of Molecular Biology*, *305*(4), 689–702.
<https://doi.org/10.1006/JMBI.2000.4328>
- Barker, M. M., Gaal, T., Josaitis, C. A., & Gourse, R. L. (2001b). Mechanism of regulation of transcription initiation by ppGpp. I. Effects of ppGpp on transcription initiation *in vivo* and *in vitro*. *Journal of Molecular Biology*, *305*(4), 673–688.
<https://doi.org/10.1006/JMBI.2000.4327>
- Barrios, H., Valderrama, B., & Morett, E. (1999). Compilation and analysis of σ^{54} -dependent promoter sequences. *Nucleic Acids Research*, *27*(22), 4305–4313.
<https://doi.org/10.1093/nar/27.22.4305>
- Battesti, A., & Bouveret, E. (2006). Acyl carrier protein/SpoT interaction, the switch linking SpoT-dependent stress response to fatty acid metabolism. *Molecular Microbiology*, *62*(4), 1048–1063. <https://doi.org/10.1111/J.1365-2958.2006.05442.X>
- Beard, S. J., Davis, P. A., Iglesias-Rodríguez, D., Skulberg, O. M., & Walsby, A. E. (2000). Gas vesicle genes in *Planktothrix* spp. from Nordic lakes: strains with weak gas vesicles possess a longer variant of *gvpC*. *Microbiology*, *146*(8), 2009–2018.
<https://doi.org/10.1099/00221287-146-8-2009>

- Beard, S. J., Handley, B. A., & Walsby, A. E. (2002). Spontaneous mutations in gas vesicle genes of *Planktothrix* spp. affect gas vesicle production and critical pressure. *FEMS Microbiology Letters*, *215*(2), 189–195. <https://doi.org/10.1111/j.1574-6968.2002.tb11390.x>
- Belenky, M., Meyers, R., & Herzfeld, J. (2004). Subunit Structure of Gas Vesicles: A MALDI-TOF Mass Spectrometry Study. *Biophysical Journal*, *86*, 499–505. [https://doi.org/10.1016/S0006-3495\(04\)74128-4](https://doi.org/10.1016/S0006-3495(04)74128-4)
- Benjamini, Y., & Hochberg, Y. (1995). Controlling the False Discovery Rate: A Practical and Powerful Approach to Multiple Testing. *Journal of the Royal Statistical Society. Series B (Methodological)*, *57*(1), 289–300. <https://doi.org/10.1111/j.2517-6161.1995.tb02031.x>
- Benson, D. A., Karsch-Mizrachi, I., Lipman, D. J., Ostell, J., & Wheeler, D. L. (2005). GenBank. *Nucleic Acids Research*, *33*(suppl 1), D34–D38. <https://doi.org/10.1093/nar/gki063>
- Bentley, S. D., Chater, K. F., Cerdeño-Tárraga, A.-M., Challis, G. L., Thomson, N. R., James, K. D., ... Hopwood, D. A. (2002). Complete genome sequence of the model actinomycete *Streptomyces coelicolor* A3(2). *Nature*, *417*, 141–147. <https://doi.org/10.1038/417141a>
- Berg, H. C., & Anderson, R. A. (1973). Bacteria Swim by Rotating their Flagellar Filaments. *Nature*, *245*(5425), 380–382. <https://doi.org/10.1038/245380a0>
- Bernardo, L. M. D., Johansson, L. U. M., Solera, D., Skarfstad, E., & Shingler, V. (2006). The guanosine tetraphosphate (ppGpp) alarmone, DksA and promoter affinity for RNA polymerase in regulation of σ^{54} -dependent transcription. *Molecular Microbiology*, *60*(3), 749–764. <https://doi.org/10.1111/j.1365-2958.2006.05129.x>
- Bertani, B., & Ruiz, N. (2018). Function and Biogenesis of Lipopolysaccharides. *EcoSal Plus*, *8*(1), 1–19. <https://doi.org/10.1128/ecosalplus.ESP-0001-2018>
- Bogomolnaya, L. M., Aldrich, L., Ragoza, Y., Talamantes, M., Andrews, K. D., McClelland, M., & Andrews-Polymenis, H. L. (2014). Identification of novel factors involved in modulating motility of *Salmonella enterica* Serotype Typhimurium. *PLoS ONE*, *9*(11), 111513. <https://doi.org/10.1371/journal.pone.0111513>
- Bonocora, R. P., Smith, C., Lapierre, P., Wade, J. T., & Sogaard-Andersen, L. (2015). Genome-Scale Mapping of *Escherichia coli* σ^{54} Reveals Widespread, Conserved Intragenic Binding. *PLoS Genetics*, *11*(10), e1005552. <https://doi.org/10.1371/journal.pgen.1005552>

- Boratyn, G. M., Schäffer, A. A., Agarwala, R., Altschul, S. F., Lipman, D. J., & Madden, T. L. (2012). Domain Enhanced Lookup Time Accelerated BLAST. *Biology Direct*, *7*(12).
<https://doi.org/10.1186/1745-6150-7-12>
- Borić, M., Danevčič, T., & Stopar, D. (2011). Prodigiosin from *Vibrio* sp. DSM 14379; A New UV-Protective Pigment. *Microbial Ecology*, *62*(3), 528–536.
<https://doi.org/10.1007/S00248-011-9857-0>
- Boucher, J. C., Schurr, M. J., & Deretic, V. (2000). Dual regulation of mucoidy in *Pseudomonas aeruginosa* and sigma factor antagonism. *Molecular Microbiology*, *36*(2), 341–351. <https://doi.org/10.1046/j.1365-2958.2000.01846.x>
- Bougdour, A., & Gottesman, S. (2007). ppGpp regulation of RpoS degradation via anti-adaptor protein IraP. *Proceedings of the National Academy of Sciences*, *104*(31), 12896–12901. <https://doi.org/10.1073/PNAS.0705561104>
- Bourdeau, R. W., Lee-Gosselin, A., Lakshmanan, A., Farhadi, A., Kumar, S. R., Nety, S. P., & Shapiro, M. G. (2018). Acoustic reporter genes for noninvasive imaging of microorganisms in mammalian hosts. *Nature*, *553*(7686), 86–90.
<https://doi.org/10.1038/nature25021>
- Bowden, M. G., & Kaplan, H. B. (1998). The *Myxococcus xanthus* lipopolysaccharide O-antigen is required for social motility and multicellular development. *Molecular Microbiology*, *30*(2), 275–284. <https://doi.org/10.1046/j.1365-2958.1998.01060.x>
- Bradley, J. S., Garau, J., Lode, H., Rolston, K. V. I., Wilson, S. E., & Quinn, J. P. (1999). Carbapenems in clinical practice: a guide to their use in serious infection. *International Journal of Antimicrobial Agents*, *11*(2), 93–100. [https://doi.org/10.1016/S0924-8579\(98\)00094-6](https://doi.org/10.1016/S0924-8579(98)00094-6)
- Branny, P., Pearson, J. P., Pesci, E. C., Köhler, T., Iglewski, B. H., & Van Delden, C. (2001). Inhibition of quorum sensing by a *Pseudomonas aeruginosa* *dksA* homologue. *Journal of Bacteriology*, *183*(5), 1531–1539. <https://doi.org/10.1128/JB.183.5.1531-1539.2001>
- Brenner, S. (1974). The Genetics of *Caenorhabditis elegans*. *Genetics*, *77*(1), 71–94.
- Brown, L., Gentry, D., Elliott, T., & Cashel, M. (2002). DksA affects ppGpp induction of RpoS at a translational level. *Journal of Bacteriology*, *184*(16), 4455–4465.
<https://doi.org/10.1128/jb.184.16.4455-4465.2002>
- Buck, M., Gallegos, M. T., Studholme, D. J., Guo, Y., & Gralla, J. D. (2000). The bacterial enhancer-dependent σ^{54} (σ^N) transcription factor. *Journal of Bacteriology*.

<https://doi.org/10.1128/JB.182.15.4129-4136.2000>

- Busenlehner, L. S., Pennella, M. A., & Giedroc, D. P. (2003). The SmtB/ArsR family of metalloregulatory transcriptional repressors: structural insights into prokaryotic metal resistance. *FEMS Microbiology Reviews*, 27, 131–143. [https://doi.org/10.1016/S0168-6445\(03\)00054-8](https://doi.org/10.1016/S0168-6445(03)00054-8)
- Bush, M., & Dixon, R. (2012). The Role of Bacterial Enhancer Binding Proteins as Specialized Activators of σ^{54} -Dependent Transcription. *Microbiology and Molecular Biology Reviews*, 76(3), 497–529. <https://doi.org/10.1128/mnbr.00006-12>
- Carver, T., Harris, S. R., Berriman, M., Parkhill, J., & McQuillan, J. A. (2012). Artemis: an integrated platform for visualization and analysis of high-throughput sequence-based experimental data. *Bioinformatics*, 28(4), 464–469. <https://doi.org/10.1093/bioinformatics/btr703>
- Casaz, P., & Buck, M. (1999). Region I modifies DNA-binding domain conformation of sigma 54 within the holoenzyme. *Journal of Molecular Biology*, 285(2), 507–514. <https://doi.org/10.1006/jmbi.1998.2328>
- Cases, I., Ussery, D. W., & De Lorenzo, V. (2003). The σ^{54} regulon (sigmulon) of *Pseudomonas putida*. *Environmental Microbiology*, 5(12), 1281–1293. <https://doi.org/10.1111/j.1462-2920.2003.00528.x>
- Chakraborty, R., & Bibb, M. (1997). The ppGpp synthetase gene (*relA*) of *Streptomyces coelicolor* A3(2) plays a conditional role in antibiotic production and morphological differentiation. *Journal of Bacteriology*, 179(18), 5854–5861. <https://doi.org/10.1128/JB.179.18.5854-5861.1997>
- Chandrangsu, P., Wang, L., Choi, S. H., & Gourse, R. L. (2012). Suppression of a *dnaKJ* Deletion by Multicopy *dksA* Results from Non-Feedback-Regulated Transcripts That Originate Upstream of the Major *dksA* Promoter. *Journal of Bacteriology*, 194(6), 1437–1446. <https://doi.org/10.1128/JB.06726-11>
- Chaney, M., Grande, R., Wigneshweraraj, S. R., Cannon, W., Casaz, P., Gallegos, M. T., ... Buck, M. (2001). Binding of transcriptional activators to sigma 54 in the presence of the transition state analog ADP-aluminum fluoride: Insights into activator mechanochemical action. *Genes and Development*, 15(17), 2282–2294. <https://doi.org/10.1101/gad.205501>
- Chao, Y., & Vogel, J. (2010). The role of Hfq in bacterial pathogens. *Current Opinion in*

- Microbiology*, 13, 24–33. <https://doi.org/10.1016/j.mib.2010.01.001>
- Chatterjee, A., Cui, Y., & Chatterjee, A. K. (2002). Regulation of *Erwinia carotovora* hrp_{L_{Ecc}}(sigma-L_{Ecc}), which encodes an extracytoplasmic function subfamily of sigma factor required for expression of the HRP regulon. *Molecular Plant-Microbe Interactions*, 15(9), 971–980. <https://doi.org/10.1094/MPMI.2002.15.9.971>
- Childs, T. S., & Webley, W. C. (2012). In vitro assessment of halobacterial gas vesicles as a *Chlamydia* vaccine display and delivery system. *Vaccine*, 30(41), 5942–5948. <https://doi.org/10.1016/J.VACCINE.2012.07.038>
- Chu, L. J., Chen, M. C., Setter, J., Tsai, Y. S., Yang, H., Fang, X., ... Ng, W. V. (2011). New Structural Proteins of *Halobacterium salinarum* Gas Vesicle Revealed by Comparative Proteomics Analysis. *Journal of Proteome Research*, 10(3), 1170–1178. <https://doi.org/10.1021/pr1009383>
- Codjoe, F. S., & Donkor, E. S. (2017). Carbapenem Resistance: A Review. *Medical Sciences*, 6(1), 1–28. <https://doi.org/10.3390/MEDSCI6010001>
- Coulthurst, S. J., Barnard, A. M. L., & Salmond, G. P. C. (2005). Regulation and biosynthesis of carbapenem antibiotics in bacteria. *Nature Reviews Microbiology*, 3(4), 295–306. <https://doi.org/10.1038/nrmicro1128>
- Coulthurst, S. J., Kurz, C. L., & Salmond, G. P. C. (2004). *luxS* mutants of *Serratia* defective in autoinducer-2-dependent “quorum sensing” show strain-dependent impacts on virulence and production of carbapenem and prodigiosin. *Microbiology*, 150(6), 1901–1910. <https://doi.org/10.1099/mic.0.26946-0>
- Cox, A. R. J., Thomson, N. R., Bycroft, B. W., Stewart, G. S. A. B., Williams, P., & Salmond, G. P. C. (1998). A pheromone-independent CarR protein controls carbapenem antibiotic synthesis in the opportunistic human pathogen *Serratia marcescens*. *Microbiology*, 144(1), 201–209. <https://doi.org/10.1099/00221287-144-1-201>
- Cunin, R., Glansdorff, N., Piérard, A., & Stalon, V. (1986). Biosynthesis and metabolism of arginine in bacteria. *Microbiological Reviews*, 50(3), 314–352. <https://doi.org/10.1128/mr.50.3.314-352.1986>
- Dalebroux, Z. D., Svensson, S. L., Gaynor, E. C., & Swanson, M. S. (2010a). ppGpp conjures bacterial virulence. *Microbiology and Molecular Biology Reviews : MMBR*, 74(2), 171–199. <https://doi.org/10.1128/MMBR.00046-09>
- Dalebroux, Z. D., & Swanson, M. S. (2012). ppGpp: magic beyond RNA polymerase. *Nature*

- Reviews Microbiology*, 10(3), 203–212. <https://doi.org/10.1038/nrmicro2720>
- Dalebroux, Z. D., Yagi, B. F., Sahr, T., Buchrieser, C., & Swanson, M. S. (2010b). Distinct roles of ppGpp and DksA in *Legionella pneumophila* differentiation. *Molecular Microbiology*, 76(1), 200–219. <https://doi.org/10.1111/J.1365-2958.2010.07094.X>
- Danevčič, T., Borić Vezjak, M., Tabor, M., Zorec, M., & Stopar, D. (2016a). Prodigiosin induces autolysins in actively grown *Bacillus subtilis* cells. *Frontiers in Microbiology*, 7, 27. <https://doi.org/10.3389/FMICB.2016.00027>
- Danevčič, T., Vezjak, M. B., Zorec, M., & Stopar, D. (2016b). Prodigiosin - A Multifaceted *Escherichia coli* Antimicrobial Agent. *PLOS ONE*, 11(9), e0162412. <https://doi.org/10.1371/JOURNAL.PONE.0162412>
- Dasgupta, N., Wolfgang, M. C., Goodman, A. L., Arora, S. K., Jyot, J., Lory, S., & Ramphal, R. (2003). A four-tiered transcriptional regulatory circuit controls flagellar biogenesis in *Pseudomonas aeruginosa*. *Molecular Microbiology*, 50(3), 809–824. <https://doi.org/10.1046/j.1365-2958.2003.03740.x>
- DasSarma, P., Negi, V. D., Balakrishnan, A., Kim, J.-M., Karan, R., Chakravorty, D., & DasSarma, S. (2015). Haloarchaeal gas vesicle nanoparticles displaying *Salmonella* antigens as a novel approach to vaccine development. *Procedia in Vaccinology*, 9, 16–23. <https://doi.org/10.1016/j.provac.2015.05.003>
- DasSarma, S., & Arora, P. (1997). Genetic analysis of the gas vesicle gene cluster in haloarchaea. *FEMS Microbiology Letters*, 153(1), 1–10. <https://doi.org/10.1111/j.1574-6968.1997.tb10456.x>
- DasSarma, S., Arora, P., Lin, F., Molinari, E., & Yin, L. R.-S. (1994). Wild-type gas vesicle formation requires at least ten genes in the *gvp* gene cluster of *Halobacterium halobium* plasmid pNRC100. *Journal of Bacteriology*, 176(24), 7646–7652. <https://doi.org/10.1128/JB.176.24.7646-7652.1994>
- Débarbouillé, M., Martin-Verstraete, I., Kunst, F., & Rapoport, G. (1991). The *Bacillus subtilis* *sigL* gene encodes an equivalent of σ^{54} from gram-negative bacteria. *Proceedings of the National Academy of Sciences of the United States of America*, 88(20), 9092–9096. <https://doi.org/10.1073/pnas.88.20.9092>
- Demarre, G., Guérout, A.-M., Matsumoto-Mashimo, C., Rowe-Magnus, D. A., Marlière, P., & Mazel, D. (2005). A new family of mobilizable suicide plasmids based on broad host range R388 plasmid (IncW) and RP4 plasmid (IncP α) conjugative machineries and their

- cognate *Escherichia coli* host strains. *Research in Microbiology*, 156(2), 245–255.
<https://doi.org/10.1016/j.resmic.2004.09.007>
- Deng, W. L., Chang, H. Y., & Peng, H. L. (1994). Acetoin catabolic system of *Klebsiella pneumoniae* CG43: Sequence, expression, and organization of the *aco* operon. *Journal of Bacteriology*, 176(12), 3527–3535. <https://doi.org/10.1128/jb.176.12.3527-3535.1994>
- Dolan, S. K., Kohlstedt, M., Trigg, S., Vallejo Ramirez, P., Kaminski, C. F., Wittmann, C., & Welch, M. (2020). Contextual Flexibility in *Pseudomonas aeruginosa* Central Carbon Metabolism during Growth in Single Carbon Sources. *MBio*, 11(2), e02684-19. <https://doi.org/10.1128/mBio.02684-19>
- Dombrecht, B., Marchal, K., Vanderleyden, J., & Michiels, J. (2002). Prediction and overview of the RpoN-regulon in closely related species of the *Rhizobiales*. *Genome Biology*, 3(12), 1–11. <https://doi.org/10.1186/gb-2002-3-12-research0076>
- Dong, T., Yu, R., & Schellhorn, H. (2011). Antagonistic regulation of motility and transcriptome expression by RpoN and RpoS in *Escherichia coli*. *Molecular Microbiology*, 79(2), 375–386. <https://doi.org/10.1111/j.1365-2958.2010.07449.x>
- Duprey, A., Taib, N., Leonard, S., Garin, T., Flandrois, J., Nasser, W., ... Reverchon, S. (2019). The phytopathogenic nature of *Dickeya aquatica* 174/2 and the dynamic early evolution of *Dickeya* pathogenicity. *Environmental Microbiology*, 21(8), 2809–2835. <https://doi.org/10.1111/1462-2920.14627>
- Durfee, T., Hansen, A. M., Zhi, H., Blattner, F. R., & Ding, J. J. (2008). Transcription profiling of the stringent response in *Escherichia coli*. *Journal of Bacteriology*, 190(3), 1084–1096. <https://doi.org/10.1128/JB.01092-07>
- Dutta, S., DasSarma, P., DasSarma, S., & Jarori, G. K. (2015). Immunogenicity and protective potential of a *Plasmodium* spp. enolase peptide displayed on archaeal gas vesicle nanoparticles. *Malaria Journal*, 14(1), 406. <https://doi.org/10.1186/s12936-015-0914-x>
- Eberl, L., Molin, S., & Givskov, M. (1999). Surface motility of *Serratia liquefaciens* MG1. *Journal of Bacteriology*, 181(6), 1703–1712. <https://doi.org/10.1128/JB.181.6.1703-1712.1999>
- Edwards, A. N., Patterson-Fortin, L. M., Vakulskas, C. A., Mercante, J. W., Potrykus, K., Vinella, D., ... Romeo, T. (2011). Circuitry linking the Csr and stringent response global regulatory systems. *Molecular Microbiology*, 80(6), 1561–1580.

<https://doi.org/10.1111/j.1365-2958.2011.07663.x>

- El-Gamal, M. I., Brahim, I., Hisham, N., Aladdin, R., Mohammed, H., & Bahaeldin, A. (2017). Recent updates of carbapenem antibiotics. *European Journal of Medicinal Chemistry*, *131*, 185–195. <https://doi.org/10.1016/J.EJMECH.2017.03.022>
- El-Gebali, S., Mistry, J., Bateman, A., Eddy, S. R., Luciani, A., Potter, S. C., ... Finn, R. D. (2019). The Pfam protein families database in 2019. *Nucleic Acids Research*, *47*(D1), D427–D432. <https://doi.org/10.1093/nar/gky995>
- Elshamy, A. A., & Aboshanab, K. M. (2020). A review on bacterial resistance to carbapenems: epidemiology, detection and treatment options. *Future Science*, *6*(3). <https://doi.org/10.2144/FSOA-2019-0098>
- Engbrecht, J., Neelson, K., & Silverman, M. (1983). Bacterial bioluminescence: Isolation and genetic analysis of functions from *Vibrio fischeri*. *Cell*, *32*(3), 773–781. [https://doi.org/10.1016/0092-8674\(83\)90063-6](https://doi.org/10.1016/0092-8674(83)90063-6)
- Englert, C., Krüger, K., Offner, S., & Pfeifer, F. (1992). Three different but related gene clusters encoding gas vesicles in halophilic archaea. *Journal of Molecular Biology*, *227*(2), 586–592. [https://doi.org/10.1016/0022-2836\(92\)90914-6](https://doi.org/10.1016/0022-2836(92)90914-6)
- Englert, C., & Pfeifer, F. (1993). Analysis of Gas Vesicle Gene Expression in *Haloferax mediterranei* Reveals That GvpA and GvpC Are Both Gas Vesicle Structural Proteins. *The Journal of Biological Chemistry*, *268*(13), 9329–9336. [https://doi.org/10.1016/S0021-9258\(18\)98354-7](https://doi.org/10.1016/S0021-9258(18)98354-7)
- Evans, T. J., Crow, M. A., Williamson, N. R., Orme, W., Thomson, N. R., Komitopoulou, E., & Salmond, G. P. C. (2010). Characterization of a broad-host-range flagellum-dependent phage that mediates high-efficiency generalized transduction in, and between, *Serratia* and *Pantoea*. *Microbiology*, *156*(1), 240–247. <https://doi.org/10.1099/mic.0.032797-0>
- Farhadi, A., Ho, G. H., Sawyer, D. P., Bourdeau, R. W., & Shapiro, M. G. (2019). Ultrasound imaging of gene expression in mammalian cells. *Science (New York, N.Y.)*, *365*(6460), 1469–1475. <https://doi.org/10.1126/science.aax4804>
- Ferullo, D. J., & Lovett, S. T. (2008). The Stringent Response and Cell Cycle Arrest in *Escherichia coli*. *PLOS Genetics*, *4*(12), e1000300. <https://doi.org/10.1371/JOURNAL.PGEN.1000300>
- Fineran, P. C., Everson, L., Slater, H., & Salmond, G. P. C. (2005a). A GntR family transcriptional regulator (PigT) controls gluconate-mediated repression and defines a

- new, independent pathway for regulation of the tripyrrole antibiotic, prodigiosin, in *Serratia*. *Microbiology*, 151(12), 3833–3845. <https://doi.org/10.1099/mic.0.28251-0>
- Fineran, P. C., Iglesias Cans, M. C., Ramsay, J. P., Wilf, N. M., Cossyleon, D., McNeil, M. B., ... Salmond, G. P. C. (2013). Draft Genome Sequence of *Serratia* sp. Strain ATCC 39006, a Model Bacterium for Analysis of the Biosynthesis and Regulation of Prodigiosin, a Carbapenem, and Gas Vesicles. *Genome Announcements*, 1(6), e01039-13. <https://doi.org/10.1128/genomeA.01039-13>
- Fineran, P. C., Slater, H., Everson, L., Hughes, K., & Salmond, G. P. C. (2005b). Biosynthesis of tripyrrole and β -lactam secondary metabolites in *Serratia*: integration of quorum sensing with multiple new regulatory components in the control of prodigiosin and carbapenem antibiotic production. *Molecular Microbiology*, 56(6), 1495–1517. <https://doi.org/10.1111/j.1365-2958.2005.04660.x>
- Fineran, P. C., Williamson, N. R., Lilley, K. S., & Salmond, G. P. C. (2007). Virulence and prodigiosin antibiotic biosynthesis in *Serratia* are regulated pleiotropically by the GGDEF/EAL domain protein, PigX. *Journal of Bacteriology*, 189(21), 7653–7662. <https://doi.org/10.1128/JB.00671-07>
- Fomsgaard, A., Freudenberg, M. A., & Galanos, C. (1990). Modification of the silver staining technique to detect lipopolysaccharide in polyacrylamide gels. *Journal of Clinical Microbiology*, 28(12), 2627–2631. <https://doi.org/10.1128/jcm.28.12.2627-2631.1990>
- Fraser, G. M., & Hughes, C. (1999). Swarming motility. *Current Opinion in Microbiology*, 2(6), 630–635. [https://doi.org/10.1016/S1369-5274\(99\)00033-8](https://doi.org/10.1016/S1369-5274(99)00033-8)
- Gallant, J., Irr, J., & Cashel, M. (1971). The Mechanism of Amino Acid Control of Guanylate and Adenylate Biosynthesis. *Journal of Biological Chemistry*, 246(18), 5812–5816. [https://doi.org/10.1016/S0021-9258\(18\)61877-0](https://doi.org/10.1016/S0021-9258(18)61877-0)
- Gardner, S. G., & McCleary, W. R. (2019). Control of the *phoBR* Regulon in *Escherichia coli*. *EcoSal Plus*, 8(2), 1–20. <https://doi.org/10.1128/ECOSALPLUS.ESP-0006-2019>
- Gatto, L., Gibb, S., & Rainer, J. (2021). MSnbase, Efficient and Elegant R-Based Processing and Visualization of Raw Mass Spectrometry Data. *Journal of Proteome Research*, 20(1), 1063–1069. <https://doi.org/10.1021/acs.jproteome.0c00313>
- Gatto, L., & Lilley, K. S. (2012). Msnbase-an R/Bioconductor package for isobaric tagged mass spectrometry data visualization, processing and quantitation. *Bioinformatics*, 28(2), 288–289. <https://doi.org/10.1093/bioinformatics/btr645>

- Grant, C. E., Bailey, T. L., & Noble, W. S. (2011). FIMO: scanning for occurrences of a given motif. *Bioinformatics*, *27*(7), 1017–1018.
<https://doi.org/10.1093/bioinformatics/btr064>
- Grimont, F., & Grimont, P. A. D. (2006). The Genus *Serratia*. In *The Prokaryotes* (pp. 219–244). Springer New York. https://doi.org/10.1007/0-387-30746-X_11
- Gristwood, T., Fineran, P. C., Everson, L., Williamson, N. R., & Salmond, G. P. C. (2009). The PhoBR two-component system regulates antibiotic biosynthesis in *Serratia* in response to phosphate. *BMC Microbiology*, *9*(112). <https://doi.org/10.1186/1471-2180-9-112>
- Grundy, F. J., Waters, D. A., Takova, T. Y., & Henkin, T. M. (1993). Identification of genes involved in utilization of acetate and acetoin in *Bacillus subtilis*. *Molecular Microbiology*, *10*(2), 259–271. <https://doi.org/10.1111/j.1365-2958.1993.tb01952.x>
- Guttenplan, S. B., & Kearns, D. B. (2013). Regulation of flagellar motility during biofilm formation. *FEMS Microbiology Reviews*, *37*(6), 849–871. <https://doi.org/10.1111/1574-6976.12018>
- Hampton, H. G., McNeil, M. B., Paterson, T. J., Ney, B., Williamson, N. R., Easingwood, R. A., ... Fineran, P. C. (2016). CRISPR-Cas gene-editing reveals RsmA and RsmC act through FlhDC to repress the SdhE flavinylation factor and control motility and prodigiosin production in *Serratia*. *Microbiology*, *162*(6), 1047–1058.
<https://doi.org/10.1099/mic.0.000283>
- Hampton, H. G., Smith, L. M., Ferguson, S., Meaden, S., Jackson, S. A., & Fineran, P. C. (2020). Functional genomics reveals the toxin–antitoxin repertoire and AbiE activity in *Serratia*. *Microbial Genomics*, *6*, mgen000458. <https://doi.org/10.1099/mgen.0.000458>
- Harris, A. K. P., Williamson, N. R., Slater, H., Cox, A. R. J., Abbasi, S., Foulds, I. J., ... Salmond, G. P. C. (2004). The *Serratia* gene cluster encoding biosynthesis of the red antibiotic, prodigiosin, shows species- and strain-dependent genome context variation. *Microbiology*, *150*(11), 3547–3560.
- Harshey, R. M., & Matsuyama, T. (1994). Dimorphic transition in *Escherichia coli* and *Salmonella typhimurium*: Surface-induced differentiation into hyperflagellate swarmer cells. *Proceedings of the National Academy of Sciences of the United States of America*, *91*(18), 8631–8635. <https://doi.org/10.1073/pnas.91.18.8631>
- Haseltine, W. A., & Block, R. (1973). Synthesis of Guanosine Tetra- and Pentaphosphate Requires the Presence of a Codon-Specific, Uncharged Transfer Ribonucleic Acid in the

- Acceptor Site of Ribosomes. *Proceedings of the National Academy of Sciences*, 70(5), 1564–1568. <https://doi.org/10.1073/PNAS.70.5.1564>
- Haugen, S. P., Ross, W., & Gourse, R. L. (2008). Advances in bacterial promoter recognition and its control by factors that do not bind DNA. *Nature Reviews Microbiology*, 6(7), 507–519. <https://doi.org/10.1038/nrmicro1912>
- Häuser, R., Pech, M., Kijek, J., Yamamoto, H., Titz, B., Naeve, F., ... Uetz, P. (2012). RsfA (YbeB) Proteins Are Conserved Ribosomal Silencing Factors. *PLOS Genetics*, 8(7), e1002815. <https://doi.org/10.1371/JOURNAL.PGEN.1002815>
- Hayes, P. K., Buchholz, B., & Walsby, A. E. (1992). Gas vesicles are strengthened by the outer-surface protein, GvpC. *Archives of Microbiology*, 157(3), 229–234. <https://doi.org/10.1007/BF00245155>
- Hayes, P. K., & Powell, R. S. (1995). The *gvpA/C* cluster of *Anabaena flos-aquae* has multiple copies of a gene encoding GvpA. *Archives of Microbiology*, 164(1), 50–57. <https://doi.org/10.1007/BF02568734>
- Hayrapetyan, H., Tempelaars, M., Groot, M. N., & Abee, T. (2015). *Bacillus cereus* ATCC 14579 RpoN (Sigma 54) is a pleiotropic regulator of growth, carbohydrate metabolism, motility, biofilm formation and toxin production. *PLoS ONE*, 10(8), e0134872. <https://doi.org/10.1371/journal.pone.0134872>
- Heeb, S., & Haas, D. (2001). Regulatory Roles of the GacS/GacA Two-Component System in Plant-Associated and Other Gram-Negative Bacteria. *Molecular Plant-Microbe Interactions*, 14(12), 1351–1363. <https://doi.org/10.1094/MPMI.2001.14.12.1351>
- Hendrickson, E. L., Guevera, P., Peñaloza-Vázquez, A., Shao, J., Bender, C., & Ausubel, F. M. (2000). Virulence of the phytopathogen *Pseudomonas syringae* pv. *Maculicola* is *rpoN* dependent. *Journal of Bacteriology*, 182(12), 3498–3507. <https://doi.org/10.1128/JB.182.12.3498-3507.2000>
- Hendrickson, E. L., Plotnikova, J., Mahajan-Miklos, S., Rahme, L. G., & Ausubel, F. M. (2001). Differential roles of the *Pseudomonas aeruginosa* PA14 *rpoN* gene in pathogenicity in plants, nematodes, insects, and mice. *Journal of Bacteriology*, 183(24), 7126–7134. <https://doi.org/10.1128/JB.183.24.7126-7134.2001>
- Henrici, R. C., Pecen, T. J., Johnston, J. L., & Tan, S. (2017). The pPSU Plasmids for Generating DNA Molecular Weight Markers. *Scientific Reports*, 7(2438), 1–9. <https://doi.org/10.1038/s41598-017-02693-1>

- Herrero, M., de Lorenzo, V., & Timmis, K. N. (1990). Transposon vectors containing non-antibiotic resistance selection markers for cloning and stable chromosomal insertion of foreign genes in gram-negative bacteria. *Journal of Bacteriology*, *172*(11), 6557–6567. <https://doi.org/10.1128/jb.172.11.6557-6567.1990>
- Hinton, J. C. D., Sidebotham, J. M., Hyman, L. J., Pérombelon, M. C. M., & Salmond, G. P. C. (1989). Isolation and characterisation of transposon-induced mutants of *Erwinia carotovora* subsp. *atroseptica* exhibiting reduced virulence. *MGG Molecular & General Genetics*, *217*(1), 141–148. <https://doi.org/10.1007/BF00330953>
- Hoeniger, J. F. M. (1965). Development of Flagella by *Proteus mirabilis*. *Journal of General Microbiology*, *40*(1), 29–42. <https://doi.org/10.1099/00221287-40-1-29>
- Hong, E., Doucleff, M., & Wemmer, D. E. (2009). Structure of the RNA Polymerase Core-Binding Domain of σ^{54} Reveals a Likely Conformational Fracture Point. *Journal of Molecular Biology*, *390*(1), 70–82. <https://doi.org/10.1016/j.jmb.2009.04.070>
- Hood, D. W., Heidstra, R., Swoboda, U. K., & Hodgson, D. A. (1992). Molecular genetic analysis of proline and tryptophan biosynthesis in *Streptomyces coelicolor* A3(2): interaction between primary and secondary metabolism — a review. *Gene*, *115*, 5–12. [https://doi.org/10.1016/0378-1119\(92\)90533-U](https://doi.org/10.1016/0378-1119(92)90533-U)
- Huang, M., Oppermann-Sanio, F. B., & Steinbüchel, A. (1999). Biochemical and molecular characterization of the *Bacillus subtilis* acetoin catabolic pathway. *Journal of Bacteriology*, *181*(12), 3837–3841. <https://doi.org/10.1128/jb.181.12.3837-3841.1999>
- Huang, M., Oppermann, F. B., & Steinbüchel, A. (1994). Molecular characterization of the *Pseudomonas putida* 2,3-butanediol catabolic pathway. *FEMS Microbiology Letters*, *124*(2), 141–150. <https://doi.org/10.1111/j.1574-6968.1994.tb07276.x>
- Huang, R., Lin, J., Gao, D., Zhang, F., Yi, L., Huang, Y., ... Zhu, X. (2019). Discovery of gas vesicles in *Streptomyces* sp. CB03234-S and potential effects of gas vesicle gene overexpression on morphological and metabolic changes in streptomycetes. *Applied Microbiology and Biotechnology*, *103*, 5751–5761. <https://doi.org/10.1007/s00253-019-09891-z>
- Hunt, T. P., & Magasanik, B. (1985). Transcription of *glnA* by purified *Escherichia coli* components: core RNA polymerase and the products of *glnF*, *glnG*, and *glnL*. *Proceedings of the National Academy of Sciences*, *82*(24), 8453–8457. <https://doi.org/10.1073/PNAS.82.24.8453>

- Hutcheson, S. W., Bretz, J., Sussan, T., Jin, S., & Pak, K. (2001). Enhancer-binding proteins HrpR and HrpS interact to regulate *hrp*-encoded type III protein secretion in *Pseudomonas syringae* strains. *Journal of Bacteriology*, *183*(19), 5589–5598. <https://doi.org/10.1128/JB.183.19.5589-5598.2001>
- Irving, S. E., Choudhury, N. R., & Corrigan, R. M. (2021). The stringent response and physiological roles of (pp)pGpp in bacteria. *Nature Reviews Microbiology*, *19*, 256–271. <https://doi.org/10.1038/s41579-020-00470-y>
- Ishimoto, K. S., & Lory, S. (1989). Formation of pilin in *Pseudomonas aeruginosa* requires the alternative σ factor (RpoN) of RNA polymerase. *Proceedings of the National Academy of Sciences of the United States of America*, *86*(6), 1954–1957. <https://doi.org/10.1073/pnas.86.6.1954>
- Itoh, T., Matsuda, H., & Mori, H. (1999). Phylogenetic Analysis of the Third Hsp70 Homolog in *Escherichia coli*; a Novel Member of the Hsc66 Subfamily and Its Possible Co-chaperone. *DNA Research*, *6*(5), 299–305. <https://doi.org/10.1093/DNARES/6.5.299>
- Iyer, L. M., Burroughs, A. M., & Aravind, L. (2006). The prokaryotic antecedents of the ubiquitin-signaling system and the early evolution of ubiquitin-like β -grasp domains. *Genome Biology*, *7*(7), R60. <https://doi.org/10.1186/gb-2006-7-7-r60>
- Jacobi, S., Schade, R., & Heuner, K. (2004). Characterization of the Alternative Sigma Factor σ^{54} and the Transcriptional Regulator FleQ of *Legionella pneumophila*, Which Are Both Involved in the Regulation Cascade of Flagellar Gene Expression. *Journal of Bacteriology*, *186*(9), 2540–2547. <https://doi.org/10.1128/JB.186.9.2540-2547.2004>
- Jacobs, M. A., Alwood, A., Thaipisuttikul, I., Spencer, D., Haugen, E., Ernst, S., ... Manoil, C. (2003). Comprehensive transposon mutant library of *Pseudomonas aeruginosa*. *Proceedings of the National Academy of Sciences of the United States of America*, *100*(24), 14339–14344. <https://doi.org/10.1073/pnas.2036282100>
- Jagannathan, A., Constantinidou, C., & Penn, C. W. (2001). Roles of *rpoN*, *fliA*, and *figR* in expression of flagella in *Campylobacter jejuni*. *Journal of Bacteriology*, *183*(9), 2937–2942. <https://doi.org/10.1128/JB.183.9.2937-2942.2001>
- Jarrell, K. F., & McBride, M. J. (2008). The surprisingly diverse ways that prokaryotes move. *Nature Reviews Microbiology*, *6*(6), 466–476. <https://doi.org/10.1038/nrmicro1900>
- Johansen, L., Bryn, K., & Stormer, F. C. (1975). Physiological and biochemical role of the butanediol pathway in *Aerobacter (Enterobacter) aerogenes*. *Journal of Bacteriology*,

- 123(3), 1124–1130. <https://doi.org/10.1128/jb.123.3.1124-1130.1975>
- Jones, D. H. A., Franklin, F. C. H., & Thomas, C. M. (1994). Molecular analysis of the operon which encodes the RNA polymerase sigma factor σ^{54} of *Escherichia coli*. *Microbiology*, 140(5), 1035–1043. <https://doi.org/10.1099/13500872-140-5-1035>
- Jones, J. G., Young, D. C., & DasSarma, S. (1991). Structure and organization of the gas vesicle gene cluster on the *Halobacterium halobium* plasmid pNRC100. *Gene*, 102(1), 117–122. [https://doi.org/10.1016/0378-1119\(91\)90549-Q](https://doi.org/10.1016/0378-1119(91)90549-Q)
- Kamaladevi, A., & Balamurugan, K. (2016). Lipopolysaccharide of *Klebsiella pneumoniae* attenuates immunity of *Caenorhabditis elegans* and evades by altering its supramolecular structure. *RSC Advances*, 6(36), 30070–30080. <https://doi.org/10.1039/C5RA18206A>
- Kang, P. J., & Craig, E. A. (1990). Identification and characterization of a new *Escherichia coli* gene that is a dosage-dependent suppressor of a *dnaK* deletion mutation. *Journal of Bacteriology*, 172(4), 2055–2064. <https://doi.org/10.1128/JB.172.4.2055-2064.1990>
- Kaniga, K., Delor, I., & Cornelis, G. R. (1991). A wide-host-range suicide vector for improving reverse genetics in Gram-negative bacteria: inactivation of the *blaA* gene of *Yersinia enterocolitica*. *Gene*, 109(1), 137–141. [https://doi.org/10.1016/0378-1119\(91\)90599-7](https://doi.org/10.1016/0378-1119(91)90599-7)
- Kashiwagi, K., Suzuki, T., Suzuki, F., Furuchi, T., Kobayashi, H., & Igarashi, K. (1991). Coexistence of the genes for putrescine transport protein and ornithine decarboxylase at 16 min on *Escherichia coli* chromosome. *Journal of Biological Chemistry*, 266(31), 20922–20927. [https://doi.org/10.1016/S0021-9258\(18\)54798-0](https://doi.org/10.1016/S0021-9258(18)54798-0)
- Kearns, D. B. (2010). A field guide to bacterial swarming motility. *Nature Reviews Microbiology*, 8(9), 634–644. <https://doi.org/10.1038/nrmicro2405>
- Köhler, T., Harayama, S., Ramos, J. L., & Timmis, K. N. (1989). Involvement of *Pseudomonas putida* RpoN sigma factor in regulation of various metabolic functions. *Journal of Bacteriology*, 171(8), 4326–4333. <https://doi.org/10.1128/jb.171.8.4326-4333.1989>
- Krantz, M. J., & Ballou, C. E. (1973). Analysis of *Halobacterium halobium* gas vesicles. *Journal of Bacteriology*, 114(3), 1058–1067. <https://doi.org/10.1128/jb.114.3.1058-1067.1973>
- Kriel, A., Bittner, A. N., Kim, S. H., Liu, K., Tehranchi, A. K., Zou, W. Y., ... Wang, J. D. (2012). Direct Regulation of GTP Homeostasis by (p)ppGpp: A Critical Component of Viability and Stress Resistance. *Molecular Cell*, 48(2), 231–241. <https://doi.org/10.1016/J.MOLCEL.2012.08.009>

- Kruger, N., Oppermann, F. B., Lorenzl, H., & Steinbuchel, A. (1994). Biochemical and molecular characterization of the *Clostridium magnum* acetoin dehydrogenase enzyme system. *Journal of Bacteriology*, *176*(12), 3614–3630.
<https://doi.org/10.1128/jb.176.12.3614-3630.1994>
- Kurz, C. L., Chauvet, S., Andrès, E., Aurouze, M., Vallet, I., Michel, G. P. F., ... Ewbank, J. J. (2003). Virulence factors of the human opportunistic pathogen *Serratia marcescens* identified by *in vivo* screening. *The EMBO Journal*, *22*(7), 1451–1460.
<https://doi.org/10.1093/emboj/cdg159>
- Kuznetsova, I., Lugmayr, A., Rackham, O., & Filipovska, A. (2021). OmicsVolcano: software for intuitive visualization and interactive exploration of high-throughput biological data. *STAR Protocols*, *2*(1), 100279. <https://doi.org/10.1016/J.XPRO.2020.100279>
- Kvint, K., Farewell, A., & Nyström, T. (2000). RpoS-dependent Promoters Require Guanosine Tetraphosphate for Induction Even in the Presence of High Levels of σ^S . *Journal of Biological Chemistry*, *275*(20), 14795–14798. <https://doi.org/10.1074/JBC.C000128200>
- Lambalot, R. H., Gehring, A. M., Flugel, R. S., Zuber, P., LaCelle, M., Marahiel, M. A., ... Walsh, C. T. (1996). A new enzyme superfamily — the phosphopantetheinyl transferases. *Chemistry & Biology*, *3*(11), 923–936. [https://doi.org/https://doi.org/10.1016/S1074-5521\(96\)90181-7](https://doi.org/https://doi.org/10.1016/S1074-5521(96)90181-7)
- Lapenda, J. C., Silva, P. A., Vicalvi, M. C., Sena, K. X. F. R., & Nascimento, S. C. (2014). Antimicrobial activity of prodigiosin isolated from *Serratia marcescens* UFPEDA 398. *World Journal of Microbiology and Biotechnology*, *31*(2), 399–406.
<https://doi.org/10.1007/S11274-014-1793-Y>
- Lee, C. M. (2019). *New Pleiotropic Co-Regulators of Gas Vesicle and Secondary Metabolite Production in Serratia sp. ATCC39006 (Doctoral Thesis)*. University of Cambridge.
<https://doi.org/https://doi.org/10.17863/CAM.38234>
- Lee, C. M., Monson, R. E., Adams, R. M., & Salmond, G. P. C. (2017). The LacI-family transcription factor, RbsR, is a pleiotropic regulator of motility, virulence, siderophore and antibiotic production, gas vesicle morphogenesis and flotation in *Serratia*. *Frontiers in Microbiology*, *8*, 1678. <https://doi.org/10.3389/fmicb.2017.01678>
- Lee, J. S., Kim, Y. S., Park, S., Kim, J., Kang, S. J., Lee, M. H., ... Yoon, J. H. (2011). Exceptional production of both prodigiosin and cycloprodigiosin as major metabolic constituents by a novel marine bacterium, *Zooshikella rubidus* S1-1. *Applied and Environmental*

- Microbiology*, 77(14), 4967–4973. <https://doi.org/10.1128/AEM.01986-10>
- Li, X., Sun, Q., Jiang, C., Yang, K., Hung, L. W., Zhang, J., & Sacchettini, J. C. (2015). Structure of Ribosomal Silencing Factor Bound to *Mycobacterium tuberculosis* Ribosome. *Structure*, 23(10), 1858–1865. <https://doi.org/10.1016/J.STR.2015.07.014>
- Lilley, B. N., & Bassler, B. L. (2000). Regulation of quorum sensing in *Vibrio harveyi* by LuxO and Sigma-54. *Molecular Microbiology*, 36(4), 940–954. <https://doi.org/10.1046/j.1365-2958.2000.01913.x>
- Lindum, P. W., Anthoni, U., Christophersen, C., Eberl, L., Molin, S., & Givskov, M. (1998). N-Acyl-L-Homoserine Lactone Autoinducers Control Production of an Extracellular Lipopeptide Biosurfactant Required for Swarming Motility of *Serratia liquefaciens* MG1. *Journal of Bacteriology*, 180(23), 6384–6388. <https://doi.org/10.1128/JB.180.23.6384-6388.1998>
- López, J. M., Thomas, B., & Rehbein, H. (1975). Acetoin Degradation in *Bacillus subtilis* by Direct Oxidative Cleavage. *European Journal of Biochemistry*, 57(2), 425–430. <https://doi.org/10.1111/j.1432-1033.1975.tb02317.x>
- Lv, M., Hu, M., Li, P., Jiang, Z., Zhang, L., & Zhou, J. (2019). A two-component regulatory system VfmIH modulates multiple virulence traits in *Dickeya zeae*. *Molecular Microbiology*, 111(6), 1493–1509. <https://doi.org/10.1111/mmi.14233>
- Magnusson, L. U., Gummesson, B., Joksimović, P., Farewell, A., & Nyström, T. (2007). Identical, independent, and opposing roles of ppGpp and DksA in *Escherichia coli*. *Journal of Bacteriology*, 189(14), 5193–5202. <https://doi.org/10.1128/JB.00330-07>
- Maltezou, H. C., Tryfinopoulou, K., Katerelos, P., Ftika, L., Pappa, O., Tseroni, M., ... Vatopoulos, A. (2012). Consecutive *Serratia marcescens* multiclone outbreaks in a neonatal intensive care unit. *American Journal of Infection Control*, 40(7), 637–642. <https://doi.org/10.1016/j.ajic.2011.08.019>
- Marin-Rodriguez, M. C., Orchard, J., & Seymour, G. B. (2002). Pectate lyases, cell wall degradation and fruit softening. *Journal of Experimental Botany*, 53(377), 2115–2119. <https://doi.org/10.1093/jxb/erf089>
- Martínez-Costa, O. H., Arias, P., Romero, N. M., Parro, V., Mellado, R. P., & Malpartida, F. (1996). A *relA/spoT* Homologous Gene from *Streptomyces coelicolor* A3(2) Controls Antibiotic Biosynthetic Genes. *Journal of Biological Chemistry*, 271(18), 10627–10634. <https://doi.org/10.1074/JBC.271.18.10627>

- Matilla, M. A., Stöckmann, H., Leeper, F. J., & Salmond, G. P. C. (2012). Bacterial Biosynthetic Gene Clusters Encoding the Anti-cancer Haterumalide Class of Molecules BIOGENESIS OF THE BROAD SPECTRUM ANTIFUNGAL AND ANTI-OOMYCETE COMPOUND, OOCYDIN A. *Journal of Biological Chemistry*, *287*(46), 39125–39138.
- McAlister, G. C., Nusinow, D. P., Jedrychowski, M. P., Wühr, M., Huttlin, E. L., Erickson, B. K., ... Gygi, S. P. (2014). MultiNotch MS3 enables accurate, sensitive, and multiplexed detection of differential expression across cancer cell line proteomes. *Analytical Chemistry*, *86*(14), 7150–7158. <https://doi.org/10.1021/ac502040v>
- McGowan, S. J., Sebahia, M., Porter, L. E., Stewart, G. S. A. B., Williams, P., Bycroft, B. W., & Salmond, G. P. C. (1996). Analysis of bacterial carbapenem antibiotic production genes reveals a novel β -lactam biosynthesis pathway. *Molecular Microbiology*, *22*(3), 415–426. <https://doi.org/10.1046/j.1365-2958.1996.00125.x>
- McNeil, M. B., Clulow, J. S., Wilf, N. M., Salmond, G. P. C., & Fineran, P. C. (2012). SdhE Is a Conserved Protein Required for Flavinylation of Succinate Dehydrogenase in Bacteria. *Journal of Biological Chemistry*, *287*(22), 18418–18428. <https://doi.org/10.1074/JBC.M111.293803>
- McNeil, M. B., Iglesias-Cans, M. C., Clulow, J. S., & Fineran, P. C. (2013). YgfX (CptA) is a multimeric membrane protein that interacts with the succinate dehydrogenase assembly factor SdhE (YgfY). *Microbiology*, *159*, 1352–1365. <https://doi.org/10.1099/MIC.0.068510-0>
- Mehra, R. K., & Drabble, W. T. (1981). Dual Control of the *gua* Operon of *Escherichia coli* K12 by Adenine and Guanine Nucleotides. *Microbiology*, *123*(1), 27–37. <https://doi.org/10.1099/00221287-123-1-27>
- Mellacheruvu, D., Wright, Z., Couzens, A. L., Lambert, J. P., St-Denis, N. A., Li, T., ... Nesvizhskii, A. I. (2013). The CRAPome: A contaminant repository for affinity purification-mass spectrometry data. *Nature Methods*, *10*(8), 730–736. <https://doi.org/10.1038/nmeth.2557>
- Merrick, M. J. (1993). In a class of its own — the RNA polymerase sigma factor σ^{54} (σ^N). *Molecular Microbiology*, *10*(5), 903–909. <https://doi.org/10.1111/j.1365-2958.1993.tb00961.x>
- Merrih, H., Ferrazzoli, A. E., & Lovett, S. T. (2009). Growth phase and (p)ppGpp control of IraD, a regulator of RpoS stability, in *Escherichia coli*. *Journal of Bacteriology*, *191*(24),

- 7436–7446. <https://doi.org/10.1128/JB.00412-09>
- Mogull, S. A., Runyen-Janecky, L. J., Hong, M., & Payne, S. M. (2001). *dksA* is required for intercellular spread of *Shigella flexneri* via an RpoS-independent mechanism. *Infection and Immunity*, *69*(9), 5742–5751. <https://doi.org/10.1128/IAI.69.9.5742-5751.2001>
- Molina-Henares, A. J., Krell, T., Eugenia Guazzaroni, M., Segura, A., & Ramos, J. L. (2006). Members of the IclR family of bacterial transcriptional regulators function as activators and/or repressors. *FEMS Microbiology Reviews*, *30*(2), 157–186. <https://doi.org/10.1111/j.1574-6976.2005.00008.x>
- Monson, R. E., Smith, D. S., Matilla, M. A., Roberts, K., Richardson, E., Drew, A., ... Salmond, G. P. C. (2015). A plasmid-transposon hybrid mutagenesis system effective in a broad range of Enterobacteria. *Frontiers in Microbiology*, *6*(1442). <https://doi.org/10.3389/fmicb.2015.01442>
- Monson, R. E., Tashiro, Y., & Salmond, G. P. C. (2016). Overproduction of individual gas vesicle proteins perturbs flotation, antibiotic production and cell division in the enterobacterium *Serratia* sp. ATCC 39006. *Microbiology*, *162*(9), 1595–1607. <https://doi.org/10.1099/mic.0.000347>
- Morgenstein, R. M., Clemmer, K. M., & Rather, P. N. (2010). Loss of the *waaL* O-antigen ligase prevents surface activation of the flagellar gene cascade in *Proteus mirabilis*. *Journal of Bacteriology*, *192*(12), 3213–3221. <https://doi.org/10.1128/JB.00196-10>
- Muhl, D., & Filloux, A. (2014). Site-Directed Mutagenesis and Gene Deletion Using Reverse Genetics. In *Pseudomonas Methods and Protocols* (pp. 521–539). Humana Press, New York, NY. https://doi.org/10.1007/978-1-4939-0473-0_40
- Nakanishi, N., Abe, H., Ogura, Y., Hayashi, T., Tashiro, K., Kuhara, S., ... Tobe, T. (2006). ppGpp with DksA controls gene expression in the locus of enterocyte effacement (LEE) pathogenicity island of enterohaemorrhagic *Escherichia coli* through activation of two virulence regulatory genes. *Molecular Microbiology*, *61*(1), 194–205. <https://doi.org/10.1111/J.1365-2958.2006.05217.X>
- Nasser, W, Reverchon, S., & Robert-Baudouy, J. (1992). Purification and functional characterization of the KdgR protein, a major repressor of pectinolysis genes of *Erwinia chrysanthemi*. *Molecular Microbiology*, *6*(2), 257–265. <https://doi.org/10.1111/j.1365-2958.1992.tb02007.x>
- Nasser, William, Dorel, C., Wawrzyniak, J., Van Gijsegem, F., Groleau, M. C., Déziel, E., &

- Reverchon, S. (2013). Vfm a new quorum sensing system controls the virulence of *Dickeya dadantii*. *Environmental Microbiology*, 15(3), 865–880.
<https://doi.org/10.1111/1462-2920.12049>
- Nealson, K. H., & Hastings, J. W. (1979). Bacterial bioluminescence: its control and ecological significance. *Microbiological Reviews*, 43(4), 496. <https://doi.org/10.1128/mr.43.4.496-518.1979>.
- Ng, W. V, Kennedy, S. P., Mahairas, G. G., Berquist, B., Pan, M., Shukla, H. D., ... DasSarma, S. (2000). Genome sequence of *Halobacterium species* NRC-1. *Proceedings of the National Academy of Sciences of the United States of America*, 97(22), 12176–12181.
<https://doi.org/10.1073/pnas.190337797>
- Niehus, E., Gressmann, H., Ye, F., Schlapbach, R., Dehio, M., Dehio, C., ... Josenhans, C. (2004). Genome-wide analysis of transcriptional hierarchy and feedback regulation in the flagellar system of *Helicobacter pylori*. *Molecular Microbiology*, 52(4), 947–961.
<https://doi.org/10.1111/j.1365-2958.2004.04006.x>
- Ninfa, A. J., & Magasanik, B. (1986). Covalent modification of the *glnG* product, NR(I), by the *glnL* product, NR(II), regulates the transcription of the *glnALG* operon in *Escherichia coli*. *Proceedings of the National Academy of Sciences of the United States of America*, 83(16), 5909–5913. <https://doi.org/10.1073/pnas.83.16.5909>
- Norton, J. P., & Mulvey, M. A. (2012). Toxin-Antitoxin Systems Are Important for Niche-Specific Colonization and Stress Resistance of Uropathogenic *Escherichia coli*. *PLoS Pathogens*, 8(10), e1002954. <https://doi.org/10.1371/journal.ppat.1002954>
- Oppermann, F. B., & Steinbuchel, A. (1994). Identification and molecular characterization of the *aco* genes encoding the *Pelobacter carbinolicus* acetoin dehydrogenase enzyme system. *Journal of Bacteriology*, 176(2), 469–485.
<https://doi.org/10.1128/jb.176.2.469-485.1994>
- Oren, A. (2013). The Function of Gas Vesicles in Halophilic Archaea and Bacteria: Theories and Experimental Evidence. *Life*, 3(1), 1–20. <https://doi.org/10.3390/life3010001>
- Österberg, S., Peso-Santos, T. del, & Shingler, V. (2011). Regulation of Alternative Sigma Factor Use. *Annual Review of Microbiology*, 65, 37–55.
<https://doi.org/10.1146/ANNUREV.MICRO.112408.134219>
- Paerl, H. W., & Huisman, J. (2008). Blooms like it hot. *Science*, 320, 57–58.
<https://doi.org/10.1126/science.1155398>

- Parker, W. L., Rathnum, M. L., Wells, J. S. J., Trejo, W. H., Principe, P. A., & Sykes, R. B. (1982). SQ 27, 860, A simple carbapenem produced by species of *Serratia* and *Erwinia*. *The Journal of Antibiotics*, *35*(6), 653–660. <https://doi.org/10.7164/antibiotics.35.653>
- Paul, B. J., Barker, M. M., Ross, W., Schneider, D. A., Webb, C., Foster, J. W., & Gourse, R. L. (2004a). DksA: a critical component of the transcription initiation machinery that potentiates the regulation of rRNA promoters by ppGpp and the initiating NTP. *Cell*, *118*(3), 311–322. <https://doi.org/10.1016/j.cell.2004.07.009>
- Paul, B. J., Berkmen, M. B., & Gourse, R. L. (2005). DksA potentiates direct activation of amino acid promoters by ppGpp. *Proceedings of the National Academy of Sciences of the United States of America*, *102*(22), 7823–7828. <https://doi.org/10.1073/pnas.0501170102>
- Paul, B. J., Ross, W., Gaal, T., & Gourse, R. L. (2004b). rRNA Transcription in *Escherichia coli*. *Annual Review of Genetics*, *38*, 749–770. <https://doi.org/10.1146/ANNUREV.GENET.38.072902.091347>
- Pfeifer, F. (2012). Distribution, formation and regulation of gas vesicles. *Nature Reviews Microbiology*, *10*(10), 705–715. <https://doi.org/10.1038/nrmicro2834>
- Plotkowski, M. C., Saliba, A. M., Pereira, S. H. M., Cervante, M. P., & Bajolet-Laudinat, O. (1994). *Pseudomonas aeruginosa* selective adherence to and entry into human endothelial cells. *Infection and Immunity*, *62*(12), 5456–5463. <https://doi.org/10.1128/iai.62.12.5456-5463.1994>
- Pontes, M. H., Lee, E.-J., Choi, J., & Groisman, E. A. (2015). *Salmonella* promotes virulence by repressing cellulose production. *Proceedings of the National Academy of Sciences*, *112*(16), 5183–5188. <https://doi.org/10.1073/PNAS.1500989112>
- Potrykus, K., & Cashel, M. (2008). (p)ppGpp: Still Magical? *Annual Review of Microbiology*, *62*(1), 35–51. <https://doi.org/10.1146/annurev.micro.62.081307.162903>
- Potts, A. H., Vakulskas, C. A., Pannuri, A., Yakhnin, H., Babitzke, P., & Romeo, T. (2017). Global role of the bacterial post-transcriptional regulator CsrA revealed by integrated transcriptomics. *Nature Communications*, *8*(1596), 1–15. <https://doi.org/10.1038/s41467-017-01613-1>
- Poulter, S., Carlton, T. M., Spring, D. R., & Salmond, G. P. C. (2011). The *Serratia* LuxR family regulator CarR₃₉₀₀₆ activates transcription independently of cognate quorum sensing signals. *Molecular Microbiology*, *80*(4), 1120–1131. <https://doi.org/10.1111/J.1365->

2958.2011.07634.X

- Poulter, S., Carlton, T. M., Su, X., Spring, D. R., & Salmond, G. P. C. (2010). Engineering of new prodigiosin-based biosensors of *Serratia* for facile detection of short-chain *N*-acyl homoserine lactone quorum-sensing molecules. *Environmental Microbiology Reports*, 2(2), 322–328. <https://doi.org/10.1111/j.1758-2229.2010.00140.x>
- Preston, A., Maskell, D., Johnson, A., & Moxon, E. R. (1996). Altered lipopolysaccharide characteristic of the I69 phenotype in *Haemophilus influenzae* results from mutations in a novel gene, *isn*. *Journal of Bacteriology*, 178(2), 396–402. <https://doi.org/10.1128/jb.178.2.396-402.1996>
- Prigent-Combaret, C., Zghidi-Abouzid, O., Effantin, G., Lejeune, P., Reverchon, S., & Nasser, W. (2012). The nucleoid-associated protein Fis directly modulates the synthesis of cellulose, an essential component of pellicle–biofilms in the phytopathogenic bacterium *Dickeya dadantii*. *Molecular Microbiology*, 86(1), 172–186. <https://doi.org/10.1111/J.1365-2958.2012.08182.X>
- Prossliner, T., Winther, K. S., Sørensen, M. A., & Gerdes, K. (2015). Ribosome Hibernation. *Annual Review of Genetics*, 52, 321–348. <https://doi.org/10.1146/ANNUREV-GENET-120215-035130>
- Prouty, M. G., Correa, N. E., & Klose, K. E. (2001). The novel σ^{54} - and σ^{28} -dependent flagellar gene transcription hierarchy of *Vibrio cholerae*. *Molecular Microbiology*, 39(6), 1595–1609. <https://doi.org/10.1046/j.1365-2958.2001.02348.x>
- Quintero-Yanes, A. (2019). *Novel pleiotropic regulators of gas vesicle biogenesis in Serratia (Doctoral thesis)*. University of Cambridge. <https://doi.org/https://doi.org/10.17863/CAM.35703>
- Quintero-Yanes, A., Lee, C. M., Monson, R., & Salmond, G. P. C. (2020). The FloR master regulator controls flotation, virulence and antibiotic production in *Serratia* sp. ATCC 39006. *Environmental Microbiology*, 22(7), 2921–2938. <https://doi.org/10.1111/1462-2920.15048>
- Quintero-Yanes, A., Monson, R. E., & Salmond, G. P. C. (2019). Environmental potassium regulates bacterial flotation, antibiotic production and turgor pressure in *Serratia* through the TrkH transporter. *Environmental Microbiology*, 21(7), 2499–2510. <https://doi.org/10.1111/1462-2920.14637>
- R Core Team. (2020). R: A language and environment for statistical computing. R Foundation

- for Statistical Computing, Vienna, Austria. URL: <http://www.R-project.org/>.
- Ramsay, J. P., Williamson, N. R., Spring, D. R., & Salmond, G. P. C. (2011). A quorum-sensing molecule acts as a morphogen controlling gas vesicle organelle biogenesis and adaptive flotation in an enterobacterium. *Proceedings of the National Academy of Sciences of the United States of America*, *108*(36), 14932–14937.
<https://doi.org/10.1073/pnas.1109169108>
- Reitzer, L., & Magasanik, B. (1985). Expression of *glnA* in *Escherichia coli* is regulated at tandem promoters. *Proceedings of the National Academy of Sciences of the United States of America*, *82*(7), 1979–1983. <https://doi.org/10.1073/pnas.82.7.1979>
- Reitzer, L., & Schneider, B. L. (2001). Metabolic Context and Possible Physiological Themes of σ^{54} -Dependent Genes in *Escherichia coli*. *Microbiology and Molecular Biology Reviews*, *65*(3), 422–444. <https://doi.org/10.1128/membr.65.3.422-444.2001>
- Retchless, A. C., & Lawrence, J. G. (2010). Phylogenetic incongruence arising from fragmented speciation in enteric bacteria. *Proceedings of the National Academy of Sciences of the United States of America*, *107*(25), 11453–11458.
<https://doi.org/10.1073/pnas.1001291107>
- Reverchon, S., Nasser, W., & Robert-Baudouy, J. (1991). Characterization of *kdgR*, a gene of *Erwinia chrysanthemi* that regulates pectin degradation. *Molecular Microbiology*, *5*(9), 2203–2216. <https://doi.org/10.1111/j.1365-2958.1991.tb02150.x>
- Ritchie, M. E., Phipson, B., Wu, D., Hu, Y., Law, C. W., Shi, W., & Smyth, G. K. (2015). Limma powers differential expression analyses for RNA-sequencing and microarray studies. *Nucleic Acids Research*, *43*(7), e47. <https://doi.org/10.1093/nar/gkv007>
- Robichon, D., Gouin, E., Debarbouille, M., Cossart, P., Cenatiempo, Y., & Hechard, Y. (1997). The *rpoN* (σ^{54}) gene from *Listeria monocytogenes* is involved in resistance to mesentericin Y105, an antibacterial peptide from *Leuconostoc mesenteroides*. *Journal of Bacteriology*, *179*(23), 7591–7594. <https://doi.org/10.1128/jb.179.23.7591-7594.1997>
- Römling, U., & Galperin, M. Y. (2015). Bacterial cellulose biosynthesis: diversity of operons, subunits, products, and functions. *Trends in Microbiology*, *23*(9), 545–557.
<https://doi.org/10.1016/J.TIM.2015.05.005>
- Rosenfeld, Y., & Shai, Y. (2006). Lipopolysaccharide (Endotoxin)-host defense antibacterial peptides interactions: Role in bacterial resistance and prevention of sepsis. *Biochimica*

- et Biophysica Acta*, 1758(9), 1513–1522.
<https://doi.org/10.1016/j.bbamem.2006.05.017>
- Ross, W., Sanchez-Vazquez, P., Chen, A. Y., Lee, J. H., Burgos, H. L., & Gourse, R. L. (2016). ppGpp Binding to a Site at the RNAP-DksA Interface Accounts for Its Dramatic Effects on Transcription Initiation during the Stringent Response. *Molecular Cell*, 62(6), 811–823. <https://doi.org/10.1016/J.MOLCEL.2016.04.029>
- Ross, W., Vrentas, C. E., Sanchez-Vazquez, P., Gaal, T., & Gourse, R. L. (2013). The Magic Spot: A ppGpp Binding Site on *E. coli* RNA Polymerase Responsible for Regulation of Transcription Initiation. *Molecular Cell*, 50(3), 420–429.
<https://doi.org/10.1016/J.MOLCEL.2013.03.021>
- RStudio Team. (2021). RStudio: Integrated Development Environment for R. RStudio, PBC, Boston, MA URL: <http://www.rstudio.com/>.
- Ryazantseva, I. N., Andreyeva, I. N., Klementyeva, G. S., Ogorodnikova, T. I., & Petrov, V. Y. (1995). Pigment-dependent light influence on the energetics of *Serratia marcescens*. *Thermochimica Acta*, 251, 63–67. [https://doi.org/10.1016/0040-6031\(94\)02148-H](https://doi.org/10.1016/0040-6031(94)02148-H)
- Sadhu, S., & Maiti, T. K. (2013). Cellulase Production by Bacteria: A Review. *British Microbiology Research Journal*, 3(3), 235–258.
<https://doi.org/10.9734/BMRJ/2013/2367>
- Sambrook, J., & Green, M. (2012). *Molecular Cloning: A Laboratory Manual* (4th ed.). New York: Cold Spring Harbor Laboratory Press.
- Schreiber, G., Ron, E. Z., & Glaser, G. (1995). ppGpp-mediated regulation of DNA replication and cell division in *Escherichia coli*. *Current Microbiology*, 30(1), 27–32.
<https://doi.org/10.1007/BF00294520>
- Seganish, J. L., & Davis, J. T. (2005). Prodigiosin is a chloride carrier that can function as an anion exchanger. *Chemical Communications*, 46, 5781–5783.
<https://doi.org/10.1039/B511847F>
- Shapiro, M. G., Goodwill, P. W., Neogy, A., Yin, M., Foster, F. S., Schaffer, D. V., & Conolly, S. M. (2014). Biogenic gas nanostructures as ultrasonic molecular reporters. *Nature Nanotechnology*, 9(4), 311–316. <https://doi.org/10.1038/nnano.2014.32>
- Sharma, A. K., & Payne, S. M. (2006). Induction of expression of *hfq* by DksA is essential for *Shigella flexneri* virulence. *Molecular Microbiology*, 62(2), 469–479.
<https://doi.org/10.1111/j.1365-2958.2006.05376.x>

- Shimada, T., Momiyama, E., Yamanaka, Y., Watanabe, H., Yamamoto, K., & Ishihama, A. (2017). Regulatory role of XynR (YagI) in catabolism of xylonate in *Escherichia coli* K-12. *FEMS Microbiology Letters*, 364(22). <https://doi.org/10.1093/femsle/fnx220>
- Shingler, V. (2011). Signal sensory systems that impact σ^{54} -dependent transcription. *FEMS Microbiology Reviews*, 35(3), 425–440. <https://doi.org/10.1111/j.1574-6976.2010.00255.x>
- Shukla, H. D., & DasSarma, S. (2004). Complexity of gas vesicle biogenesis in *Halobacterium* sp. strain NRC-1: identification of five new proteins. *Journal of Bacteriology*, 186(10), 3182–3186. <https://doi.org/10.1128/jb.186.10.3182-3186.2004>
- Sivamaruthi, B. S., Prasanth, M. I., & Balamurugan, K. (2015). Alterations in *Caenorhabditis elegans* and *Cronobacter sakazakii* lipopolysaccharide during interaction. *Archives of Microbiology*, 197(2), 327–337. <https://doi.org/10.1007/s00203-014-1064-1>
- Slater, H., Crow, M. A., Everson, L., & Salmond, G. P. C. (2003). Phosphate availability regulates biosynthesis of two antibiotics, prodigiosin and carbapenem, in *Serratia* via both quorum-sensing-dependent and-independent pathways. *Molecular Microbiology*, 47(2), 303–320. <https://doi.org/10.1046/j.1365-2958.2003.03295.x>
- Spiers, A. J., Bohannon, J., Gehrig, S. M., & Rainey, P. B. (2003). Biofilm formation at the air–liquid interface by the *Pseudomonas fluorescens* SBW25 wrinkly spreader requires an acetylated form of cellulose. *Molecular Microbiology*, 50(1), 15–27. <https://doi.org/10.1046/j.1365-2958.2003.03670.x>
- Sproer, C., Mendrock, U., Swiderski, J., Lang, E., & Stackebrandt, E. (1999). The phylogenetic position of *Serratia*, *Buttiauxella* and some other genera of the family Enterobacteriaceae. *International Journal of Systematic Bacteriology*, 49(4), 1433–1438. <https://doi.org/10.1099/00207713-49-4-1433>
- Stuart, E. S., Morshed, F., Sremac, M., & DasSarma, S. (2004). Cassette-based presentation of SIV epitopes with recombinant gas vesicles from halophilic archaea. *Journal of Biotechnology*, 114(3), 225–237. <https://doi.org/10.1016/j.JBIOTEC.2004.01.005>
- Studholme, D. J. (2002). Enhancer-Dependent Transcription in *Salmonella enterica* Typhimurium: New Members of the σ^N Regulon Inferred from Protein Sequence Homology and Predicted Promoter Sites. *Journal of Molecular Microbiology and Biotechnology*, 4(4), 367–374.
- Sun, J., Hesketh, A., & Bibb, M. (2001). Functional analysis of *relA* and *rshA*, two *relA/spoT*

- homologues of *Streptomyces coelicolor* A3(2). *Journal of Bacteriology*, *183*(11), 3488–3498. <https://doi.org/10.1128/JB.183.11.3488-3498.2001>
- Sunaga, S., Li, H., Sato, Y., Nakagawa, Y., & Matsuyama, T. (2004). Identification and Characterization of the *pswP* Gene Required for the Parallel Production of Prodigiosin and Serrawettin W1 in *Serratia marcescens*. *Microbiology and Immunology*, *48*(10), 723–728. <https://doi.org/10.1111/j.1348-0421.2004.tb03597.x>
- Suryawanshi, R. K., Patil, C. D., Koli, S. H., Hallsworth, J. E., & Patil, S. V. (2016). Antimicrobial activity of prodigiosin is attributable to plasma-membrane damage. *Natural Product Research*, *31*(5), 572–577. <https://doi.org/10.1080/14786419.2016.1195380>
- Suzuki, K., Babitzke, P., Kushner, S. R., & Romeo, T. (2006). Identification of a novel regulatory protein (CsrD) that targets the global regulatory RNAs CsrB and CsrC for degradation by RNase E. *Genes & Development*, *20*(18), 2605–2617. <https://doi.org/10.1101/GAD.1461606>
- Syed, A., & Gralla, J. D. (1997). Isolation and properties of enhancer-bypass mutants of sigma 54. *Molecular Microbiology*, *23*(5), 987–995. <https://doi.org/10.1046/j.1365-2958.1997.2851651.x>
- Tashiro, Y., Monson, R. E., Ramsay, J. P., & Salmond, G. P. C. (2016). Molecular genetic and physical analysis of gas vesicles in buoyant enterobacteria. *Environmental Microbiology*, *18*(4), 1264–1276. <https://doi.org/10.1111/1462-2920.13203>
- Thakur, B. R., Singh, R. K., Handa, A. K., & Rao, M. A. (1997). Chemistry and uses of pectin — A review. *Critical Reviews in Food Science and Nutrition*, *37*(1), 47–73. <https://doi.org/10.1080/10408399709527767>
- Thomson, N. R., Cox, A. R. J., Bycroft, B. W., Stewart, G. S. A. B., Williams, P., & Salmond, G. P. C. (1997). The Rap and Hor proteins of *Erwinia*, *Serratia* and *Yersinia*: a novel subgroup in a growing superfamily of proteins regulating diverse physiological processes in bacterial pathogens. *Molecular Microbiology*, *26*(3), 531–544. <https://doi.org/10.1046/j.1365-2958.1997.5981976.x>
- Thomson, N. R., Crow, M. A., McGowan, S. J., Cox, A. R. J., & Salmond, G. P. C. (2000). Biosynthesis of carbapenem antibiotic and prodigiosin pigment in *Serratia* is under quorum sensing control. *Molecular Microbiology*, *36*(3), 539–556. <https://doi.org/10.1046/j.1365-2958.2000.01872.x>
- Tichy, E. M., Hardwick, S. W., Luisi, B. F., & Salmond, G. P. C. (2017). 1.8 Å resolution crystal

- structure of the carbapenem intrinsic resistance protein CarF. *Acta Crystallographica Section D: Structural Biology*, 73(7), 549–556.
<https://doi.org/10.1107/S2059798317002236/JM5021SUP1.PDF>
- Tichy, E. M., Luisi, B. F., & Salmond, G. P. C. (2014). Crystal Structure of the Carbapenem Intrinsic Resistance Protein CarG. *Journal of Molecular Biology*, 426(9), 1958–1970.
<https://doi.org/10.1016/J.JMB.2014.02.016>
- Toguchi, A., Siano, M., Burkart, M., & Harshey, R. M. (2000). Genetics of swarming motility in *Salmonella enterica* serovar Typhimurium: Critical role for lipopolysaccharide. *Journal of Bacteriology*, 182(22), 6308–6321. <https://doi.org/10.1128/JB.182.22.6308-6321.2000>
- Tomme, P., Warren, R. A. J., & Gilkes, N. R. (1995). Cellulose Hydrolysis by Bacteria and Fungi. *Advances in Microbial Physiology*, 37, 1–81. [https://doi.org/10.1016/S0065-2911\(08\)60143-5](https://doi.org/10.1016/S0065-2911(08)60143-5)
- Totten, P. A., Lara, J. C., & Lory, S. (1990). The *rpoN* gene product of *Pseudomonas aeruginosa* is required for expression of diverse genes, including the flagellin gene. *Journal of Bacteriology*, 172(1), 389–396. <https://doi.org/10.1128/JB.172.1.389-396.1990>
- Traxler, M. F., Summers, S. M., Nguyen, H.-T., Zacharia, V. M., Hightower, G. A., Smith, J. T., & Conway, T. (2008). The global, ppGpp-mediated stringent response to amino acid starvation in *Escherichia coli*. *Molecular Microbiology*, 68(5), 1128–1148.
<https://doi.org/10.1111/J.1365-2958.2008.06229.X>
- Tsai, C.-M., & Frasch, C. E. (1982). A sensitive silver stain for detecting lipopolysaccharides in polyacrylamide gels. *Analytical Biochemistry*, 119(1), 115–119.
[https://doi.org/10.1016/0003-2697\(82\)90673-X](https://doi.org/10.1016/0003-2697(82)90673-X)
- Tsai, C.-S., & Winans, S. C. (2010). LuxR-type quorum-sensing regulators that are detached from common scents. *Molecular Microbiology*, 77(5), 1072–1082.
<https://doi.org/10.1111/J.1365-2958.2010.07279.X>
- Tsau, J. L., Guffanti, A. A., & Montville, T. J. (1992). Conversion of pyruvate to acetoin helps to maintain pH homeostasis in *Lactobacillus plantarum*. *Applied and Environmental Microbiology*, 58(3), 891–894. <https://doi.org/10.1128/aem.58.3.891-894.1992>
- Tsui, H. C., Feng, G., & Winkler, M. E. (1996). Transcription of the *mutL* repair, *miaA* tRNA modification, *hfq* pleiotropic regulator, and *hflA* region protease genes of *Escherichia*

- coli* K-12 from clustered σ^{32} -specific promoters during heat shock. *Journal of Bacteriology*, 178(19), 5719–5731. <https://doi.org/10.1128/JB.178.19.5719-5731.1996>
- Tsui, H. C., Leung, H.-C. E., & Winkler, M. E. (1994). Characterization of broadly pleiotropic phenotypes caused by an *hfq* insertion mutation in *Escherichia coli* K-12. *Molecular Microbiology*, 13(1), 35–49. <https://doi.org/10.1111/j.1365-2958.1994.tb00400.x>
- Turner, A. K., Lovell, M. A., Hulme, S. D., Zhang-Barber, L., & Barrow, P. A. (1998). Identification of *Salmonella typhimurium* genes required for colonization of the chicken alimentary tract and for virulence in newly hatched chicks. *Infection and Immunity*, 66(5), 2099–2106. <https://doi.org/10.1128/IAI.66.5.2099-2106.1998>
- Valle, A. H. del, Seip, B., Cervera-Marzal, I., Sacheau, G., Seefeldt, A. C., & Innis, C. A. (2020). Ornithine capture by a translating ribosome controls bacterial polyamine synthesis. *Nature Microbiology*, 5(4), 554–561. <https://doi.org/10.1038/s41564-020-0669-1>
- Vigneshkumar, B., Pandian, S. K., & Balamurugan, K. (2012). Regulation of *Caenorhabditis elegans* and *Pseudomonas aeruginosa* machinery during interactions. *Archives of Microbiology*, 194(4), 229–242. <https://doi.org/10.1007/s00203-011-0750-5>
- Wadhams, G. H., & Armitage, J. P. (2004). Making sense of it all: bacterial chemotaxis. *Nature Reviews Molecular Cell Biology*, 5(12), 1024–1037. <https://doi.org/10.1038/nrm1524>
- Walsby, A. E. (1969). The permeability of blue-green algal gas-vacuole membranes to gas. *Proceedings of the Royal Society of London. Series B. Biological Sciences*, 173(1031), 235–255. <https://doi.org/10.1098/rspb.1969.0049>
- Walsby, A. E. (1972). Structure and function of gas vacuoles. *Bacteriological Reviews*, 36(1), 1–32. <https://doi.org/10.1128/br.36.1.1-32.1972>
- Walsby, A. E. (1994). Gas vesicles. *Microbiological Reviews*, 58(1), 94–144. <https://doi.org/10.1128/mr.58.1.94-144.1994>
- Walsby, A. E., & Bleything, A. (1988). The Dimensions of Cyanobacterial Gas Vesicles in Relation to Their Efficiency in Providing Buoyancy and Withstanding Pressure. *Microbiology*, 134(10), 2635–2645. <https://doi.org/10.1099/00221287-134-10-2635>
- Walsby, A. E., & Hayes, P. K. (1988). The Minor Cyanobacterial Gas Vesicle Protein, GvpC, Is Attached to the Outer Surface of the Gas Vesicle. *Microbiology*, 134(10), 2647–2657. <https://doi.org/10.1099/00221287-134-10-2647>
- Walsby, A. E., & Hayes, P. K. (1989). Gas vesicle proteins. *The Biochemical Journal*, 264(2),

- 313–322. <https://doi.org/10.1042/bj2640313>
- Walsh, N. P., Alba, B. M., Bose, B., Gross, C. A., & Sauer, R. T. (2003). OMP peptide signals initiate the envelope-stress response by activating DegS protease via relief of inhibition mediated by its PDZ domain. *Cell*, *113*(1), 61–71. [https://doi.org/10.1016/S0092-8674\(03\)00203-4](https://doi.org/10.1016/S0092-8674(03)00203-4)
- Walton, J. D. (1994). Deconstructing the Cell Wall. *Plant Physiology*, *104*(4), 1113–1118. <https://doi.org/10.1104/pp.104.4.1113>
- Watanabe, M., Kojima, H., & Fukui, M. (2018). Review of *Desulfotomaculum* species and proposal of the genera *Desulfallas* gen. nov., *Desulfofundulus* gen. nov., *Desulfofarcimen* gen. nov. and *Desulfohalotomaculum* gen. nov. *International Journal of Systematic and Evolutionary Microbiology*, *68*(9), 2891–2899. <https://doi.org/10.1099/IJSEM.0.002915>
- Waters, C. M., & Bassler, B. L. (2005). QUORUM SENSING: Cell-to-Cell Communication in Bacteria. *Annual Review of Cell and Developmental Biology*, *21*, 319–346. <https://doi.org/10.1146/ANNUREV.CELLBIO.21.012704.131001>
- Webb, C., Moreno, M., Wilmes-Riesenberg, M., Curtiss III, R., & Foster, J. W. (1999). Effects of DksA and ClpP protease on sigma S production and virulence in *Salmonella typhimurium*. *Molecular Microbiology*, *34*(1), 112–123. <https://doi.org/10.1046/j.1365-2958.1999.01581.x>
- Weiss, V., & Magasanik, B. (1988). Phosphorylation of nitrogen regulator I (NR(I)) of *Escherichia coli*. *Proceedings of the National Academy of Sciences of the United States of America*, *85*(23), 8919–8923. <https://doi.org/10.1073/pnas.85.23.8919>
- Whitfield, C., Amor, P. A., & Köplin, R. (1997). Modulation of the surface architecture of gram-negative bacteria by the action of surface polymer:lipid A-core ligase and by determinants of polymer chain length. *Molecular Microbiology*, *23*(4), 629–638. <https://doi.org/10.1046/j.1365-2958.1997.2571614.x>
- Widdel, F., & Pfennig, N. (1977). A New Anaerobic, Sporing, Acetate-Oxidizing, Sulfate-Reducing Bacterium, *Desulfotomaculum* (emend.) *acetoxidans*. *Archives of Microbiology*, *112*, 119–122. <https://doi.org/10.1007/bf00446665>
- Wigneshweraraj, S., Bose, D., Burrows, P. C., Joly, N., Schumacher, J., Rappas, M., ... Buck, M. (2008). Modus operandi of the bacterial RNA polymerase containing the σ^{54} promoter-specificity factor. *Molecular Microbiology*, *68*(3), 538–546.

<https://doi.org/10.1111/j.1365-2958.2008.06181.x>

- Wilf, N. M., Reid, A. J., Ramsay, J. P., Williamson, N. R., Croucher, N. J., Gatto, L., ... Salmond, G. P. C. (2013). RNA-seq reveals the RNA binding proteins, Hfq and RsmA, play various roles in virulence, antibiotic production and genomic flux in *Serratia* sp. ATCC 39006. *BMC Genomics*, *14*(1), 822. <https://doi.org/10.1186/1471-2164-14-822>
- Wilf, N. M., & Salmond, G. P. C. (2012). The stationary phase sigma factor, RpoS, regulates the production of a carbapenem antibiotic, a bioactive prodigiosin and virulence in the enterobacterial pathogen *Serratia* sp. ATCC 39006. *Microbiology*, *158*(Pt_3), 648–658. <https://doi.org/10.1099/mic.0.055780-0>
- Wilf, N. M., Williamson, N. R., Ramsay, J. P., Poulter, S., Bandyra, K. J., & Salmond, G. P. C. (2011). The RNA chaperone, Hfq, controls two *luxR*-type regulators and plays a key role in pathogenesis and production of antibiotics in *Serratia* sp. ATCC 39006. *Environmental Microbiology*, *13*(10), 2649–2666. <https://doi.org/10.1111/j.1462-2920.2011.02532.x>
- Williams, R. P., Gott, C. L., Qadri, S. M., & Scott, R. H. (1971). Influence of temperature of incubation and type of growth medium on pigmentation in *Serratia marcescens*. *Journal of Bacteriology*, *106*(2), 438–443. <https://doi.org/10.1128/jb.106.2.438-443.1971>
- Williamson, N. R., Fineran, P. C., Gristwood, T., Chawrai, S. R., Leeper, F. J., & Salmond, G. P. C. (2007). Anticancer and immunosuppressive properties of bacterial prodiginines. *Future Microbiology*, *2*(6), 605–618. <https://doi.org/10.2217/17460913.2.6.605>
- Williamson, N. R., Fineran, P. C., Leeper, F. J., & Salmond, G. P. C. (2006). The biosynthesis and regulation of bacterial prodiginines. *Nature Reviews Microbiology*, *4*(12), 887–899. <https://doi.org/10.1038/nrmicro1531>
- Williamson, N. R., Fineran, P. C., Ogawa, W., Woodley, L. R., & Salmond, G. P. C. (2008). Integrated regulation involving quorum sensing, a two-component system, a GGDEF/EAL domain protein and a post-transcriptional regulator controls swarming and RhIA-dependent surfactant biosynthesis in *Serratia*. *Environmental Microbiology*, *10*(5), 1202–1217. <https://doi.org/10.1111/j.1462-2920.2007.01536.x>
- Williamson, N. R., Simonsen, H. T., Ahmed, R. A. A., Goldet, G., Slater, H., Woodley, L., ... Salmond, G. P. C. (2005). Biosynthesis of the red antibiotic, prodigiosin, in *Serratia*: identification of a novel 2-methyl-3-n-amylopyrrole (MAP) assembly pathway, definition

- of the terminal condensing enzyme, and implications for undecylprodigiosin biosynthesis in *Streptomyces*. *Molecular Microbiology*, *56*(4), 971–989.
<https://doi.org/10.1111/j.1365-2958.2005.04602.x>
- Wong, C., Tintut, Y., & Gralla, J. D. (1994). The domain structure of sigma 54 as determined by analysis of a set of deletion mutants. *Journal of Molecular Biology*, *236*(1), 81–90.
<https://doi.org/10.1006/jmbi.1994.1120>
- Xiao, Z., & Xu, P. (2007). Acetoin metabolism in bacteria. *Critical Reviews in Microbiology*, *33*(2), 127–140. <https://doi.org/10.1080/10408410701364604>
- Xu, B.-Y., Dai, Y.-N., Zhou, K., Liu, Y.-T., Sun, Q., Ren, Y.-M., ... Zhou, C.-Z. (2014). Structure of the gas vesicle protein GvpF from the cyanobacterium *Microcystis aeruginosa*. *Acta Crystallographica Section D Biological Crystallography*, *70*(11), 3013–3022.
<https://doi.org/10.1107/S1399004714021312>
- Xu, L., Wang, Q., Xiao, J., Liu, Q., Wang, X., Chen, T., & Zhang, Y. (2010). Characterization of *Edwardsiella tarda* *waal*: Roles in lipopolysaccharide biosynthesis, stress adaptation, and virulence toward fish. *Archives of Microbiology*, *192*(12), 1039–1047.
<https://doi.org/10.1007/s00203-010-0635-z>
- Xu, T., Yu, M., Liu, J., Lin, H., Liang, J., & Zhang, X.-H. (2019). Role of RpoN from *Labrenzia aggregata* LZB033 (*Rhodobacteraceae*) in flagellar formation, motility, biofilm formation and environmental adaptation. *Applied and Environmental Microbiology*, *85*(7), e02844-18. <https://doi.org/10.1128/AEM.02844-18>
- Yenkeje, R. A., Sam, M. R., & Esmaeillo, M. (2017). Targeting survivin with prodigiosin isolated from cell wall of *Serratia marcescens* induces apoptosis in hepatocellular carcinoma cells. *Human & Experimental Toxicology*, *36*(4), 402–411.
<https://doi.org/10.1177/0960327116651122>
- Youn, M., Lee, K. M., Kim, S. H., Lim, J., Yoon, J. W., & Park, S. (2013). *Escherichia coli* O157: H7 LPS O-side chains and pO157 are required for killing *Caenorhabditis elegans*. *Biochemical and Biophysical Research Communications*, *436*(3), 388–393.
<https://doi.org/10.1016/j.bbrc.2013.05.111>
- Yu, V. L. (1979). *Serratia marcescens*: historical perspective and clinical review. *The New England Journal of Medicine*, *300*(16), 887–893.
<https://doi.org/10.1056/NEJM197904193001604>
- Yun, J., Jeon, B., Barton, Y. W., Plummer, P., Zhang, Q., & Ryu, S. (2008). Role of the DksA-

- like protein in the pathogenesis and diverse metabolic activity of *Campylobacter jejuni*. *Journal of Bacteriology*, 190(13), 4512–4520. <https://doi.org/10.1128/JB.00105-08>
- Zhang, G., Meredith, T. C., & Kahne, D. (2013). On the essentiality of lipopolysaccharide to Gram-negative bacteria. *Current Opinion in Microbiology*, 16, 779–785. <https://doi.org/10.1016/j.mib.2013.09.007>
- Zhang, Y., & Inouye, M. (2011). RatA (YfjG), an *Escherichia coli* toxin, inhibits 70S ribosome association to block translation initiation. *Molecular Microbiology*, 79(6), 1418–1429. <https://doi.org/10.1111/j.1365-2958.2010.07506.x>
- Zielinski, N. A., Maharaj, R., Roychoudhury, S., Danganan, C. E., Hendrickson, W., & Chakrabarty, A. M. (1992). Alginate synthesis in *Pseudomonas aeruginosa*: Environmental regulation of the *algC* promoter. *Journal of Bacteriology*, 174(23), 7680–7688. <https://doi.org/10.1128/jb.174.23.7680-7688.1992>